THE UNIVERSITY OF
WARWICK

University of Warwick institutional repository: http://go.warwick.ac.uk/wrap

A Thesis Submitted for the Degree of PhD at the University of Warwick

http://go.warwick.ac.uk/wrap/72497

This thesis is made available online and is protected by original copyright.

Please scroll down to view the document itself.

Please refer to the repository record for this item for information to help you to cite it. Our policy information is available from the repository home page.

Low Energy Electron Diffraction from Metal Surfaces

by

R.J. Reid, B.Sc.

A Thesis

Submitted for the Degree of

Doctor of Philosophy

of the

University of Warwick

August, 1971.

Preamble

The work reported in this Thesis was performed by myself in the School of Physics of the University of Warwick, except insofar as is specifically acknowledged in the references in the text. No part of the work has been included in a Thesis submitted in respect of any other Degree of any University. Parts of Chapter 4 have been published in the British Journal of Applied Physics, Journal of Physics D, 2 (1969); 145, and some of the results presented in Chapter 6 have been published in Physica Status Solidi (a), 2 (1970), K109 and 4 (1971), K211. The bulk of Chapters 5 and 6 have been submitted to the journal Surface Science for publication. It has proved convenient to list the references cited in each chapter at the end of that chapter, rather than en masse at the end of the Thesis.

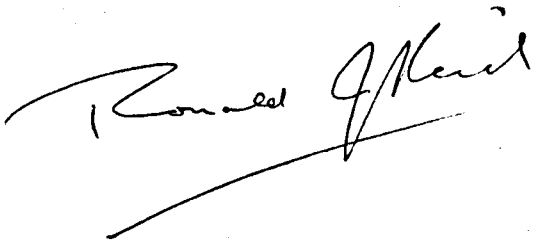

Ronald J. Reid.

Acknowledgements

I wish to express my sincere thanks to my supervisor Dr. H. Mykura for introducing me to the subject of LEED and for his unfailing encouragement and support during the course of this work, and to Professor A.J. Forty for the provision of facilities within the School of Physics.

I would also like to thank the many members of the School of Physics who have assisted me in any way during this period, and in particular Drs. D.P. Woodruff and M.P. Seah whose collaboration and advice in matters experimental were invaluable and Dr. B.W. Holland who patiently guided me through some of the many mysteries of the theory of the LEED process. In addition, I am indebted to Mr. O.S. Simpson for his excellent technical support.

The provision of a maintenance grant by the Science Research Council during the period of this work is also gratefully acknowledged.

Finally, I would like to thank my mother Mrs. M. Reid for her careful typing of this Thesis.

SUMMARY

Although Low Energy Electron Diffraction (LEED) has become relatively well established as a technique for the study of some aspects of the surfaces of crystalline systems, it is only comparatively recently that close attention has been paid to the physics of the diffraction process. The work presented in this thesis was therefore carried out in an attempt to elucidate some of these aspects of the process.

Firstly, we show that it is not necessary for the surface under examination to be an atomically perfect crystal surface, or even a macroscopically perfect surface over the entire area sampled by the electron beam, by a consideration of the diffraction patterns produced from faceted metal foils. This shows that provided the surface contains small areas of good crystal order larger than the coherence area of the electron beam used to produce the diffraction pattern, only as little as 10% of the sampled area of surface need be occupied by these areas of good crystalline order to produce no visible degradation of the diffraction pattern.

A short discussion of the properties of an ideal set of experimental data against which theoretical calculations of LEED intensity-energy spectra should be checked is followed by a set of experimental results which goes some way towards meeting these criteria. This comprises a complete set of intensity-energy spectra for the specular LEED beam from a single crystal copper (100) surface in an azimuth close to ⟨110⟩ , covering a large planar area of k-space bounded by the approximate energies 20 and 350eV, and the angles of incidence 6 and 22°, the spectra being taken at 1° intervals, together with a similar set of data for the

(111) surface in a $\langle 11\bar{2} \rangle$ azimuth, the spectra being taken in this case at 2^{o} intervals. The (110) surface of copper proved to be impossible to clean satisfactorily in a UHV environment, and a short discussion of its adsorption properties in that environment is given.

These sets of spectra demonstrate that although the main features of the intensity-energy spectrum lie close to the kinematical Bragg scattering conditions, the details of the spectra can only be explained by the use of proper dynamical calculations, in accord with the latest theories of LEED. Some correlations between the features of the spectra and the emergence of new non-specular diffraction beams are discussed.

Finally, a detailed discussion is presented on the effects of specimen temperature on the intensity-energy spectra obtained from the Cu(100) surface and the Cu(111) surface, the results for the (100) surface being rather more detailed than those for the (111) surface. These results demonstrate that the principal effect of temperature is the diminution in intensity of the diffraction peaks in the intensity-energy spectra, and that this diminution in intensity can be characterised by an effective Debye temperature. As the specimen temperature is changed, these peaks also shift in energy in a non-simple way, which, while not in itself important when comparing experimental results with rigid lattice theoretical spectra, must be taken into account in evaluating the Debye temperature for each peak. However, the width and overall shape of diffraction peaks which are well isolated from other peaks in the spectra appear to be independent of temperature. The detailed study of the measured Debye temperatures and peak shifts for all the diffraction peaks as a function

of the experimental diffraction parameters - energy and crystal orientation - proves them to be highly sensitive to the diffraction conditions. Such results cannot therefore be interpreted in the traditional kinematical manner, and hence cannot be used with confidence in extracting information about surface atom vibrations, surface lattice expansions, etc. The importance of including thermal effects when comparing theory with experiment is emphasised, and a particularly interesting experimental result is discussed in the light of a very recent calculation.

Table of Contents

Appendices Page

List of Figures

Chapter 2

Chapter 3

List of Tables

BLANK IN ORIGINAL

CHAPTER 1

HISTORICAL PERSPECTIVE AND SCOPE OF THIS THESIS

Following the accidental discovery of electron diffraction by Davisson and Germer in 1927[1], some use was made of the phenomenon to study certain aspects of the surface properties of crystalline systems by the back diffraction of slow electrons (e.g. references 2 and 3). Reproducibility of results, however, was not a notable feature of these experiments, mainly due to the relatively poor vacuum techniques available at that time. It was not until the development of ultra high vacuum techniques and the discovery of simple cleaning procedures for crystal surfaces[4] that Low Energy Electron Diffraction (LEED) became established as a promising technique. Since the early 1960's, however, the growth of experimental surface studies using LEED has been rapid (see, for example, the Bibliography published by Jackson *et al*[5]), although in many cases the results have proved somewhat disappointing. It is, in fact, only very recently that the full complexity of the problem of understanding the nature of the LEED process has been realised, let alone tackled. Indeed, the LEED problem has been described as one of the most difficult problems in solid state physics which is at present being tackled.

The characteristic of much of the published LEED work has been the reliance on insufficient data. In many cases, little has been described apart from the geometry of the LEED pattern, and perhaps one or two intensity - energy spectra, at perhaps a couple of angles of incidence. While such data can give a certain amount of information on, for example, the

symmetry of gas - solid adsorption structures, proceeding from such results to complicated analyses of the chemical and physical nature of the surface system, and of the nature of the interaction of low energy electrons with that system - as is very often done - appears to us to be a somewhat hazardous procedure. Recently, however, it has been realised that the complexity of the problem is such that extensive and detailed series of experimental data are required, and a few studies have gone some way towards meeting this requirement[6,7,8,9]. In Chapter 5 we describe some of the characteristics of an ideal set of experimental data and in what measure the results presented in this thesis go towards meeting these criteria.

The experimental content of this thesis falls into two distinct sections. Firstly, in Chapter 4, there is a brief study indicating the surface requirements which must be fulfilled by a real crystal system in order that a LEED pattern should be visible, and this will, in fact, demonstrate that these conditions are much less stringent than was at one time thought necessary. The second and major portion of the thesis occupies Chapters 5 and 6, and is an attempt to meet some of the requirements of the type of study outlined above. Here, the studies are restricted to a small range of systems, namely the "clean" low index faces of copper, and, within the specific limits described in Chapters 5 and 6, an attempt is made to provide a relatively complete set of data for the specularly reflected diffraction beam from the (100) surface, i.e. a set of intensity - energy spectra covering a large planar area of $\underline{k}$ - space, and a description of the effects of temperature on these spectra. For the (111) surface, a rather less complete set of data is presented. What we shall seek to demonstrate is that the results can not be interpreted on any naïve model

of the scattering process, but indicate that detailed calculations will have to be performed before significant conclusions can be drawn regarding the nature of the surfaces and of the mechanisms involved. Secondly, the importance of the effects of temperature on the LEED process, a hitherto much neglected parameter, will be demonstrated. Where possible, we shall also describe how present theoretical studies can indicate, however imperfectly, the correct interpretation of these results.

REFERENCES

1) C.J. Davisson and L.H. Germer, Phys. Rev. 30 (1927), 705.

2) H.E. Farnsworth, Phys. Rev. 34 (1929), 1287.

3) L.H. Germer, Z. Phys. 54 (1929), 408.

4) H.E. Farnsworth, R.E. Schlier, T.H. George and R.M. Burger, J. Appl. Phys. 26 (1955), 252.

5) A.G. Jackson, M.P. Hooker, T.W. Haas, G.J. Dooley and J.T. Grant, "A Bibliography on LEED and Related Techniques", Office of Aerospace Research, U.S.A.F., Report No. ARL 69-0003 (1969).

6) E.G. McRae and C.W. Caldwell, Surface Science 2 (1964), 509.

7) M.P. Seah, Surface Science 17 (1969), 181.

8) M.G. Lagally, Z. Naturforsh. 25a (1970), 1567.

9) F. Jona, I.B.M. J. Res. & Dev. 14 (1970), 444.

CHAPTER 2

LOW ENERGY ELECTRON DIFFRACTION

2.1 - Surface Crystallography

2.1.1 - Definition of a Surface

A crystal is a regular array of atoms whose centres lie at the points of a three dimensional lattice possessing translational symmetries and a certain set of point symmetries (i.e. reflections, rotations, etc.). The mathematical definition of a lattice is a set of points all of which are spatially equivalent, and so it is clear that, strictly speaking, a regular solid can only be a crystal if it is infinite in extent, with no defects in its structure. It is convenient and conventional, however, to talk about the lattice of a crystal, and this is derived by taking a representative portion of the perfect bulk solid and assuming that this is extended to infinity via its translational symmetry operators. The set of point and translational symmetry operators of this lattice is then known as the space group of the crystal.

When we come to discuss the surface of a crystal, that is some plane on which the atomic array is truncated, we no longer have full three-dimensional symmetry, and we cannot describe the structure of the surface in terms of a space lattice. However, the surface of a crystal has periodicity - and hence translational symmetry - in the two dimensions of the surface plane, although it may well be aperiodic in the third dimension into the crystal. Accordingly, if we restrict the three-space definition of a lattice to the

two-space of the surface plane, we can define a net of points, all of which are spatially equivalent in the two-space. Again we ignore the fact that a real crystal will not be infinite in these directions.

It is relatively straightforward to show that there are only five unique nets (called Bravais nets) of this type. In an analogous way to the space group of a three-space lattice, we can define the plane group of a two-space net, and there are seventeen of such plane groups[1]. However, when dealing with a real crystal surface, it is often useful to be able to describe the surface structure in three-space, and Wood[2] has shown that there are eighty space groups which are diperiodic in three-space. A complete table of such groups has been published[3].

For our purposes, however, it is most convenient to consider the surface structure as being related in some way to the bulk structure since, in the present state of LEED theory, it is impossible to deduce exactly where the surface atoms are in relation to the bulk atoms, although the solution of this problem may be aided by the relatively new technique of ESCA (Electron Spectroscopy for Chemical Analysis)[4]. Accordingly, one relates the net of actual surface structures to the hypothetical net obtained by slicing through the bulk structure parallel to the exposed surface plane.

There are two current notations for describing the relationship between these two nets, due to Wood[5] and to Park[6]. Wood's convention expresses the chosen primitive translation vectors (p.t.v.'s) of the surface unit mesh in terms of the p.t.v.'s of the substrate unit mesh. (The unit mesh of a net is the smallest unit of the net which, when operated on by the translation operators of the net, reproduces the net. Although the

choice of p.t.v.'s is somewhat arbitrary, it is most common to choose the two vectors representing the edges of the unit mesh of the net). For example, in Figure 2.1-1, $\underline{a}_s = 2\underline{a}$ and $\underline{b}_s = 2\underline{b}$. This structure would be described by the shorthand notation (2 x 2). If the p.t.v.'s of the surface unit mesh are not parallel to those of the substrate mesh, then, to obtain the shorthand notation, one rotates the unit mesh of the substrate until it is parallel to that of the surface, and uses as the reference vectors the primitive translation vectors of the unrotated substrate along these new directions. For example, Fig. 2.1-2 shows a (5 x 1)-R45° structure, the "R45°" denoting that the substrate unit mesh has been rotated through 45°. The full vector description of this surface structure is

$$\begin{aligned} \underline{a}_s &= 5\underline{a} - 5\underline{b} \\ \underline{b}_s &= \underline{a} + \underline{b} \end{aligned} \qquad (2.1 - 1)$$

A description of an adsorption structure in this notation would be, for example, Ni(011) - (3 x 1) - O, denoting the structure of adsorbed oxygen on a Nickel (011) surface.

In Park's notation, one describes the surface structure by the matrix transformation between the surface unit mesh and the substrate unit mesh, e.g. for the vector transformation of equation 2.1-1, the matrix

$$\underline{\underline{M}} = \begin{bmatrix} 5 & -5 \\ 1 & 1 \end{bmatrix}$$

describes the change of basis. Equation 2.1-1 may thus be written as

$$\underline{S} = \underline{\underline{M}}\,\underline{B} \qquad (2.1 - 2)$$

with an obvious notation.

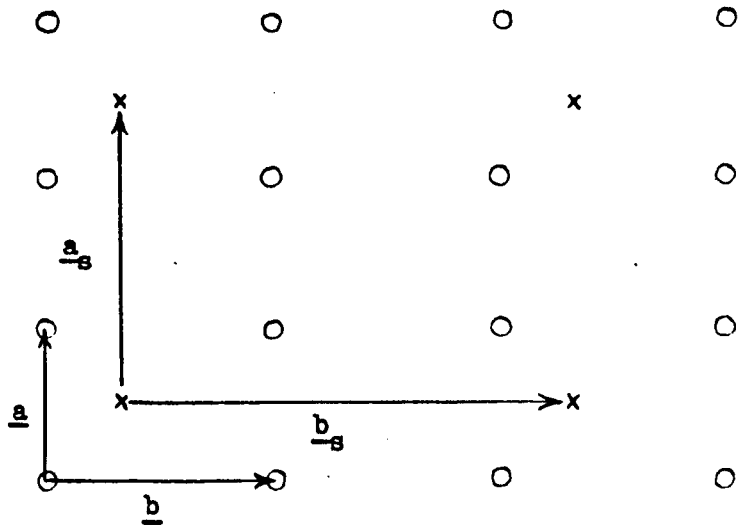

○ - Substrate atom

× - Surface atom

Figure 2.1-1. An example of a (2 x 2) surface structure.

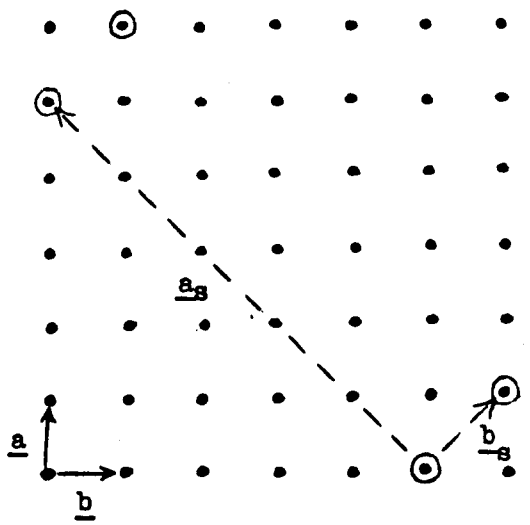

• - Substrate atom

○ - Surface atom

Figure 2.1-2. An example of a (5 x 1)-R45° surface structure.

It is sometimes more convenient to describe the surface structure in terms of a centred unit mesh rather than a primitive mesh, in much the same way as it is convenient to talk about face- or body-centred cubic lattices. In these cases the derivation of notations for the structure is exactly as described above, but a distinguishing "c" is added as c - (2 x 1), for example.

2.1.2 - The Surface Reciprocal Net

It is often useful in diffraction theory to work in terms of reciprocal space rather than direct space. To this end, we therefore define the reciprocal net of a surface direct net as follows. Let the direct net of the surface be represented by the primitive translation $\underline{a}_1, \underline{a}_2$. Then the reciprocal net is defined by the primitive translation $\underline{a}_1^*, \underline{a}_2^*$ such that

$$\underline{a}_i \cdot \underline{a}_j^* = 2\pi \delta_{ij} \qquad (i,j = 1,2) \qquad (2.1 - 3)$$

where δ_{ij} is the Kronecker delta and reciprocal two-space is defined to coincide with direct two-space (i.e. they both occupy the same planar section of three-space). The factor 2π is introduced for convenience, since this makes the reciprocal net integral in the units of k, the magnitude of the wave vector of the radiation whose diffraction we are considering.

Projection of the two-space reciprocal net into three-space gives a line extending to $\pm\infty$ through each reciprocal net point, parallel to the third basis vector of the three-space, usually defined to be perpendicular to the plane of the two-space. We shall refer to these lines as the

three-space reciprocal net rods of the direct surface net, or more simply as the reciprocal net rods.

The reciprocal net rods of the surface may be related to the three-space reciprocal lattice of the bulk crystal in the following manner. We choose the three p.t.v.'s of the direct space lattice of the crystal such that two of these lie in the surface and are the p.t.v.'s of a surface net. Equation 2.1-3 is then extended to three-space by letting the i,j run over 1,2,3. This then defines a lattice of points, and, because of the way we have chosen our p.t.v's, each of these points lies on one of the reciprocal net rods of the surface net.

2.2 - The Geometry of LEED

2.2.1 - The Formation of LEED Patterns

Low Energy Electron Diffraction may be conveniently defined as the elastic scattering of a beam of monoenergetic electrons from a crystal surface (or other object which displays some form of periodicity). Consider a beam of electrons of wave vector $\underline{k}$ incident on a planar array of scatterers. We wish to look at the intensity of electrons scattered into the direction $\hat{\underline{k}}_i$ ($\hat{\underline{k}}_i$ denotes a unit vector in the direction of the vector $\underline{k}_i$ i.e. $\underline{k}_i = k_i\hat{\underline{k}}_i$). The scattering will be totally defined by the two conservation laws - energy and total momentum. The first law means that

$$\frac{\hbar^2 k_i^2}{2m} = \text{constant} = \frac{\hbar^2 k^2}{2m} \qquad (2.2 - 1)$$

It may readily be shown (see § 2.4.2) that conservation of total momentum (i.e. electron momentum plus crystal momentum) reduces to the conservation of the component of electron momentum parallel to the scattering net modulo $\hbar\underline{g}$, where $\underline{g}$ is a reciprocal net vector of the net of scatterers. Thus, if $\underline{k} = \underline{k}_{\parallel} + \underline{k}_{\perp}$, where $\underline{k}_{\parallel}$ and $\underline{k}_{\perp}$ are respectively the components of the electron wave vector parallel and perpendicular to the net of scatterers, conservation of momentum leads to the condition

$$\hbar\underline{k}_{i\parallel} = \hbar\underline{k}_{\parallel} + \hbar\underline{g}$$

$$\text{i.e. } \underline{k}_{i\parallel} = \underline{k}_{\parallel} + \underline{g} \qquad (2.2 - 2)$$

The diffraction pattern of the net - in most cases that is of the crystal surface - is thus a series of discrete beams whose wave vectors satisfy 2.2-2, and hence the pattern reflects the geometry of the reciprocal net.

Because of the condition 2.2-2, the positions of the diffracted beams immediately give the periodicities of the surface net, but can give no information regarding the actual positions of the atoms within the surface unit mesh.

Diffraction spots are labelled with the ordered pair of indices which defines the appropriate reciprocal net vector giving rise to the spot in terms of the basis vectors of the reciprocal net. For example, the (h,k) diffraction spot is that for which h,k satisfy the equation

$$\underline{k}_{i\parallel} = \underline{k}_{\parallel} + h\underline{a}^* + k\underline{b}^* \qquad (2.2 - 3)$$

where $\underline{a}^*, \underline{b}^*$ are the basic vectors of the surface reciprocal net.

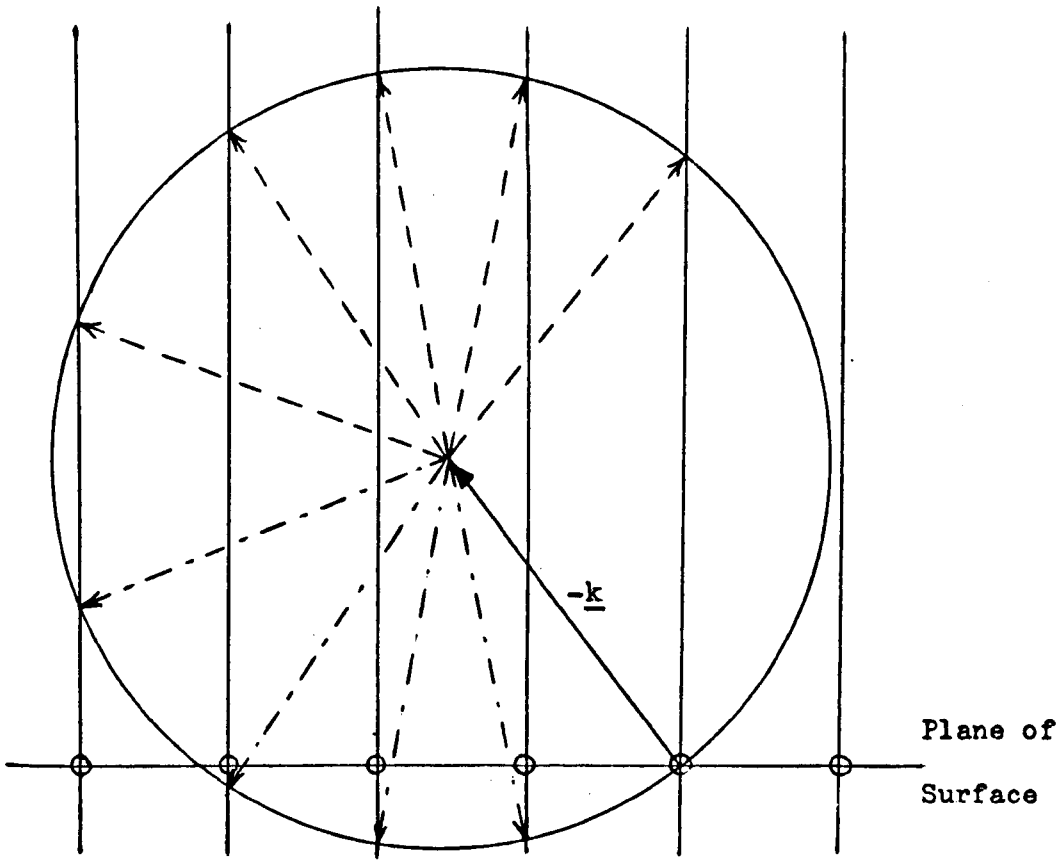

Figure 2.2-1. A two dimensional slice of the Ewald Sphere Construction for non-penetrating radiation of incident wave vector $\underline{k}$. The open circles *O* are the reciprocal net points of the surface mesh, lying in the two-space of the surface plane, and the lines through these points perpendicular to the plane of the surface are the corresponding three space reciprocal net rods.

PAGE NUMBERING AS IN THE ORIGINAL THESIS

2.2.2 - The Ewald Sphere Construction

The directions of beams diffracted by any particular structure can readily be determined by a modification of the Ewald Sphere Construction widely used in X-ray and High Energy Electron Diffraction[7,8]. The procedure, illustrated in Fig. 2.2-1, is to construct the three-space reciprocal net rods of the surface net as described in § 2.1.2. From the origin of the two-space reciprocal net, the vector $-\underline{k}$ is drawn, where $\underline{k}$ is the wave vector of the incident electrons. The tip of this vector is then the centre of the Ewald sphere for these diffraction conditions, the sphere of radius k being described about this point. Vectors drawn from the centre of the sphere to the points of intersection of the sphere with the reciprocal net rods then give the directions of all possible diffracted beams - into or out of the crystal.

The kinematical (i.e. single scattering) theory of LEED (§ 2.4.2) predicts that the diffracted beams will be most intense when the incident beam is in a Bragg scattering condition, i.e. when electron waves scattered from successive atomic planes in the crystal interfere constructively. These conditions may be derived from the Ewald sphere construction as follows.

On the reciprocal net rods is superimposed the reciprocal lattice of the bulk crystal, the points lying, as we described earlier, on the rods. A two-dimensional slice through such a sphere is shown in Fig. 2.2-2. Whenever the Ewald sphere passes through one of these points, that beam is in a Bragg scattering condition, and the corresponding maximum in the intensity of the beam is called a Bragg peak.

These concepts will be discussed rather more fully in § 2.4.2, where the kinematical theory of LEED is discussed.

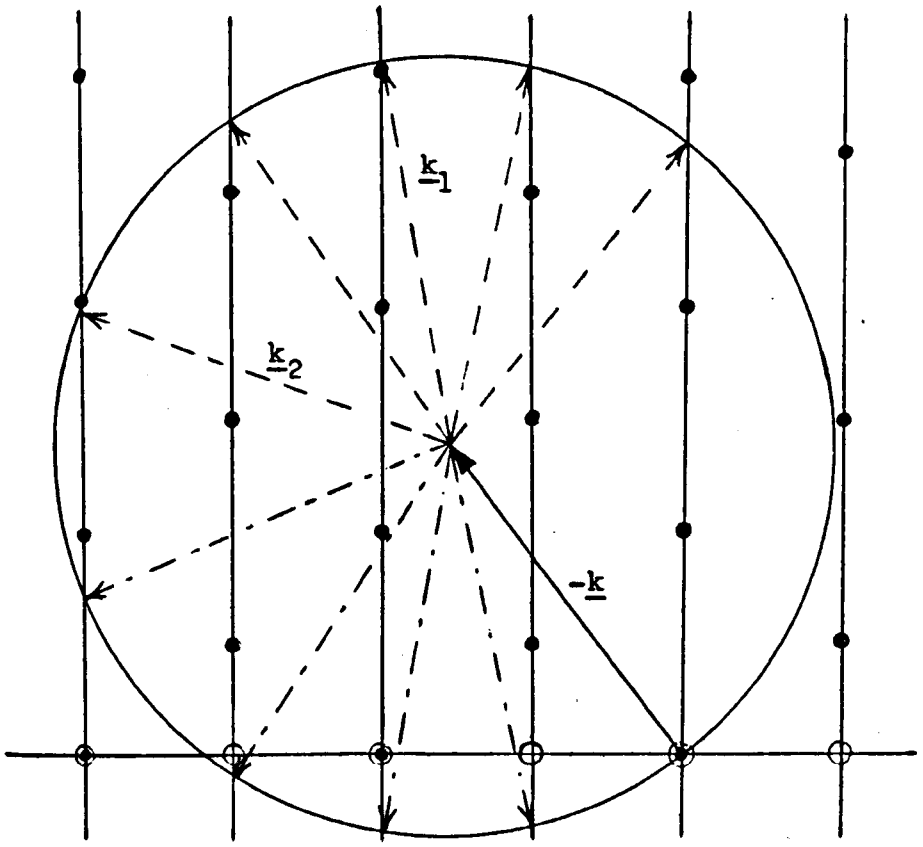

Figure 2.2-2. The Ewald Sphere Construction of Figure 2.2-1, with the reciprocal lattice points of the appropriate section of the three-space crystal lattice superimposed (full circles). Penetrating radiation is then in a kinematical Bragg scattering condition when a possible diffracted beam has a wave vector the tip of which intersects a reciprocal lattice point e.g. the vectors $\underline{k}_1$ and $\underline{k}_2$ in the Figure are almost in such a condition.

2.2.3 - Double Diffraction

At the energies of interest in LEED, the scattering cross sections for electrons are large enough for there to be a significant probability of the electrons suffering more than one elastic scattering event before leaving the crystal[9]. It is therefore possible for any beam diffracted into the crystal by the surface layer to act as an incident beam for the next crystal plane, producing its own diffraction pattern superimposed on the surface layer diffraction pattern, and so on[10]. If the surface plane and subsequent planes exhibit the same symmetry parallel to the surface, no difference in pattern geometries will occur, and this "double diffraction" will be undetectable. However, if the surface plane has a different primitive translation from the substrate plane, then "extra" diffraction spots may arise, satisfying the condition

$$\underline{k}_{i\parallel} = \underline{k}_{\parallel} + \underline{g}_{surf} + \underline{g}_{sub} \qquad (2.2 - 4)$$

where $\underline{g}_{surf}$ is a reciprocal net vector of the surface layer

$\underline{g}_{sub}$ is a reciprocal net vector of the substrate layer.

In this manner, quite complex diffraction patterns can arise from simple surface structures.

For example, suppose a hexagonal overlayer is situated on, and parallel to, a hexagonal substrate, so that the p.t.v.'s of each net are parallel but of different magnitudes, then some of the possible diffracted beams are as illustrated in Figure 2.2-3.

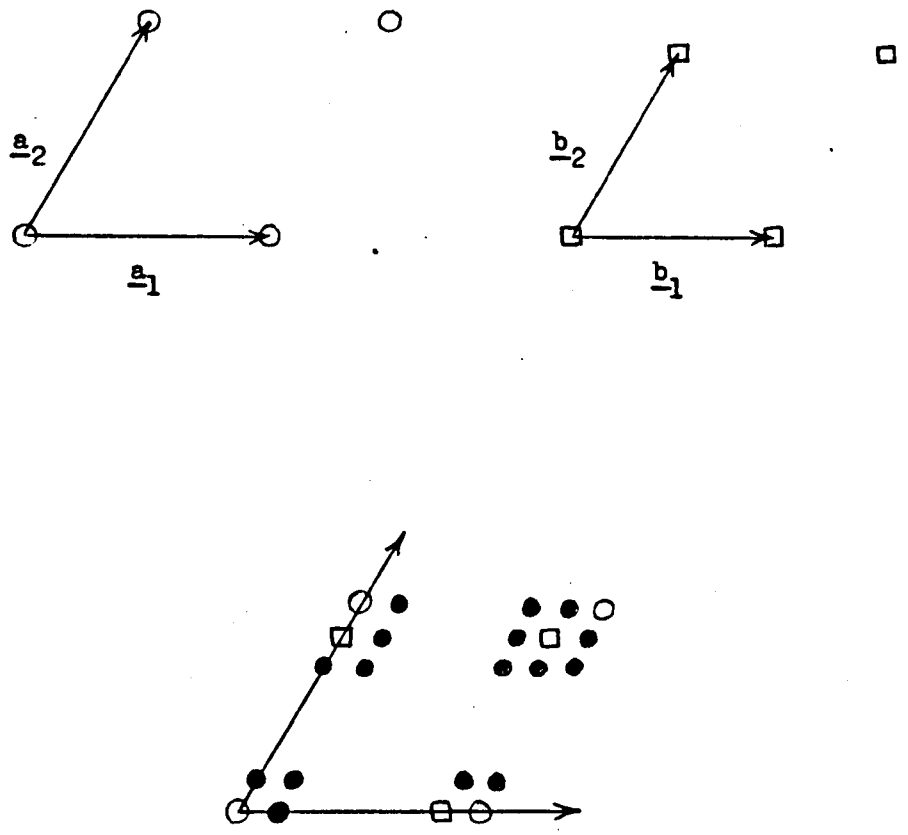

Figure 2.2-3. Some of the possible double diffraction beams arising from multiple reflections between the surface unit mesh ($\underline{b}_1$,$\underline{b}_2$) situated on and parallel to the substrate unit mesh ($\underline{a}_1$,$\underline{a}_2$).

2.3 - LEED Intensity - Energy Spectra

2.3.1 - Introduction and Definition of Parameters

In X-ray diffraction, structural information regarding the distribution of scatterers within the unit cell is obtained from reflection curves. These are obtained by rotating the crystal in a beam of X-rays of fixed wavelength and picking out the successive values of angle of incidence which give rise to the various diffracted beams corresponding to the spacings between different crystal planes[11]. (American authors often call these "rocking curves"). In LEED, however, it is experimentally simpler to vary the incident energy (and hence the wavelength) of the electrons rather than the angle of incidence, so what is generally plotted is the variation in intensity of a diffracted beam with incident energy. Stern[12] calls these curves "pseudo - rocking curves", but the term Intensity - Energy Spectra, or I(E) curves, is preferable.

The parameters open to variation are thus the energy of the incident beam E, the angle of incidence θ, and the azimuthal angle ϕ.

In LEED the angle of incidence θ is usually taken to be the angle between the incident beam and the surface normal. The azimuthal angle ϕ is defined as the angle between the plane of incidence (i.e. the plane containing the incident beam and the surface normal) and some arbitrary line in the surface plane - usually a low index crystallographic direction. These angles are illustrated in Fig. 2.3-1. It is usual to describe an azimuth in terms of the Miller indices of the plane of incidence.

The energy, E, of the incident beam is related to the magnitude of the

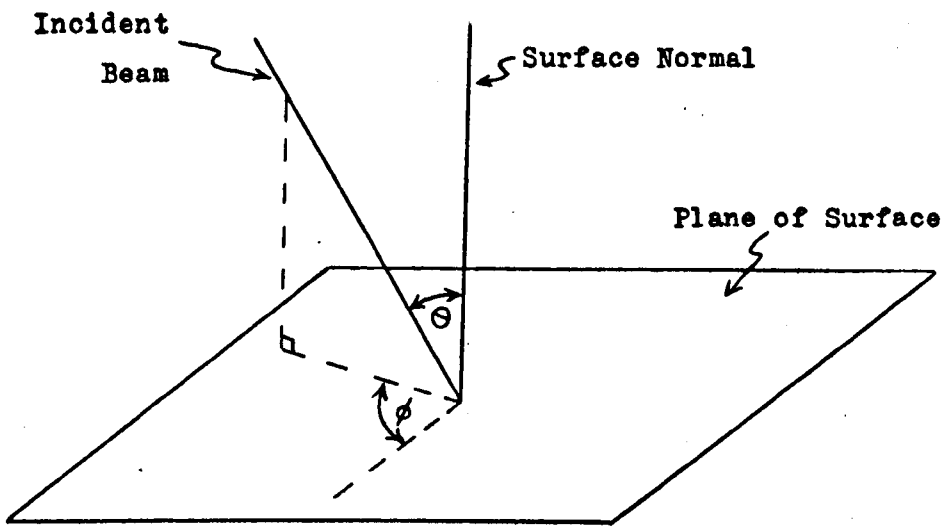

Figure 2.3-1. Definitions of angle of incidence θ, and azimuthal angle ϕ.

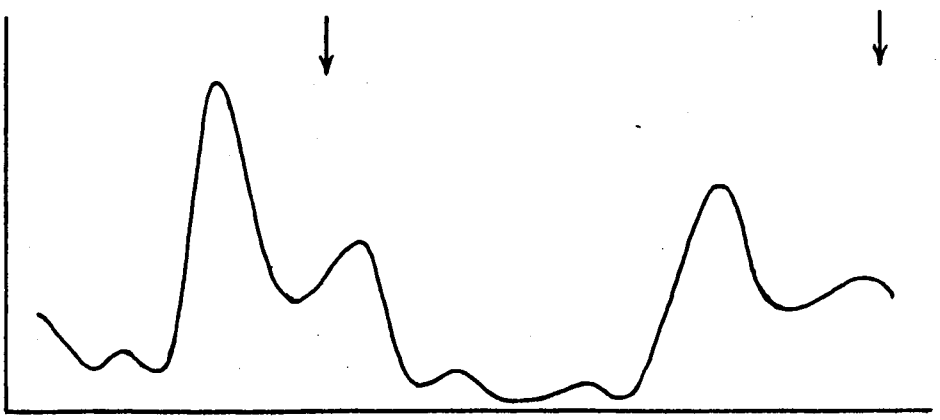

Figure 2.3-2. A typical Intensity-Energy Spectrum. The arrows show the positions of kinematical Bragg peaks.

incident wave vector $\underline{k}$ via the relation

$$k = 2\pi\sqrt{\frac{2mE}{h}} = 2\pi\sqrt{\frac{E}{150.4}} \quad \text{Å}^{-1} \qquad (2.3 - 1)$$

where E is in electron volts, and m is the mass of the electron. This expression arises by direct substitution in the de Broglie equation. The associated electron wavelength is then

$$\lambda = \frac{2\pi}{k} = \sqrt{\frac{150.4}{E}} \quad \text{Å} \qquad (2.3 - 2)$$

2.3.2 - k-space Plots

A typical intensity-energy spectrum is shown in Fig. 2.3-2, and it will be observed that it displays a considerable amount of structure. In order to be able to compare a large number of such curves, it is useful to be able to reduce the data to a more easily handled form. One method of reduction is due to Seah[13].

The section of the reciprocal lattice of the bulk crystal in the plane of incidence is drawn, and on this section through $\underline{k}$-space are plotted the tips of the vectors $-\underline{k}_i$ where $\{\underline{k}_i\}$ is the set of wave vectors of the incident beam each of which gives rise to a peak in the intensity-energy spectrum of the diffraction beam under consideration. The origin of the $-\underline{k}_i$ is the origin of reciprocal space. In other words, the plotted points are the centres of the Ewald spheres corresponding to the incident beam diffraction conditions for each of the diffraction peaks. The relative heights of the diffraction peaks are suggested by the relative sizes of the dots. Illustrative diagrams are presented in Fig. 2.3-3.

On the same diagram, lines may be drawn to represent the intersections of

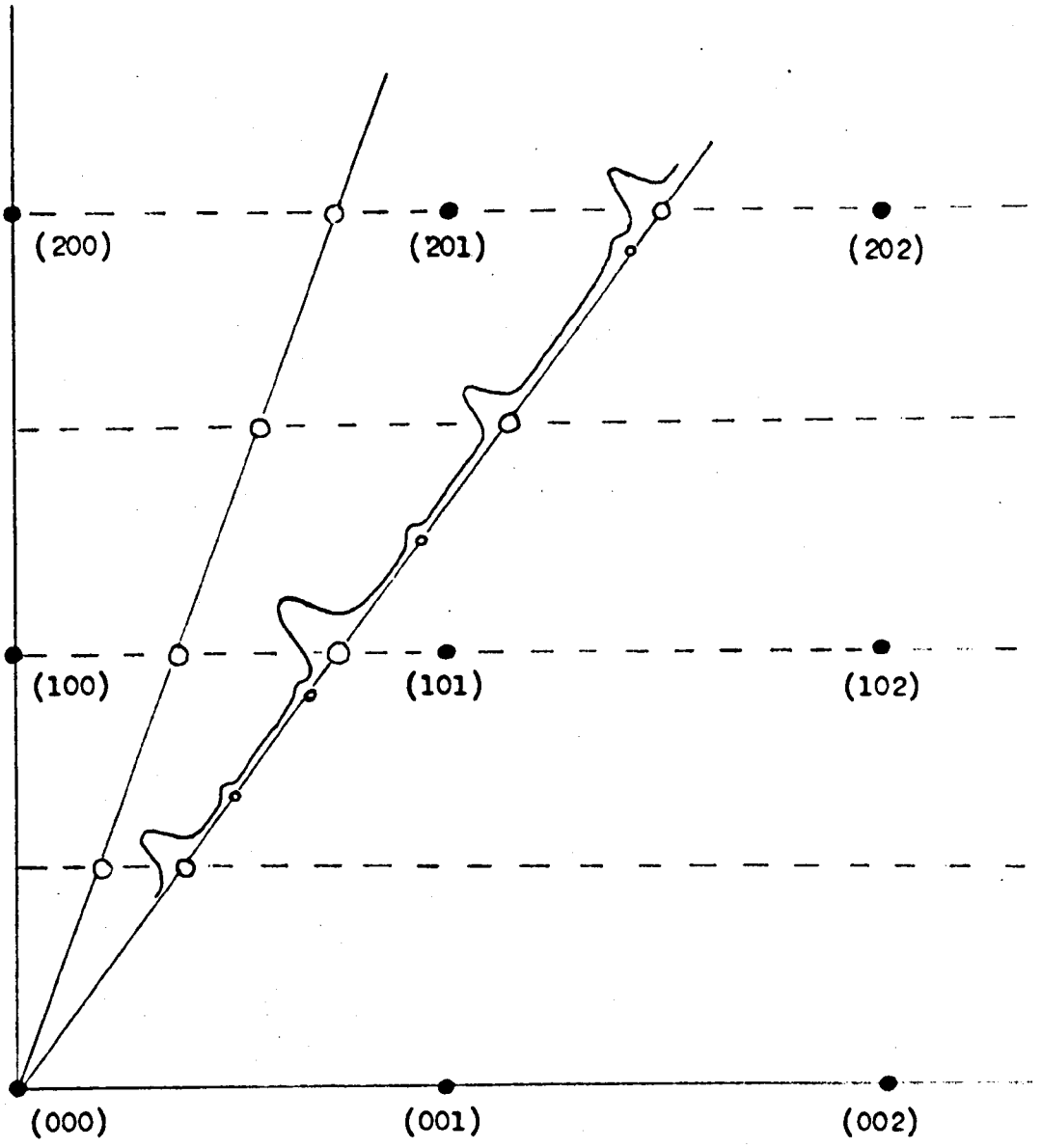

Figure 2.3-3. Section through the reciprocal lattice of a crystal (full circles), showing the centres of Ewald Spheres (open circles) corresponding to hypothetical diffraction peaks at two angles of incidence, and the intensity-energy spectrum at one of these angles of incidence.

this plane with the various Brillouin zone planes of the reciprocal lattice, these lines being known as zone lines. In the simple kinematical theory, dots representing Bragg peaks in the (h,k) beam are expected to lie, for all azimuths, on the zone lines corresponding to reciprocal lattice points on the (h,k) reciprocal net rod. These zone lines are then called Bragg zone lines, and are labelled with the indices of the appropriate Bragg reflection.

2.3.3 - The Reciprocity Theorem

The discussion presented above on the geometry of the LEED process has shown that the symmetries of the crystal are reflected in the diffraction process. These symmetries are therefore liable to be expressed in intensity-energy spectra to the extent that such spectra taken for beams which are in directions which are crystallographically identical are expected to be identical.

However, before applying this principle to real crystals, there is one further symmetry operation which must be taken into account[14], that of Time Reversal Symmetry. When applied to LEED, this may be expressed in terms of the Reciprocity Theorem which says

$$I_{-\underline{k}_i \rightarrow -\underline{k}} = I_{\underline{k} \rightarrow \underline{k}_i} \qquad (2.3 - 3)$$

that is, the time reversed intensity must be identical to the normal (i.e. forward time) intensity. An elegant experimental proof of this theorem has been presented by Woodruff and Holland[14].

When this symmetry is superimposed on the crystal symmetry, the effect is to mirror each half of the $\underline{k}$-space plot in the (0,0) reciprocal net

rod, thus producing a symmetrical arrangement of points representing peaks in the intensity-energy spectra, even though the crystal lattice may not be symmetrical about the (0,0) reciprocal net rod in this azimuth.

2.4 - Theories of LEED

2.4.1 - Introduction

The theory of the LEED process has progressed rapidly in the last few years, and has now reached a point where reasonably significant correlation of calculated intensity-energy spectra for simple crystals with the experimental results is just about being achieved[15]. However, since the purpose of this thesis is not to provide a detailed experimental substantiation of any one theoretical approach, nor to define completely the diffraction mechanisms operating in LEED, only a brief outline of the various theoretical approaches will be presented. The section will conclude with a brief discussion of the spirit of interpretation of the LEED data which will be adopted here.

Only selected references are quoted here, but a relatively complete list of sources for the kinematical theory is quoted by Lander[9] and those for the remaining sections may be found in the work of McRae[19] and of Holland *et al*[15].

2.4.2 - The Simple Kinematical Theory

The simple kinematical theory of LEED assumes that the cross section for elastic scattering (i.e. where the electron suffers no energy loss) of

low energy electrons by the atoms of a crystal is low, but that that for inelastic scattering (i.e. where the electron suffers some loss in energy) is high. The effect is for the majority of electrons either to suffer one elastic collision and leave the crystal in a beam defined by equation 2.2-3, or to suffer one inelastic collision and be lost to the LEED detection system. This treatment proceeds by direct analogy with the calculations performed for x-ray diffraction intensities, and an extensive discussion has been presented by Lander[9].

Consider a beam of electrons to be represented by a plane wave of wave vector $\underline{k}$ and amplitude A, and to be incident on an array of identical scattering centres defined by the set of position vectors $\{\underline{r}_n\}$. Let each scattering centre produce a scattered wave of amplitude $f_o A$ coherent with the incident wave, where f_o is a function of k and of the scattering angle $\cos^{-1}(\hat{\underline{k}}\cdot\hat{\underline{k}}_i)$ where $\hat{\underline{k}}_i$ is a unit vector along the direction in which we are measuring the scattered intensity. Then the total scattered amplitude A' along $\hat{\underline{k}}_i$ is given by[16]

$$A' = Af_o \sum_n \exp\left\{2\pi i(\underline{k}-\underline{k}_i)\cdot\underline{r}_n\right\} \qquad (2.4-1)$$

and the corresponding intensity is given by

$$I = |A'|^2 = A'A'^*$$

$$= A^2|f_o|^2 \sum_{\substack{m,n \\ m\neq n}} \exp\left\{2\pi i(\underline{k}-\underline{k}_i)\cdot\underline{r}_{mn}\right\} \qquad (2.4-2)$$

where $\underline{r}_{mn} = \underline{r}_m - \underline{r}_n$.

The electrons see a structure which is periodic in the two dimensions of the surface, although possibly aperiodic in the surface normal direction. If the periodicity of the surface is represented by the set of surface

reciprocal net vectors $\{\underline{g}_m\}$ then the intensity given by 2.4-2 vanishes unless

$$(\underline{k} - \underline{k}_i)_{\parallel} = \underline{g}_m \qquad (2.4 - 3)$$

where $(\underline{k} - \underline{k}_i)_{\parallel}$ is the projection of $\underline{k} - \underline{k}_i$ on the plane of the surface. This is the result stated in § 2.2-1.

The simple kinematical theory then states, by analogy, that the intensity of a diffracted beam will be at a maximum when the normal component of $\underline{k} - k_i$, i.e. $(\underline{k} - \underline{k}_i)_{\perp}$, is such that $\frac{2\pi}{(\underline{k} - \underline{k}_i)_{\perp}}$ is an integral multiple of the spacing between any two crystal planes in this direction.

In this case, equation 2.4-1 can be shown to reduce to[9]

$$A_{hk} = A_o N \sum_j f_j \exp\left\{2\pi i\left[hx_j + ky_j + \frac{1}{2\pi}(\underline{k} - \underline{k}_i)\cdot\underline{Z}_j\right]\right\} \qquad (2.4 - 4)$$

for the (h,k) beam, where $\{\underline{Z}_j\}$ is a set of vectors representing depth within the crystal, not necessarily a periodic function. This expression also allows for a distribution of scatterers of "strengths" f_j at positions (x_j, y_j) within the unit mesh of the surface.

Because of the relatively high probability posited for inelastic scattering it is assumed that the electrons "see" rather more or less of the three dimensional structure of the bulk crystal, depending on the strength chosen for the inelastic scattering. By direct analogy with optical diffraction theory, the electrons "see" a "grating" of more or less "elements", and the more "elements" they "see", the sharper will be the resultant diffraction maxima.

We can picture this by imagining that in the Ewald sphere construction, the density of a reciprocal net rod at any point is proportional to the intensity of electrons scattered to that point where the Ewald sphere intersects that point. By plotting the density of the rod as a function of position along the rod, measured from the plane of the surface reciprocal net, we would reproduce the intensity-energy spectrum of the diffracted beam scattered to that rod. Then, if initially we have very high inelastic scattering, so that the electrons cannot penetrate the solid at all, the rods will be of uniform density. As we progressively switch off the inelastic scattering, the electrons penetrate deeper and deeper into the crystal, and the density of the rods becomes modulated, gradually peaking around the reciprocal lattice points (assuming that the crystal is, in fact, periodic in the third dimension). Eventually, as the inelastic scattering becomes weaker, the rods split up into elongated sections centred on the reciprocal lattice points. Eventually, in the limit of no inelastic scattering, we have delta functions in density at these points, with nothing in between. What is assumed to be the case in reality is an intermediate case with broadish diffraction maxima near the reciprocal lattice points, i.e. moderately strong inelastic scattering.

This then predicts only simple Bragg maxima in the intensity-energy curves, whereas real I(E) curves show a much greater amount of structure. However, peaks in the spectra are often to be found at positions reasonably close to the positions predicted by 2.4-4, especially at higher energies, where the theory is expected to be better in any case. Consequently a "fudge factor" was introduced and related to the Inner Potential of the Sommerfeld Box Model of a solid. This then gives a kind of refractive index which could be used to bring the experimental peak positions into

coincidence with the Bragg peak positions. The inner potential defined in this way is now in fact found to be a somewhat erratic function of the energy and angle of incidence of the incident electrons.

It was for long felt that the kinematical theory should predict the main features of the experimental intensity-energy spectra, and that modifications to include dynamical scattering effects would simply introduce the observed fine structure. Consequently, many ingenious suggestions were put forward to explain the fine structure, e.g. variation of lattice spacing near the surface[17], "shadowing" of atoms in lower planes by those nearer the surface[18], and so on. Many such modifications are described in detail by Lander[9].

It is comparatively easy to obtain a reasonable fit to experimental data over a limited range of energy and angles of incidence by a suitable choice of such "corrections", but in no case has it proved possible to obtain the requisite amount of detailed fit over wide variations of the experimental parameters.

2.4.3 - The Multiple Scattering Theory

The first approach to show real promise of a reasonable correlation between theory and experiment was the multiple scattering treatment of E.G. McRae[19] based on early work by Lax[20]. This treatment recognised that the cross sections for scattering of low energy electrons are large[9] and so the probability of multiple elastic collisions is significant. It is not proposed to discuss the details of the theory, but it is worth mentioning the salient features of the treatment.

The diffraction process is assumed to be dominated by the elastic scattering so inelastic scattering can be formally ignored, and the elastic scattering is assumed to be symmetrical, i.e. s-wave, in character. The crystal model for which all calculations using this model have so far been performed is "simple cubium", i.e. a simple cubic lattice of scattering centres, each of which is represented by a muffin-tin type of potential. Discussion is thus limited to a somewhat artificial case. Nevertheless, this model is capable of reproducing in many respects the detail of experimental results, since it predicts the existence of both simple Bragg peaks (i.e. single scattering peaks) and secondary Bragg peaks (multiple scattering peaks).

The theory considers that the incident electron wave field, when it interacts with each scattering centre in the crystal gives rise to a scattered wave field, which may be propagating or non-propagating (i.e. evanescent). This scattered wave field then interacts back with the incident wave field, so that the effective wave field incident on each individual scattering centre is the sum of the incident wave field and the wave fields emitted by all the other atoms in the crystal. By suitably iterating this procedure the calculation can be made fully self consistent. Secondary peaks then arise due to "beating" (interferences) between the various components of the effective wave field[21].

Kambe[22] has presented a more complete formulation of this type of multiple scattering theory which gives results identical with those of McRae for the simple cubium model.

2.4.4 - The Band Structure Approach

An independent method of tackling the LEED problem based on the very early work of Bethe[23], Morse[24] and others was developed by Boudreaux and Heine[25] and subsequently by Pendry[26], Capart[27], Marcus and Jepsen[28] and by Gibbons[29] among others.

The basis of this approach is the recognition that if an electron incident on a crystal surface has a wave vector $\underline{k}$ such that the real part of $\underline{k}$ inside the crystal lies in a band gap of the electronic band structure of the crystal, then the only Bloch waves which can be excited within the crystal are those with imaginary wave vectors, i.e. they are non-propogating or evanescent. Matching of the electron wave fields inside and outside the crystal across the surface region then leads to total reflection of the incident electron in this case.

Pendry[26] has studied in detail the calculation of band structures near a free surface, but the approach nevertheless requires the presence of Bloch waves propogating through the crystal, which is not, in general, the case (see § 2.4.5). However, some agreement with experiment has been achieved. Recently Jones and Strozier[30] have obtained reasonably good fits to experimental data on Be(0001) using a reformulated band matching approach with a realistic crystal potential. In this modification, the inelastic scattering is included formally into the problem by splitting the crystal potential into real and imaginary parts. The real part then describes the elastic scattering, and the imaginary part describes the inelastic scattering. Very recently, Capart[31] has performed calculations on Copper (100) by recalculating the band structure in a very detailed way in the presence of the inelastic scattering potential, and obtained a

reasonable fit to experiment. The results of this calculation will be discussed further in Chapter 5.

2.4.5 - The Inelastic Collision Model

The basis of this model[32] lies in the realisation that the cross section for inelastic scattering of low energy electrons is high enough for the electrons to penetrate only a few atomic layers of the crystal[33]. This renders any formalism neglecting the effects of such inelastic scattering fundamentally unrealistic. The formalism takes as its model for the crystal a lattice of ion cores bathed in a uniform homogeneous gas of electrons. It is, of course, a gross approximation to assume that the electron gas is homogeneous near the surface, but present techniques of mathematical physics are unable to handle the problem of the inhomogeneous electron gas, and it is assumed that the main qualitative results of calculations at least ought to remain valid.

It is assumed that the dominant inelastic scattering channel is through the electron-electron interaction, the mean free path for such processes being estimated to be of the order of a few lattice spacings. The main electron-electron inelastic scattering processes in a metal are electron-hole pair production and volume- and surface-plasmon creation. At LEED energies, it is thought that electron-hole pair production is the dominant mode[34]. The electron-phonon interaction is thought not to be of major importance in this context, since this would give rise to temperature dependent peak widths, which are not observed in practise[34].

The procedure is to calculate the elastic scattering of the electrons by

the ion cores in the presence of the heavy damping introduced by the inelastic scattering in the electron gas. The scattering is calculated using the propogator formalism developed by Beeby[35] with the electron self energy being made complex to include the effects of inelastic scattering. The electron which is injected into the electron gas is regarded as being "dressed" to form a quasi-particle through its interaction with the electron gas. Such quasi-particles have a finite lifetime and may therefore be regarded as having complex self energies. The real part of the self energy is effectively the inner potential of the crystal into which the electron is injected, and the imaginary part is related to the lifetime of the quasi-particle, and hence to its mean free path in the electron gas.

The scattering is then expressed in terms of a multiple scattering series, i.e. a summation over single scattering, double scattering.....n-fold scattering events.

It is not proposed to discuss the mathematical details of this model, which have been presented by Duke and Tucker[32], but a brief summary of some of the more important conclusions drawn from specific calculations based on the model[15] is appropriate in this context.

Within the limitations of the model, calculations of intensity-energy spectra are found to be in reasonable agreement with experiment over a wide range of energies and angles of incidence. In the model calculations of Holland *et al*[15] on two radically different systems (LiF and Ni) it was found that little or no inner potential was required for the specular beam at low energies. However at higher energies, the LiF results

required a correction of 10-15eV to bring the calculations into agreement with experiment, whereas for Ni, no such correction was required over the entire energy range studied. However, the non-specular beams from Ni required an inner potential correction of about 20eV.

It is found that it is not very meaningful to try to ascribe definite diffraction processes to each peak in the intensity-energy spectra, i.e. calling some simple Bragg peaks, others secondary Bragg peaks, etc., since, in general, many different diffraction processes contribute to any one peak. Likewise, it is very definitely wrong to assume that the main features of intensity-energy spectra are determined by kinematical processes and the dynamical treatment simply adds the fine structure. Indeed, Holland showed that by progressively switching on the multiple scattering, a simple Bragg peak calculated on a single scattering basis was progressively annihilated and replaced by a multiple scattering peak a few eV away.

In a recent paper, Tucker and Duke[36] have shown that a calculation based on this model locates the main features of intensity-energy spectra near the kinematical Bragg scattering conditions, but that this does not mean that they are kinematical events. Indeed, what they have demonstrated is that the intensity-energy spectrum consists mainly of a very large number of inter-layer multiple scattering peaks which overlap to form a quasi-continuous spectrum, but that the overall intensity distribution is determined by an envelope function which peaks near the Bragg conditions in many cases.

2.4.6 - Interpretation of LEED Results

In view of the comments in the last section, in this thesis, we shall make no attempt to interpret peaks occurring in the intensity-energy spectra which we reproduce in terms of simple Bragg peaks, etc. Nevertheless, it will often be found convenient to plot results on $\underline{k}$-space plots of the type described in § 2.3.2, and simple Bragg zone lines will be plotted on these. In view of the results of calculations on nickel, and since all results presented here are for the specular beam from copper, no inner potential corrections are made to any of the results, such corrections being left until such time as full calculations for copper have been performed. For simplicity, however, main features of the intensity-energy spectra located near the Bragg zone lines will often be referred to as Nominal Bragg Peaks, without in any way prejudging the actual scattering mechanisms involved. The appropriate inner potential correction required to bring such features into coincidence with the Bragg zone lines will often be quoted, but never used. In passing it may be noted that in his calculations on copper, Capart[31] assumes a constant inner potential of 15eV.

REFERENCES

1) International Tables for X-Ray Crystallography 2 (Kynoch Press, Birmingham, 1959)

2) E.A. Wood, Bell Syst. Tech. Journ. 43 (1964), 541.

3) E.A. Wood, Bell Syst. Tech. Pubs. Monograph No. 4680.

4) K. Seigbahn et al, 'ESCA, Atomic, Molecular and Solid State Structures Studied by Means of Electron Spectroscopy' (Almquist & Wiksells, Uppsala, 1967)

5) E.A. Wood, J.Appl.Phys. 35 (1964), 1306.

6) R.L. Park, Surface Science 11 (1968), 188.

7) P.P. Ewald, Z. Kristallogr. 56 (1921), 129.

8) R.W. James, 'Optical Principles of the Diffraction of X-Rays' (G.Bell & Sons, London, 1962), p.6.

9) J.J. Lander, Progr. in Sol. State Chem. 2 (1965), 26.

10) E. Bauer, Surface Science 7 (1967), 351.

11) R.W. James, op. cit., p.282.

12) S. Friedman and R.M. Stern, Surface Science 17 (1969), 214.

13) M.P. Seah, Surface Science 17 (1969), 181.

14) D.P. Woodruff and B.W. Holland, Phys. Lett. 31A (1970), 207.

15) B.W. Holland, R.W. Hannum and A.M. Gibbons, Surface Science 25 (1971), 561

B.W. Holland, R.W. Hannum, A.M. Gibbons and D.P. Woodruff, Surface Science 25 (1971), 576.

16) G.H. Wannier, 'Elements of Solid State Theory' (C.U.P., 1960), p.39.

17) A.U. McRae and L.H. Germer, Ann. N.Y. Acad. Sci. 101 (1963), 627.

18) R.L. Gerlach and T.N. Rhodin, Surface Science 8 (1967), 1.

19) E.G. McRae, J. Chem. Phys. 45 (1966), 3258.

20) M. Lax, Rev. Mod. Phys. 23 (1951), 287.

---, Phys. Rev. 85 (1952), 621.

21) E.G. McRae, Surface Science 8 (1967), 14.

22) K. Kambe, Z. Naturforsh. A22 (1967), 322; A23 (1968), 1280.

23) H. Bethe, Ann. der Physik 87 (1928), 55.

24) P.M. Morse, Phys. Rev. 35 (1930), 1310.

25) D.S. Boudreaux and V. Heine, Surface Science 8 (1967), 426.

26) J.B. Pendry, J.Phys.C 2 (1969), 2273; 2283.

27) G. Capart, Surface Science 13 (1969), 361.

28) P.M. Marcus and D.W. Jepsen, Phys. Rev. Lett. 20 (1968), 925.

29) A.M. Gibbons, Ph.D. Thesis, University of Warwick (1969).

30) R.O. Jones and J.A. Strozier, Phys. Rev. Lett. 25 (1970), 516.

31) G. Capart, Surface Science, 26 (1971), 429.

32) C.B. Duke and C.W. Tucker, Surface Science 15 (1969), 231.

---, Phys. Rev. Lett. 23 (1969), 1163.

C.B. Duke, J.R. Anderson and C.W. Tucker, Surface Science 19 (1970), 127.

33) H.E. Farnsworth, Phys. Rev. 49 (1936), 605.

34) M.P. Seah and D.P. Woodruff, Phys. Lett. 30A (1969), 250.

35) J.L. Beeby, J.Phys.C 1 (1968), 82.

36) C.W. Tucker and C.B. Duke, Surface Science 24 (1971), 31.

CHAPTER 3

APPARATUS AND EXPERIMENTAL TECHNIQUES

3.1 - General Survey of LEED Apparatus

3.1.1 - Historical

The original apparatus of Davisson and Germer, in which the phenomenon of electron diffraction was first observed[1] used a beam of electrons which was focussed onto a large crystal, and the scattered electrons were collected in a Faraday cup which could be rotated about one axis in the crystal surface. The physical labour involved in elucidating a diffraction pattern with this system was considerable, and this prompted Germer and his co-workers[2,3] to investigate the possibility of some sort of visual display system. The system which they evolved was based on one developed earlier by Ehrenberg[4].

The energy of the electrons one is trying to detect makes it difficult to obtain a stable phosphor with a high enough quantum efficiency to enable direct conversion of the low energy electrons to photons to give a useable light output[5]. However, in LEED, one is generally interested only in the pseudo-elastically scattered electrons, i.e. those which have either been elastically scattered or have scattered off phonons in the crystal lattice, so some sort of energy filter is required to remove those electrons which have lost energy. The simplest way to filter the electrons is to use a system of two or more fine meshes in front of the display screen, at appropriate electrical potentials. It is then a simple enough matter to apply a suitably large potential between the final mesh and the screen to enable the electrons to gain enough energy to strike the screen

with enough velocity for efficient conversion to take place. This was the basis of the apparatus built by Scheibner et al[2], and is essentially identical with most of the LEED systems still in use. The operation of such a system will be described in a later section.

Farnsworth and his multitudinous colleagues continued to use the Faraday cup type of apparatus, however, and developed such systems to a high degree of precision over the period 1928 - 60, when little or no other work was being done in the field[6].

A great revival of interest in the field of LEED took place in the Sixties. The main reason for this was not some great advance in the techniques of electron diffraction, although the field of High Energy Electron Diffraction (HEED) had indeed developed greatly in the interim, but lay rather in the revolution in vacuum technique which enabled vacua of the order of nanotorr (10^{-9} mm of mercury) to be routinely attainable. The early LEED work had been plagued with the problem of maintaining "clean" or, rather, reproducible surfaces for any reasonable period of time, simply because of the relatively poor vacua at the disposal of the experimenters. The advent of UHV (Ultra High Vacuum) seemed the answer to this problem.

3.1.2 - The Display Type LEED Apparatus

As we mentioned earlier, in the display type LEED apparatus, after the electrons have scattered from the crystal, they pass through an electrostatic energy analyser and are accelerated onto a fluorescent screen. The most usual arrangement is as indicated in Figure 3.1-1, where the target is at the centre of curvature of the concentric spherical grids and screen,

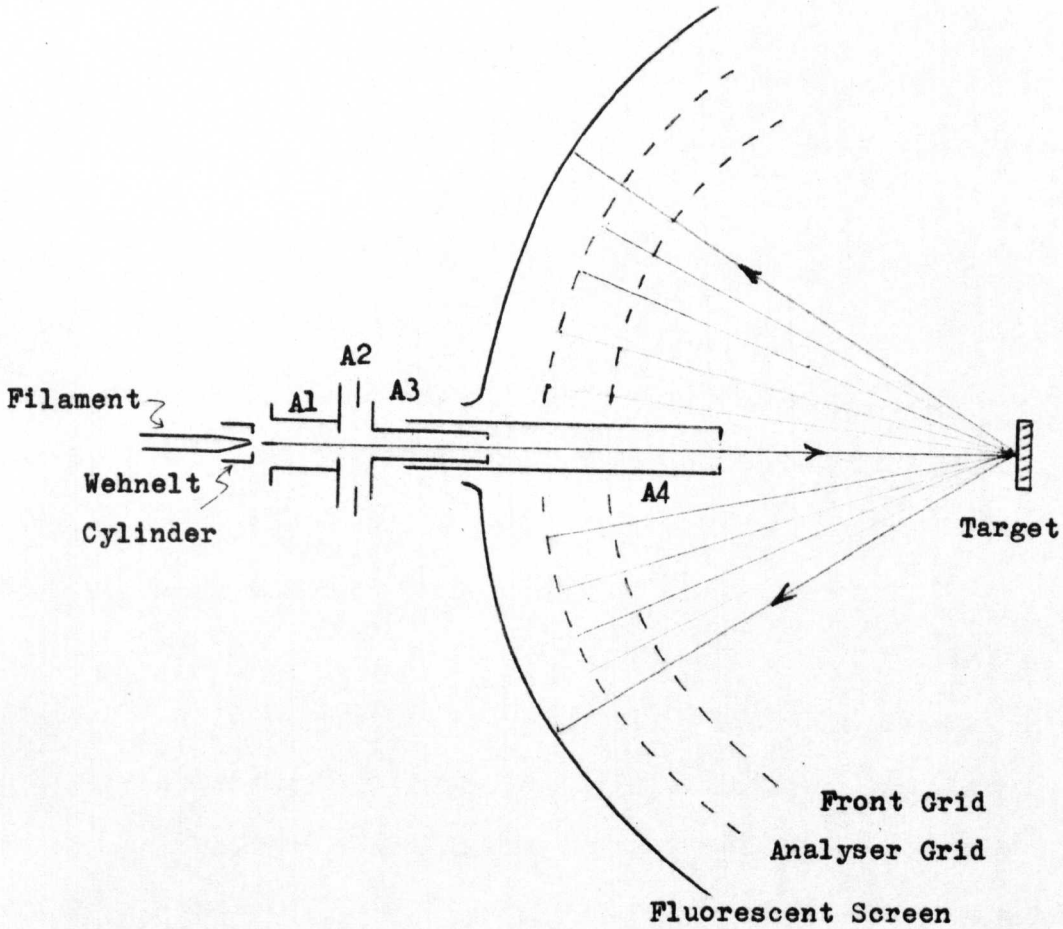

Figure 3.1-1. Typical layout of a two grid LEED optics.

and the screen is viewed from behind the specimen i.e. through the grids. Systems employing two, three or four grids are in common use.

The grid - screen system usually subtends an angle of about 112° at the specimen, but systems with flat or cylindrical grids[7,8] have been constructed, and these can subtend much larger angles. The advantage of the spherical grid system is that the pattern of diffraction spots on the screen is undistorted. Distortions are introduced when the screen is viewed from some distance away, and these are discussed in § 3.3.1.

In the most usual mode of operation of the two grid system, the front grid, the specimen and the final anode of the electron gun, which projects through the grids, are all maintained at earth potential, so that after scattering, the electrons move in an electrostatically field free space. The second grid is then operated as a repeller to perform the required energy analysis of the electrons, and the screen is held a few kilovolts positive. In the three grid system, first and second grids are usually strapped together as the analyser, and the first grid is again at earth potential. These modes of operation will be dealt with more thoroughly in § 3.2.3.

The display system possesses numerous inherent disadvantages, especially when one requires quantitative measurements, and these will be discussed in detail in § 3.1.4.

3.1.3 - The Faraday Cup Type LEED Apparatus

In this type of apparatus, the reflected electrons are collected in a

moveable Faraday cup which subtends some small angle at the crystal, and which can scan some part of the solid angle into which electrons can be scattered by the specimen. Because of the difficulty of applying the necessary two independent motions to the collector to enable it to cover this area, it is usually found to be the case that the collector moves on a great circle of a sphere centred on the specimen, and the specimen is rotated about a perpendicular axis to scan out the whole surface of the sphere[9].

The most common construction for the Faraday cup is three or more coaxial cylinders, of which the innermost is the actual collector, and the others form the energy analyser and potential guards. By the use of suitable electronic techniques, good resolution of the elastic and inelastic components of the scattered electrons can be obtained.

A different type of Faraday cup collector has been developed by Seah[10]. In this system, the collector is a small plate which moves behind a grid system similar to that found in the conventional display system. This has the advantage that only one electrical contact needs to be made to the moving collector, rather than the three or more in a conventional Faraday cup, and any possibility of leakage currents is completely eliminated.

3.1.4 - Critique and Future Trends

Up till the present time, the vast majority of work in LEED has been performed in display type LEED apparatus. The main reason for this is

that is is inherently cheaper and simpler than the Faraday cup system. The supreme advantage of the display system over the Faraday cup system is that the diffraction pattern is visible, so any gross changes are immediately discernible. This can be very useful when studying gas-solid interactions which involve changes in the surface symmetry, and it is in this field that LEED has been mainly used. Lately, however, there has been much interest in the diffraction process itself.

For this sort of problem, one requires to look in detail at the intensities of diffraction beams, and here one runs into difficulties with the display apparatus. For the specularly reflected beam, which does not move when the energy of the incident electrons changes, it is a comparatively easy matter to focus a spot photometer onto the diffraction spot on the fluorescent screen and to monitor its intensity as a function of energy, but this is no easy task for any other spot. Further, if one wishes to look at, say, the change in intensity of a diffraction beam with angle of incidence at a given energy, things become extremely difficult, since even a change in angle of 1^{o} can make a tremendous difference to the intensity-energy spectrum.

There are also basic difficulties inherent in the fluorescent screen - photometric technique, which will be discussed in more detail in § 3.3.

For intensity measurements, the Faraday cup is inherently more accurate, with its direct measurement of scattered electron flux, using well proven electrical measurement techniques, but it has the disadvantage of requiring a moveable detector inside the vacuum system, and a non - visible pattern.

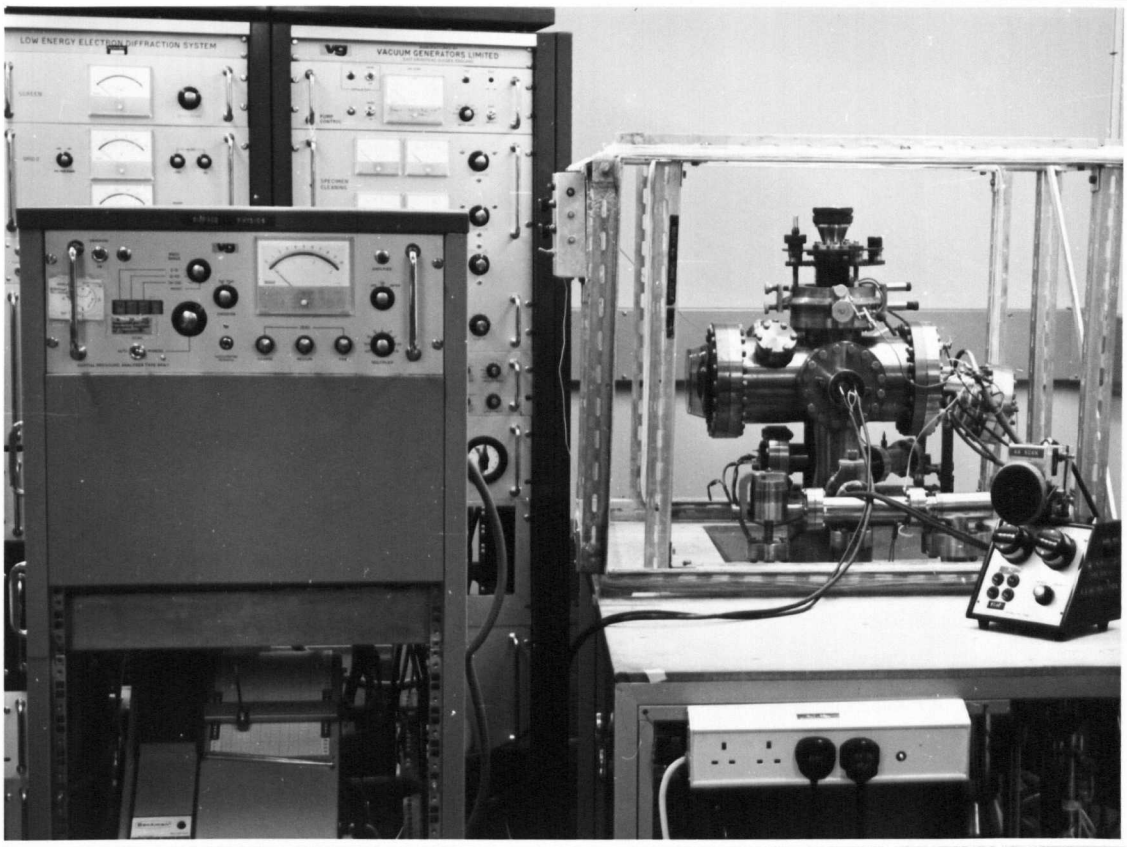

Figure 3.2-1. The Vacuum Generators LEED System. In this photograph, the magnetic compensation coils and the friction wheel for driving the A4 potentiometer are both clearly visible.

The obvious development is a combination of the two techniques. Several systems with this facility have been constructed[9,10], but these are systems where the two parts have been in effect bolted together, and each operates as a separate, independent system. However, new systems are now being developed, both in this department and in the U.S.A.[11], where the Faraday cup will scan in front of the conventional display optics, so that entire patterns can be monitored continuously, and simultaneous, accurate intensity measurements can be performed. It is to be expected that this type of system will be of the most use in the future.

3.2 - The Vacuum Generators LEED-1 System

3.2.1 - General Introduction

The LEED apparatus used in these studies is virtually a standard display type LEED unit manufactured by Vacuum Generators, Ltd. One or two minor modifications will be described where appropriate, but description of the standard items will be brief, since full specifications are readily available[12]. The system, which is fabricated in a non-magnetic stainless steel alloy, is shown in Figure 3.2-1.

3.2.2 - The Diffraction Chamber

The diffraction chamber is shown in Fig.3.2-2. The combined electron gun and LEED optics assembly is mounted on an eight inch 'Conflat' type flange at the rear of the chamber, and a similar flange at the front

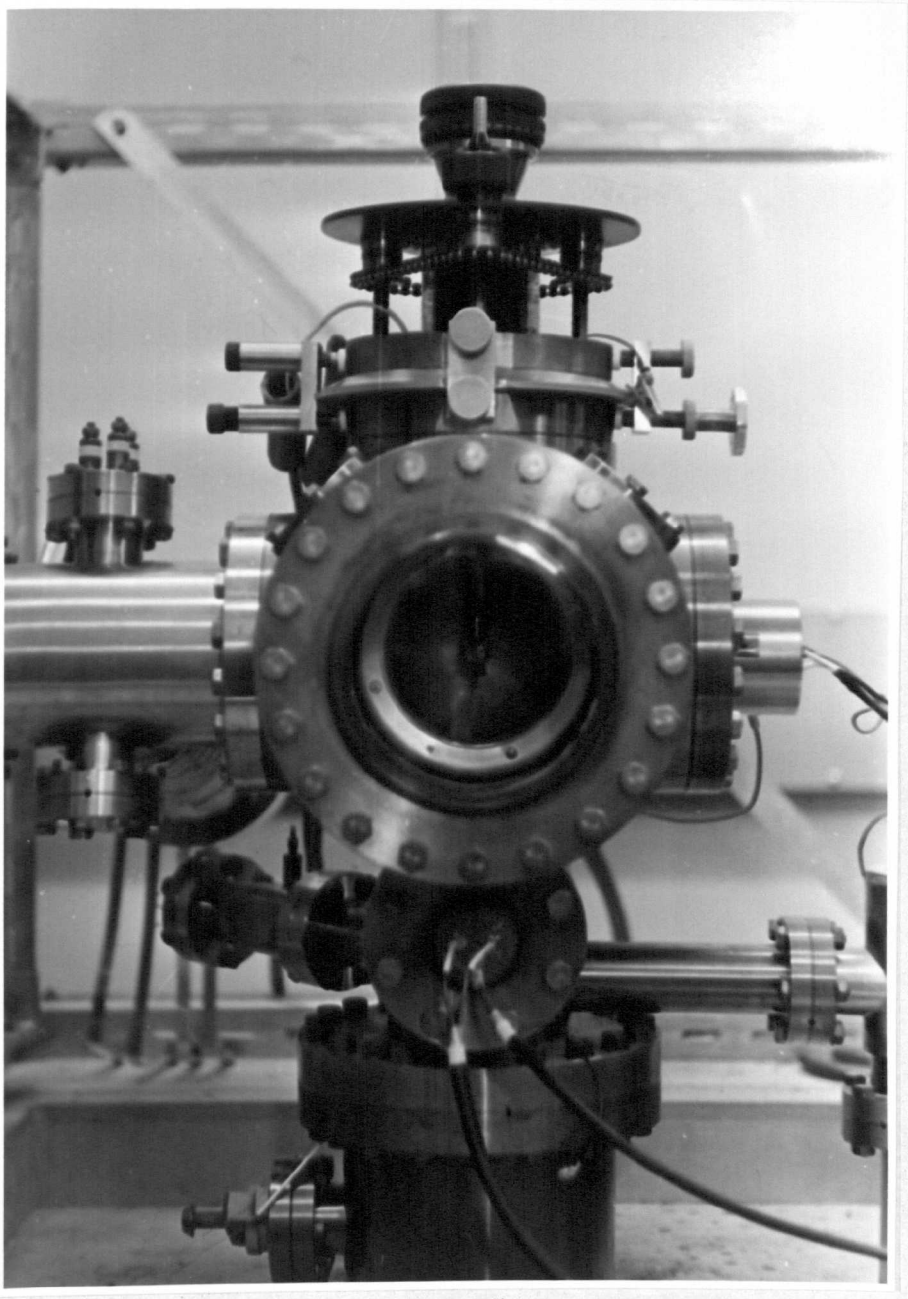

Figure 3.2-2. Close-up of the diffraction chamber. The hot stage containing the specimen can be seen through the viewing port, in front of the grids. The argon ion gun is directly to the right of the specimen, and the services well to the left.

carries a $4\frac{1}{2}$" Kodial viewing port. A six inch flange on the right hand side of the chamber carries the argon ion gun, while a similar port on the left leads to a small services well and a 4" water-cooled titanium sublimation pump. The whole chamber sits on top of a 6" tube leading to the main pumping station.

The specimen is carried on a Vacuum Generators Type U.M.D. 1 specimen manipulator, mounted on top of the chamber. This enables the specimen to be moved vertically through about 3", horizontally through about ± 1 cm. laterally and fore-and-aft, and tilted through about ± 5° from the vertical in any direction about the centre of curvature of the screen. Rotation through 360° about the vertical axis is normally possible, but this is restricted to about ± 110° when the special hot stage used in these studies is in position.

Pressures in the chamber are measured with a Mullard Type 10G 12 Bayard-Alpert ionisation gauge head, calibrated for nitrogen. All pressures quoted in this thesis are therefore equivalent nitrogen pressures.

A Vacuum Generators Type PPA 1 mass spectrometer head is fitted to the main chamber, so that residual gas analyses may be carried out, down to total residual gas pressures of about 10^{-8}T.

3.2.3 - The Electron Optics

(a) Two Grid LEED Optics

Two grid optics are usually used in systems where only LEED work is done, but those equipped for Auger Electron Analysis[13] have the three

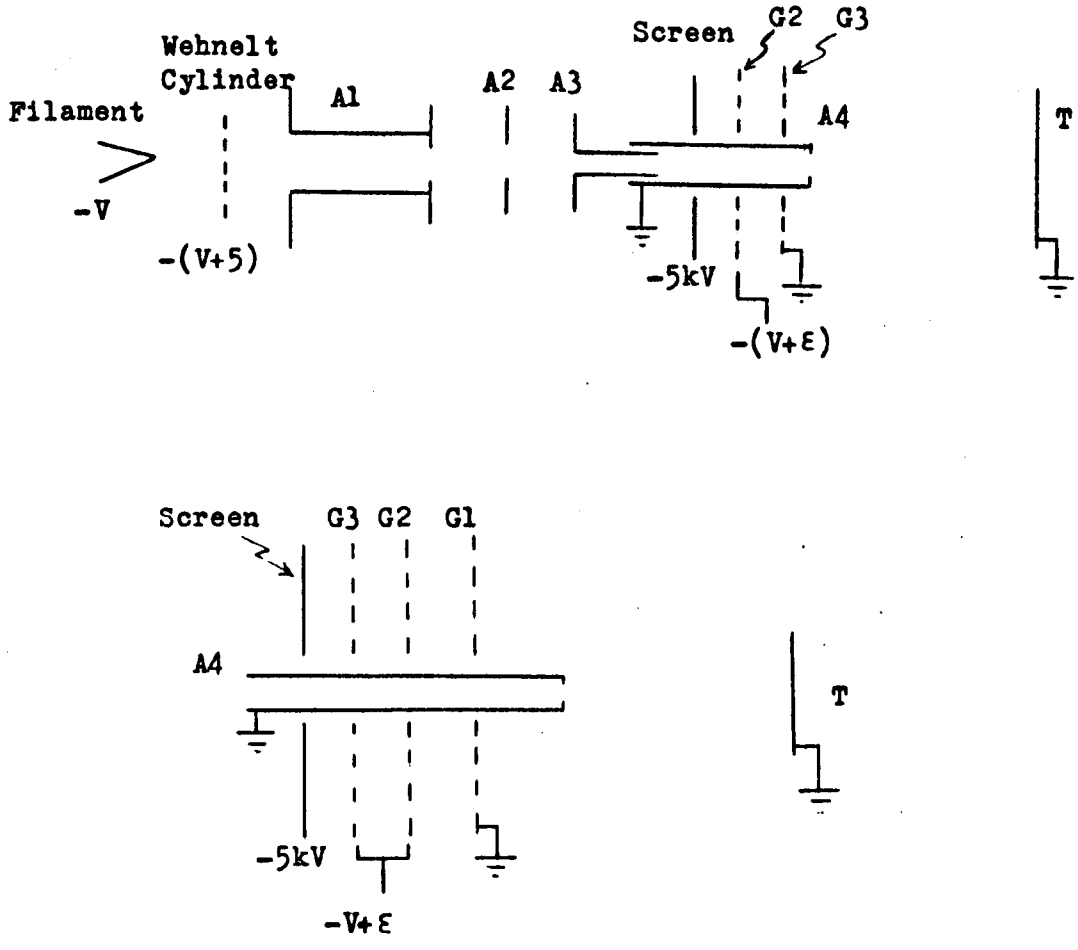

Figure 3.2-3. Essential electrical details of the two grid (upper) and three grid (lower) LEED optics. The electron gun in each case is similar, and so is only shown in the upper sketch. Typical operating potentials are shown below most of the components, apart from the anodes of the electron gun. The potentials of these depend on the accelerating potential V.

grid optics system which is described below, or may even have a fourth grid added. The essential electrical features of both types of optics are shown in Figure 3.2-3, and the geometrical layout was shown in Figure 3.1.1. A photograph of the two grid optics is shown in Figure 3.2-4.

In Figure 3.2-3, G1 and the specimen T are held at earth potential, so in the intervening space the electrons scattered from T move in straight lines, provided that there are no magnetic fields present. Most of the electrons penetrate G1, since these grids have very high transparencies. Ideally, these electrons would then see a potential gradient down to the potential -V, where V is the accelerating potential of the incident beam of electrons. This would then repel all but the elastic component of the scattered flux, which would just penetrate through G2 to see the high accelerating potential which shoots them onto the screen. However, the screen and G2 are separated only by about 2mm and the massive potential gradient between them ($\sim$20kV cm^{-1}) penetrates the very open mesh of the grid, causing the equipotential surface to bulge out between the wires of the grid, thus reducing the already poor energy resolution of the filter system. To partially cancel out this field penetration, G2 is run at a potential $-(V+\varepsilon)$ where ε is a small potential determined by trial and error, selected so that a small increase in ε causes all the scattered electrons to be repelled. It is generally found that ε is of the order of 5V.

(b) Three Grid LEED Optics

As mentioned above, three grid optics are usually found in systems equipped for Auger Electron Analysis. They have, however, some advantages

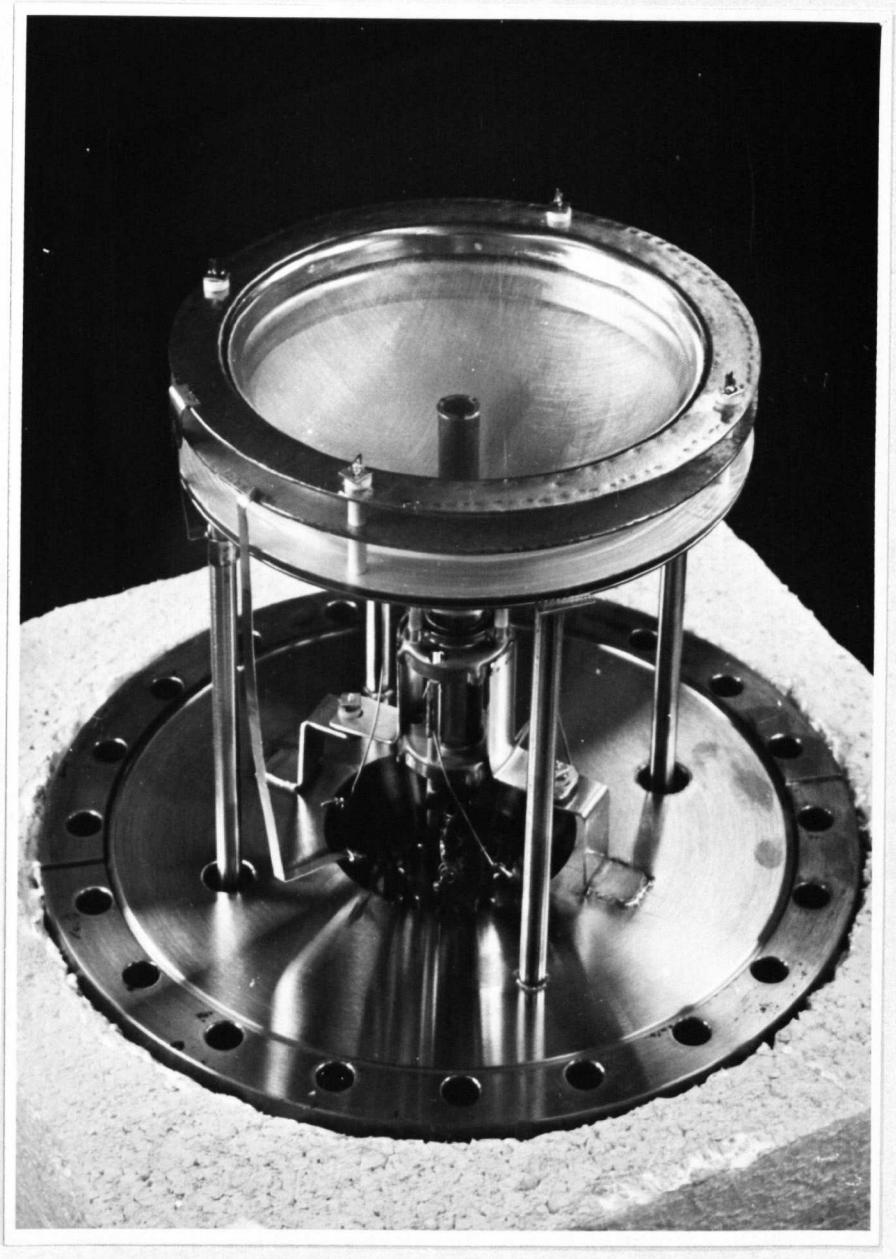

Figure 3.2-4. The two grid LEED optics.

when used for LEED, but the extra grid reduces the transparency of the system for both electrons and photons. The main advantage is that the energy resolution of the system is increased, since field penetration from the screen to the analyser (centre) grid can be drastically reduced either by strapping the third (inner) grid to the front grid (earth) or to the second grid. In these cases, the analysing potential is held just slightly positive of -V.

In this work, both types of optics were used at various times.

3.2.4 - The Electron Guns

The electron guns used in the two and three grid optics vary slightly in the details of their mechanical construction, but are similar in electrical operation. The main electrical details are as sketched in Figure 3.2.5. The final electrode A4 takes the form of a drift tube which penetrates the optics, and is held at earth potential. To obtain the necessary accelerating potentials, the centre point of the heated filament is sunk negative with respect to earth. The gun potentials are derived from a common 1kV supply by means of potential dividers. The bottom end of this supply is connected to the centre of the filament, and the supply floats about an earth defined by the slider of the potentiometer A4, connected across the supply as shown in the Figure. This potentiometer thus controls the energy of the incident electron beam. The filament supply is a fully floating d.c. supply, and the variable 5kV screen supply and the optics grid supplies are tied to the bottom end of the 1kV power supply.

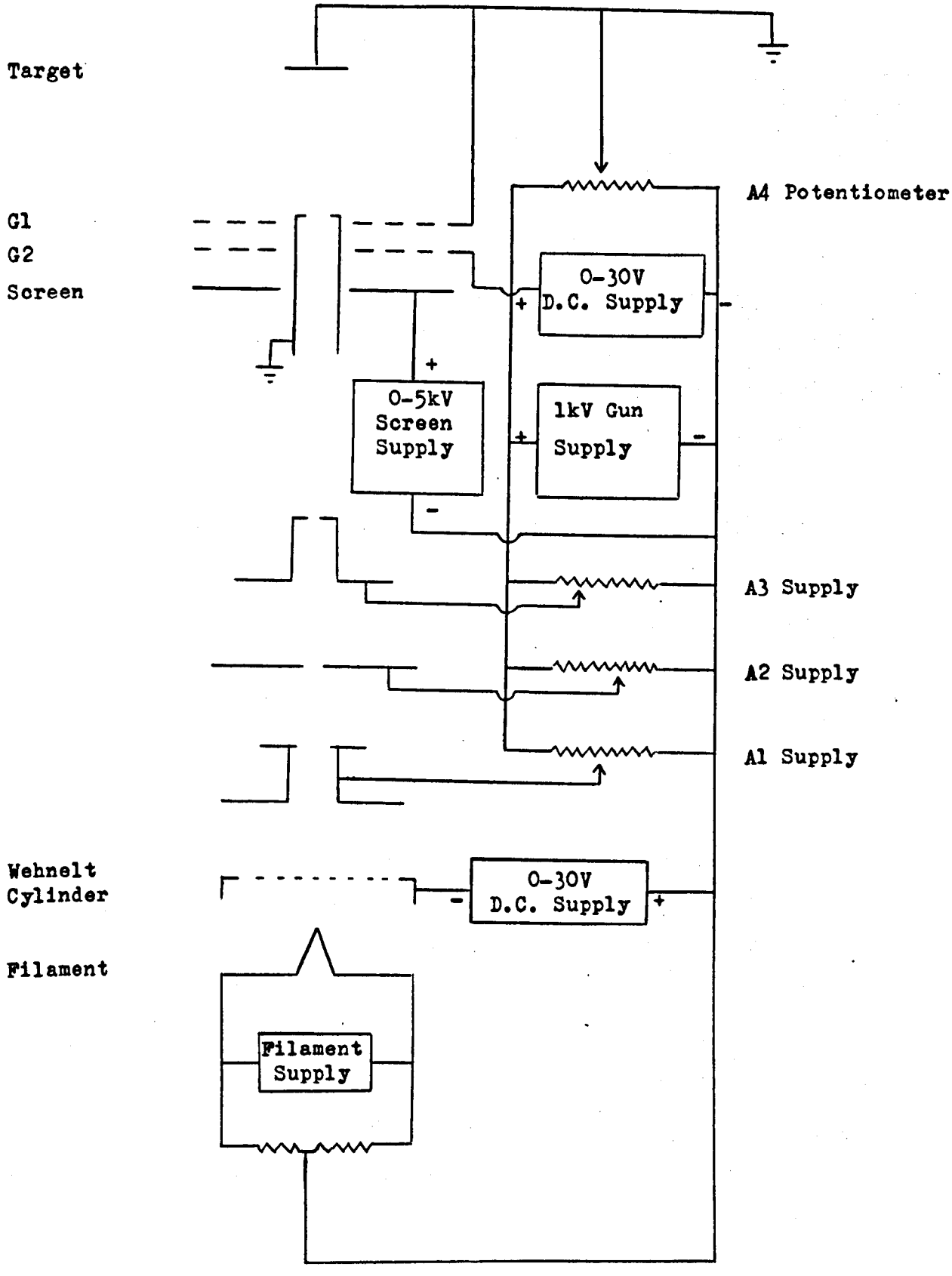

Figure 3.2-5. General arrangement of the electron gun and LEED optics (two grid optics) power supplies.

During operation of the system, problems of ripple on the filament supply and on the accelerating potential were experienced. These were eliminated by putting extra R-C smoothing in the filament supply, and connecting the common line to earth through a large ($8\mu F$) capacitor.

The beam focussing in the gun is entirely electrostatic in nature, obviating magnetic field problems. The output of the gun is approximately $1\mu A$, and is reasonably flat over the energy range 15 - 1000eV, a typical output characteristic being shown in Figure 3.2.6. Best focus conditions produce a spot of about 1mm in diameter above about 15eV, but the focussing conditions vary over the total energy range. The whole range may be reasonably covered in three steps, 15-80eV, 50-150eV and 150-1000eV with relatively constant focussing in each range. This is illustrated in Figure 3.2-7, where it is assumed that the size of the diffraction spot is beam limited.

3.2.5 - The Pumping Station

The pumping station comprises two separate complementary pumping systems, viz., a trapped mercury diffusion pumping line for roughing the system and serving the gas handling line, and an ionisation pump/sublimation pump system integral with the diffraction chamber to produce and maintain a clean UHV environment. (See Figure 3.2-8).

Initial roughing is achieved with two MSS 100 liquid nitrogen cooled zeolite sorption pumps. After a 15 minute prechill, one of these is used to 'sweep' the system down to a few mm of mercury, which it does in

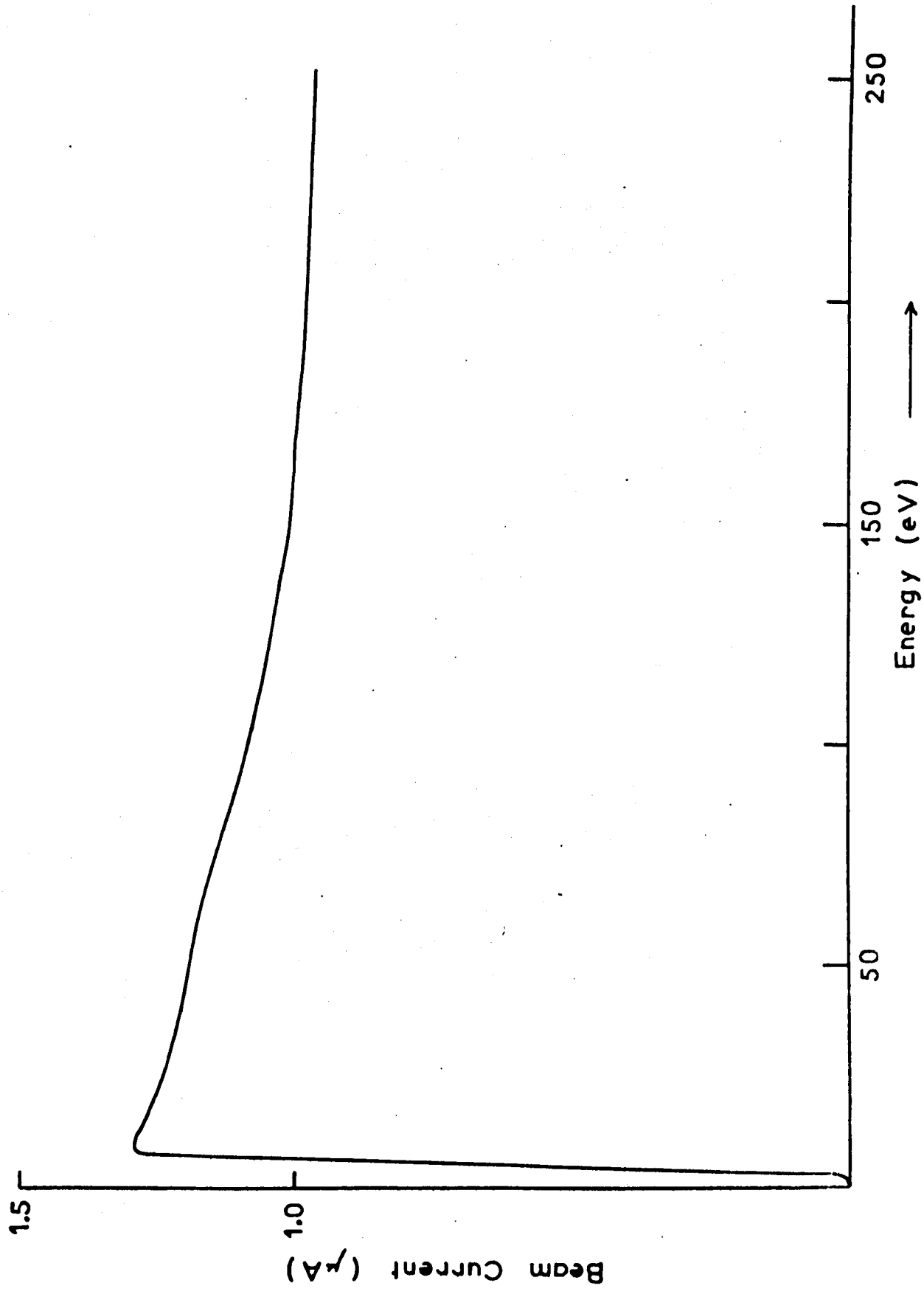

Figure 3.2-6. Output characteristic of the electron gun for a typical set of operating conditions.

(a)

(b)

(c)

Figure 3.2-7. LEED patterns from copper (100) at energies of (a) 30eV (b) 50eV and (c) 120eV to illustrate the relative beam sizes under "best focus" conditions over a range of energies. In each case, it is assumed that the size of the diffraction spots is beam limited, i.e. no diffraction broadening is ocurring. The 30eV pattern is at an angle of incidence of 10°, the others are at normal incidence.

a few minutes. This pump is then valved off, and the other pump opened up. This will usually take the system down to about 10^{-3}T. in approximately 20-30 minutes. The system is then pumped out by the liquid nitrogen trapped Edwards EM2-A mercury vapour diffusion pump, which is backed by a further MSS 100 sorption pump. In a few hours, this will take the system down to about 10^{-7}T.

The entire diffraction chamber plus ion pump well is then baked for about eight hours at 300-350°C. into the diffusion pump, allowed to cool and the mercury pump is valved off. During this bakeout, the filaments of the titanium sublimation pump are thoroughly outgassed. The Ferranti 140 ls^{-1} titanium sputter ion pump is then switched on, and the diffraction chamber is baked into this for a further 24 hours. When the system has cooled, the pressure is usually about 10^{-9}T. The 4" water cooled titanium sublimation pump is then fired for periods of two minutes at intervals of a few hours over the next twenty four hours, and all heated filaments inside the system are thoroughly outgassed. This procedure usually results in an ultimate vacuum in the low 10^{-10}T. range.

Care was always taken to ensure that the tubulation behind any valve being baked (especially the M6 leak valve to the gas handling line) was always evacuated before bakeout, to prevent oxidation of the valve seats.

3.2.6 - The Gas Handling System

The gas handling system comprises a small chamber fitted with an ionisation gauge head and bakeable Pirani gauge head, with an inlet manifold of three separately valved ports, usually occupied by a silver oxygen diffusion tube,

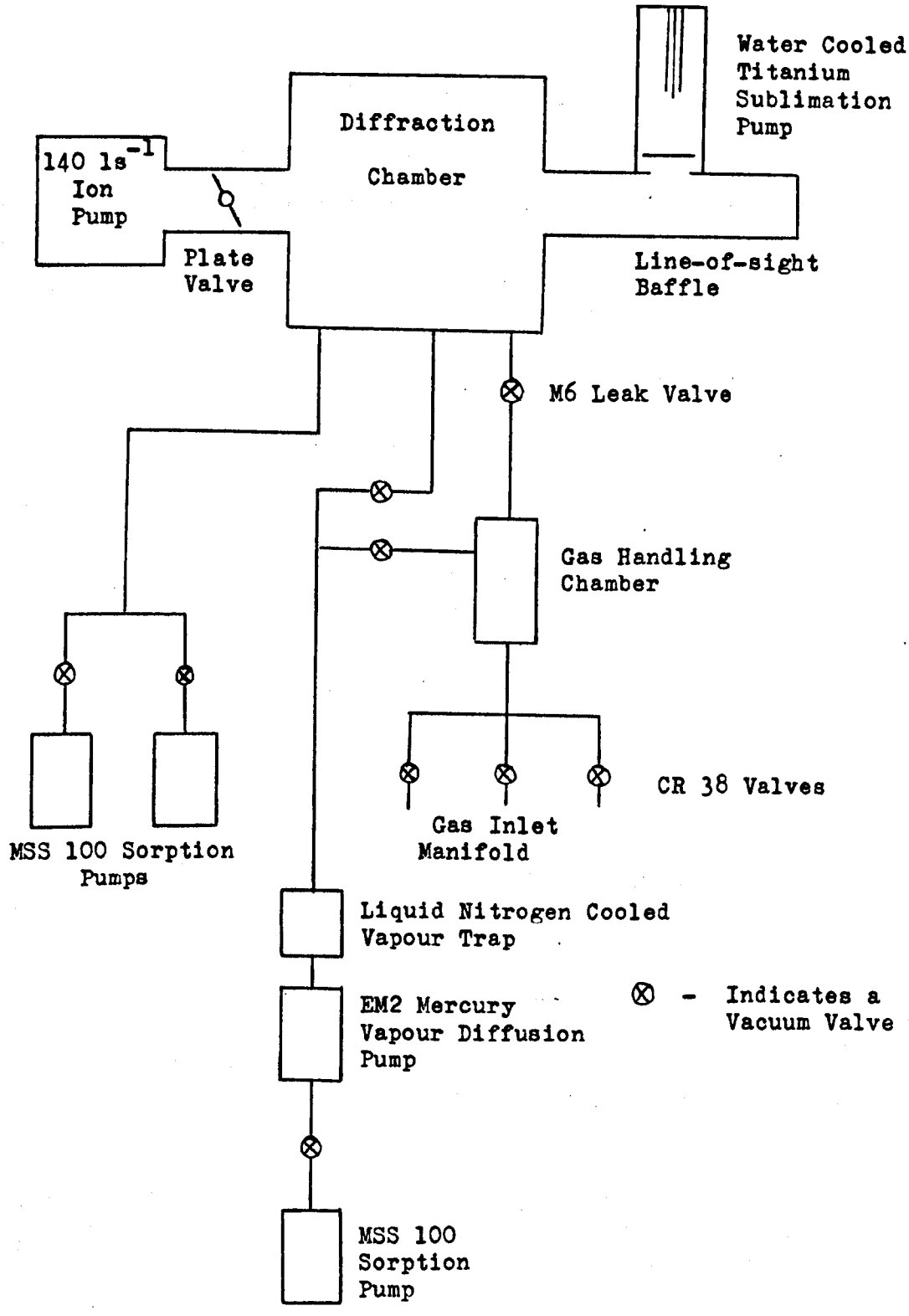

Figure 3.2-8. Schematic layout of the vacuum system and pumping station.

a palladium hydrogen diffusion tube and an argon gas bottle repectively. The chamber is connected to the main system via the M6 bakeable leak valve, and may be separately pumped with the mercury diffusion pump. It is capable of being baked into the mercury pump, and normally has an ultimate vacuum of 10^{-7}T.

3.2.7 - Magnetic Field Compensation

One of the major problems in LEED is that very small magnetic fields can cause large deflections of the slow electrons, so that, as the electron energy is varied, the incident beam scans a region of the crystal surface, with changing angle of incidence, etc.

In much early LEED work, the magnetic fields inside the chamber were cancelled out by hanging small bar magnets at strategic points around the chamber, but this is too crude to prevent small beam movements which are undesirable for accurate work.

The most satisfactory way of reducing the field inside the diffraction chamber is to screen out the earth's field and any stray magnetic fields with double-walled magnetic screening of a material such as Mumetal or Conetic AA in the manner described by Seah[5]. This however involves the use of specially selected non-magnetic materials for everything inside the screening including, for instance, glass-to-metal seals, which are most commonly made from Kovar, which is magnetic. This was obviously impracticable on an existing system, so a set of square, Helmholtz-type coils was constructed to cancel out the magnetic fields inside the chamber.

Two sets of large square coils[14] were constructed, one with the field aligned in a horizontal plane perpendicular to the gun axis, and the other in the vertical plane. Each set of coils consisted of a number of separate coils of varying numbers of turns in parallel, which could be switched in and out to vary the degree of compensation.

The coils were made large (66cm. and 84cm. square respectively) both to allow easy access to the working space inside and to give a reasonably large region of fairly homogeneous magnetic field near the centre, where the gun was situated. The coils, which were removable for bakeout, were wound from 24swg double cotton covered copper wire on an aluminium 'Handy Angle' former, and they can be seen in the photograph in Figure 3.2-1. The coils were powered by a Westinghouse Brake and Signal Co., Ltd., Westat Type WS 320 constant potential 12V power supply, rated at 26.6A.

It was decided that a sufficient criterion for compensation would be that no motion of the specular beam would occur at low energies of the incident beam, for high angles of incidence, when the incident energy was varied. In practice, if there were any insulators present in the chamber, these tended to charge up at low energies of the incident beam - tertiary emission from the grids is thought to be the source of this charge - and some deflection of the incident beam would occur. Nevertheless, using this system, the specular beam has been monitored for energies as low as 6eV - in the field free mode of operation as described in § 3.2.3 - although at this energy the beam was greatly defocussed.

Using only the two sets of coils, of course, still leaves the possibility of there being a magnetic field along the axis of the electron gun.

This would result in rotation of the diffraction pattern as the beam energy is varied. Although this was looked for, it was never seen, so that it was assumed that, perhaps fortuitously, no compensation was required in this direction.

3.3 - Measurements in Display Type LEED System

3.3.1 - Measurements of Pattern Geometry

Although in § 3.1.2 it was stated that using a spherical grid-screen system of optics gives an undistorted pattern of diffraction spots on the screen, this is only strictly true provided that the intersection of the incident beam and the surface of the specimen is at the centre of curvature of the screen, that all magnetic fields are cancelled out, and that all electrostatic fields are strictly radial. In practise, these conditions are usually obeyed accurately enough for any effects to be ignored, although some attention must be given to the position of the specimen with regard to the available fore-and-aft translation.

Nevertheless, even if these conditions are accurately obeyed, the screen is viewed from a distance which is large compared to the radius of curvature, and so the pattern appears distorted. Additionally, diffraction angles are usually calculated from photographs of patterns, where the projection of the spherical surface onto a plane introduces further distortions. The computation of diffraction angles from photographs may be carried out using a procedure similar to that described by Taylor[15], which is described in Appendix A1.

Alternatively, the screen may be 'calibrated' by taking a sequence of photographs of a given diffraction pattern at various angles of incidence, and plotting the position of the specular spot. This is the more satisfactory method if there is any doubt of the specimen not being at the centre of curvature of the screen, since it eliminates lengthy calculations.

3.3.2 - Intensity Measurements

As mentioned earlier, spot photometric measurements of anything but intensity-energy spectra of the specular beam are extremely difficult to make. Measurements on the other spots are difficult because of their motion with changing energy, necessitating movement of the photometer head to follow them, which is not easy, since one is peering at a dim screen through a tiny eyepiece and only a small fraction of the light incident on the photometer optics is passed to the eyepiece. The photomultiplier tube only accepts light from a small solid angle, the periphery of which is delineated by a dark circle in the centre of the field of view of the telescope. Thus if one has a "good" LEED pattern, i.e. one consisting of bright spots on a dark background, it is often impossible to see the sighting ring against the background.

Nevertheless, the spot photometer is the only convenient way of measuring intensities in a display type LEED system.

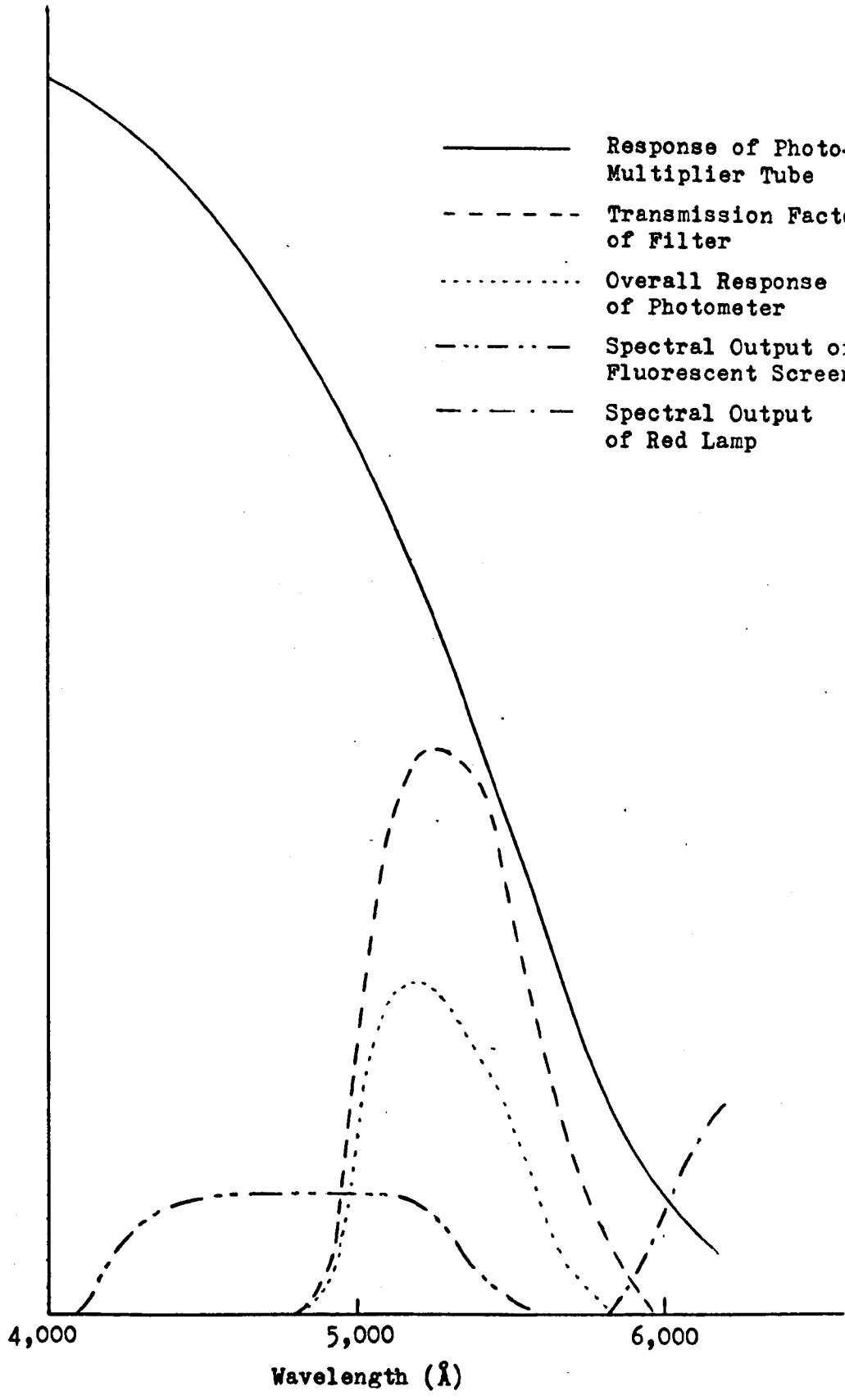

Figure 3.3-1. Comparison of the relative spectral responses of the photometer system and the spectral outputs of the fluorescent screen and the red lamp used for working illumination.

3.3.3. - The Spot Photometer

The spot photometer used was a Hollywood Photo Research Corporation Type SB¼, with an acceptance angle of ¼°. When in use it was mounted on a standard heavy photographic tripod, with full raise, pan and tilt facilities. To supplement these, a horizontal traverse with a screw controlled drive was fitted. In place of one of the standard range of filters incorporated in the photometer head, an Ilford Type 408 Narrow Cut Tricolour Green gelatin filter was fitted. Figure 3.3-1 shows the quoted spectral response of the photomultiplier tube (RCA Type 931A, S4 characteristic), the transmission properties of the filter, and the spectral output of the light from the fluorescent screen of the LEED set. This latter was measured using a simple prism spectrometer. The overall response of the system to red light is thus seen to be rather low, and this enabled work to be carried out under a relatively bright red light.

The angular resolution of the spot photometer was also measured by traversing the photometer across three narrow, equally spaced illuminated slits at various distances from the head. The results of such traverses are shown in Figure 3.3-2. These give an angular resolution of 16.5 ± 1.5 minutes of arc, which is comparable to the angular width of LEED beams. This made it impossible to measure k-space profiles of LEED beams with this photometer.

It was found that when working with the low level light intensities available in this work, the overall noise level in the photometer was too high to be tolerated. A large amount of ripple at 50Hz (about 10%) was found on the H.T. line to the photomultiplier tube dynode chain, and by incorporating extra R-C smoothing, this was cut to about 1%. Even this

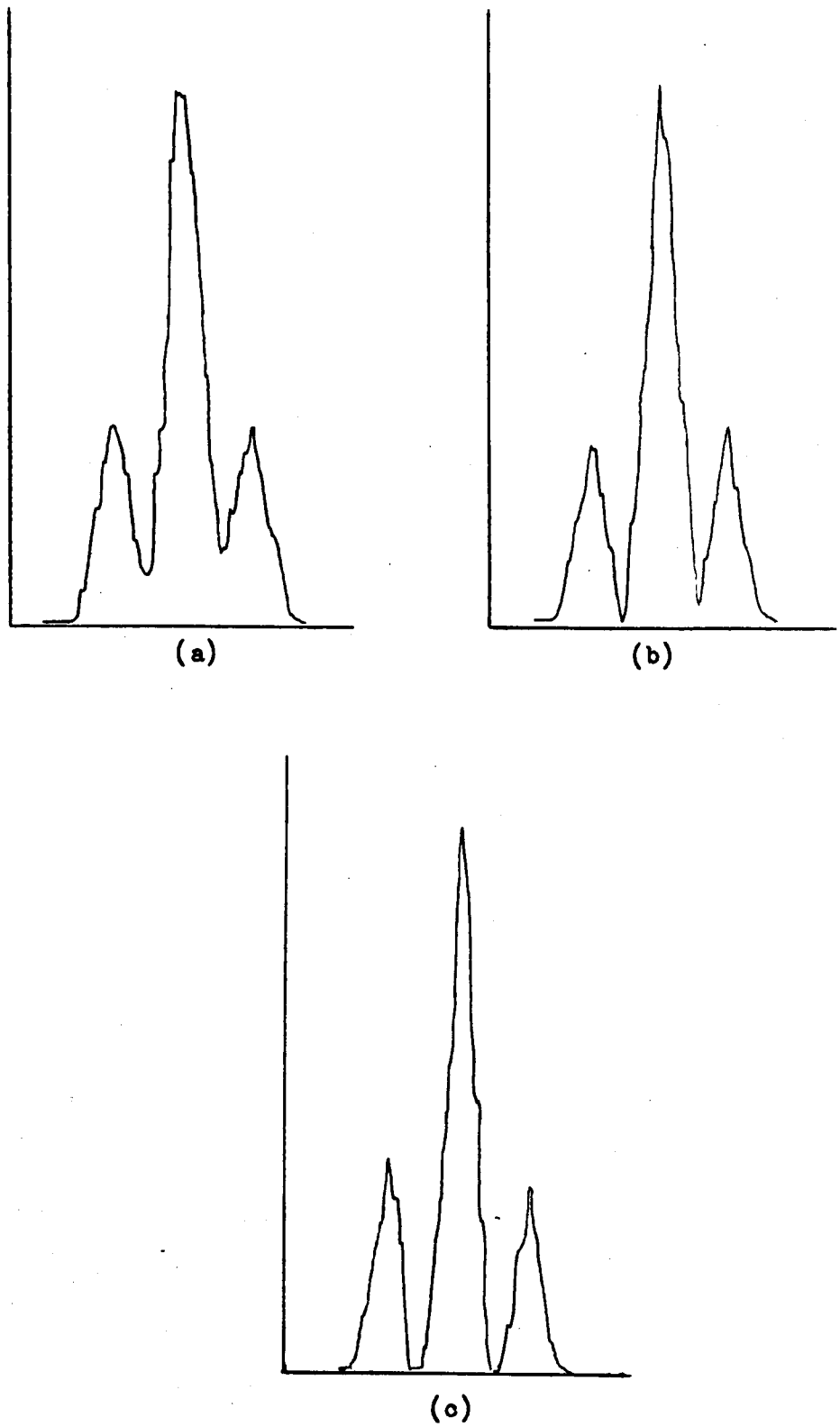

Figure 3.3-2. Determination of the angular resolution of the spot photometer. The photometer was traversed across three unequally illuminated slits each of width 5mm and separated by 5mm at distances of (a) 39inches (b) 40inches and (c) 41inches. The 5mm gap between the slits was just resolved at 40", so this gives a measure of the angular resolution of the instrument.

amount of ripple caused undue levels of noise, so the photomultiplier power supply was replaced by an AERE Type 1359A variable H.T. Power Supply, manufactured by General Radiological, Ltd., of London.

The internal amplifier in the photometer head was also disconnected because it was too noisy, and the output of the photomultiplier tube fed directly to the input head of a Keithley Model 417 fast picoammeter by a short piece of low noise coaxial cable.

These procedures reduced the overall noise levels to more manageable proportions, and what was left could generally be removed by using the variable response time facility on the Keithley. Calculations in fact showed the residual noise levels to be not greatly in excess of the shot noise level of the photomultiplier tube. Further reduction of the noise level might be effected by cooling the photomultiplier tube, but this was not deemed practicable, nor really necessary.

A possible way of improving the sensitivity of the system by reducing the noise levels might be to apply a series of blanking pulses to the suppressor grid at a moderate frequency, and to detect the photomultiplier signal with a phase sensitive detector[16]. Phase sensitive detection is a standard technique in Auger electron analysis spectroscopy, and might prove worthwhile in this case, but could not be attempted in this system.

3.3.4 - The Inherent Problem of Spot Photometry

There are many problems inherent in the spot photometric technique for measuring LEED beam intensities. That of noise has been discussed in

the previous section, and some of the physical difficulties of using the instrument were discussed earlier. Other problems of an equally fundamental nature remain.

The essentials of the LEED system are sketched in block diagram form in Figure 3.3-3. The portion of the process within dotted lines is that part peculiar to the display type apparatus. The last two operations in this part - i.e. those within the photomultiplier tube - are efficient and reasonably well behaved. The other two operations are those open to fundamental objections.

It is extremely difficult to produce a stable phosphor of large area with uniform properties, and so one cannot be absolutely certain that variations in the intensity of a diffraction spot as it moves across the screen are not in some part due to variations in the quantum efficiency of the conversion process.

One also has to assume linearity in the response of the phosphor. It is unlikely, however, that the range of intensities with which we are dealing in LEED will either cause saturation at one end of the scale, or produce enough light to be visible when the response tails off at the bottom end of the scale.

We therefore ignore effects due to these processes, except, of course, in the case of gross defects in the phosphor which are visible to the naked eye.

In the LEED optics, we have a spherical grid situated about 2mm from a spherical screen with a large electric field between them. This

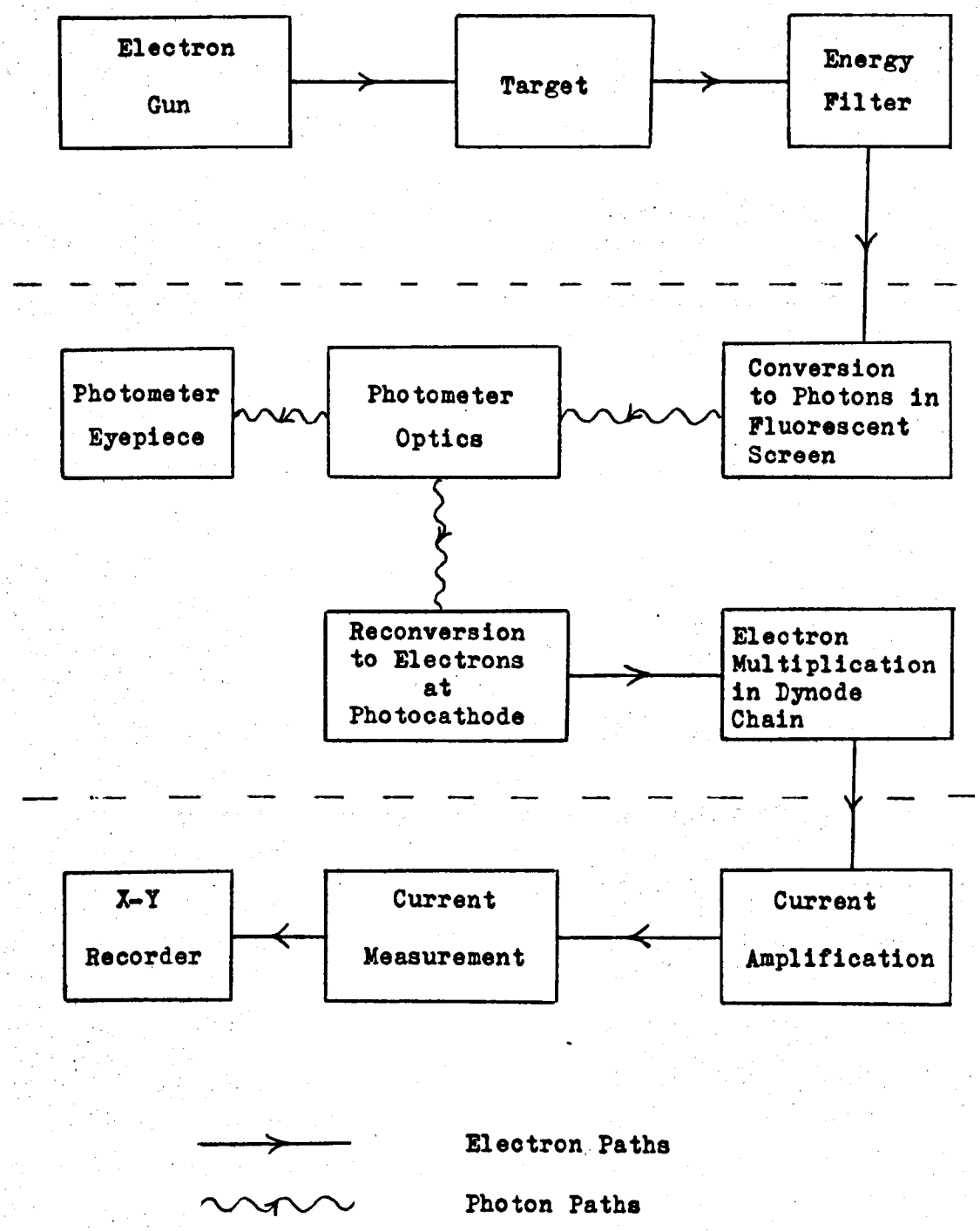

Figure 3.3-3. Block diagram of the processes in a display type LEED apparatus, with photometric measurement of diffraction intensities.

potential gradient is sufficient to cause field emission from any 'spiky' defects in the mesh of the grid, and these can give rise to quite bright spots of light on the fluorescent screen. These must, if at all possible, be avoided when making measurements of low light intensities.

The grids cause problems in themselves. Although they are about 80-90% transparent at normal incidence, at oblique viewing angles, this transparency falls off. This can be minimised by keeping the optical axis of the spot photometer as nearly normal to the grids as possible, but this is not always possible, especially when using a reasonably long focus spot photometer at high diffraction angles. Further, one often sees Moiré fringes[17] due to optical interference between the grids, and these can give rise to spurious effects.

3.3.5 - The Recording of Results

Diffraction patterns were photographed directly onto 35 mm film with a camera held directly in front of the diffraction chamber viewing port. With Ilford HPX film stock, exposures of 12 seconds at f/4 were generally found to be adequate.

The intensity-energy spectra were recorded continuously on an X-Y recorder, usually a Bryans Series 26000 A3 Metric, by plotting the output of the Keithley electrometer on one axis and the accelerating potential on the other.

Energy changes of the incident beam were effected by driving a ten-turn potentiometer directly with a friction wheel attached to a synchronous

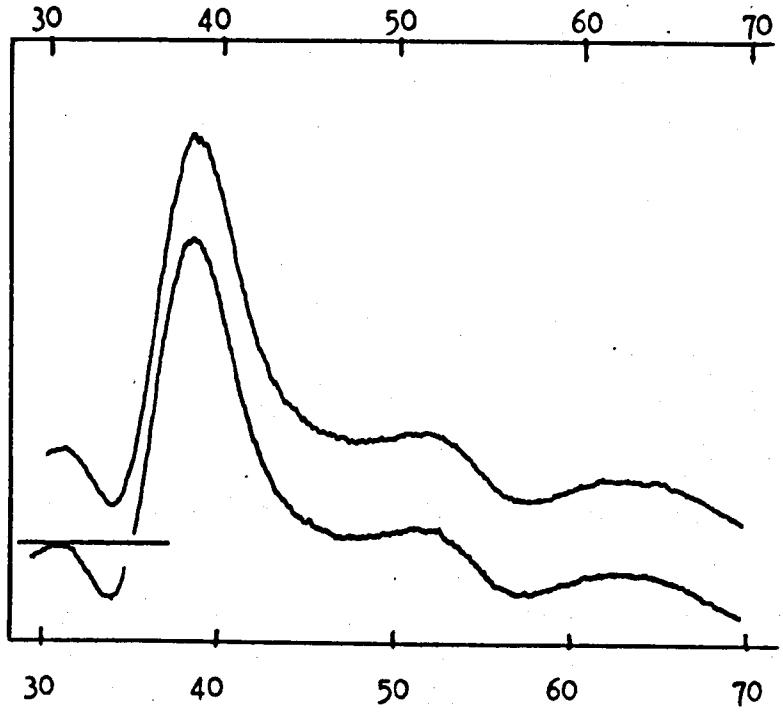

(a) Total scan time = 40secs.

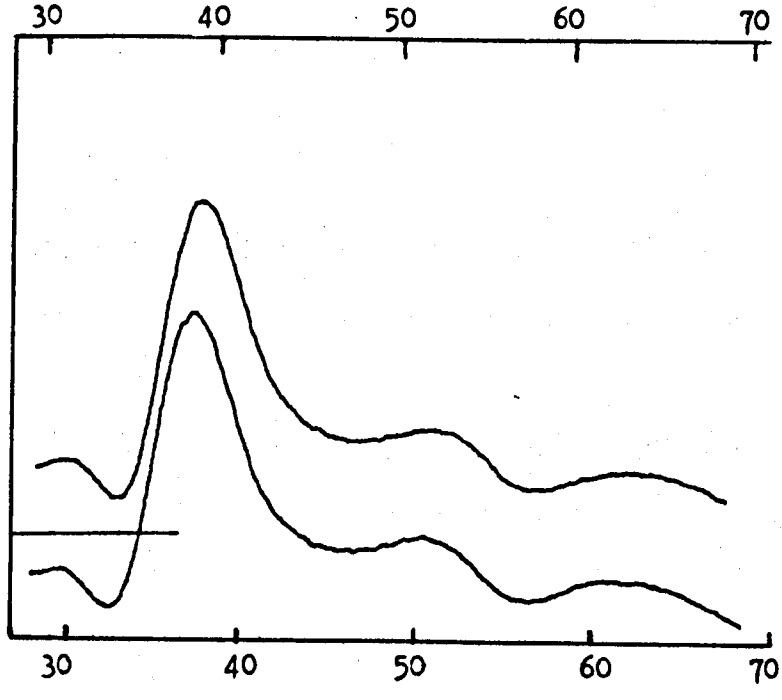

(b) Total scan time = 14.5secs.

Figure 3.3-4. The effect of decreasing the scan time across a given intensity-energy spectrum is to cause hysteresis between scans taken with increasing energy (upper trace and energy scale in each panel) and those taken with decreasing energy (lower trace and scale)

motor fitted with a 1:750 reduction gear box. This gave a scanning speed of the order of 1eV s^{-1}, suitable for the rather low overall response speed of the system. The use of a faster energy scan results in marked hysteresis between scans taken with increasing and decreasing energies (See Figure 3.3-4). The response time of the system is limited by the time constant of the smoothing capacitor used to reduce the ripple in the LEED optics, connected between the negative end of the A4 potentiometer and ground (§ 3.2.4), and to a certain extent by the variable response time setting on the Keithley.

3.4 - Initial Specimen Preparation and Cleaning

3.4.1 - Single Crystal Specimens

Single crystal copper rods 12mm in diameter and of nominal 99.999% purity were purchased from Metals Research, Ltd., of Cambridge.

Short lengths of this rod were sawn from the bar using an acid string saw of the type described by Simmons[18], although Terylene thread was used rather than stainless steel wire. The cutting solution used was nine parts of concentrated nitric acid to one part of water. With this arrangement, however, it was not possible to produce a smooth, accurate surface. The specimens were mounted on a special goniometer rig which was interchangeable between a Philips X-ray Laue camera, a Metals Research Corporation Servomet spark machiner, the string saw and an acid polishing wheel.

The specimens were oriented to within 1° of the desired orientation by

X-ray Laue back diffraction, and polished to this orientation on an acid wheel using the technique described by Simmons[18], the polishing solution being concentrated hydrochloric acid saturated with cuprous chloride. Cuprous ions were regenerated in the solution by 'topping up' periodically with twenty volume hydrogen peroxide. After polishing was completed, the crystal was washed in concentrated HCl and distilled water.

After the acid wheel polish was completed, the orientation was checked in the Laue camera, and any small corrections made - again to within 1°. A slice about 1mm thick was then machined off on the spark machiner, using a low cutting speed to minimise the depth of penetration of damage from the (back) surface of the specimen. That no significant damage was introduced into the crystal during these processes was inferred from the absence of any major recrystallisation induced by the later annealing cycles.

The slice was then fixed onto a Tufnol or Teflon rod with Durofix, and the surface polished by hand on a flat bed polisher of the type described by Mitchell *et al*[19], using the same polishing solution as on the acid wheel. The surface was carefully monitored by optical microscopy until the best surface was obtained.

Further smoothing of the surface was achieved by polishing in a bath of warm (60°C) solution of 20% concentrated nitric acid (S.G. 1.82), 55% orthophosphoric acid (S.G. 1.75) and 25% glacial acetic acid[20]. Again this polish was administered in small 'doses' and the surface monitored by optical microscopy.

The final surface was obtained by electropolishing on a Shandon 6500 electropolisher, using as electrolyte 40% orthophosphoric acid (S.G. 1.75), 40% Industrial Methylated Spirits and 20% water. Best polishing conditions were found by trial and error, once more using optical microscopy as a monitor. This treatment resulted in a surface which, while not completely flat, having a slight 'orange peel' finish, was reasonably smooth and only lightly pitted. Annealing in the UHV environment of the LEED system removed many of these irregularities.

Immediately after each stage, the specimen was washed in distilled water, and just prior to insertion into the specimen holder of the LEED set was washed in distilled water, acetone and alcohol, and dried in a hot air blast.

Figure 3.4-1 shows various stages of surface polish.

3.4.2 - Foil Specimens

In part of the work described in this thesis, faceted specimens of copper foil were used. These were prepared by annealing pieces of Analar quality (99.9% pure) copper foil in an oil diffusion pumped silica tube vacuum furnace. Pressures of the order of 10^{-6}T. were used, and the foil was enclosed in a Purox (recrystallised alumina) boat with a copper foil lid.

Widely varying anneal times and temperatures were used to produce varying degrees of faceting and sizes of facet, but a typical anneal schedule might be one day at 1000°C., followed by two days at 800°C. and then

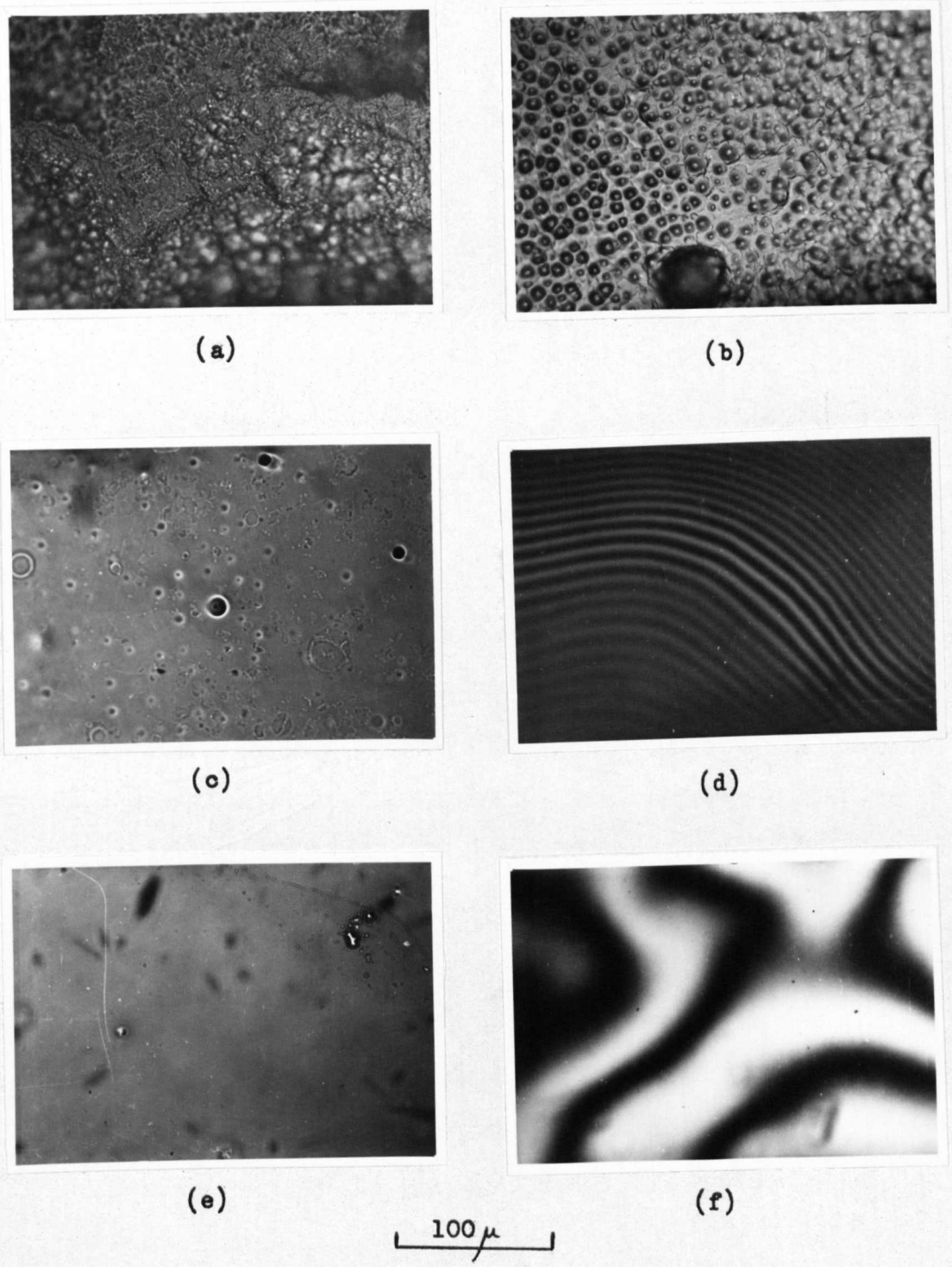

Figure 3.4-1. States of polish of the specimen surface at various stages of the polishing treatment.

(a) After flat-bed polish
(b) After chemical polish
(c) After 20 min. electropolish
(d) Interferogram of stage (c)
(e) After further 35 min. electropolish - final surface
(f) Interferogram of final surface

quenched to room temperature. Fuller details regarding the formation of simple linear facets may be found in the literature[21,22].

No cleaning techniques - other than bakeout - were used in the LEED system for these foil specimens.

3.5 - In Situ Operations on the Specimens

3.5.1 - Specimen Heating

In this study, it was felt to be desirable to heat the specimens by some means which would allow observation of the LEED patterns during the heating cycles. This ruled out electron bombardment heating and infra-red heating through the viewing port. A small radiative heating oven was therefore constructed. Details may be seen in Figures 3.5-1 and 2. The nature of the heater winding, however, meant that when current was flowing through the heater, a residual magnetic field aligned along the axis of the electron gun was present. This caused some distortion of the pattern, but this was not too important for visual monitoring purposes.

A cylindrical Purox crucible was used as the body of the oven, and a narrow slot was cut as near the open end of the crucible as possible, to take the specimen. The slot was made deep enough for the specimen to fill the opening at the front completely. The specimen was held in position by small pieces of Analar copper foil wedged behind it. Into one of these pieces of copper foil was spot welded a chromel-alumel (T1-T2) thermocouple. (See Figure 3.5-2).

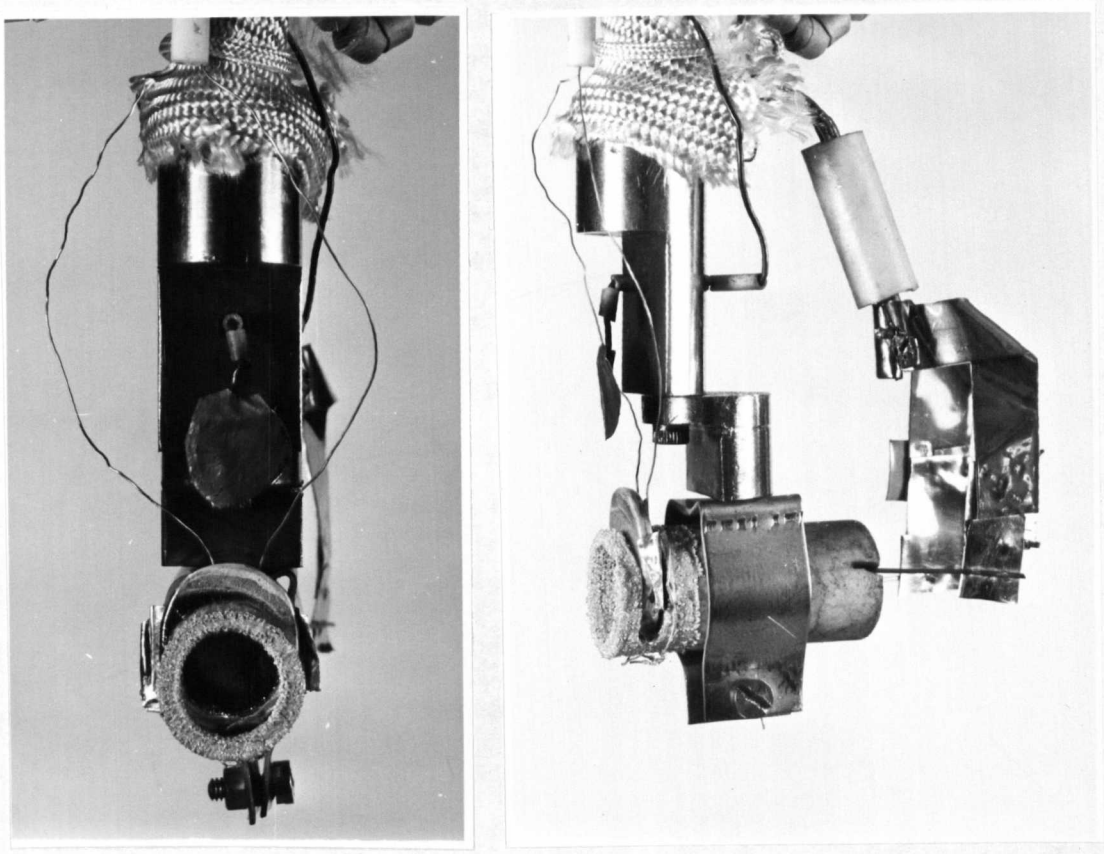

Figure 3.5-1. The special hot stage used in these studies. Details of the conducting coating of electro-deposited copper which can be clearly seen at the front of the oven are given in Figure 3.5-2. Also visible is the thermocouple spot-welded into a piece of copper foil wedged behind the specimen. The flat disc above the specimen is a soot-covered piece of Ferry sheet, used as a simple Faraday cup for measurement of the incident beam intensity.

The heater coil was wound from 200 micron (35swg) tungsten wire, and was placed in the crucible behind the specimen. Current leads of Ferry tape were spot welded to the ends of the coil and these were joined to heavy copper wire leads inside Purox insulator tubes, strapped to the specimen manipulator rod, as may be seen in the photograph (Figure 3.5-1).

If no precautions are taken, the Purox will of course charge up under the influence of the direct electron beam, or one of the tertiary electrons produced at the first grid of the electron optics by the backscattered primary or secondary electrons.

The first method used to overcome this charging was to coat the whole crucible with a thin film of tin oxide. This was performed in the manner described by Seah[5] after Gomer[23], giving a film of resistivity a few ohms per square, which was high enough to avoid short circuiting the heater winding, but low enough to eliminate the charging problem very successfully. However, it was found that at quite modest temperatures, the tin became mobile and diffused across the surface of the copper, forming a surface alloy which gave rise to very complicated diffraction patterns. Further, after many argon ion bombardments the coating lost its continuity and further charging occurred.

Primarily to obviate the problem of foreign atom diffusion contamination, it was decided to cover the Purox with a layer of copper. Firstly, several layers of Liquid Bright Platinum (Johnson Matthey Chemicals, Ltd.) were burned into the surface of the Purox with a high temperature oxygen-natural gas flame, to give a mechanically bound, electrically continuous conducting layer over the front of the oven (see Figure 3.5-2 for details).

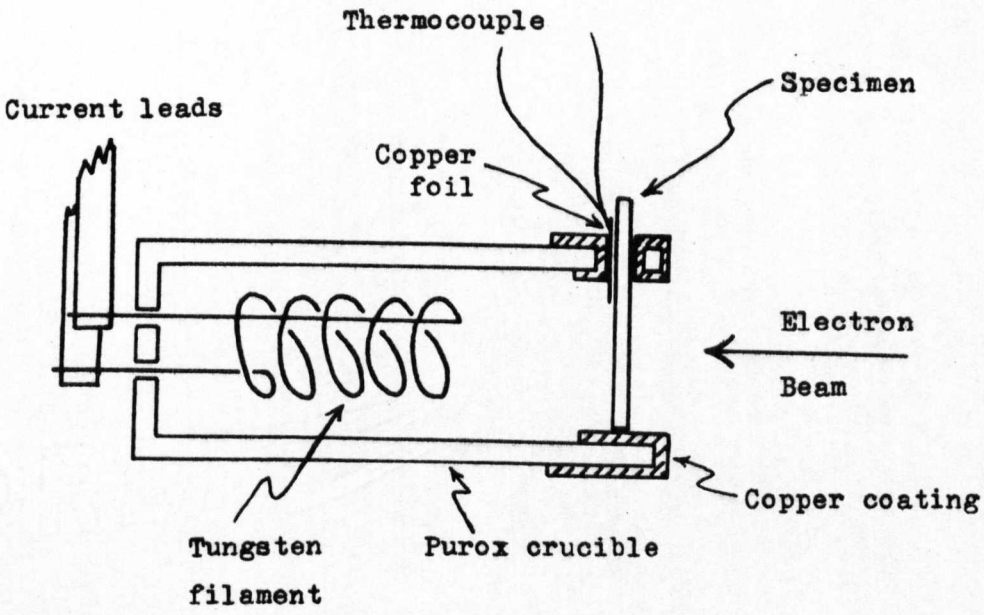

(a) Section through specimen heater.

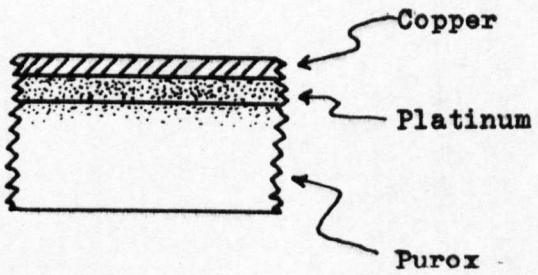

(b) Details of conductive coating.

Figure 3.5-2. The special hot stage used in these studies. The conductive coating of copper over the front of the Purox crucible is to prevent the charging up of the Purox by the electron beam.

A thin copper wire was bound tightly over the coated part of the tube and covered with Liquid Bright Platinum which was reduced to metallic platinum in a low temperature flame. Using this wire as a contact, a thickish layer of copper was then slowly electrodeposited onto the platinum in a copper-copper sulphate electrolytic cell, all materials being of Analar grade.

The oven was then annealed in a silica tube vacuum furnace at 850°C. and 10^{-5}T. for two hours. A further electrodeposit of copper was plated on top of the first layer, and the oven annealed under the same conditions as above for a further fifteen hours.

This resulted in a very low resistance, electrically continuous film of copper, very well keyed into the Purox, although some 'balling up' of the copper film occurred during the anneals. A little copper had been vapour deposited onto the uncoated Purox during the anneals, but this did not form an electrically continuous film. This oven has performed very successfully in UHV throughout many annealing and argon bombardment cycles, with no recurrence of charging, and no outgassing problems.

In the LEED set, the copper film could be earthed either through the embedded copper wire, or through the specimen thermocouple - the specimen made good contact with the film simply by mechanical pressure.

With this oven, temperatures approaching 1000°C. are readily attainable.

3.5.2 - Argon Ion Bombardment

In situ cleaning of the specimens were performed using alternate argon ion bombardment and annealing cycles [24].

The beam of argon ionsis produced in a gun of conventional design. The original gun as supplied by Vacuum Generators was mounted on a small eight-way feed through, which necessitated the leads being fairly close together. When the filament got hot, it tended to sag and would short out to one of the grids. By constructing a gun of similar design on a Ferranti eight-way feed through, where all the pins are led through separate insulators, all the leads could be further apart, and this obviated the problem. This gun has performed satisfactorily throughout many cycles.

In use the gun is run in an atmosphere of 10^{-4}T. of argon, and gives a beam current of approximately 0.8μA. at 500eV, with a beam diameter at the specimen such that the area bombarded is about $1cm^2$.

With this particular vacuum system, it was not possible to isolate the ion pump from the diffraction chamber, so during argon ion bombardment, the pump had to be switched off. This leads to a certain amount of regurgitation of CO, CH_4, etc. A typical mass spectrum of such regurgitation is shown in Figure 3.5-3. The procedure for admitting argon gas to the main system was therefore as follows. The gas handling system, which had previously been baked and only exposed to an argon atmosphere since the bakeout, was evacuated to 10^{-7}T. with the mercury diffusion pump. Argon gas (British Oxygen Company Argon Gas, Grade X) of high purity was bled into the gas handling line to a pressure of 10^{-2}T.

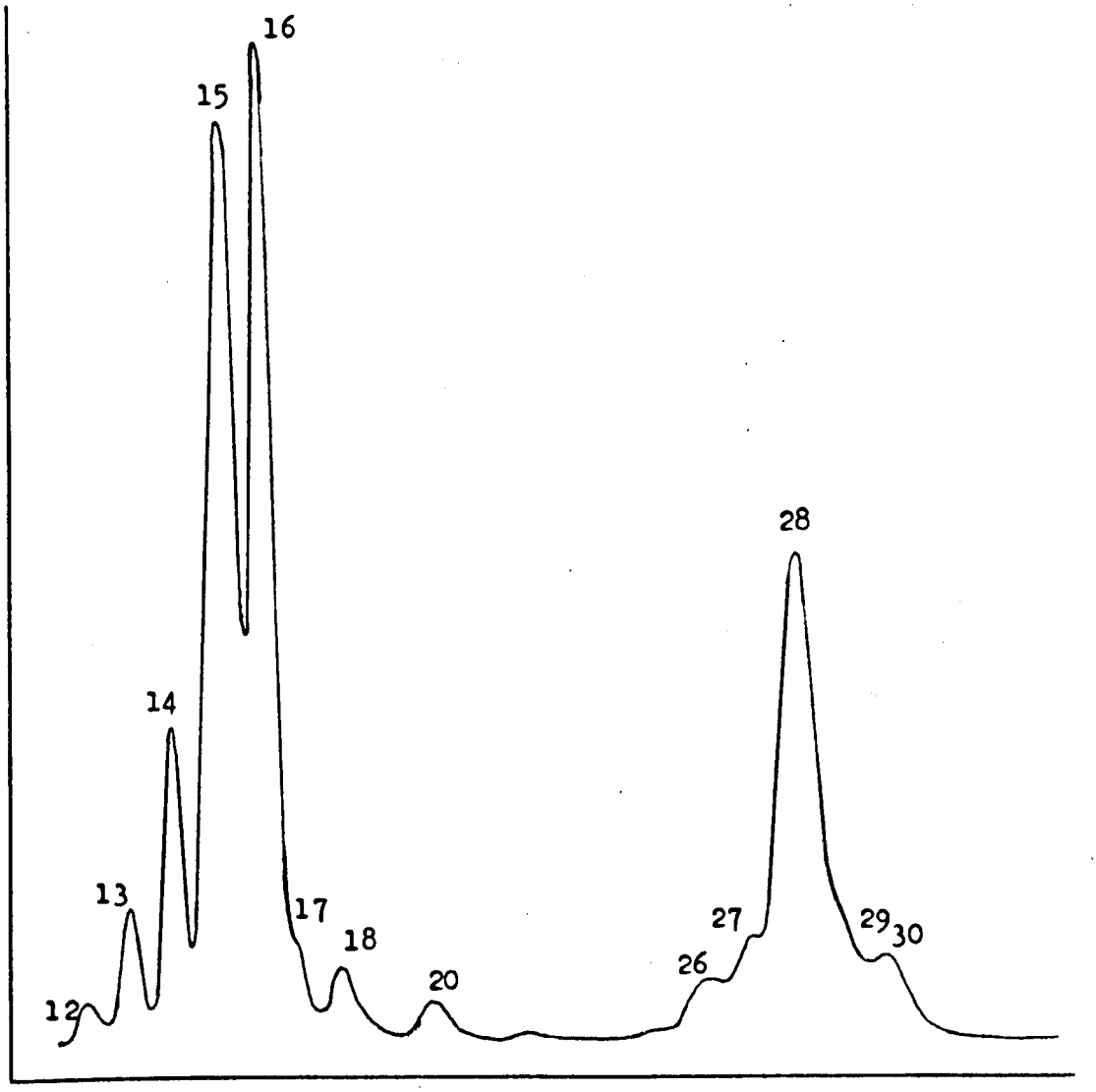

Figure 3.5-3. Typical mass spectrum of the residual gas in the vacuum system resulting from the regurgitation of gases by the ion pump when it is switched off.

from a one litre glass bottle. The bleed rate was controlled by carefully cracking open the CR 38 valve between the bottle and the gas line (see Figure 3.2-8). This valve was then closed, and this fill of argon pumped away. Argon was then readmitted to the gas handling line to the same pressure as above. In this way any small quantities of gaseous impurities released by the admission of the first fill of argon gas would be swept away. The sublimation pump in the main chamber was fired for two minutes, and the M6 leak valve cracked open. As soon as argon gas began to bleed into the main system, the ion pump - whose pumping line had been throttled by the plate valve - was switched off. The argon was then allowed to bleed into the main chamber fairly quickly, until the pressure reached 10^{-4}T. The argon ion gun, which had previously been well outgassed in UHV, was switched on and the crystal turned to face the aperture of the gun.

When the bombardment had finished, the argon was quickly evacuated from the chamber with the diffusion pump, the sublimation pump was fired again and the ion pump switched on. Using this procedure, pressures of a few times 10^{-10}T. could be consistently attained a few minutes after the end of the bombardment.

3.5.3 - Cleaning Procedures

Single crystal slices of copper, oriented to all three low index faces were subjected to the same cleaning procedure. Typically, this would involve annealing the specimen at 400°C. for about 24 hours, argon ion bombardment for 5 hours, annealing at 600°C. for 12 hours, repeating these two stages and then cycling argon ion bombardments of half an hour

and anneals at 600°C. for half an hour until, firstly, only "clean" diffraction spots were visible, and secondly, until the low energy (i.e. 20-100eV) intensity-energy spectrum was unchanged by a further cycle. This portion of the spectrum was apparently the part most susceptible to change by contamination in the ranges of energy available. The specimen was then flashed to 850°C., cooled, and the whole procedure repeated, if necessary, until a stable intensity-energy spectrum resulted. This is closely similar to the technique of Andersson[25] for cleaning copper. He also made use of Energy Analysis of the scattered electrons as a monitor of cleanliness, but such facilities were not available to us for the greater portion of this work. . We therefore assume the rather less satisfactory criterion of stability of the intensity-energy spectrum as being an adequate one for cleanliness.

REFERENCES

1) C.J. Davisson and L.H. Germer, Phys.Rev. 30 (1927), 705.

2) E.D. Scheibner, L.H. Germer and C.D. Hartmann, Rev.Sci.Instrum. 31 (1960), 112.

3) L.H. Germer and C.D. Hartman, Rev.Sci.Instrum. 31 (1960), 784.

4) W.H. Ehrenberg, Phil.Mag. 18 (1934), 878.

5) M.P. Seah, Thesis, University of Bristol (1969).

6) See e.g. H.E. Farnsworth, 'Surface Chemistry of Metals and Semiconductors' (Wiley, New York, 1959), p. 21.

7) C.W. Tucker, Jr., J.Appl.Phys. 35 (1964), 1897.

8) K. Fujiwara, K. Hayakawa and S. Miyake, Jap.J.Appl.Phys. 5 (1966), 295.

9) See e.g. E.R. Jones, Thesis, University of Wisconsin (1965).

10) M.P. Seah and A.J. Forty, J.Phys.E, 3 (1970), 833.

11) Perkin-Elmer Corp., Palo Alto, Calif., Model 100 Analytical LEED Microscope.

12) Vacuum Generators, Ltd., East Grinstead, Sussex.

13) P.W. Palmberg and T.N. Rhodin, J.Appl.Phys. 39 (1968), 2425.

14) A.H. Firester, Rev.Sci.Instrum. 37 (1966), 1264.

15) N.J. Taylor, Varian Ass., Palo Alto, Calif., Technical Leaflet VR-29.

16) P.C.G. Danby, Electronic Engng. 42 (1970), No.1, p.36.

17) R.W. Ditchburn, 'Light' (Blackie, London and Glasgow, 1963), p. 176.

18) G.W. Simmons, Thesis, University of Virginia (1967), published as U.S.At.Energy Comm. Report No. ORO-3109-5.

19) J.W. Mithcell, J.C. Chevrier, B.J. Hockey and J.P. Monaghan, Can.J.Phys. 45 (1967), 453.

20) W.J.McG. Tegart, 'The Electrolytic and Chemical Polishing of Metals' (Pergamon, London, 1959), p. 100.

21) A.J.W. Moore, Acta Metall. 12 (1958), 293.

--- , 'Metal Surfaces: Structure, Energetics and Kinetics' (American Society for Metals, Ohio, 1963), 155.

22) W.M. Robertson, Acta Metall. 12 (1964), 241.

23) R. Gomer, Rev.Sci.Instrum. 24 (1953), 993.

24) H.E. Farnsworth, R.E. Schlier, T.H. George and R.M. Burger, J.Appl.Phys. 26 (1955), 252.

25) S. Andersson, Surface Science 18 (1969), 325.

CHAPTER 4

LEED AND SURFACE PERFECTION

4.1 - Introduction

The work reported in this Chapter was performed as a preliminary exercise to the main corpus of work reported in this thesis. It comprises a brief study of some of the conditions required for production of a "good" LEED pattern, i.e. a pattern of sharp, intense diffraction spots superimposed on a low background intensity at room temperatures.

The primary object of the experimental work (§ 4.5) is an attempt to define the area of crystal surface required to produce a "good" pattern. This work has been briefly reported in the literature[1,2].

4.2 - The Concept of Coherence

The concept of coherence is applicable to any physical waveform, but for simplicity we will discuss the concept for the special case of electromagnetic waves and then show how this may be carried over to the case of matter waves.

When any two waveforms interfere, the parameter which determines the nature of the interference is the phase difference between the two waveforms. In most experimental cases of interference phenomena, the two waveforms are derived from the same physical source, and therefore the phase difference

is determined by the optical path difference between the two interfering waveforms (i.e. the difference in distance between source and detector for each waveform). Experimentally, however, it is found that there is a finite limit to the optical path difference which can be used in practice.

This limit is known as the coherence length of the waveform, and may be simply understood as detailed below for the case of an electromagnetic wave. Electromagnetic waves are spontaneously emitted when an excited system de-excites. In general, the energy levels of the system from which, and to which, it decays have a finite width, i.e. spread of energies. Thus the emitted wave will have an energy which is uncertain by the amount ΔE, where ΔE is the sum of the widths of the energy levels of the excited and de-excited states. This is a fundamental uncertainty, and ignores line broadening introduced by the physical state of the system, such as pressure broadening and Doppler broadening. Corresponding to the energy uncertainty, there is the associated momentum uncertainty, Δp. The coherence length Δx is then defined as the associated uncertainty in position derived from the Heisenberg Uncertainty Principle

$$\Delta p_x \Delta x \gtrsim \hbar \qquad (4.2 - 1)$$

where Δp_x is the uncertainty in momentum of the x-component of the wave.

In addition to the coherence length determined by the energy uncertainty, there can be defined a coherence width Δy due to the uncertainty in the momentum of the wave transverse to the direction of propogation of the wave caused by the angular spread of the beam - any waveform in the form of a beam emitted by a finite aperture has an inherent angular spread - even

for perfectly monochromatic radiation. Again,

$$\Delta p_y \Delta y \gtrsim \hbar \qquad (4.2 - 2)$$

Of course, in any real situation, the Δp in each case (longitudinal or transverse) will contain an element of the uncertainty in the other component, so that, for a real beam, the total momentum spread along the axis of propogation will be determined by the total spread in components of momentum along that axis, and similarly for the momentum perpendicular to that axis.

The coherence length Δx and the coherence width Δy are usually distinguished by being referred to as temporal (or time) coherence and spatial coherence respectively.

(Note that cylindrical symmetry about the direction of the axis of propogation has been assumed, so that there is only one coherence width. If this were not the case, e.g. if we had an asymmetrical source such as a rectangle, there would be different coherence widths in different directions transverse to the axis).

In essence, the coherence length determines the length of the wave train of the emitted radiation (i.e. the "length" of the photon) and the coherence width determines its divergence (i.e. the "breadth" of the photon, or the area of its wavefront at any point).

When we come to consider particulate interference, it is convenient to consider the particles as wave packets whose "length" is determined by the time coherence length associated with the uncertainty in energy of each particle, and whose "width" is determined by the spatial coherence width

associated with the uncertainty in the direction of propogation of the particles.

In particular, we consider the interaction of a beam of particles with a lattice of scatterers in such a way as to produce a diffraction pattern. Firstly it is important to observe that it is not the interference of one particle with another after each has been scattered by the lattice that produces the diffraction pattern, but that the interaction of each particle individually with the lattice produces its own diffraction pattern. The observed pattern is the summation of all these individual patterns. In other words, the diffraction is not a steady state process, but a summation over transient processes.

Secondly, subject to the qualifications introduced by the "mixing" of uncertainties mentioned above, for a beam of particles at normal incidence on a planar array of scatterers, the time coherence places no limitation on the diffraction process, provided that

$$\Delta x > \Delta y \cos\theta \qquad (4.2 - 3)$$

where θ is the angle between incident and diffracted beams, but the spatial coherence delimits the area of the array, i.e. the total number of scatterers, which contributes to the diffraction process.

This is true for a three-dimensional array of scatterers and for any angle of incidence, provided that

(i) the penetration depth of the particles is less than the coherence length of the wavepacket

(ii) the coherence length is greater than the effective coherence

width i.e. if θ is the angle of incidence, then

$$\Delta x > \Delta y \cos \theta \qquad (4.2 - 4)$$

These two conditions are not always satisfied simultaneously in LEED.

4.3 - Coherence in LEED

The coherence length and width of an electron wave packet are defined by equations A2-1 and A2-2 (Appendix 2).

The spread in energy of the incident electron beam in a LEED camera is the summation of the thermal spread in energies of the electrons emitted by the heated cathode filament of the electron gun and of the ripples on the potentials of the anodes of the gun. The latter may be reduced to a few millivolts by careful electronic technique, but the former is a function simply of the temperature of the filament[3], at least for simple electron guns of the type used in conventional LEED systems. Seah[4] measured the energy distribution of the electrons emitted from his gun as having a beamwidth (FWHM) of 0.6eV.

The diameter of the electron source and the angular spread of the electron beam are rather more difficult quantities to estimate. Lander[5], however, estimates the beam spread to be of the order of 10^{-3}rad.

Inserting these values into equations A2-1 and A2-2 leads to the values of coherence lengths and widths displayed in Table 4.1.

E (eV)	x (Å)	y (Å)
10	20	600
100	65	200
1000	200	60

Table 4.1 - Coherence Lengths and Widths of Low Energy Electrons.

In calculating the figures for the coherence length in Table 4.1, we have assumed that the uncertainty in energy of each electron is the total spread in energy of the entire beam. This is not strictly true, since we could further energy analyse the electron beam, leading to electrons of greater "length". The figures are therefore the lower limit of the coherence length, but give a useful working figure.

Park[6] has estimated the coherence width of the electron beam in his system by measuring the broadening of emergent diffraction beams at high diffraction angles, and finds a coherence width of (110 ± 10)Å at 90eV, and (310 ± 60)Å at 10eV, in broad agreement with the figures in Table 4.1. The rather lower measured values suggest a beam divergence smaller than 10^{-3}.

Simple diffraction theory[7] predicts that the angular width of a diffracted beam, $\Delta\theta$, will depend in a simple fashion on the number of scatterers, N, with which the incident beam interacts, viz.,

$$\Delta\theta = \frac{\lambda}{Nd \cos\theta} \qquad (4.3 - 1)$$

where θ is the angle between incident and scattered beams and d is the spacing between scatterers.

(Single scattering diffraction theory is appropriate here, since multiple scattering is a summation over single scattering events).

In a typical LEED situation, the width of the electron beam is about 1mm and the target - screen distance is about 100mm, so beam broadenings of less than 10^{-2} radians are undetectable. At near normal incidence, with 150eV electrons (λ = 1Å) this corresponds to a value of Nd = 100Å. For 25eV electrons (λ = 2.45Å) this value goes up to 250Å. In these cases, the coherence width is greater than the diffraction broadening "width", so broadening due to the limited coherence area will not be observed. However, if we go to higher diffraction angles, e.g. $\theta = 56^{\circ}$, we find for 150eV electrons, Nd = 165Å, and here the coherence width is about 160Å. Similarly, for 250eV electrons, these values are 200Å and 120Å respectively. Thus at high angles, the breadth of diffraction spots may be enhanced due to the limited coherence area of the incident beam.

One effect of the limited coherence lengths of the electrons at LEED energies and beam fluxes is that each electron acts totally independently. Indeed, it may readily be shown that any given electron arrives at the surface, interacts with the lattice, and either departs or is absorbed before the next electron arrives, provided that the interaction time is less than about 10^{-12} seconds.

Fairly comprehensive accounts of the effects of coherence in LEED have been given by Park[6], Houston and Park[8] and Heckingbottom[9].

4.4 - LEED from Polycrystalline and Faceted Specimens

Because of the limited coherence width of the electrons, the actual area of crystalline surface with which each electron interacts is limited, and the observed LEED pattern is the summation of many individual electron-lattice

diffraction patterns. A LEED pattern will therefore be built up on a fluorescent screen provided two conditions are satisfied.

(i) Each individual electron LEED pattern must overlap all the others.

(ii) The electron flux is sufficient to cause a persistent visual image to appear on the screen.

In the case of a specimen which is single crystal over the whole area illuminated by the electron beam, the first condition is automatically satisfied, since the symmetry of the LEED pattern is invariant with respect to translations in the plane of the crystal surface. The second condition is a purely experimental variable.

However, consider a specimen whose surface is composed of small areas of single crystal, contiguous with other small areas of single crystal, separated by some sort of boundary region (i.e. a polycrystalline specimen) or a specimen whose surface consists of small areas of low index crystalline surface separated by areas of high index surface (i.e. a faceted specimen). It is then relevant to ask what sort of diffraction pattern will be formed by these surfaces.

We will assume that each small area of single crystal surface (either grain or facet) is comparable in size to the coherence area of the electron beam, or larger than it, in order to obviate any diffraction broadening effects. We can then consider the diffraction process as the interaction of single electrons with one or other of these grains or facets.

Consider first a polycrystalline sample. There are two extreme cases which we may consider. Firstly, let us take the case of a sample where

each grain exhibits a different surface orientation from each of its neighbours, and whose surface normal is not parallel to those of its neighbours, so that, on average, all possible crystal orientations are presented to the electron beam. Here, it is evident that the observed LEED pattern will be the sum of many randomly oriented LEED patterns and will exhibit no clear diffraction features. In the unlikely event of randomly oriented grains with parallel surface normals, we would, however, always see a specularly reflected spot. The other extreme is where a sample consists of a large number of grains which all expose the same crystal face to the electron beam and whose surface normals are parallel, but where the crystal axes lying in the surface plane of each grain are in random orientations (i.e. rotational asymmetry). Here the result would be a series of uniform diffraction rings, with the angular diameter of the rings being determined by the atom spacings in the surface of the grains. If the rotational asymmetry were not complete, i.e. if some directions were preferred over others in the sample surface, then the rings would have modulated intensities round their circumferences, reflecting these preferred orientations.

Cases intermediate between these two extremes would exhibit intermediate behaviour.

An exception to the behaviour described for the randomly oriented polycrystalline sample would occur if the sample were composed of atoms such that the atomic scattering factor exhibits marked asymmetry[10], i.e. if scattering from a single atom is markedly different from a spherically symmetrical radially outgoing wave. These asymmetries in the atomic scattering factor would then be reflected in the LEED pattern as radial intensity modulations of the background.

If we now turn our attention to consideration of a faceted specimen, it may readily be seen that if the surface consists of number of facets of one crystal orientation, each of which is greater in area than the coherence area of the incident beam, and separated by distances comparable with the coherence width of the beam, then each facet will interact with one or other of the electrons exactly as if they were part of a much larger single crystal surface. Thus all the individual facet patterns sum to give a total diffraction pattern identical in geometry with that to be expected from a single crystal of the same orientation.

If facets of two or three different crystal faces are exposed to the electron beam in comparable numbers, then the net pattern will consist of the superimposition of the LEED patterns from each of the different sets of facets, each centred on its own specular spot.

If the facets are smaller than the coherence area, but still well separated and not small enough to give rise to beam broadening effects, then the effect is simply to reduce the intensity of the resultant facet pattern.

An extensive discussion of the types of pattern to be expected from a surface containing large numbers of small, closely spaced facets, especially in the case where the whole surface can be regarded as being made up of facets on an atomic scale (terraces) separated by atomic steps, has been given by Rhead[11]. He shows that scattering from the successive steps can lead to splitting of the diffraction spots and other effects.

Returning to the case of well-separated facets, we must consider what happens to the electrons which strike the complex, high index surface

between the facets. The nature of the interaction is determined by exactly the same considerations as determine the formation of a LEED pattern by a large area of any crystal surface, i.e. the existence of sufficient areas of two-dimensional periodicity (or possibly one dimensional periodicity) in the surface. If no such periodicities exist, the electrons striking this part of the surface will be backscattered in a diffuse manner, giving rise to a general background on the LEED screen.

It is therefore pertinent to ask the question, what percentage area of the crystal surface sampled by the incident beam of electrons would have to be occupied by any one crystal orientation in order to give rise to clearly discernable diffraction spots?

Several LEED studies of faceting have been published (for example, references 12 and 13 among others) but these have mainly dealt with crystal surfaces where the major part of the surface was well ordered and gave rise to a sharp diffraction pattern, with the facet LEED pattern superimposed on this one. The experiments to be described in the next section deal with crystals where the low index facets occupy a relatively small area of the total crystal surface, and are separated by large stretches of high index crystal surface.

4.5 - Experimental LEED Study of Faceted Metal Crystals

The formation of simple linear facets has been described by Moore[14] and by Robertson[15]. Copper and silver are known to facet to the low index (111) and (100) planes through the mechanism of thermal etching under

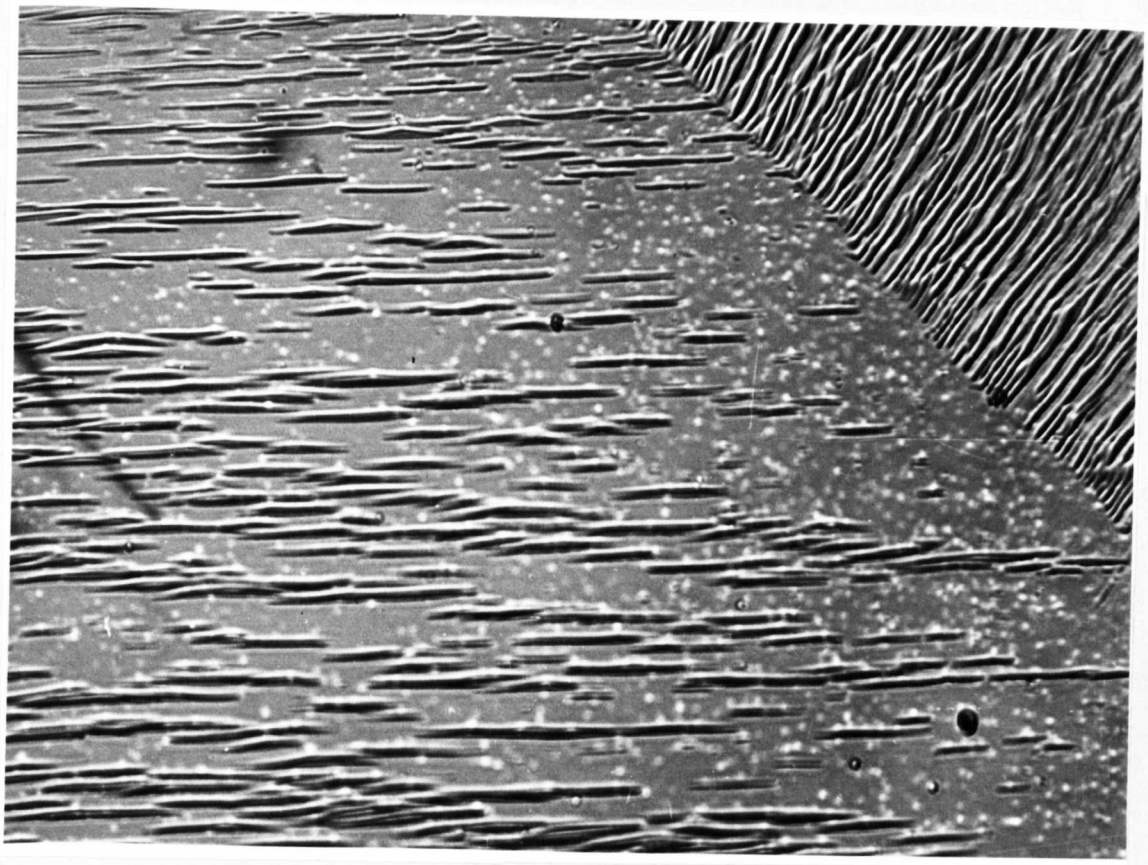

Figure 4.5-1. Optical micrograph of a faceted copper foil. The facets are the dark lenticular areas, and are typically 15μm by 2μm in size. Also to be seen is a twin boundary running diagonally across one corner of the photograph.

vacuum. In such conditions, the crystal surfaces tend to be covered with adsorbed monolayers of oxygen. By a suitable choice of initial surface orientation and of the thermal treatment, the proportion of low index facet on the surface can be varied, and so the effect on the diffraction process of varying the amount of low index crystal surface exposed to the electron beam can be studied.

Results are presented here for copper, and similar studies on silver have recently been presented by Schön[15].

Faceted specimens of copper foil were prepared as described in § 3.4.2. They were examined by optical microscopy, optical interference microscopy and by LEED. Fig. 4.5-1 is an optical micrograph of a typical faceted specimen, and Fig. 4.5-2 shows a typical surface profile as determined by optical interference microscopy.

The facets on these specimens appear optically flat in the micrographs, but this does not preclude the existence of steps and other irregularities of sizes less than the resolution of such a technique. The continuation surface between the facets has areas of high curvature, but the central regions between the facets exhibit large areas of optically flat surface.

The specimens were examined in the LEED camera after bakeout, and good quality LEED patterns were usually observed from most faceted parts of the foil specimens. One such pattern is illustrated in Fig. 4.5-3. This particular pattern arises from a specimen which is almost entirely single crystal, and is fairly uniformly faceted to (100) over its entire surface.

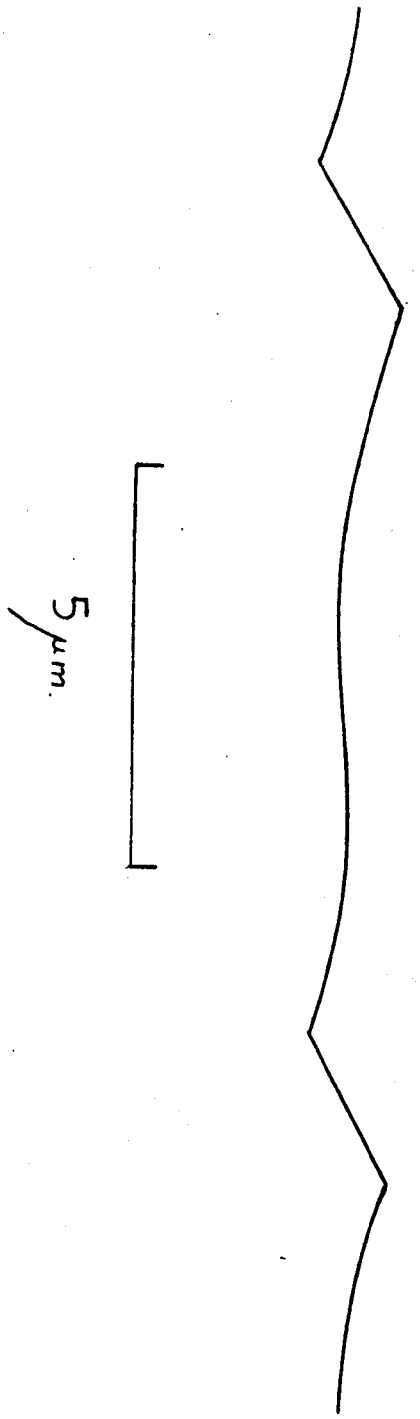

Figure 4.5-2. Typical surface profile of a faceted copper crystal as determined by optical interference microscopy.

The density of facets on the surface is such that the proportional area of facet is about 15%. The facets are typically 15μm x 2μm in size, and spaced on average by about 10μm. The flat portions of the complex surface are close to (831) in orientation. The diffraction pattern comprises a series of clear sharp spots, of angular width comparable with the instrumental resolution, superimposed on a background of low intensity.

From examination of many such faceted specimens, faceted to both (100) and (111), it is concluded that clear patterns, superimposed on somewhat higher backgrounds, could readily be observed even when the facet area occupied as little as 5% of the sampled area of the specimen.

The pattern reproduced in Fig. 4.5-3 is very similar to that observed by Ertl[17] from a copper (100) surface onto which he had adsorbed a monolayer of oxygen by exposing a clean Cu(100) surface to N_2O. The direction of the specularly reflected spot and the behaviour of the pattern with changing energy of the electron beam and with changing angle of incidence show quite unambiguously that all the observed diffraction spots come from the facets, and so we conclude that the facets are indeed Cu(100) covered with a monolayer of oxygen as we projected earlier.

Although no beam broadening effects are discernable in the diffraction spots, this does not unambiguously preclude the existence of microfacets of dimensions greater than those required to produce beam broadening (say, 300Å), but smaller than the resolution of the optical microscope (say, 5,000Å), so that the optically observed facet area may not include all the areas giving rise to the observed low index diffraction pattern.

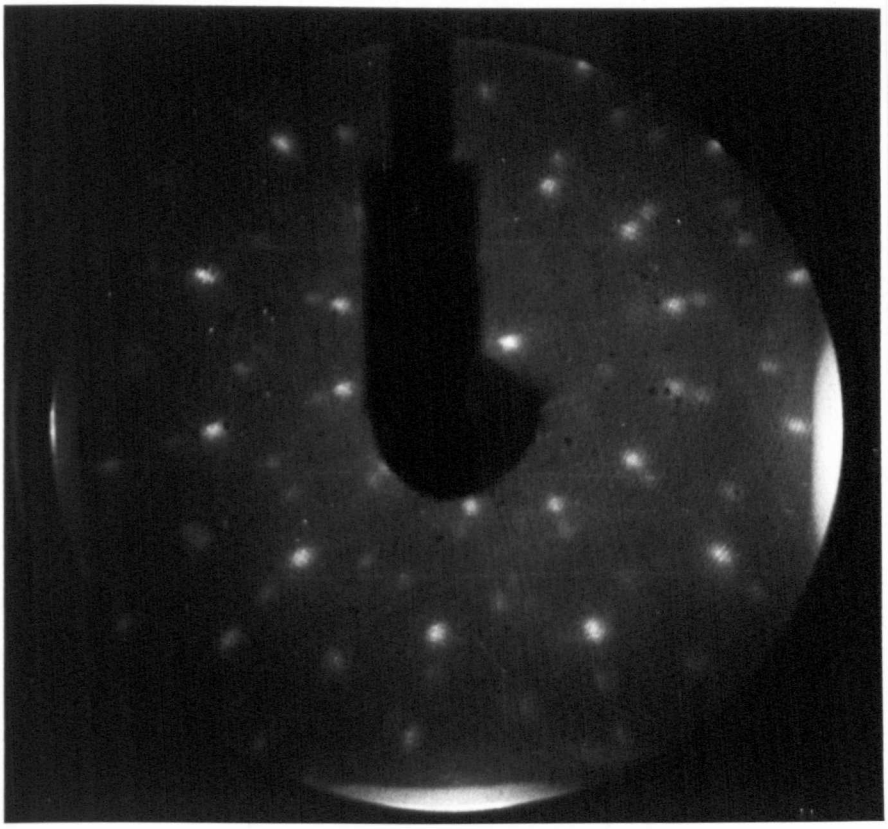

Figure 4.5-3. LEED pattern from a faceted copper foil taken with electrons of energy 116eV at an angle of incidence of about 4^{o}. The specularly reflected spot is that just above the shadow of the final anode of the electron gun, to the right of the specimen holder. The pattern which exhibits pseudo-twelvefold symmetry probably arises from two equivalent hexagonal overlayers of oxygen on the facets of Cu(100), the p.t.v.s of the two overlayers being at right angles to each other.

However, since there exist areas of crystal surface which do not exhibit LEED patterns on these specimens, and no patterns were observed from a platinum specimen smoothed by high temperature annealing, we are led to the conclusion that the complex surface does not contain sufficient microfacets to contribute significantly to the observed low index pattern, and that in general, this surface does not exhibit sufficient periodicity to generate a pattern of its own.

In summary, we conclude that while the existence of a sharp, intense diffraction pattern superimposed on a low background is a necessary condition for the existence of large areas of perfect periodicity in the surface, it is by no means a sufficient one, indicating only that there are sufficient small areas of perfect periodicity in the surface, each of which is greater than the coherence area of the sampling electron beam, to occupy more than about 10% of the sampled area.

REFERENCES

1) R.J. Reid and H. Mykura, Harwell LEED Conference (1968), Paper A3.

2) R.J. Reid and H. Mykura, J. Phys. D 2 (1969), 145.

3) K.R. Spangenberg, "Fundamentals of Electron Devices" (McGraw-Hill New York, 1957).

4) M.P. Seah and A.J. Forty, J.Phys. E 3 (1970), 833.

5) J.J. Lander, Progr. in Sol. State Chem. 2 (1965), 26.

6) R.L. Park, "Structure and Chemistry of Solid Surfaces" (Wiley & Son, New York, 1969), Paper 28.

7) F.A. Jenkins and H.E. White, "Fundamentals of Optics" (McGraw-Hill, Kogakusha, Tokyo, 1957), 337.

8) J.E. Houston and R.L. Park, Surface Science 21 (1970), 209.

9) R. Heckingbottom, Surface Science 17 (1970), 394.

10) J.J. Lander and J. Morrison, J. Appl. Phys. 34 (1963), 3517.

11) G.E. Rhead and J. Perdereau, "Structure et Proprietes des Surfaces de Solides" (CNRS, Paris, 1969), 37.

12) J.W. May, Industr. Engng. Chem. 57(7) (1965), 18.

13) G.W. Simmons, D.F. Mitchell and K.R. Lawless, Surface Science 8 (1967), 180.

14) A.J.W. Moore, Acta Metall. 6 (1958), 293.

--- , "Metal Surfaces; Structure, Energetics and Kinetics" (American Society for Metals, Ohio, 1963), 155

15) W.M. Robertson, Acta Metall. 12 (1964), 241.

16) G. Schön, Surface Science 18 (1969), 437.

17) G. Ertl, Surface Science 6 (1967), 208.

CHAPTER 5

THE LOW INDEX FACES OF COPPER

5.1 - Introduction

Although, as we have seen, LEED is eminently suitable for the study of some aspects of the surfaces of crystalline systems, and has rapidly become established as a technique for such purposes as the study of the symmetry properties of gaseous adsorption on solid surfaces, it is only comparatively recently that theoretical approaches to the calculation of intensity-energy spectra have reached a point where it seems likely that significant correlation with experimental results will be achieved. However, in the literature, there exists a paucity of the type of detailed experimental results against which these theories can be measured.

From the theorist's point of view, an ideal set of experimental results would comprise a complete set of intensity-energy spectra from zero to a few hundred electron volts in energy, taken for a wide, finely-graded range of angles of incidence, for all of the diffracted beams. Preferably, absolute intensities would be measured. Additionally, we will argue in the next chapter that experimental information on the effects of temperature on the intensity-energy spectra is an important parameter of the system.

It is scarcely to be wondered at that such a set of results has not yet been published for any given crystal system, although a few studies approaching this ideal have been reported for LiF[1], Ag[2,3] and Al[4].

The data presented in this chapter and the following chapter provide for the (100) surface of copper a reasonably complete set of such results for the specular beam in the energy range 20 - 350eV at angles of incidence 6 - 22° spaced at 1° intervals in the ⟨110⟩ azimuth (See Fig. 5.2-2). For the (111) surface a rather less detailed set of results is presented over the same range of energy and angles of incidence spaced at 2° intervals in the ⟨11$\bar{2}$⟩ azimuth (see Fig. 5.3-2).

Copper has been relatively well studied by LEED since 1928 (there are about thirty eight papers published prior to 1970), but apart from one or two recent studies, the published work concentrates almost exclusively on its adsorption properties. The most detailed intensity-energy spectra published so far are those of Andersson[5] who reports spectra for several of the diffracted beams from the (100) surface, but these are confined to a few angles of incidence. Single intensity-energy spectra for the (111) surface are to be found in several places[6,7,8,9], but no detailed study has yet been published. The (110) surface has been studied only from the point of view of its adsorption properties[7,10].

5.2 - The (100) Surface

The (100) surface proved reasonably easy to clean and remained clean in the vacuum system in the mid 10^{-10}T. range of pressure for periods in excess of 24 hours, at least remained clean within the limits of the definition of cleanliness stated in § 3.5.3 After about 48 hours, however, small changes in the intensity-energy spectra could be observed. Consequently, anneal and bombardment cycles were performed each day prior to the sequence of observations on the surface.

An interesting point which was noted with regard to this surface was that after many argon ion bombardment and anneal cycles, the surface became extremely sensitive to bombardment. The "normal" behaviour of the surface was that diffraction spots, albeit somewhat diffuse, were clearly visible after many hours bombardment, although the extremely diffuse spots reported by other authors[7] were never observed. However, for the "sensitive" surface, a few seconds exposure to the argon ion beam would completely destroy the diffraction pattern. A short anneal would, however, completely restore the pattern, and in this manner an apparently clean surface was produced. At this juncture, the crystal was removed from the vacuum system and examined under the optical microscope. The surface appeared to consist of large flat facets of (100) orientation, separated by a few terraces, and no signs of recrystallisation were present. The specimen was repolished according to the original procedure (§ 3.4.1) and replaced in the vacuum system, where its diffraction properties proved identical to those of the original surface. The reasons for this sudden onset of sensitivity to bombardment - a sensitivity which did not recur with the repolished specimen - are unknown.

The diffraction pattern (Fig. 5.2-1) revealed the crystal to be orientated such that rotation of the crystal caused the electron beam to move in one of the ⟨110⟩ azimuthal planes (Fig. 5.2-2). In fact, the crystal was misoriented by about 3°. An accurate determination of the normal incidence position of the crystal was effected by finding two positions, one on either side of the surface normal which gave rise to identical intensity-energy spectra for the specular beam.

Figure 5.2-1. LEED pattern from the (100) surface of copper taken with electrons of energy 150eV i.e. of wavelength 1Å, at normal incidence.

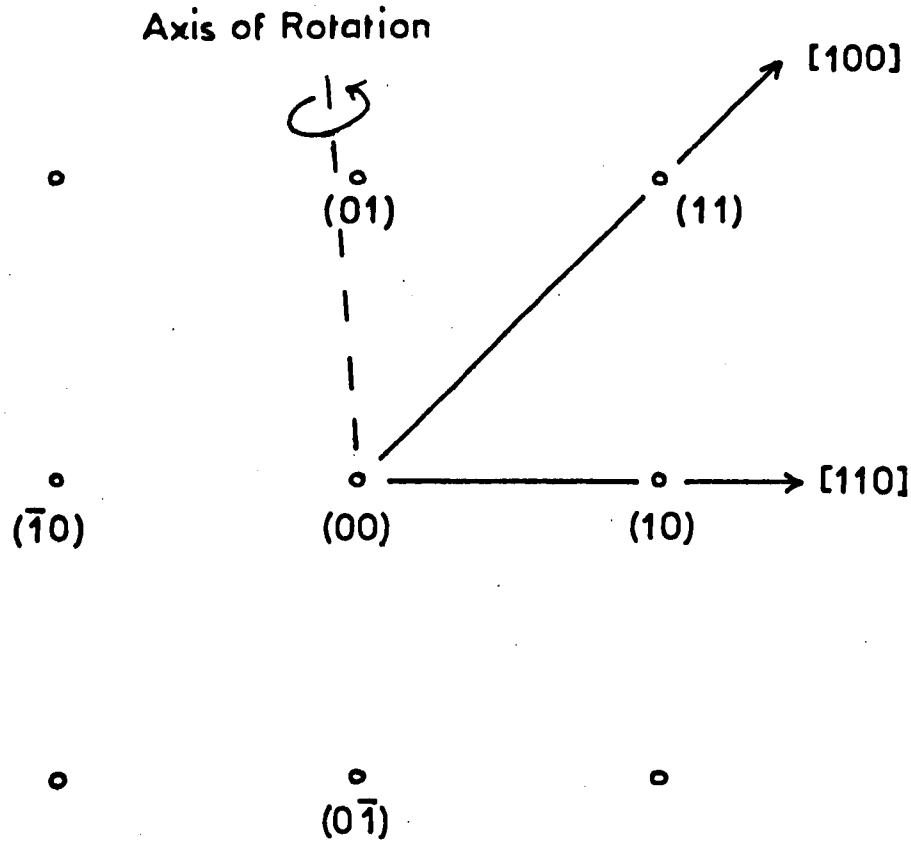

Figure 5.2-2. Definitions of the co-ordinates of the non-specular diffraction beams and of the surface azimuths for the (100) surface.

Figures 5.2-3 through 5.2-7 reproduce the intensity-energy spectra for the specular beam as detailed in the figure captions, and Figure 5.2-8 is a redrawn part of the spectrum set out for greater clarity. The results are reproduced in the form of a $\underline{k}$-space plot (§ 2.3.2) in Figure 5.2-9. In this figure, in accordance with our previous discussion, no inner potential corrections have been made.

Inspection of Figure 5.2-9 shows that the major peaks appearing in the spectrum lie close to the Bragg zone lines,but at some distance below them. Addition of a constant small energy to each of the peaks in a group can shift them up towards the Bragg zone line (and incidentally change the angle of incidence in a manner analogous to Snell's Law of refraction[2]) so that each set of such peaks can be brought into coincidence with the appropriate zone line. As a matter of convenience, we refer to such sets of peaks as Nominal Bragg Peaks, without in any way implying that they constitute genuine, single scattering, kinematical Bragg Peaks. However, the energy required by any given peak in a group varies from that required by the other members of the group in a rather random manner. A rough mean of these individual values, which we call for convenience inner potentials, is listed in Table 5.1 for four of these nominal Bragg peaks, and Table 5.2 lists the individual values for each of the peaks in the (800) nominal Bragg peak.

Holland *et al*[12] have argued that it is qualitatively reasonable that the inner potential should increase with increasing energy of the incident electron, as appears to be the case here. However the existence of the detailed variation of the inner potential makes it difficult to place any precise physical interpretation on the measured values, and again illustrates the danger of over-simplifying the LEED process.

Figures 5.2-3 to 5.2-8 The Intensity-Energy Spectrum of the specular LEED beam diffracted from the (100) surface of Copper in the ⟨110⟩ azimuth. The energy region and angle of incidence for each individual spectrum is detailed in the appropriate Figure. Figure 5.2-8 is a section of the spectrum redrawn for greater clarity. In each case the intensity scale is in arbitrary units.

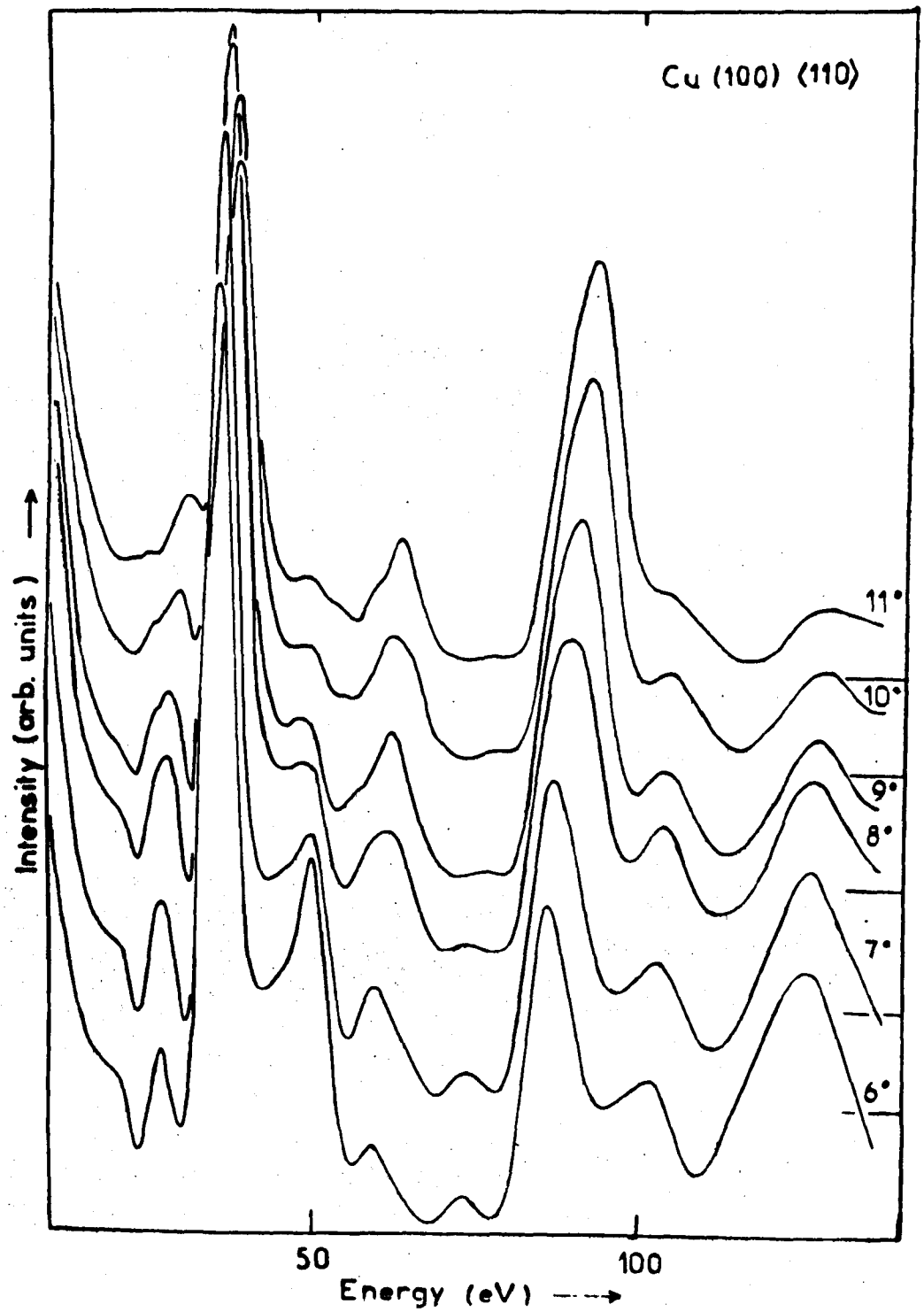

Figure 5.2-3.

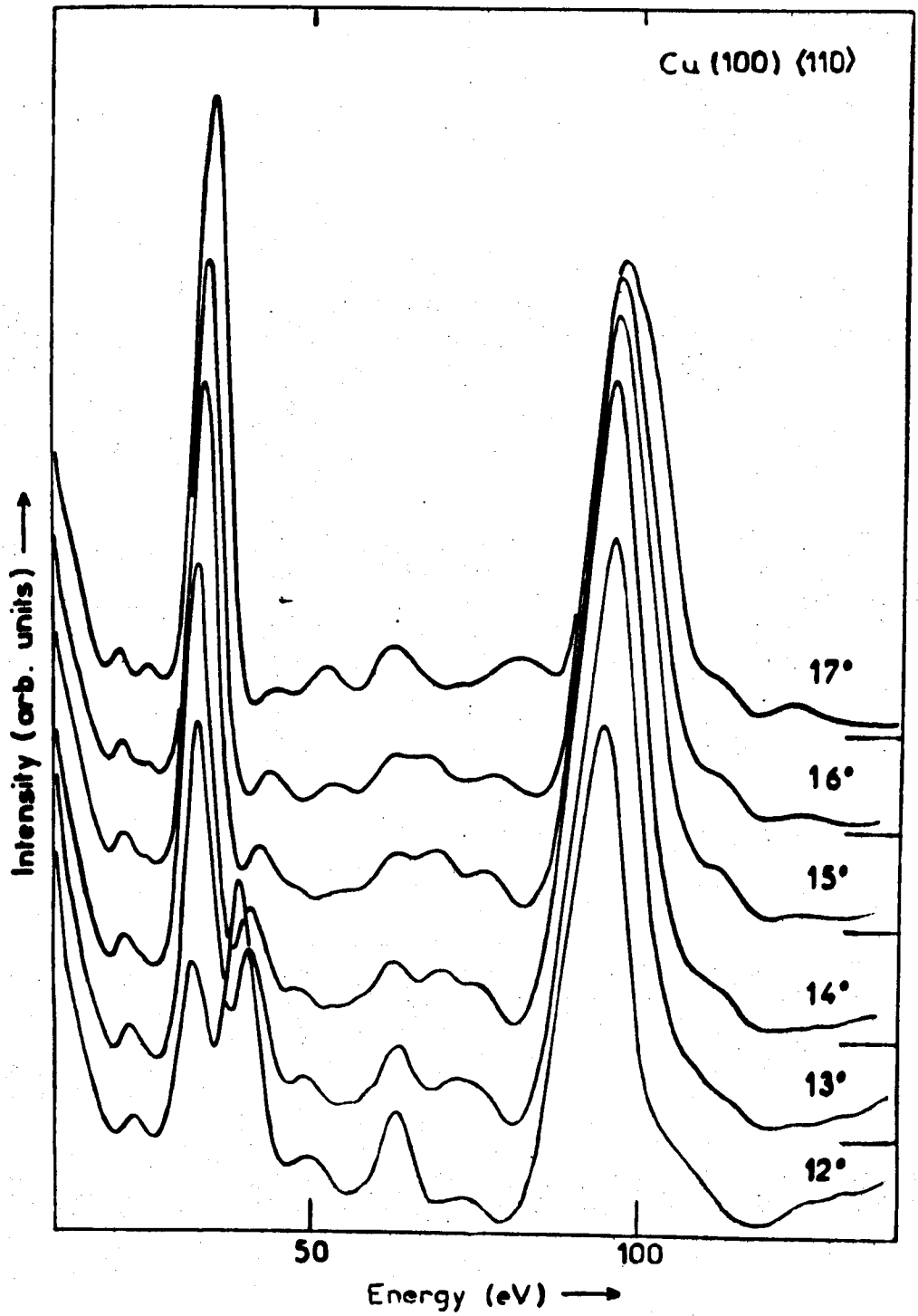
Cu (100) ⟨110⟩
Intensity (arb. units) ⟶
17°
16°
15°
14°
13°
12°
50
100
Energy (eV) ⟶

Figure 5.2-4

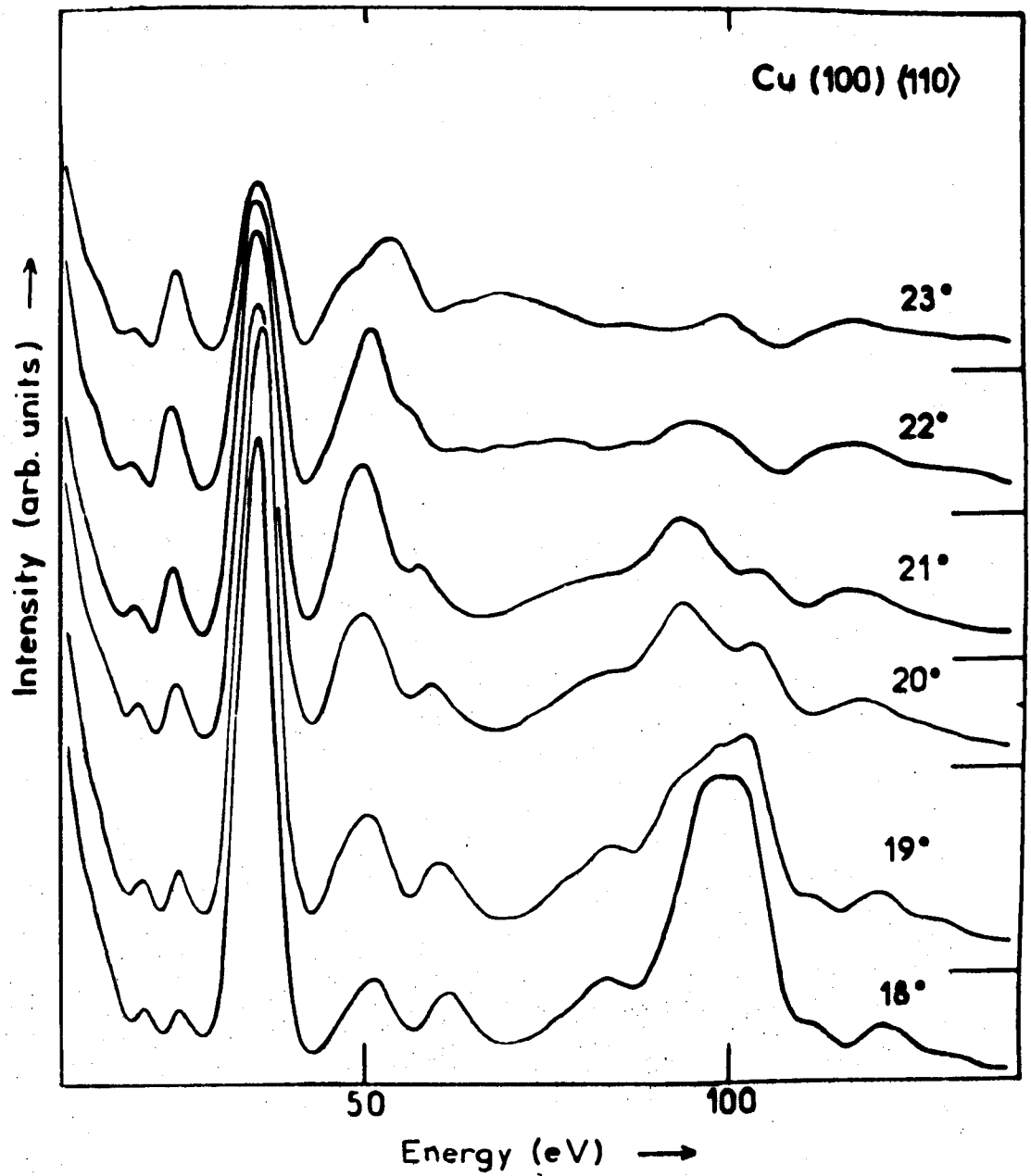
Cu (100) ⟨110⟩
23°
22°
21°
20°
19°
18°
Intensity (arb. units) →
50
100
Energy (eV) →

Figure 5.2-5.

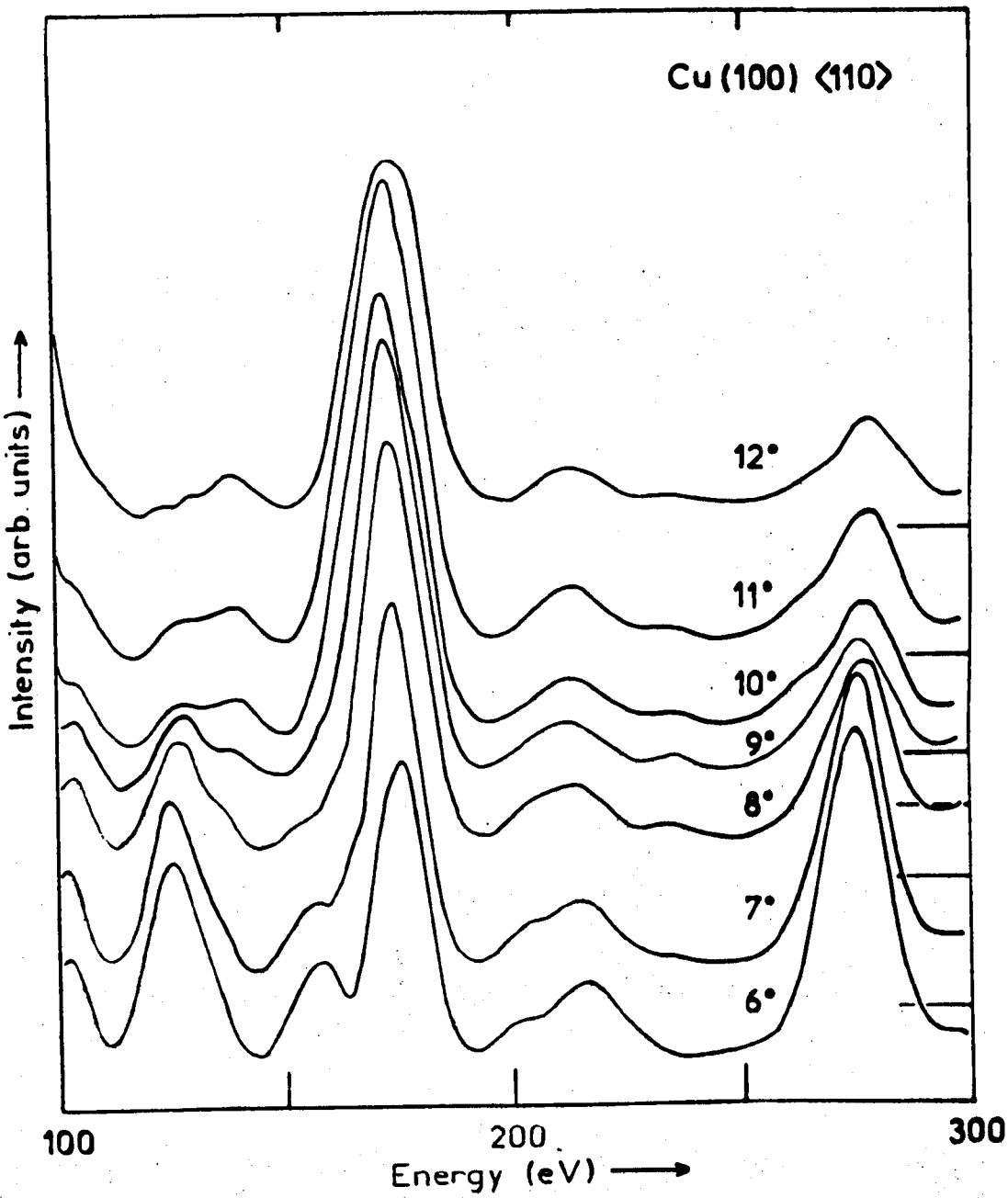
Cu (100) ⟨110⟩
Intensity (arb. units) ⟶
12°
11°
10°
9°
8°
7°
6°
100
200
300
Energy (eV) ⟶

Figure 5.2-6.

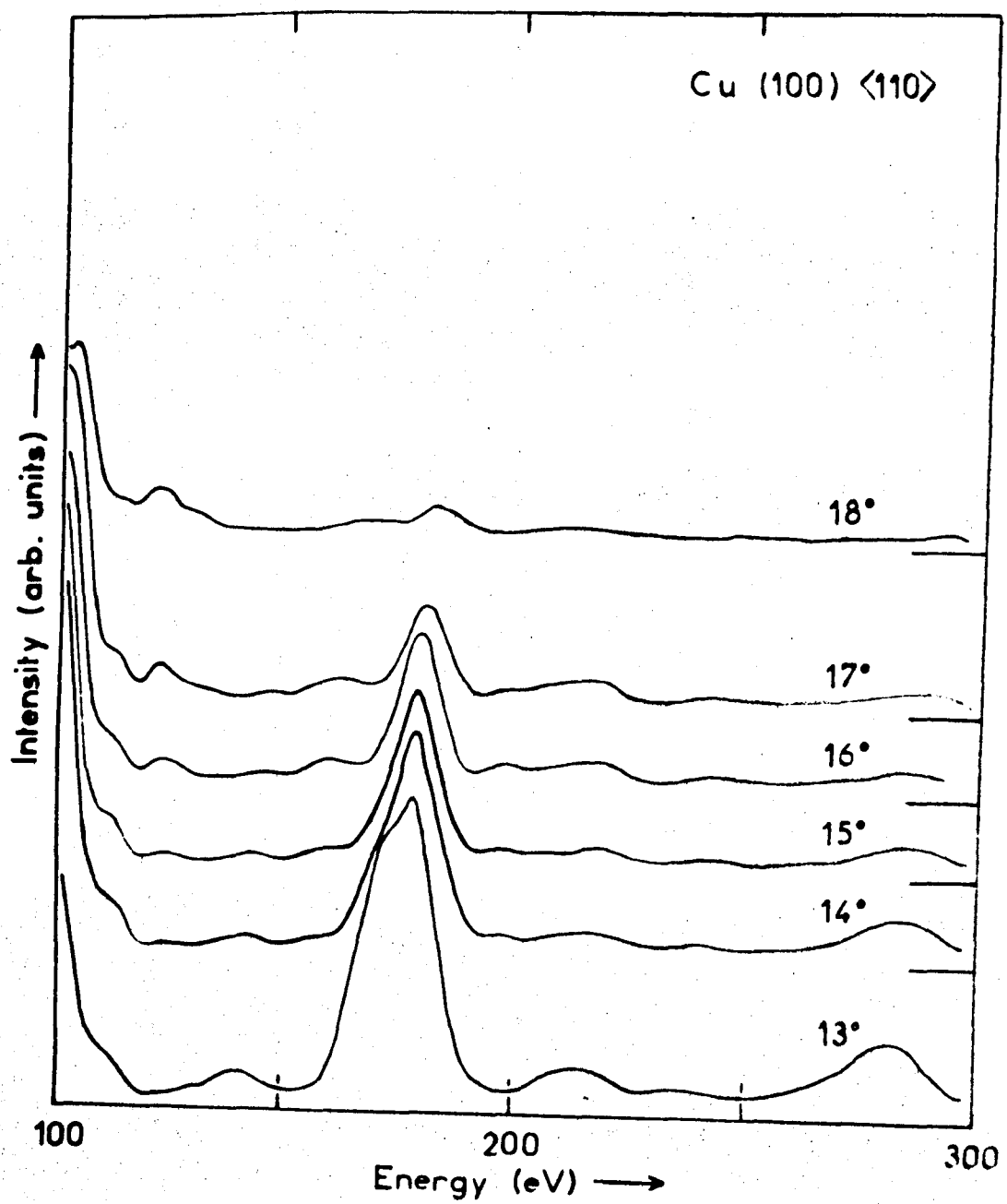
Cu (100) ⟨110⟩
Intensity (arb. units) ⟶
18°
17°
16°
15°
14°
13°
100
200
300
Energy (eV) ⟶

Figure 5.2-7.

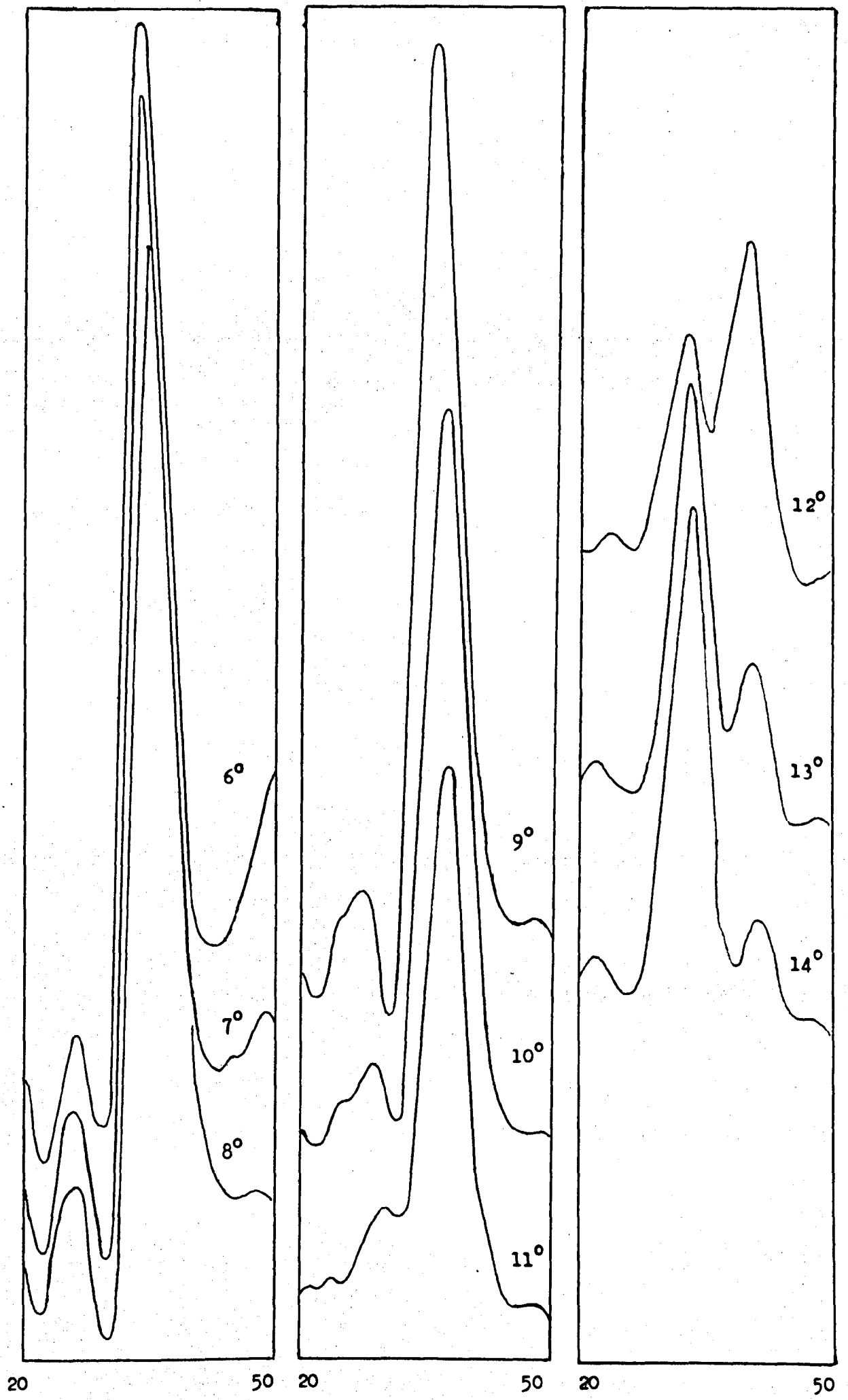

Energy (eV)

Figure 5.2-8.

Figure 5.2-9 The Intensity-Energy Spectrum of Figures 5.2-3 through 5.2-7 redrawn as a polar plot in $\underline{k}$-space. The dots each represent the centre of the Ewald Sphere corresponding to the diffraction conditions appropriate to a peak in the Intensity-Energy Spectrum, with no Inner Potential corrections applied. The relative sizes of the dots reflect the relative sizes of the diffraction peaks. The labelled horizontal lines show the kinematical Bragg scattering conditions for the diffraction beam.

Figure 5.2-10 The $\underline{k}$-space plot of Figure 5.2-9 redrawn with the emergence conditions of the non-specular diffraction beam superimposed on it. These loci are determined as described in the text, and a few are labelled with the coordinates of the appropriate beam. The labelling convention for these beams was shown in Figure 5.2-2.

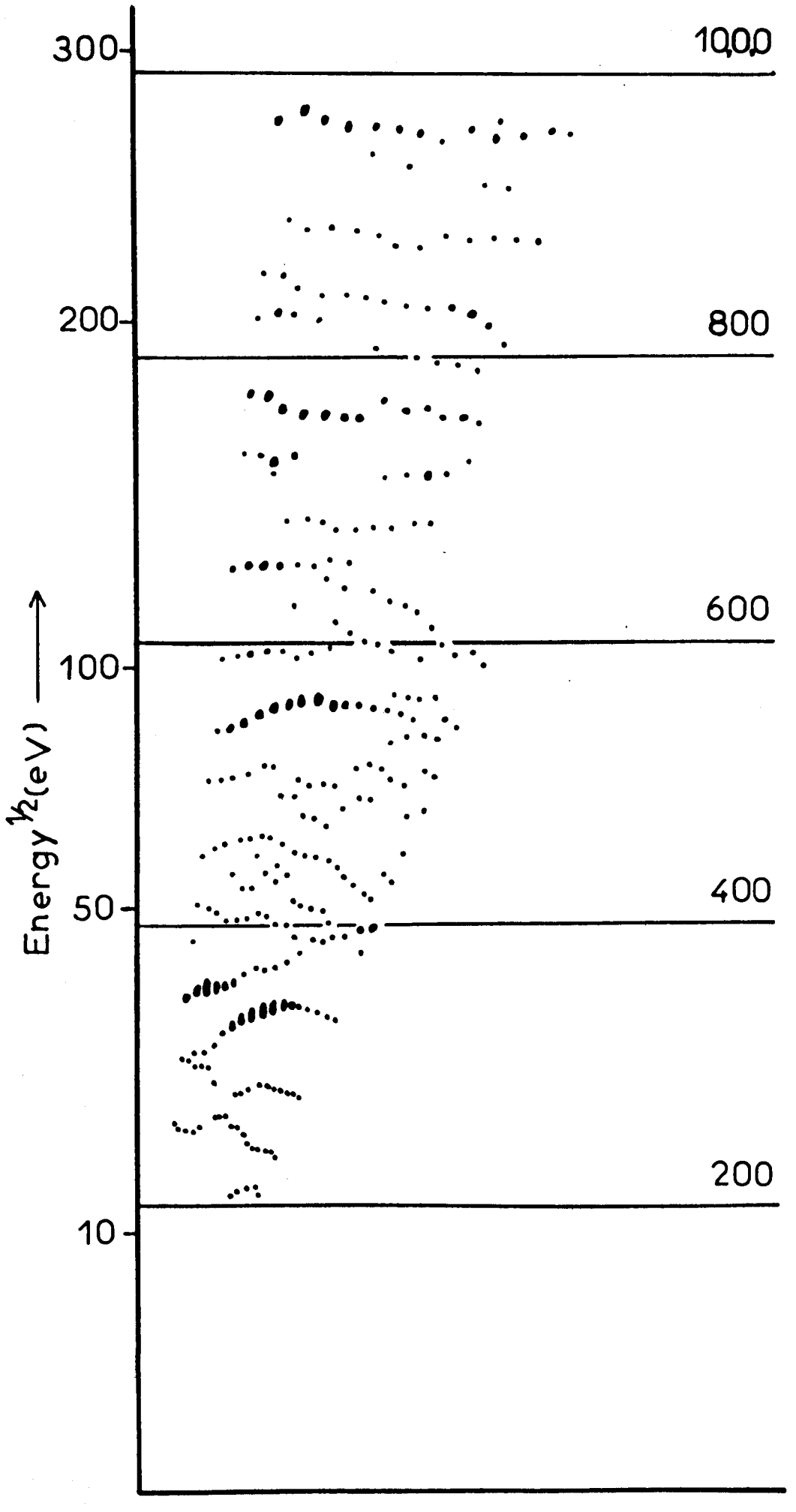
300
200
100
50
10
Energy ½(eV)
1000
800
600
400
200

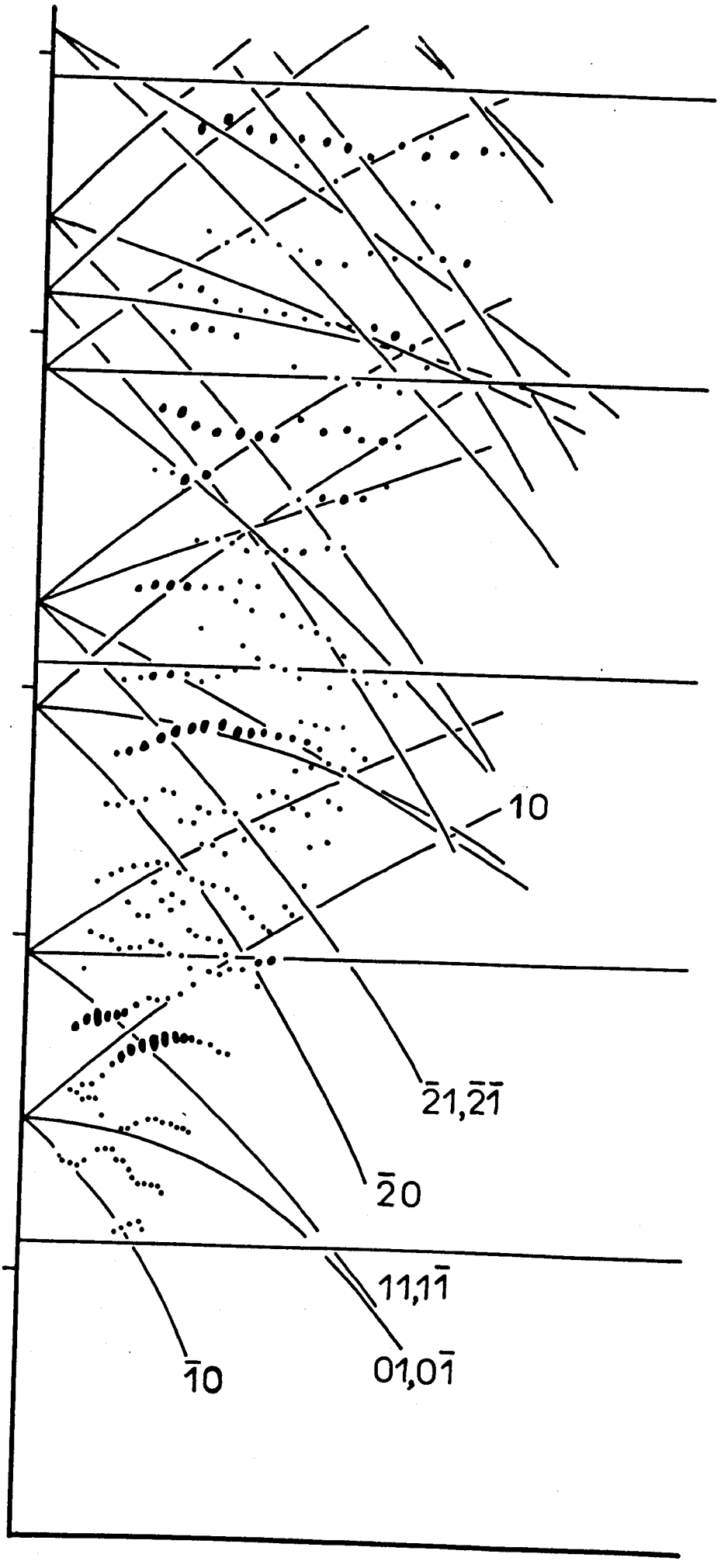
10
$\bar{2}1,\bar{2}\bar{1}$
$\bar{2}0$
$11,1\bar{1}$
$01,0\bar{1}$
$\bar{1}0$

TABLE 5.1

Nominal Bragg Peak	Inner Potential (eV)
400	10
600	14
800	15
10,0,0	18

Inner Potentials for Nominal Bragg Peaks from Cu(100)

TABLE 5.2

Angle of Incidence	Inner Potential (eV)
6	12
7	13
8	17
9	18
10	18
11	19
12	20
13	14
14	15
15	15

Detailed Variation of the Inner Potential for the (800) Nominal Bragg Peak as a Function of the Angle of Incidence

The most striking feature of this spectrum is the behaviour of the group of peaks which we have assigned to the (400) nominal Bragg peak, i.e. those lying in the energy range 30-50eV. The main peaks in this group appear as a doublet in which the ratio of the intensities of the two elements of the doublet varies rapidly as the angle of incidence is varied, passing through unity at an angle of incidence of about 12.5°.

The complete intensity-energy spectrum of the specular beam is re-drawn in $\underline{k}$-space in Figure 5.2-10 with the emergence conditions of the non-specular beams superimposed on it. These loci are determined geometrically by ascertaining the values of $\underline{k}'$ which satisfy the equation

$$\underline{k}'_{\parallel} = \underline{k}_{\parallel} + \underline{g}$$

where $\underline{k}$ is the wave vector of the incident electron.

In this diagram, the horizontal lines represent the kinematical Bragg scattering conditions for the specular beam, and should therefore in the simplest analyses be associated with intensity maxima in this beam. The other lines, the emergence conditions for the non-specular beams, therefore represent competing reflections into the other beams, not necessarily in the same azimuth, and in such analyses would therefore be associated with minima in the specular beam.

It will be observed that the two elements of the doublet discussed above lie one on either side of the emergence condition of the (10) beam, (see Fig. 5.2-2 for the definition of beam coordinates) and it is therefore plausible to postulate that some sort of sharp valley is traversing a single large diffraction peak in the intensity-energy spectrum, and that this valley may be associated with the emergence of this new diffraction

beam. The group of peaks could therefore be referred to as a split (400) nominal Bragg peak. Accordingly, in Figure 5.2-11, the position of the bottom of this valley is plotted in k-space over the beam emergence condition. The position of the valley does not lie precisely on the emergence condition except at low angles of incidence, after which it gradually drops below it. As the valley traverses the maximum of the postulated main peak, the locus of the minimum breaks back to meet the emergence condition and then falls away again. This is indeed the behaviour to be expected when a narrow valley traverses a relatively broad peak, since the minimum in the composite peak occurs when the sum of the gradients of the two components is zero. This should then result in a displacement of the observed minimum from that of the true minimum of the sharp valley away from the maximum of the main peak. Thus as the valley approaches the peak maximum, the observed minimum should be at a lower energy than the true minimum, and as the valley moves away from the peak, the observed minimum should be at higher energies than the valley position. Clearly there is thus some sort of correlation between the two events, but there is also some more complex interaction, and, without more detailed calculations being performed, the precise nature of the correlation cannot be specified.

Behaviour of this type might be interpreted as evidence for the existence of a McRae surface wave resonance[11], but Holland et al[12] point out that it is more likely to be associated with the opening of a new scattering channel (the new diffracted beam) "robbing" the other scattering channels of flux. It is however, difficult to see why on this model the valley should lie completely below the beam emergence condition. It might be pointed out that we have so far ignored the effects of the inner potential

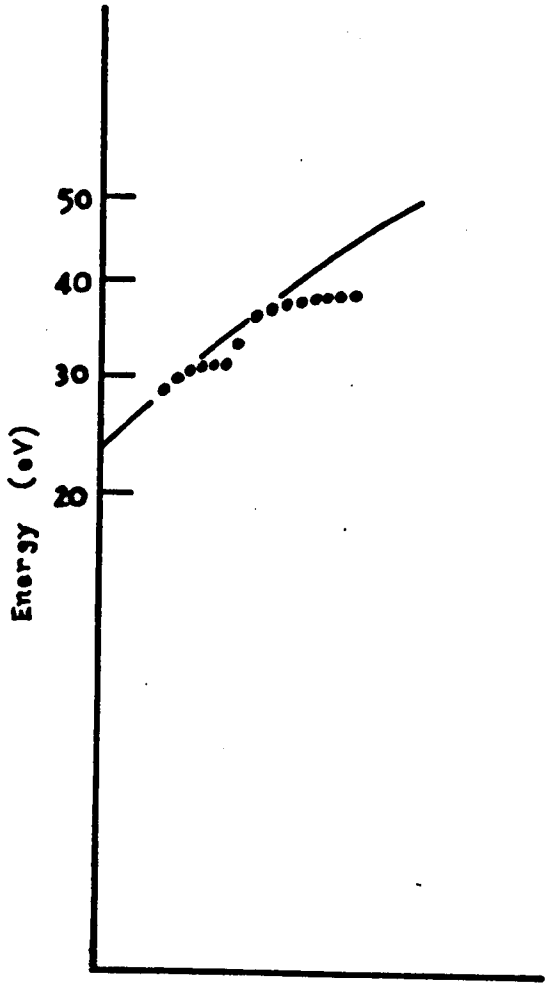

Figure 5.2-11. The position of the valley crossing the "split" (400) Nominal Bragg Peak (full circles) plotted as a polar plot in $\underline{k}$-space along with the emergence condition of the $(10)'$ diffraction beam (solid line).

and the detailed mechanisms of the transport of the electrons across the surface-vacuum interface. It is indeed correct to ignore the inner potential here, since the beam emergence conditions are solely derived from the conservation of momentum parallel to the interface across the interface, and so the beam emergence is independent of the inner potential. Similarly, the effects of the transport across the boundary - such as contact potential differences, etc. - affect only the normal component of the momentum, but affect equally the absolute values of beam emergence energies and the energies of the incident electrons.

Close examination of Figure 5.2-10 reveals that although there are no further striking correlations between the positions of peaks and the beam emergence conditions, nevertheless some weaker effects are discernable. For instance, in several cases, where a beam emergence crosses the locus of a diffraction peak, a "kink" appears in that locus, e.g. where the $2\bar{2},\bar{2}2$ beam emergence crosses the nominal (1000) Bragg peak. Similarly the nominal (600) Bragg peak appears to try to "avoid" the $12,\bar{1}2$ emergence. However the overall level of correlation is too low to allow definite conclusions to be drawn. Nevertheless this appears to be a factor to be considered in the analysis of LEED data.

It is instructive to compare these results with other experimental studies and with calculations where this is possible. The only detailed study published to date is that of Andersson[5]. In this case, the crystal was oriented in a ⟨100⟩ azimuth, i.e. rotated by 42° with respect to the azimuth used in this work. Nevertheless, at low angles of incidence, azimuthal differences are not expected to be very pronounced. In Figure 5.2-12 we present the results of Andersson at 3° and 6° incidence (centre

Figure 5.2-12 Comparison between the results of this work, that of Andersson and the calculations of Capart.

(a) This work at an angle of incidence of 6° in the 110 azimuth extrapolated to $0^{\circ}K$ and normalised as described in the text.

(b) The result of Andersson at an angle of incidence of 6° in the 100 azimuth at room temperature.

(c) Andersson's result at 3° incidence.

(d) The result of Capart's normal incidence, rigid lattice calculation.

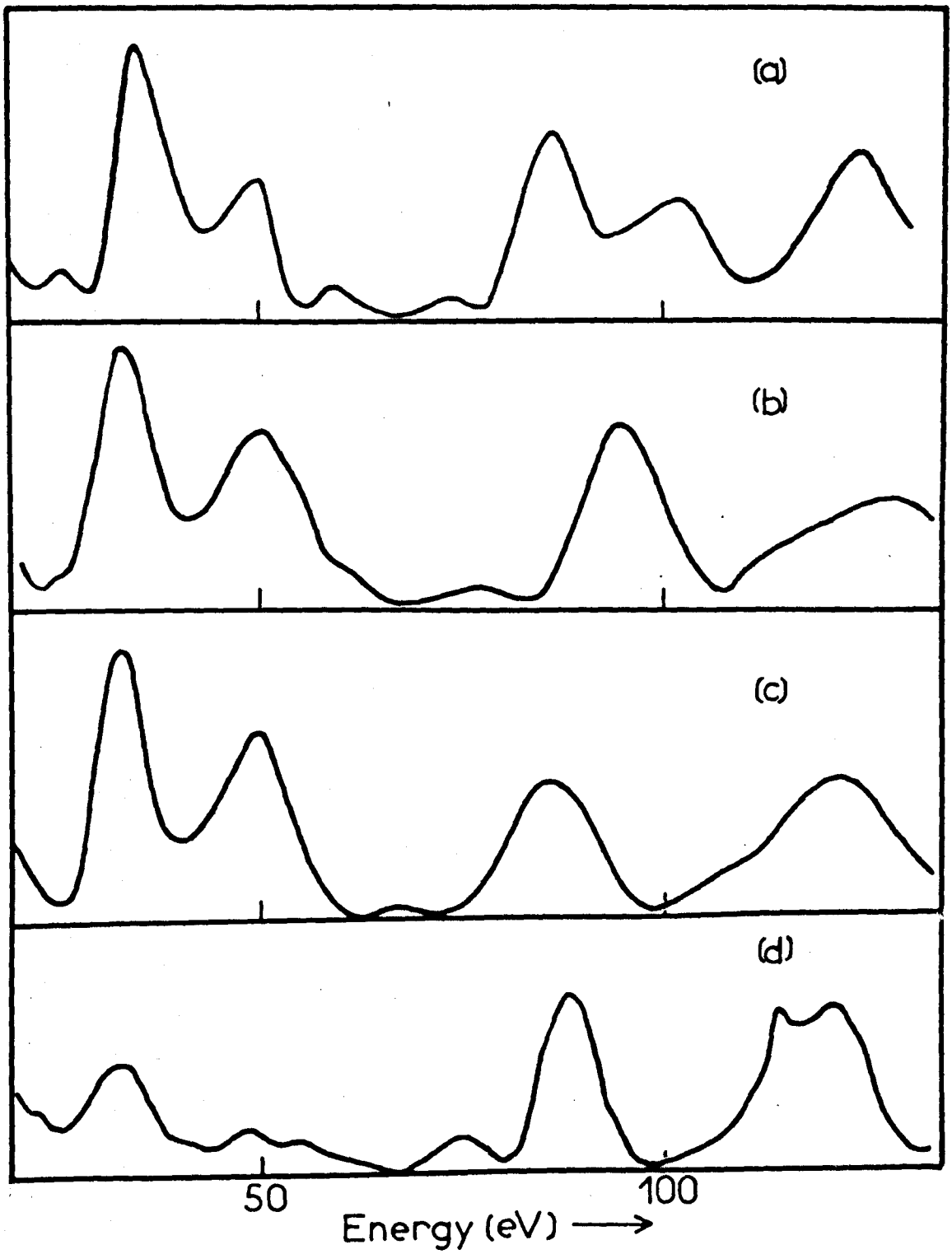
(a)
(b)
(c)
(d)
50
100
Energy (eV) ⟶

panels) and compare these with our result at 6° incidence (top panel). Here, we have extrapolated this curve to 0°K in the manner described in the following chapter, and normalised the peak at 35eV to the peak at 34eV in curve (c). The two 6° curves, (a) and (b), agree well in their principle features, especially below about 80eV. However, in this work, between 80 and 105eV there appears a doublet rather than the single peak shown in (b).

The bottom panel of this figure shows the results of Capart's normal incidence calculation[13], which includes an inner potential correction of 15eV. Comparing this curve with both Andersson's 3° curve and his 6° curve, there does not appear to be much difference in the agreement of the calculated curve with either of the measured curves, so it is justifiable for us to compare our 6° curve with the theory. Making due allowance for the difference in angle of incidence and azimuth, and ignoring the large peak at 100eV in our results, which may be simply an azimuthal effect, the agreement with Capart's calculation appears to be no better and no worse than with the data of Andersson. However, before meaningful comparisons can be made, calculations at non-normal incidence in both azimuths are required.

Figure 5.2-13 is a double logarithmic plot of the peak width at half height against energy for several selected peaks in the intensity-energy spectra - selected to be those which are not obviously composed of two or more unresolved peaks. The values are somewhat scattered as is generally found to be the case, but a least squares fit to the data is shown as a straight line of slope (0.63 ± 0.06). This value is rather higher than the more usual value of 0.5[5,14], but is still well below

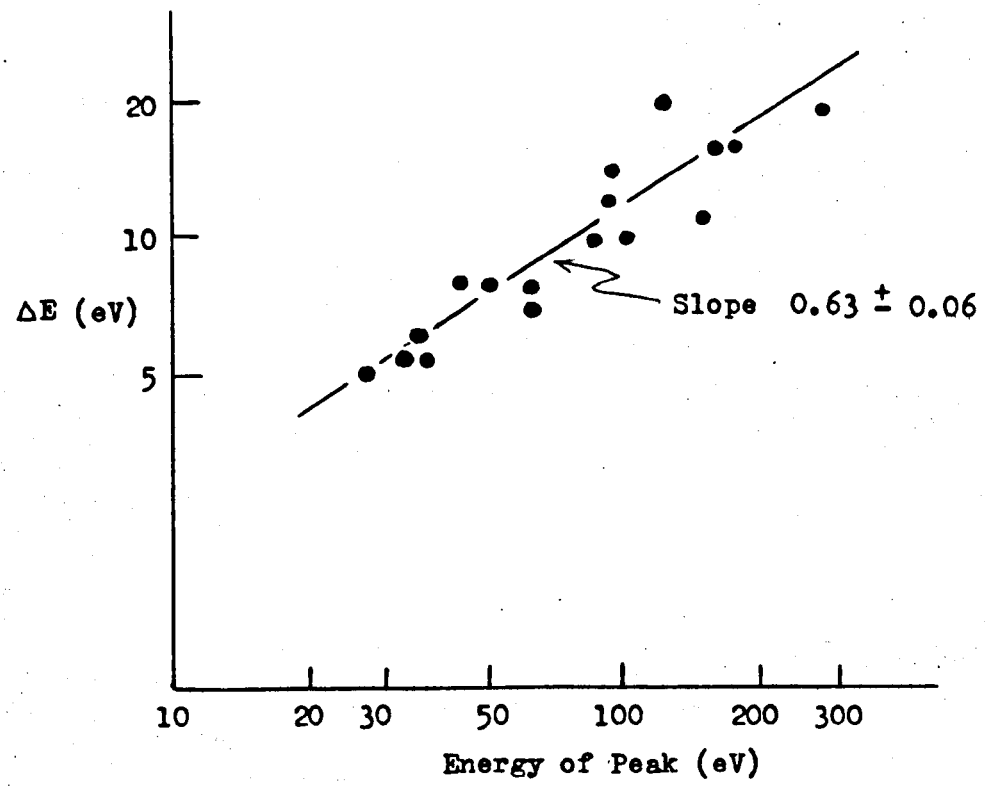

Figure 5.2-13.

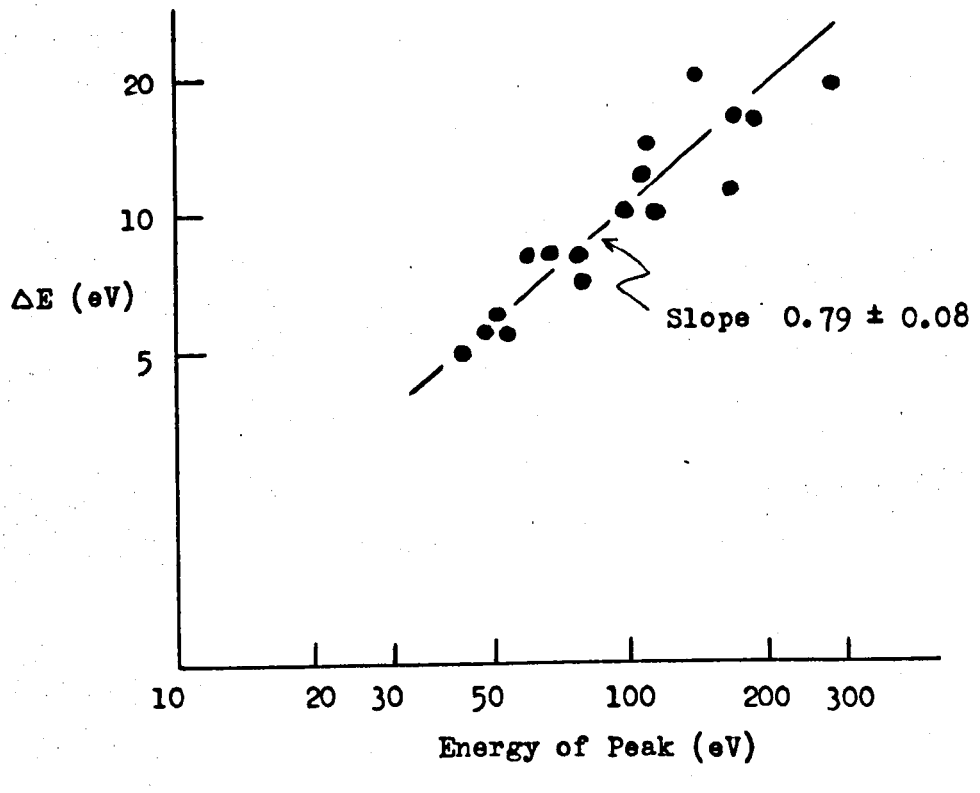

Figure 5.2-14.

Figure 5.2-13. Double logarithmic plot of the width of diffraction peaks measured at half height, ΔE, against peak energy. No inner potential correction has been made.

Figure 5.2-14. As the above Figure, but with an inner potential correction of 15eV added.

that obtained by Heine and Pendry[15] - 0.75 - by a theoretical argument. Addition of a mean inner potential of 15eV to the data, however, increases this slope to (0.79 ± 0.08) - much higher than any other reported value, as shown in Figure 5.2-14.

5.3 - The (111) Surface

As was the case with the (100) surface, the (111) surface was easily cleaned, and within the limits of our definition of cleanliness, remained clean in a vacuum of 10^{-10}T. for many days. This lower reactivity of the (111) surface compared to the (100) surface is in agreement with the results of Simmons *et al*[7] on the initial oxidation of these surfaces, and the generally low reactivity of the surface is comparable with Seah's observations on (111) silver[2].

The diffraction pattern (Figure 5.3-1) revealed the crystal to be oriented in a $\langle 11\bar{2} \rangle$ azimuth (Fig. 5.3-2). The results obtained for this surface are rather less detailed than those for the (100) surface, and the complete intensity-energy spectrum is shown in Figure 5.3-3. Spectra here are taken in the range 20 - 350eV in the range of angles 6 - 22° in 2° steps. The spectra are replotted in $\underline{k}$-space in Figure 5.3-4.

As Woodruff and Seah[16] noted previously, major peaks in the spectrum can be brought into coincidence with the Bragg zone lines (222), (555) and (666) by the applications of suitable inner potential corrections, which are listed in Table 5.3. Other major peaks lie just below the (333) and (444) zone lines, but those below the (333) zone line are much dispersed,

Figure 5.3-1. LEED pattern from the (111) surface of copper taken with electrons of energy 69eV at normal incidence.

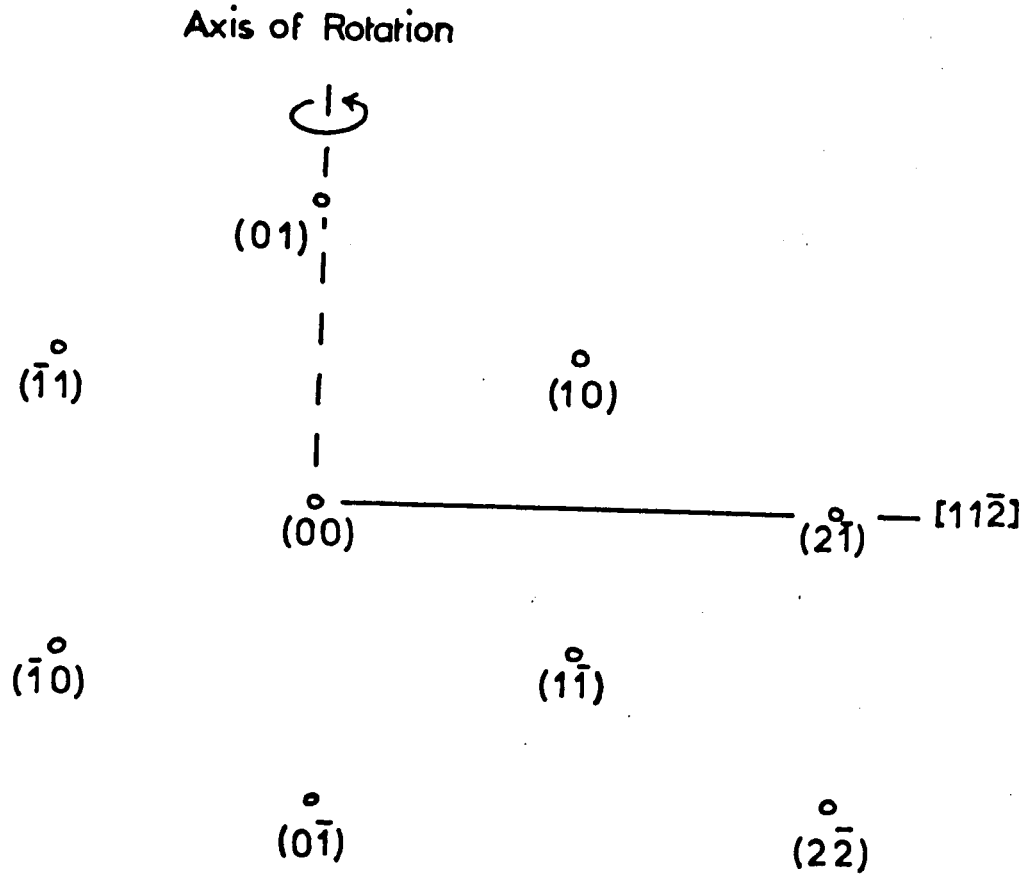

Figure 5.3-2. Definitions of the co-ordinates of the non-specular diffraction beams and of the surface azimuths for the (111) surface.

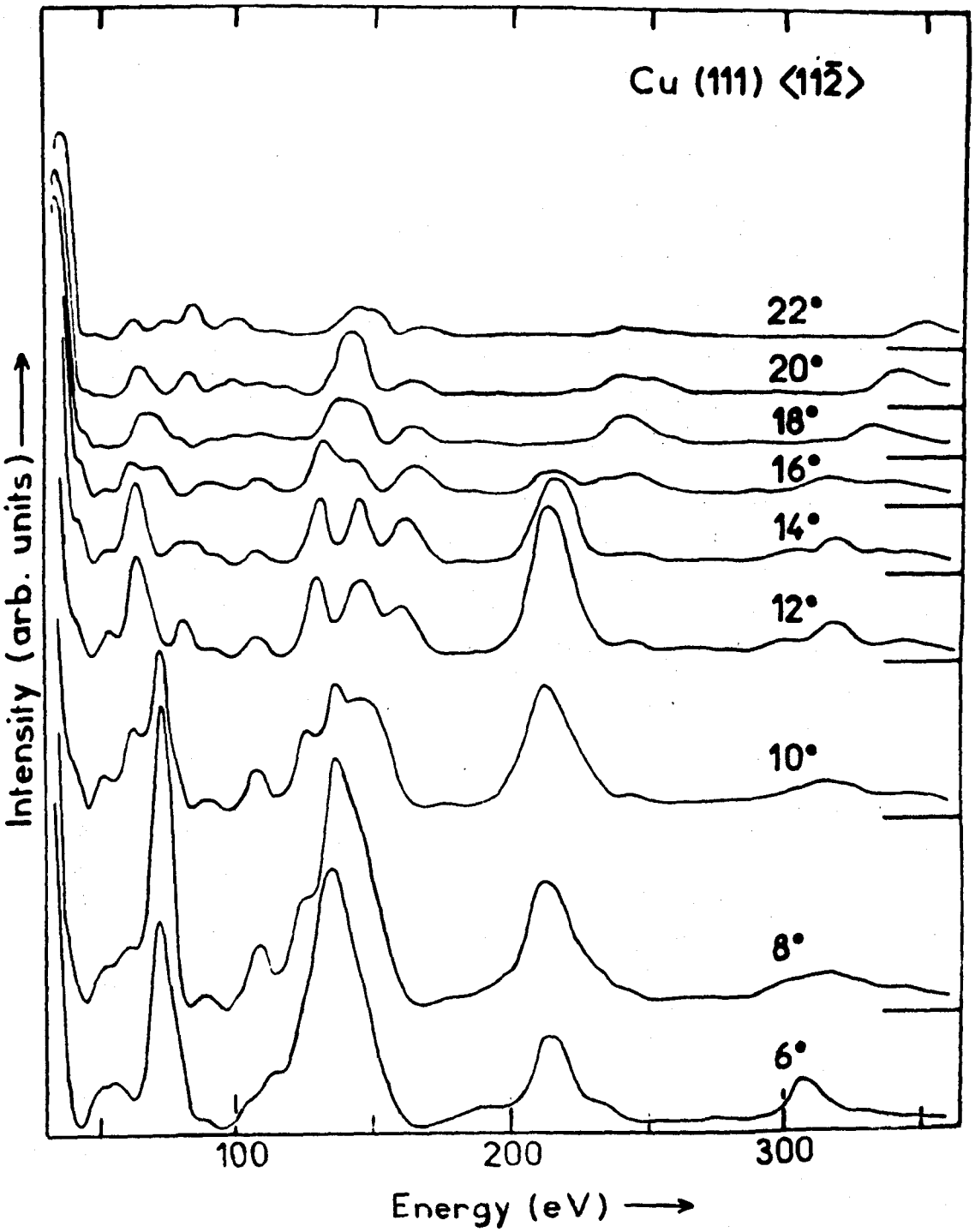
Cu (111) ⟨11$\bar{2}$⟩
22°
20°
18°
16°
14°
12°
10°
8°
6°
Intensity (arb. units) ⟶
100
200
300
Energy (eV) ⟶

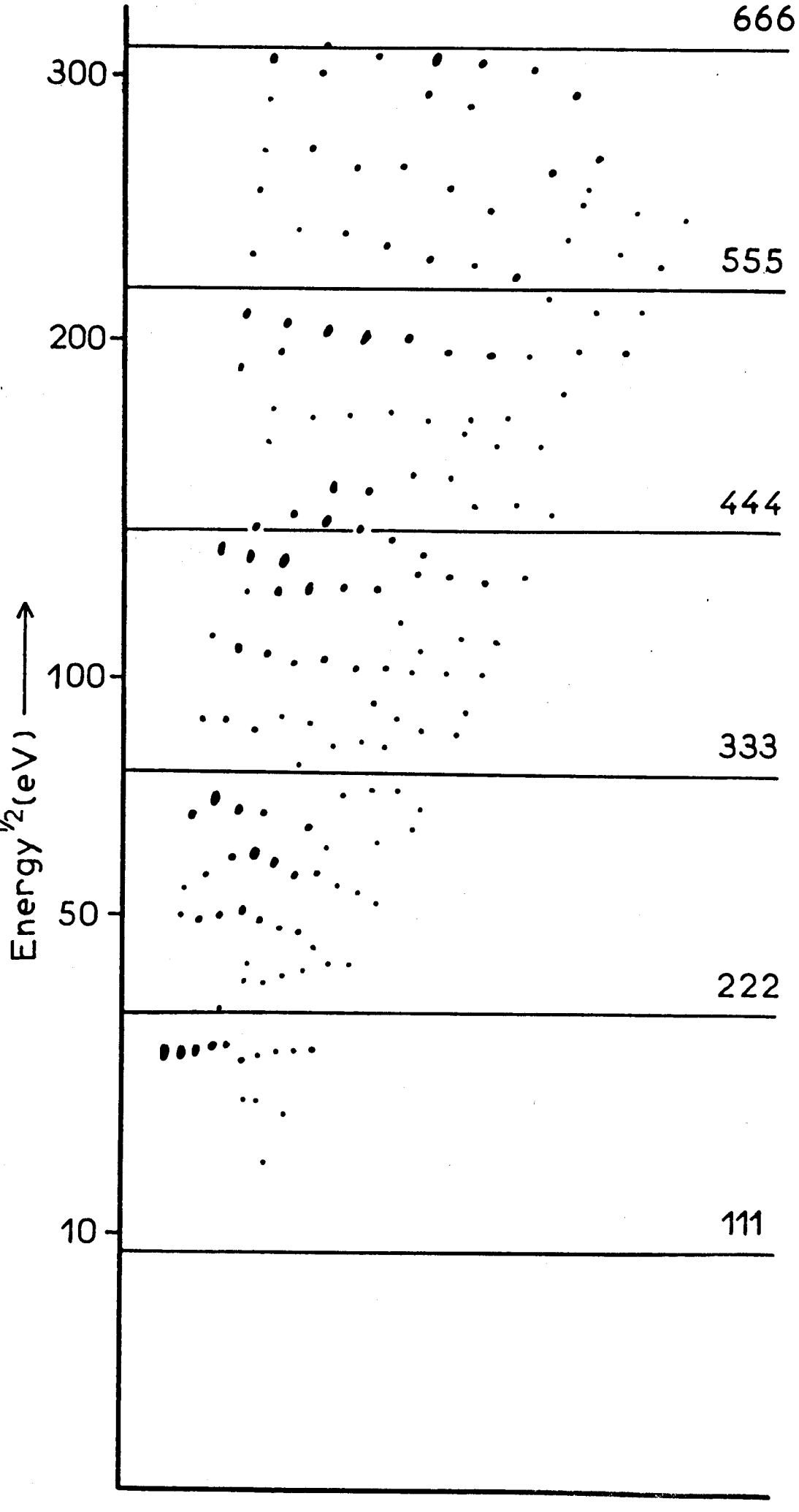
666
555
444
333
222
111
300
200
100
50
10
Energy $^{1/2}$(eV)

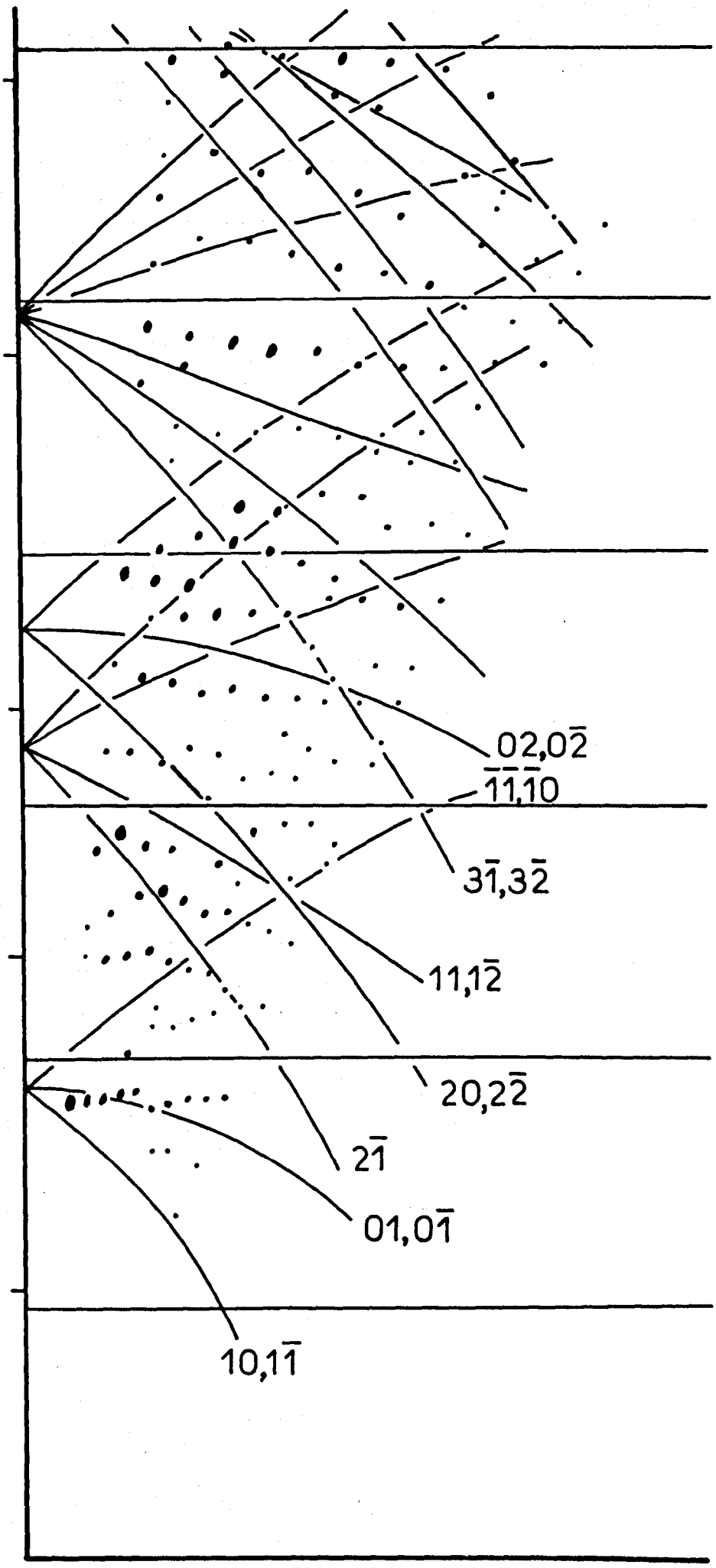
02,0$\bar{2}$
$\bar{1}\bar{1}$,10
3$\bar{1}$,3$\bar{2}$
11,1$\bar{2}$
20,2$\bar{2}$
2$\bar{1}$
01,0$\bar{1}$
10,1$\bar{1}$

TABLE 5.3

Nominal Bragg Peak	Inner Potential (eV)
222	8
333	12
444	18
555	10
666	5

Inner Potentials for Nominal Bragg Peaks from Cu(111)

and those below the (444) zone line lie on several loci. However, plausible inner potentials are listed for these peaks in the Table. It is of interest to note that for this surface, the required correction does not increase monotonically with energy, but passes through a maximum value, in contrast to the behaviour for the (100) surface. The detailed inner potentials, however, for any given peak exhibit the same type of behaviour as those obtained for the (100) surface.

The k-space plot is redrawn in Figure 5.3-5 with the beam emergence conditions superimposed. For this surface, no strong correlations are revealed, but the kink in the nominal (222) Bragg peak lies near the $01,0\bar{1}$ emergence, and the dispersed (333) and (444) nominal Bragg peaks lie in regions where many emergences intersect.

As yet, no detailed calculations on the (111) surface have been performed, so no comparisons are possible. The results presented here are, however, in good agreement with the results of other authors[6,7,8,16] insofar as comparisons can be made.

5.4 - The (110) Surface

In contrast to the other two low index surfaces, the (110) surface proved to be impossible to prepare in a clean state and to maintain in that state for any reasonable length of time in a vacuum in the high 10^{-10}T. range. A surface which had been argon ion bombarded for some time so that it exhibited only "clean" diffraction spots, but had not been annealed, gave, in point of fact, reasonably sharp diffraction spots. In less than one

hour, however, streaks appeared between the diffraction spots, parallel to the $\langle 1\bar{1}0 \rangle$ direction in the crystal surface. After two hours, these streaks became very prominent, and gradually became most intense around the positions of the half order spots (Fig. 5.4-1). As these half order spots became more intense, the streaks grew fainter, until, after 24 hours or so, the diffraction pattern consisted solely of the "clean" diffraction spots and the half order spots, with little or no streaking between them, indicating that a (2 x 1) adsorption structure had been formed over a substantial portion of the crystal surface. If the crystal were annealed for a short time after the end of the bombardment, e.g. for 15 minutes at 550°C., the streaking became visible after a slightly shorter period of time than was the case for the unannealed specimen. The overall behaviour was not, however, significantly different. Figure 5.4-2 shows a sequence of such diffraction patterns.

This much higher reactivity of the (110) surface compared to the other two low index surfaces is in accord with the results of Simmons et al[7], who find a closely similar sequence of diffraction patterns on the initial oxidation of the (110) surface. They interpret the initial gas atom sticking as being due to random adsorption in the "troughs" in the (110) surface parallel to the $\langle 1\bar{1}0 \rangle$ direction, which destroys the periodicity of the surface along this direction. As more and more gas atoms pack into the troughs, sections become completely full of adsorbed atoms, restoring the local two-dimensional periodicity. Eventually, all the troughs are filled with gas atoms, arranged such that the periodicity of the adsorption structure is twice that of the clean surface structure along the $\langle 1\bar{1}0 \rangle$ direction.

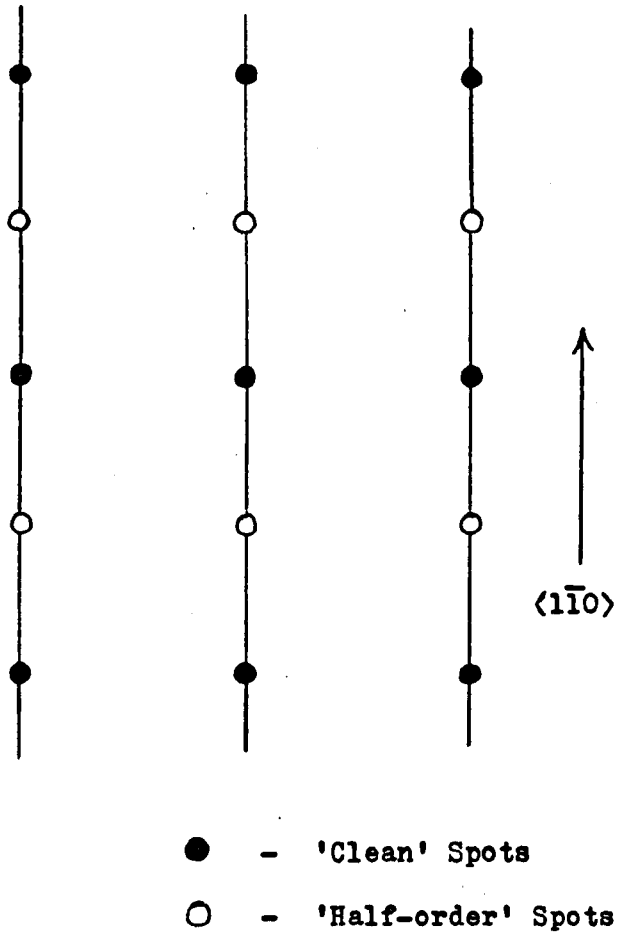

Figure 5.4-1. Sketch of the (110) copper surface diffraction pattern, showing the 'clean' surface diffraction spots (full circles), the 'half-order' contamination diffraction spots, and the streaking in the ⟨1$\bar{1}$0⟩ direction.

Figure 5.4-2 Sequence of diffraction patterns from the (110) surface of copper on adsorbing oxygen from the residual gases in the vacuum system at a total pressure of about 1×10^{-9} T.

(a) Initial pattern immediately after the end of argon ion bombardment. Energy 48eV.

(b) After 2½ hours. Energy 57eV.

(c) After 5 hours. Energy 72eV.

(d) After 24 hours. Energy 51eV.

(e) After 25 hours. The specimen has been flashed to a temperature of 500°C and allowed to cool. Energy 68eV.

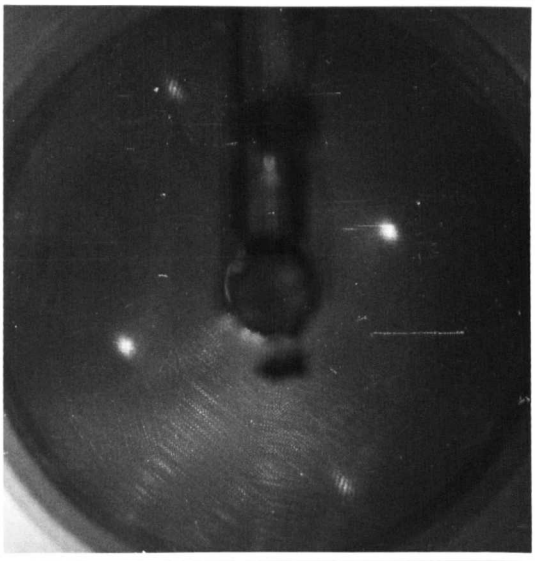

(a)

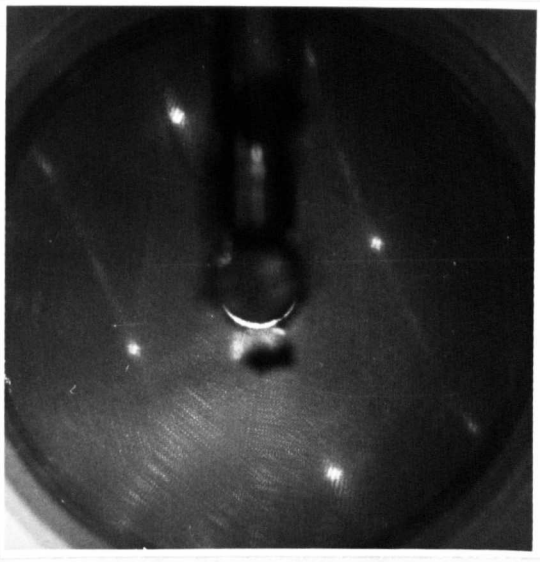

(b)

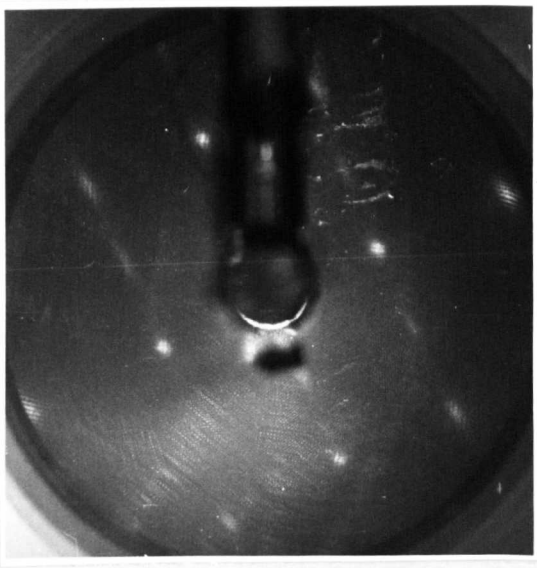

(c)

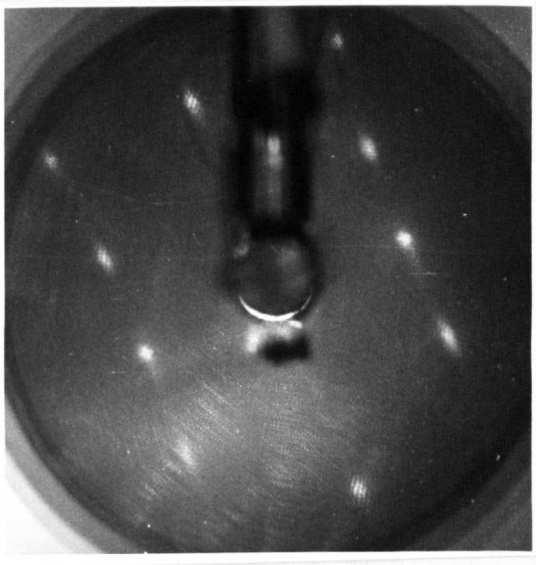

(d)

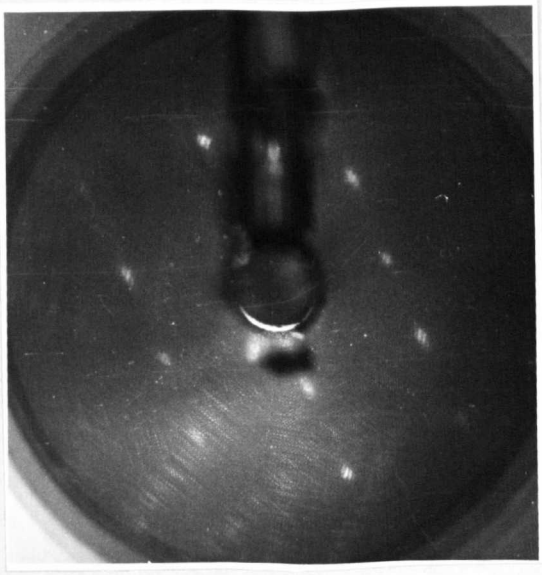

(e)

The (110) surface is known to adsorb little of the common vacuum residual gases apart from oxygen[17] and atomic hydrogen[18]. The contamination rate is apparently unaffected when there are no hot filaments present in the vacuum system, which eliminates dissociation of CO or CO_2 on the surface by the electron beam, so we therefore conclude that the surface is being oxidised.

Auger Electron Spectroscopy, however, failed to detect any oxygen on the surface. However, the overall sensitivity of the system was rather low, since at this time, the exciting beam was at normal incidence and the beam current had fallen to about 0.1μA. It is not impossible therefore that oxygen was in fact present.

Simmons et al[7] find that the onset of streaking is associated with oxygen exposures of 3×10^{-10}T-min. and the (2 x 1) structure with an exposure of 2×10^{-5}T-min. If we assume these figures, the required partial pressure of oxygen in the vacuum system is such that the residual gas would be virtually pure oxygen! It would therefore appear that the reactivity of the clean (110) copper surface is rather higher than Simmons et al suggest. Indeed, if we assume that after 24 hours the (2 x 1) structure is complete (i.e. it forms a complete half monolayer over the entire surface), a unity sticking coefficient requires a partial pressure of oxygen of 5×10^{-12}T. i.e. about five parts of oxygen per thousand of residual gas. This is probably a reasonable value, so we assume that the sticking coefficient of oxygen on clean Cu(110) is high, probably near unity. This value should not be taken too seriously, however, since detailed measurements of coverage and exposure times were not made.

Because of the high reactivity, no intensity-energy spectra for the (110) surface are presented, since no satisfactory definition of cleanliness could be achieved. For the same reason, results in Chapter 6 are confined to the (100) and (111) surfaces.

5.5 - Conclusions

Results presented in this chapter for the low index surface of copper show that the relative reactivities of each of these surfaces with the residual gases of the vacuum may be represented by the inequality

$$(110) \gg (100) \gg (111)$$

within the limits of the definition of cleanliness and contamination used here.

Detailed measurements of the intensity-energy spectra of the specular LEED beam from the (100) and (111) surfaces show that the major features of the spectra lie near the nominal Bragg conditions, as is to be expected in the light of the recent theoretical discussions of Tucker and Duke[19], but that the detailed structure is complex. Although certain inner potential corrections have been tabulated, these vary not only with energy, but, using the simplest and usually assumed definition of inner potential, with angle of incidence. Such a situation is clearly not very satisfactory, so what physical significance should be attached to these figures is far from clear. However, some of the deviations from "simple" behaviour in some of the nominal Bragg peaks may be correlated in some way with the emergence of new diffraction beams.

Comparison with theory for copper can not, as yet, be very extensive, since only one normal incidence calculation has been reported. The more general theoretical discussions of LEED so far published have been restricted to s-wave scatterers. For an element like copper, however, the higher order phase shifts are expected to be of importance. Where a comparison can be made, the agreement is not, as yet, complete.

REFERENCES

1) E.G. McRae and C.W. Caldwell, Surface Science 2 (1964), 509.

2) M.P. Seah, Surface Science 17 (1969), 181.

3) M.G. Lagally, Z. Naturforsh. 25a (1970), 1567.

4) F. Jona, I.B.M.J.Res.& Dev. 14 (1970), 444.

5) S. Andersson, Surface Science 18 (1969), 325.

6) N.J. Taylor, Surface Science 4 (1966), 161.

7) G.W. Simmons, D.F. Mitchell and K.R. Lawless, Surface Science 8 (1967), 130.

8) I. Marklund, S. Andersson and J. Martinsson, Arkiv för Fysik 37 (1968), 127.

9) D.P. Woodruff and B.W. Holland, Phys. Lett, 31A (1970), 207.

10) J.M. Charlot and R. Degeilh, C.R.Acad.Sci.Paris 259B (1964), 2977.

11) E.G. McRae, J. Chem. Phys. 45 (1966), 3258.

12) B.W. Holland, R.W. Hannum and A.M. Gibbons, Surface Science 25 (1971), 567.

13) G. Capart, Surface Science 26 (1971), 429.

14) R.M. Stern and F. Balibar, Phys.Rev.Lett. 25 (1970), 1328.

15) V. Heine and J.B. Pendry, Phys.Rev.Lett. 22 (1969), 1003.

16) D.P. Woodruff and M.P. Seah, Phys.Stat.Sol.(a) 1 (1970), 429.

17) T.A. Delchar, private communication.

18) B.M.W. Trapnell, Proc. Roy. Soc. A218 (1953), 566.

19) C.W. Tucker and C.B. Duke, Surface Science 24 (1971), 31.

CHAPTER 6

THE EFFECTS OF TEMPERATURE ON THE LEED PROCESS

6.1 - Introduction

Until recently, the full importance of the effects of temperature on the LEED process was not fully appreciated. Several authors[1-32] have discussed the various effects to be expected, but no systematic, reasonably complete study has been reported.

Temperature can affect the LEED process both as regards the geometry of the diffraction pattern, and the profiles of the intensity-energy spectra. The former effect is not a fundamental property of the diffraction process itself, but reflects changes in the physical structure of the surface under study i.e. it is caused by temperature induced phase changes, adsorption or desorption of impurities, etc. Such effects have been studied in detail by Goodman[18]. In the work reported here, once a "clean" surface had been obtained, no changes in the geometry of the diffraction pattern were observed on heating the specimen, and so such effects will not be further discussed here.

Changes in the profiles of the intensity-energy spectra are a fundamental effect of the thermal vibrations of the atoms of the crystal lattice on the detailed mechanism of the diffraction process, and form the main point of interest of the remainder of this chapter.

There are three basic effects to be discussed in this context, namely changes in intensity of the diffraction peaks, changes in the shape and width of diffraction peaks and changes in the position of these peaks.

The bulk of the literature has been concerned with the change in intensity of diffraction peaks with temperature, in particular for those peaks which occur on or near kinematical Bragg scattering conditions. The early work (e.g. references 2,6,7) demonstrated that the intensities of such diffraction peaks had an exponential temperature dependence, and so attempts were made to relate this dependence to the Debye-Waller factor of X-ray diffraction, in order to extract values of $\langle u^2 \rangle$, the mean square amplitude of vibration of atoms at or near the crystal surface. From such values, it was hoped that information could be deduced about the interatomic potentials in the surface region of the crystal, by studying the effects of the free surface on the lattice dynamics of the crystal.

In the bulk of these studies, the authors selected only those peaks lying near the kinematical Bragg scattering conditions since it was felt that they had a reasonable idea of the scattering vector operative under such conditions. Little attention was paid to the temperature dependence of other peaks in the spectra, even to the extent of not checking if they too had an exponential temperature dependence. Indeed one author[4] explicitly states that he rejected from his data any peaks not displaying such a temperature dependence.

Only a few isolated studies of peak shapes and widths[20,26] and peak shifts[21,26,29] have been reported.

The undertaking of a detailed study of the effects of temperature on the profiles of intensity-energy spectra mapping out a relatively large area of k-space is therefore pertinent, and the results of such a study are reported in the subsequent sections of this chapter. The results presented refer to the intensity-energy spectra discussed in detail in the previous chapter.

6.2 - Debye-Waller Factors

6.2.1 - The Debye-Waller Factor

It may be shown (see Appendix A3) that in a single scattering model of electron diffraction, under a fairly restrictive set of approximations, the intensity, I, of an electron beam diffracted by a vibrating lattice may be represented by

$$I = I_o e^{-2W} \qquad (6.2 - 1)$$

where I_o is the intensity diffracted from the rigid lattice (i.e. the lattice at the absolute zero of temperature) and $2W$ is the Debye-Waller factor given by

$$2W = \frac{16\pi^2}{\lambda^2} \langle u^2 \rangle \cos^2 \theta \qquad (6.2 - 2)$$

where λ is the wavelength of the incident electrons

θ is the angle of incidence

and $\langle u^2 \rangle$ is the mean square displacement of the atoms of the lattice projected along the direction of the scattering vector apposite to the diffraction conditions operating i.e. the vector difference between the wave vectors of the incident and the scattered electrons.

If we assume that the phonon spectrum of the lattice may be adequately described by the Debye model, then, as is shown in Appendix A3, $\langle u^2 \rangle$ is given by

$$\langle u^2 \rangle = \frac{3\hbar^2 T}{M k_B \Theta_D^2} \qquad (6.2 - 3)$$

where Θ_D is the so-called Characteristic Debye Temperature of the lattice

M is the mass of the vibrating atoms

T is the absolute temperature of the lattice

and k_B is the Boltzmann Constant.

The various approximations used in the derivation of Equations 6.2-2 and 6.2-3 are discussed in Appendix A3, so it will suffice here to mention only the more important limitations on the validity of the expressions. Equation 6.2-2 has been derived on the assumption that the dynamics of the crystal lattice are adequately describable within the Harmonic approximation, and the expression for $\langle u^2 \rangle$ has been evaluated for a Debye phonon spectrum in the high temperature limit, i.e. for $T \gg \Theta_D$.

The important point to notice here is that a semilogarithmic plot of the intensity of a diffracted beam against temperature, i.e. a graph of ln I against T, should be linear where these two approximations remain valid. In fact Wallis *et al*[33] have shown that in numerical evaluations of the Debye-Waller factor within the harmonic approximation, the linearity of such graphs (which we shall call Debye plots) holds to within a good degree of accuracy down to temperatures as low as $\frac{1}{2}\Theta_D$.

The analysis used in the derivation of the Debye-Waller factor here explicitly makes the assumption that the lattice vibrations are isotropic in order that the summation over the phonon spectrum can be performed (Equation A3-9). This is of course only true provided that we are dealing with a completely isotropic lattice, i.e. a cubic Bravais lattice, well away from any perturbing influences such as a free surface. However, we make the *ad hoc* assumption that even in the non-isotropic environment of the surface region of a crystal we can decouple the components of the scalar product of the scattering vector and the eigenvectors of the dynamical matrix in such a way that the Debye-Waller factor is still governed by the amplitude of vibrations of the surface atoms projected along the scattering vector of the electrons. Equation A3-10 then shows that in principle we can then determine the ratios of the mean square amplitudes of vibration apposite to different diffraction processes by taking the ratio of the gradients of the two Debye plots, without making detailed assumptions as to the nature of the phonon spectrum involved.

Because we are dealing with this anisotropic surface region of the crystal, it is to be expected that the lattice vibrations themselves will be anisotropic. The amplitudes of vibration of atoms close to the surface will be such that the component of the amplitude along the surface normal direction will be somewhat greater than that of atoms in the bulk crystal. It is difficult to say *a priori* whether the tangential component (i.e. the component parallel to the surface) of such vibrations will be much altered, since this will depend on the precise nature of the exposed surface. For close-packed surfaces, not much difference would be expected, but for rather more open surface structures, the amplitudes may well be increased, but not to as great an extent as for the normal component.

Thus by considering the temperature variation of the intensities of beams of electrons scattered under different diffraction conditions, one could, in principle, arrive at values for the vibrations of the atoms at or near the surface in various directions in the crystal.

In the derivation of the beam intensity discussed above, it has been assumed that all the electrons which have been scattered off phonons in the crystal have been lost to the detection system, so that the expression for the intensity I is strictly the intensity of the residual, purely elastically scattered electrons. This component of the total scattered flux is often referred to as the zero phonon component of the electrons scattered to the appropriate reciprocal net rod. In practice, however, the aperture of the spot photometer "sees" an appreciable area of the Brillouin zone around the reciprocal net rod, and the energy resolution of the grid filter system in front of the fluorescent screen is not good enough to reject the phonon scattered electrons. Thus the measured intensity will contain an appreciable amount of those electrons which have suffered phonon energy losses (and phonon energy gains), but have not suffered much momentum transfer parallel to the crystal surface. These phonon scattered electrons have been shown to peak in intensity at the reciprocal net rods[8,12], and will therefore give a background intensity which has to be subtracted from the measured peak intensities to leave the zero phonon component in which we are interested. This background correction will be discussed in more detail in a later section.

When considering the experimental values of peak intensities and their relative changes as the temperature of the specimen is changed, we have to make the assumption that the total decrease in the elastic component

of the scattered electrons is caused solely by the increase in the scattering of the electrons off the increased phonon density. In other words, if we include the phonon scattered electrons with the elastically scattered electrons in a pseudoelastic category, we assume that the total intensity of pseudoelastic electrons is independent of temperature. Barnes, Lagally and Webb[12] have demonstrated that this is plausible by collecting the total pseudoelastic flux over the entire Brillouin zone around a reciprocal net rod, and showing this to be independent of temperature. In actual fact, what they do is to collect the flux from areas which are respectively just greater than and just smaller than the Brillouin zone and showing that in the former case, the flux increases with temperature and in the latter case the flux decreases with temperature. They split the difference and conclude that the flux to the Brillouin zone is therefore temperature independent.

The assumption of the constancy of the pseudoelastic component of the scattered electrons is tantamount to assuming that the relative cross sections for pseudoelastic and inelastic scattering are temperature independent, so that the total inelastic component of the scattered intensity must be temperature independent. Data on this subject is somewhat sparse, but the indications are that it is indeed the case[34,35].

We therefore make the assumption that if we take the total pseudoelastic component of the scattered electrons at a fixed energy and temperature and subtract off the phonon scattered component, we are left with the genuine zero phonon component at that temperature.

It must be emphasised that the whole of the foregoing discussion on the Debye-Waller Factor and the sort of information that can be drawn from

experimentally determined values of such factors is based on the major assumption that the diffraction process is adequately describable on a single scattering model. As we have seen, however, it is by now well established that such a description is totally inadequate for discussing the origins of even the major features of LEED intensity-energy spectra. It is therefore pertinent at this point to see how the above discussion can be extended within the framework of a multiple scattering analysis of the problem, and to what extent it remains relevant.

Extension of the derivation of a Debye-Waller factor to a double[18] or even to a triple scattering model is relatively trivial, and can be shown to retain the exponential temperature dependence of the diffracted intensities. From the gradient of the Debye plot, we can derive an effective Debye temperature Θ_D^{eff} where this is then given by

$$\frac{\cos^2\theta}{\left\{\Theta_D^{eff}\right\}^2} = \sum_i \frac{\cos^2\theta_i}{\left\{\Theta_D^{i}\right\}^2} \qquad (6.2 - 4)$$

where $2\theta_i$ is the angle between the wave vectors of the incident and scattered electrons in the i th scattering event

2θ is the net scattering angle for the diffraction process considered

Θ_D^i is the Debye temperature appropriate to atomic vibrations projected along the scattering vector of the i th scattering event

and the i run over all possible scattering events which could contribute flux to the diffracted beam.

In a double or triple scattering analysis, this analysis could just about be tractable, and could yield reasonable values for the atomic vibrations

provided we can postulate a reasonably plausible diffraction scheme and make suitable guesses as to the way the atomic vibrations varied at the different scattering centres. However, when we go to a full multiple scattering analysis of the process, the summation in 6.2-4 goes over to an integration over all angles, and the integral just cannot be unfolded. In addition, there are certain other complicating factors which enter into the analysis which we cannot really discuss here, but they enter since the vibrating atoms create an anisotropic scattering centre, which means that the higher partial waves become relatively more important in the analysis.

Laramore and Duke[36] have recently incorporated thermal vibrations into the framework of their inelastic collision model of the LEED process, and have shown that in this analysis, the linearity of the Debye plots is preserved, but that it is virtually meaningless to try to extract values of atom vibrations from the gradients of the graphs, since these depend in a very sensitive way on the precise diffraction parameters involved.

What one can probably say, however, is that since in the final resort a multiple scattering series is simply a summation over a large number of single scattering events, then the lowest measured value of Debye temperature obtained for diffraction from any given surface sets an upper limit on the real value of the Debye temperature which would be obtained from a single scattering event with a surface atom such that the scattering vector is normal to the crystal surface, and hence sets a lower limit on the amplitude of the normal component of the surface atom vibrations.

What we will show in the experimental results presented later in this chapter is that any peak in the intensity-energy spectra studied here

has a linear Debye plot, and hence can be assigned an effective Debye temperature. Although such Debye temperatures cannot be used to extract values of such things as atomic vibrations according to the arguments presented in the above paragraphs, we will argue that they are a useful experimental parameter of the diffraction process. Detailed analyses of the variation of measured Debye temperatures with diffraction parameters will show that the kinematical and pseudokinematical arguments presented at the beginning of the section do not provide a suitable explanation of the results.

Before going on to discuss the experimental results, however, there is one further point to be considered. It is well known that the harmonic approximation for the dynamics of a crystal lattice is insufficient for discussing many of the properties of the lattice, e.g. in such a model, the lattice does not expand on heating. Maradudin and Flinn[37] have discussed the effects of including certain of the lower order anharmonic terms (the cubic and quartic terms) in the analysis of the effects of temperature on X-ray diffraction intensities. It is not necessary for us to discuss in detail the effects of the inclusion of such terms into the analysis, but it will suffice to note that the main effect is to cause the effective Debye temperature to decrease with increasing temperatures. Thus the Debye plot is linear at low temperatures, but gradually drops below this line at higher temperatures as the melting point of the crystal is approached. Although the X-ray diffraction intensities are evaluated in a kinematical analysis, intuitively one would expect that including anharmonic terms into a multiple scattering analysis of LEED intensities would lead to qualitatively similar effects. This deviation of the Debye plot from linearity at high temperatures is well known experimentally in X-ray diffraction[38].

6.2.2 - Experimental Techniques

In much of the previous work in determining LEED Debye temperatures, the procedure has been to "tune" the system such that the diffraction conditions of the incident electron beam were such as to give rise to a peak in the intensity of the scattered beam near an expected kinematical Bragg peak at room temperature and then to monitor the intensity of that peak as a function of temperature at that constant energy. However, as Woodruff and Seah[21] have pointed out, the position of a diffraction maximum in energy space tends to change as the temperature of the sample changes, and so this procedure leads to exaggerated values of the gradient of Debye plots, with consequent lowering of the values of the derived Debye temperatures. Typically, underestimates in the value of Debye temperatures obtained in this way are of the order of 10%. In addition, utilising this procedure automatically throws away the information which can be obtained about the shifts of diffraction maxima with temperature, and any changes in the peak widths and shapes which may occur.

Ideally, what one wants to do is to take series of intensity-energy spectra while the crystal is held at various constant temperatures. It is difficult, however, to devise a form of specimen heater which gives no residual magnetic field at the specimen during the heating operation, and still allows the usual measurements to be made on the LEED beams. Any form of electrical heating gives some magnetic field at or near the specimen, which will distort the electron trajectories near the surface. Electron bombardment heating requires large electrical fields near the specimen, again distorting the low energy electron trajectories. Infra-red heating is difficult to achieve while still permitting use of the spot photometer to measure the diffracted intensities. Tracy[39] has

described a device which uses pulsed heating currents and blanks off the LEED pattern during these pulses by applying a synchronised negative going blanking pulse to the analyser grid of the LEED optics. No such device was available to us during the course of the work described here, and so the simple procedure described below was adopted.

The specimen was heated to a reasonably high temperature (600-700°C) in the simple hot stage described earlier, and the heater current switched off. A rapid series of intensity-energy spectra restricted to a limited range of energy at a fixed angle of incidence were taken, always scanning the energy in a fixed direction (i.e. always increasing or always decreasing the energy across the energy range of interest in any given set of results) and noting the temperatures at spot marks along the curves. Since the mass of the specimen plus specimen holder is relatively large, the specimen took quite some time ($\sim$1 hour) to cool from 600°C. to room temperature and so quite a large number of spectra could be taken during any one cooling cycle, giving a reasonable number of data points in any one Debye plot. In practice, because of the inordinately long time a specimen could take to cool through the last part of the temperature range, most runs were terminated at about 50°C above room temperature. The whole procedure was then repeated scanning the energy in the opposite direction, so that by taking the mean of the two sets of results, effects due to the variation of temperature across any one intensity-energy spectrum could be eliminated. Intensity-energy spectra at room temperature taken before and after such runs were identical for "clean" specimens, showing that adsorption during the run was negligible. A Xerox copy of a typical set of "raw" data obtained during one such run is shown in Figure 6.2-1.

Figure 6.2-1 Xerox copy of a typical set of temperature-dependent intensity-energy spectra as plotted directly on the X-Y recorder. The figures noted against various points on the traces give the temperature at these points in millivolts as indicated by the chromel-alumel thermocouple. The base line of each successive trace is displaced vertically by a known amount.

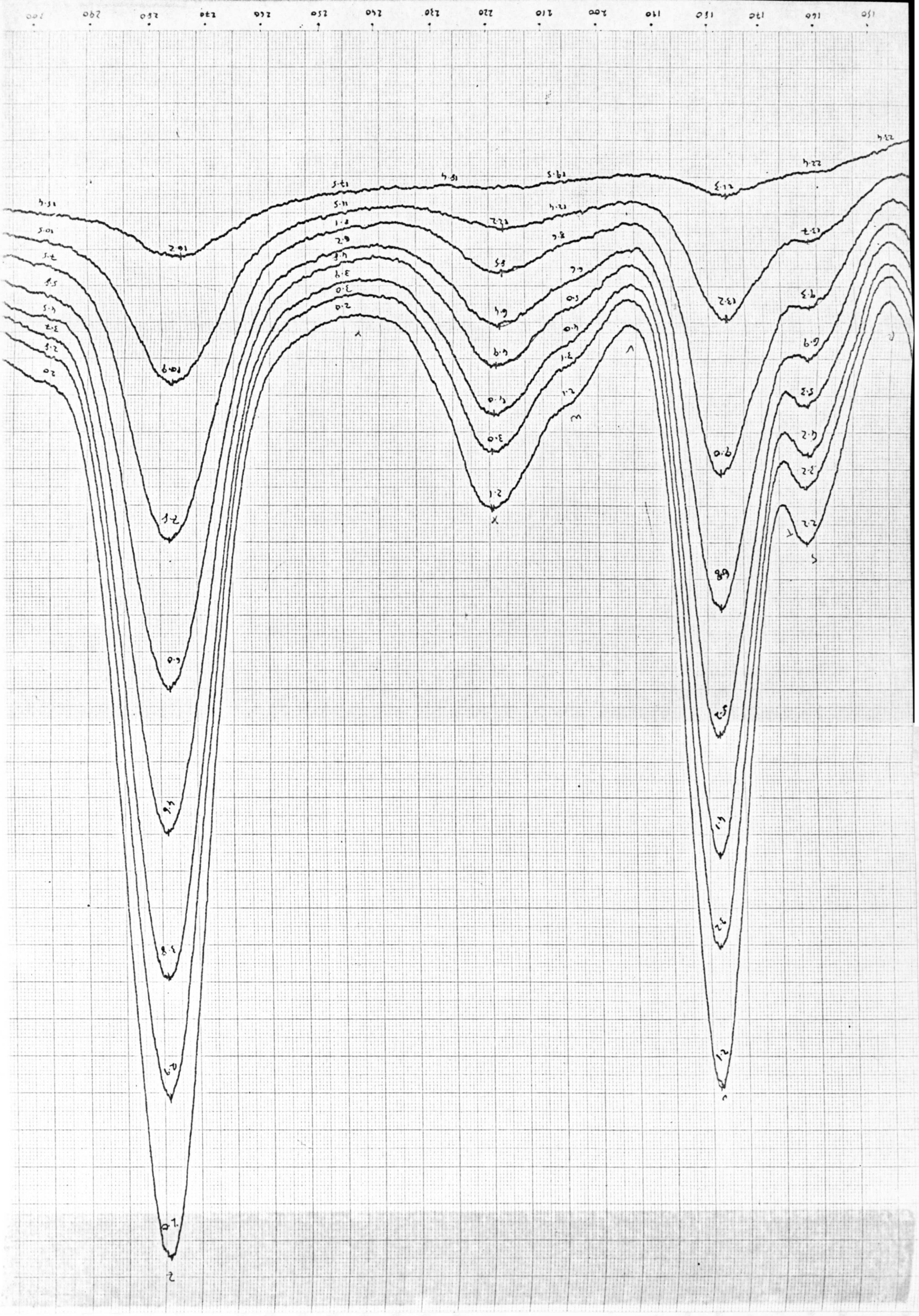

By repeating this procedure for various fixed ranges of energy at various angles of incidence, a complete picture of the effects of temperature on the entire intensity-energy spectrum for the specular beam from the two surfaces under study was built up.

This procedure is fairly straightforward when we are dealing with the specular beam which does not move with changing energy, as the spot photometer can be set up on the beam at room temperature and then left in position for the entire run - changes in beam direction due to warping of the specimen holder as it heats up, etc., were found to be negligible in practice and easily detectable in the few cases where they did occur. However, extension of the technique to the non-specular beams which do move with changing energy is well-nigh impossible, and so in the work which is reported here, results are confined entirely to the specular beam.

6.2.3 - Subtraction of Backgrounds from Diffraction Intensities

Before proceeding to discuss the measured values of Debye temperatures in detail, we must return to the consideration of the removal of the background intensity from the measured diffraction intensities. That such a correction is necessary is shown in Figure 6.2-2, where the upper trace is the uncorrected diffraction intensity of one particular diffraction peak, and it will be seen to tend towards a constant value at high temperatures.

The background intensity arises from two distinct sources, firstly due to those electrons which have scattered off phonons in the crystal lattice

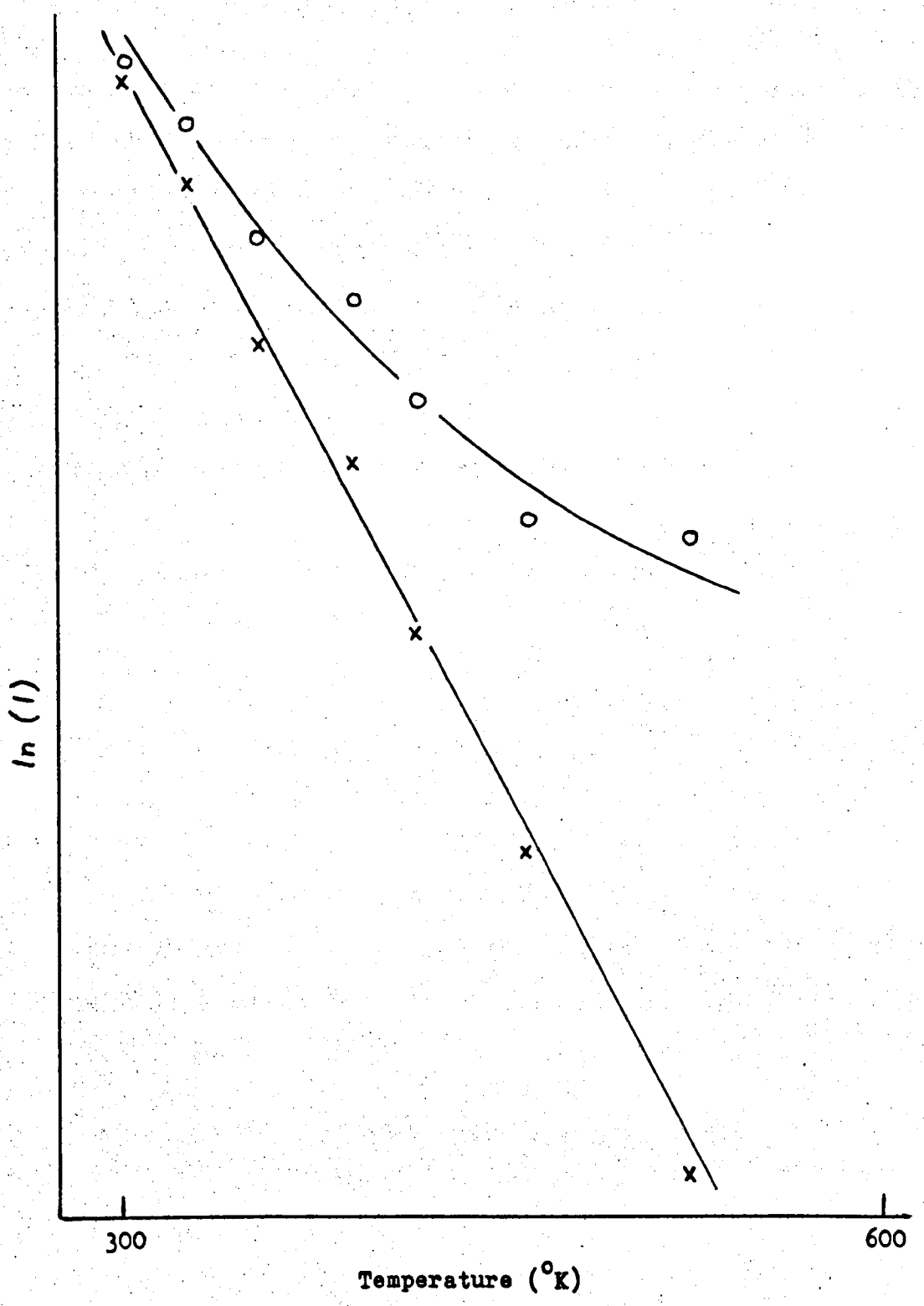

Figure 6.2-2. Debye plot for a peak at 310eV in the Intensity-Energy Spectrum for Cu(111). The open circles are the intensities of the diffraction peak with no background correction, and the crosses are the intensities corrected for a background in the manner described in the text.

but have not experienced sufficient momentum transfer parallel to the crystal surface to remove them from the acceptance circle of the spot photometer, and secondly due to those electrons which have been incoherently scattered from the disorder, defects and impurities which are of necessity found in a real crystal surface. The phonon scattered electrons give rise to a background which is both energy and temperature dependent[8], increasing as both these parameters increase, and the incoherent electrons give a background which is energy dependent but temperature independent to first order[26] in a well annealed specimen. In general, for a good crystal surface as carefully prepared as these specimens were, the phonon scattered background would be expected to be predominant.

Two distinct approaches have been used to assess the required background correction. The first approach is essentially empirical and was widely used in the early work on deriving LEED surface Debye temperatures. It consists of determining by trial and error that subtraction which must be applied to the experimental data points to give a linear Debye plot[4,5,6]. Obviously, there must be some limitation placed on the way in which this correction is assessed, so it is often assumed that the temperature dependence of the phonon background is weak enough for a temperature independent background to be subtracted[4]. This approximation has been shown to introduce an error of only about 2% into the derived value of the Debye temperature[26]. This method, however, suffers from the disadvantage that it essentially begs the question of demonstrating the linearity of the Debye plots.

The second approach has been to make an experimental estimate of the background correction required. This can then take into account even

highly temperature dependent background corrections. Two distinct ways of making this experimental estimate have been used. That due to Wilson[24,28] involves moving the spot photometer just off the diffraction spot and measuring the intensity at that point. The disadvantage of this method is that the spatial distribution of the phonon scattered electrons across the Brillouin zone is not uniform, and has been shown to peak at the reciprocal net rods[8,12], so the measured intensity just off the diffraction spot provides an underestimate of the phonon intensity in the diffraction spot. This is not too serious an inaccuracy, however, and will be within the other experimental errors. However, to obtain the correct energy and temperature dependence of the background involves making measurements of the intensity both on and off the spot as both these parameters are varied, so a constant specimen temperature is really required during each set of measurements. Woodruff and Seah have demonstrated[26] that a sensible value of the background correction for any given diffraction peak can be derived from the temperature dependent intensity-energy spectra themselves, by taking the intensity of the nearest "deep" valley in the spectrum as the datum level for measuring the intensity of that peak at that temperature. This essentially assumes that all the intensity in these valleys is of phonon scattered origin together with the incoherently scattered electrons. This is shown not to be strictly true in the calculations of LEED spectra which take inelastic scattering into account, where intensity is nearly always present at all points along the reciprocal net rods, even at $0^{\circ}K$. In addition, if we may anticipate the discussion of the experimental results, the examination of several hundred such valleys in the intensity-energy spectra has failed to reveal any in which the intensity increases with temperature as a genuine phonon scattered intensity would. Although many such valleys are of constant

intensity, the majority in fact decrease with temperature in a way comparable to the diffraction peaks themselves. We are therefore over-correcting for the background by using this method, and subtracting off some of the proper multiply scattered elastic component of the intensity. However, if the intensity in the valley is small compared to the peak under consideration, the error introduced is small. The precise extent of this overcorrection is rather difficult to estimate, since it will vary with both the ratio of phonon scattered electrons in the background to the multiply scattered elastic electrons and to other background electrons and also with the ratio of the background intensity to the intensity of the peak under study. Generally, however, it will be no greater than of the order of 2-3%. The fact that we are also subtracting the background appropriate to an energy different from that of the peak is likewise not too serious, since the phonon scattering is a relatively weak function of the energy[5,8], and one can usually find a "deep" valley at an energy fairly close to the peak energy. This therefore is the method adopted in this work.

Experimentally, it is found that a background correction must be applied to all diffraction peaks above about 75eV. Below this energy, however, when we consider the temperature dependence of intense diffraction peaks - and the most intense peaks are generally to be found in this energy region - the background correction may be small, and a negligible difference in the slope of the Debye plot may be caused by its inclusion. Nevertheless, even in this energy range, the correction is still important for the less intense peaks, where the background may be a significant fraction of the intensity in the diffraction peak.

6.2.4 - Measured Debye Temperatures For Cu(100)

Although the detailed results obtained in the course of the experimental work involved in the studies reported in this thesis comprise many traces of the type illustrated in Figure 6.2-1 and many more Debye plots derived from them, it would be unproductive to reproduce all of these in detail here. Figures 6.2-1 amd 6.2-3 are therefore presented as being reasonably typical examples of respectively the "raw" experimental data and the type of Debye plot which can be derived from such series of temperature dependent intensity-energy spectra. The two Debye plots reproduced in Figure 6.2-3 illustrate the general features of the Debye plots which can be derived for all peaks in the intensity-energy spectra, for those which might be classified as nominal Bragg peaks and for those which lie well away from the kinematical Bragg scattering conditions. They will serve to illustrate one or two general points which we can discuss in a qualitative manner before turning to a detailed discussion of the specific results.

Figure 6.2-3(a) is typical of the type of Debye plot obtained for a low energy diffraction peak, in this case, one at 40eV. The semilogarithmic plot of intensity against temperature is a reasonable fit to a straight line for temperatures below about 700°K. Above this sort of temperature, however, the measured intensity drops off more rapidly than the linear dependence would predict. That such deviations from linearity are not simply the result of the application of an overcorrection for background intensity discussed earlier is demonstrated by the fact that such effects are most prominent for the low energy diffraction peaks for which little or no background correction is required. As we discussed earlier, this is the type of behaviour which can be associated with the onset of significant effects of the anharmonic terms in the force constants of the

Figure 6.2-3 Debye plots i.e. graphs of the logarithm of the intensity of a diffraction peak as a function of temperature for diffraction peaks at (a) 40eV and (b) 181eV in the intensity-energy spectrum of the specular LEED beam from the (100) surface of Copper. The departure from linearity of the plot for the lower energy peak is discussed in the text.

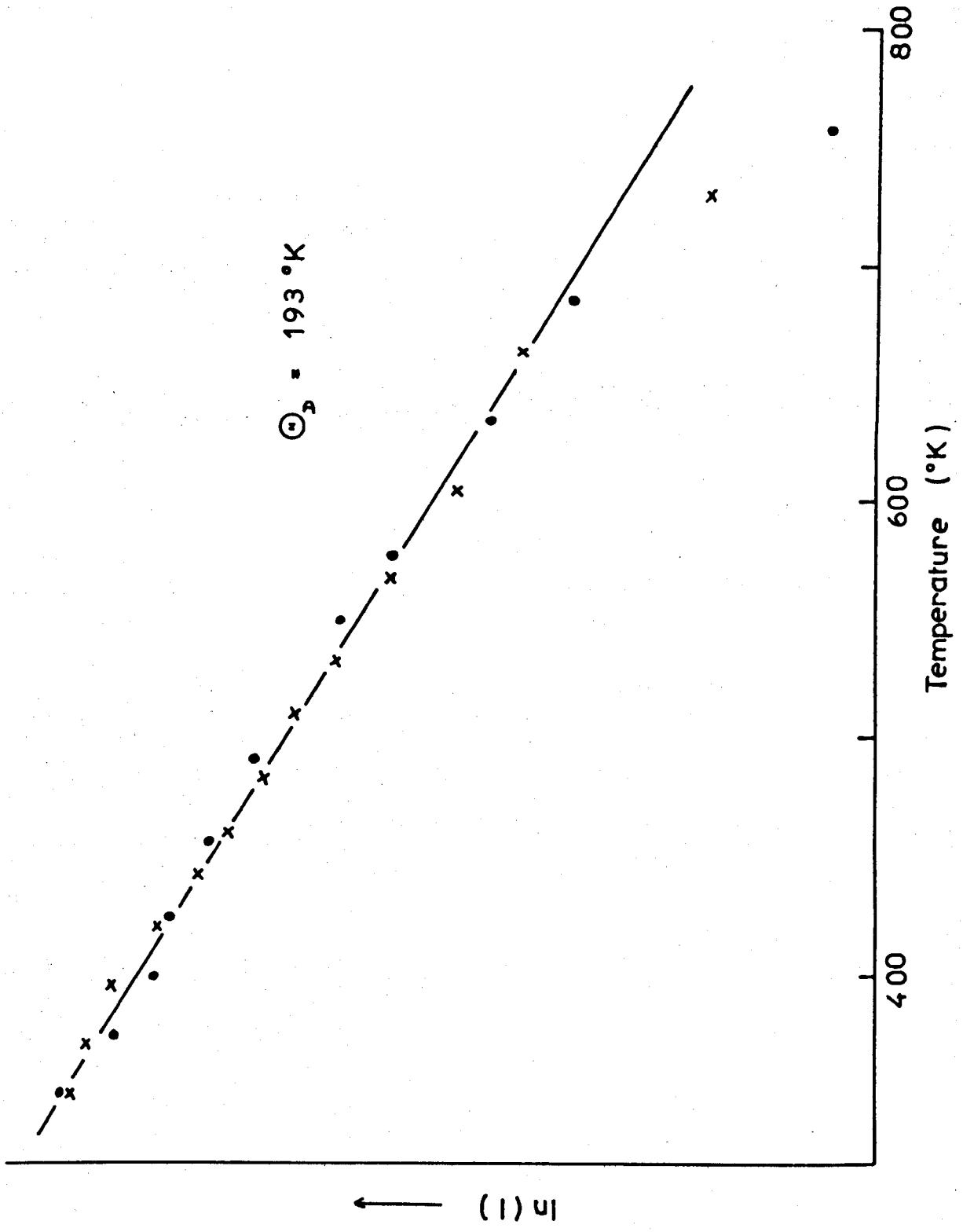

Figure 6.2-3 (a)

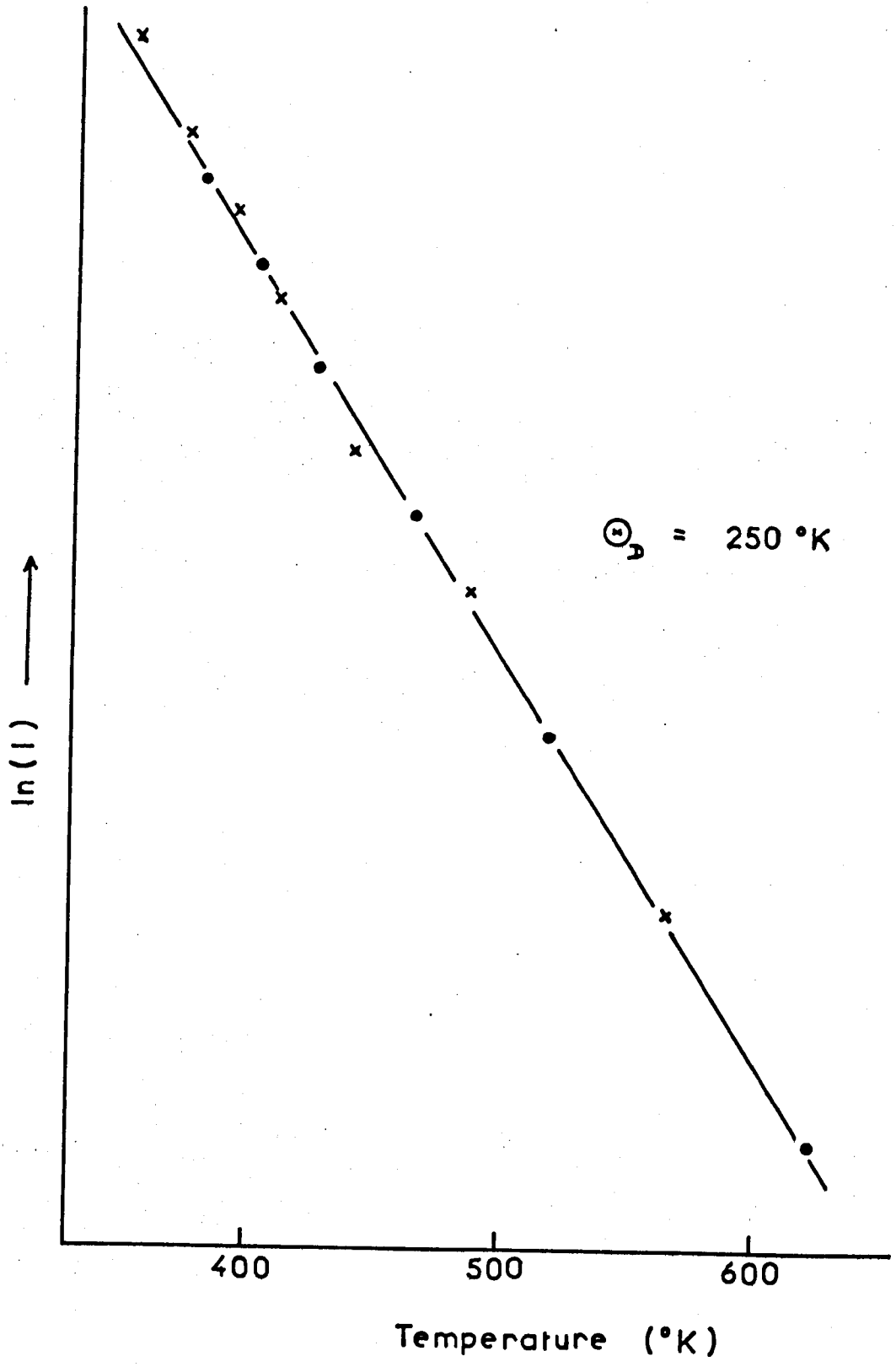

Figure 6.2-3 (b)

lattice. No such deviations from linearity are apparent in the Debye plot for the peak at the rather higher energy of 181eV reproduced in Figure 6.2-3(b). The temperature scale in this case is much shorter than in the Debye plot for the lower energy peak, since, by the time the temperature has reached 700°K, the 181eV peak has all but disappeared into the background intensity, and errors have become proportionately larger. This virtual disappearance of higher energy peaks at higher temperature, is, of course, due to the specific energy dependence of the Debye-Waller factor, and is not necessarily due to a higher Debye temperature. As far as may be determined, there is no significant variation in the temperature at which these anharmonic effects become noticeable with different diffraction conditions.

Both these Debye plots show data points derived from intensity-energy spectra taken with energy scans in both directions, and in each case, no really significant differences can be detected between the two sets of data, indicating that the varying temperature across any one scan is not introducing any serious distortion into the results.

The derivation of a Debye temperature from such Debye plots requires the exercise of a little care. The first point to note is that due to the curvature of the plot at higher temperatures, the derived Debye temperature is related to the gradient of the linear, low temperature portion of the curve. Secondly, the expression for the Debye temperature specifically includes the energy of the incident electrons, and this, as we have mentioned earlier is in itself temperature dependent if we are always to remain on a diffraction maximum. This in itself will introduce a slight curvature into the Debye plot, which is, since most peaks move down in

energy as the temperature is increased, in the opposite direction to the curvature introduced by anharmonicity. This effect is very small however, and we ignore it in the subsequent discussion, and use the room temperature value of the peak energy in evaluating Debye temperature.

Finally, with regard to the evaluation of Debye temperatures from Debye plots, the expression for the Debye temperature, which is, inserting LEED parameters into equations 6.2-2 and 6.2-3

$$\Theta_D^2 = 152.84 \frac{E \cos^2\theta}{M} \frac{\Delta T}{\Delta(\ln I)} \qquad (6.2 - 5)$$

contains the energy and angle of incidence of the electrons inside the crystal. As we have mentioned at several points in this thesis, we have not made any corrections for the inner potential of the crystal, since we do not have as yet any independent estimates of its magnitude. The effect of including an inner potential is to increase the effective energy of the electron inside the lattice, and to decrease its angle of incidence. Obviously, inserting such corrections into equation 6.2-5 will make a difference to the absolute magnitude of the calculated effective Debye temperature. Indeed, if the inner potential is ΔE eV, then the correction to Θ_D^2 is the multiplicative factor

$$\left(1 + \frac{\Delta E}{E}\right)\left(1 - \frac{\Delta E}{E} \tan^2\theta\right) \qquad (6.2 - 6)$$

assuming a Snell's Law type of boundary correction. An inner potential of 15eV, a typically used sort of value, operative on a diffraction peak at 30eV for a normally incident electron beam would therefore increase the calculated Debye temperature by about 25%, but this correction decreases rapidly with increasing energy and angle of incidence. Since we shall be more interested in the detailed variation in the magnitudes of Debye temperatures with diffraction conditions rather than with their absolute

magnitudes, we ignore such effects, but they should be borne in mind in comparisons with other work.

Errors quoted in the values of Debye temperatures derived from Debye plots in this work are simply obtained from the scatter of data points about the straight line which has been fitted to the low temperature part of the curve by eye. Other errors which could be introduced through the energy, angle of incidence and temperature terms in Equation 6.2-5 are assumed small compared to those derived in this manner.

We now turn to examining the detailed values of Debye temperature obtained in the manner discussed above for many of the peaks in the intensity-energy spectra of the specular beam from the (100) surface of copper.

A comprehensive list of these Debye temperatures is presented in Table 6.1. From this table, it will be observed that the Debye temperatures cover a wide range of values. There are two relationships between these values and the diffraction conditions which we examine, namely the variation of the Debye temperature with energy at a constant angle of incidence, and the variation of Debye temperature with angle of incidence at a constant energy.

The first relationship is important, since this is the one which has often been used in the past to study the variation in atomic vibrations with depth into the crystal, and to draw conclusions about the penetration depth of the electrons themselves. Simple kinematical theory tells us that Bragg peaks of successively higher orders represent scattering from layers deeper and deeper into the crystal. Thus the Debye temperatures for such peaks will be low for the lower order Bragg peaks and will increase to the

TABLE 6.1

Measured Effective Debye Temperature for Cu (100)

Angle of Incidence	Energy (eV)	Debye Temp. (°K)
6	29	210 ± 11
6	37	235 ± 4
6	52	221 ± 5
6	61	261 ± 9
6	76	211 ± 5
6	90	228 ± 5
6	105	221 ± 4
6	128	260 ± 3
6	161	290 ± 4
6	179	250 ± 4
6	219	260 ± 5
6	277	298 ± 3
6	401	291 ± 4
6	556	351 ± 9
7	30	195 ± 8
7	38	222 ± 3
7	90	311 ± 5
7	105	222 ± 4
7	128	248 ± 3
8	30	192 ± 4
8	38	229 ± 6
8	92	307 ± 3
8	106	215 ± 4
8	129	265 ± 4
8	175	281 ± 5
8	216	259 ± 5
8	279	297 ± 3
9	39	227 ± 4
9	93	246 ± 3
9	107	215 ± 3
9	129	250 ± 4
10	40	191 ± 4
10	94	255 ± 2
10	106	234 ± 2
10	130	250 ± 3
10	175	288 ± 3
10	215	267 ± 3
10	280	299 ± 3
11	41	217 ± 3
11	95	245 ± 2
12	35	175 ± 3
12	42	210 ± 3
12	95	239 ± 2
12	176	284 ± 3
12	214	263 ± 5
12	280	288 ± 2
13	35	312 ± 9
13	42	202 ± 4
13	97	247 ± 2
14	36	277 ± 6
14	44	212 ± 4
14	97.5	249 ± 3
14	180	271 ± 3
14	284	289 ± 4
15	36	243 ± 3
15	98	246 ± 2
16	41	234 ± 5
16	100	254 ± 3
16	181	250 ± 2
17	38	223 ± 6
17	100	248 ± 2
18	39	218 ± 3
18	55	218 ± 4
18	100.5	249 ± 2
19	39	213 ± 3
19	55	229 ± 4
19	87	232 ± 3
19	101.5	253 ± 3
20	39	203 ± 3
20	54	196 ± 3
20	87.5	241 ± 3
20	102	262 ± 3

bulk value for the higher order Bragg peaks. It is rather more difficult to say a priori what the simple multiple scattering theories can tell us about the Debye temperatures of non-Bragg like peaks, since these will depend on the precise multiple scattering mechanisms involved. If we assume that the total mean free path of the electrons in the crystal depends only on the energy of the electron and is independent of the number of elastic scatterings it has undergone, the multiple scattering peaks will arise from scatterings nearer the surface than the nearby Bragg peaks. The atomic vibrations governing the thermal behaviour of these peaks will then be a mixture of vibrations normal to the surface larger than those relating to nearby Bragg peaks and vibrations parallel to the surface which may or may not be larger in amplitude than the normal vibrations relating to those Bragg peaks, and might even be smaller. Thus the precise behaviour of any one peak will be determined by the details of the mixture of these vibrations, and could give a Debye temperature either larger or smaller than that for nearby Bragg peaks. A full multiple scattering analysis, however, tells us that all peaks in the intensity-energy spectrum are to be regarded as being made up from contributions from many different multiple scattering events, so we cannot therefore predict the behaviour of the Debye temperature as a function of energy.

Figures 6.2-4 through 6.2-8 show this function for five given angles of incidence, and closely similar results could be shown for other angles. The bulk Debye temperature of $322 \pm 22^{\circ}K$ derived from X-ray data[40] is indicated by the horizontal dashed line. The most striking feature of each of these figures is the extreme variability of the Debye temperature from peak to peak, in sharp contrast to much of the published work. Even if we select those peaks which lie close to the expected kinematical Bragg

Figures 6.2-4 to 6.2-8 The Debye temperatures measured for various peaks in the intensity-energy spectrum of the specular LEED beam from the (100) surface of copper plotted as a function of peak energy for the angles of incidence of 6°, 8°, 10°, 12° and 20° respectively. In each Figure, the short arrows at the top of the panel indicate the kinematical Bragg scattering conditions at that angle. In Figure 6.2-4, the horizontal dashed line represents the bulk X-ray Debye temperature of $322^{\circ}K$.

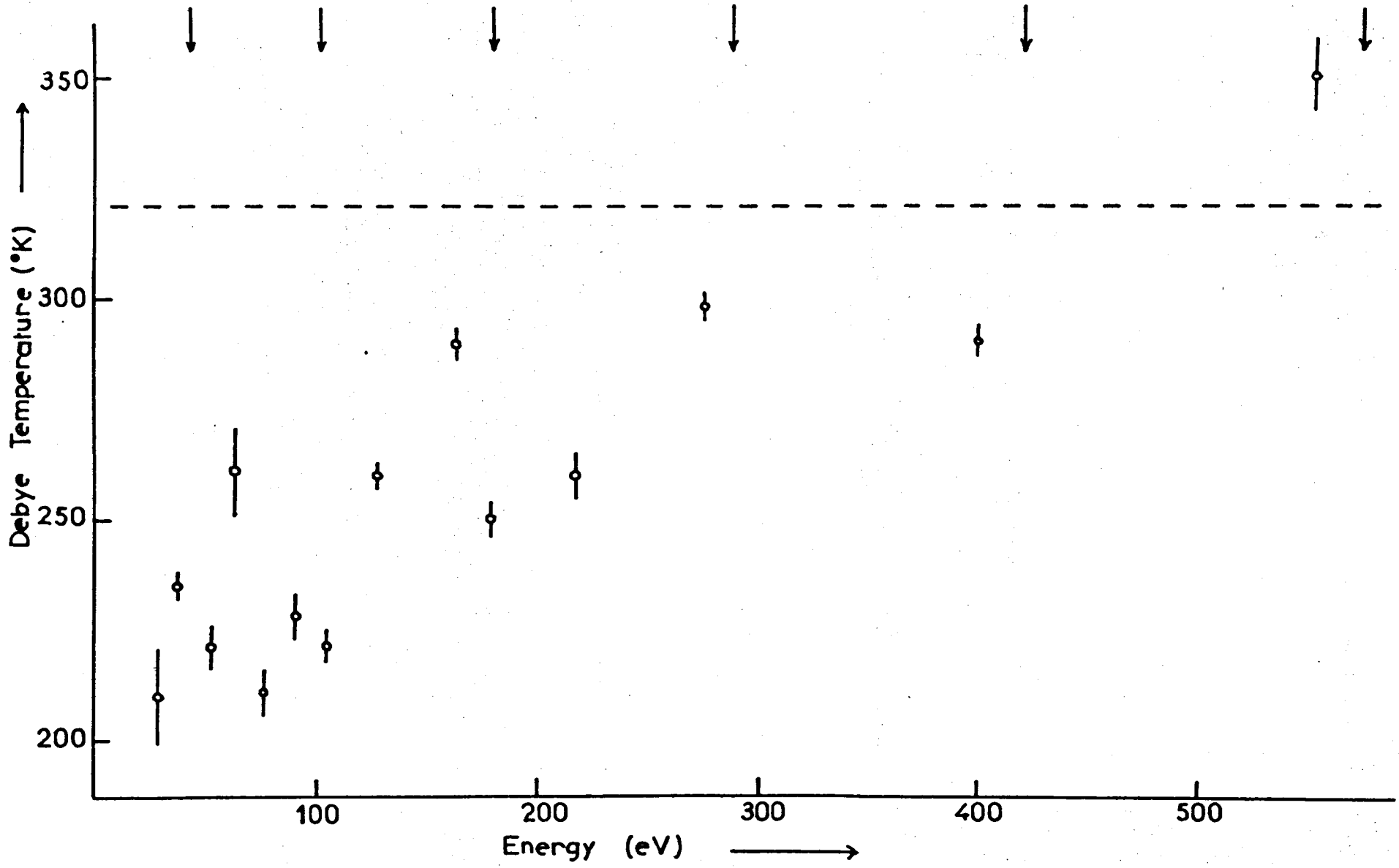
Debye Temperature (°K)
350
300
250
200
100
200
300
400
500
Energy (eV)

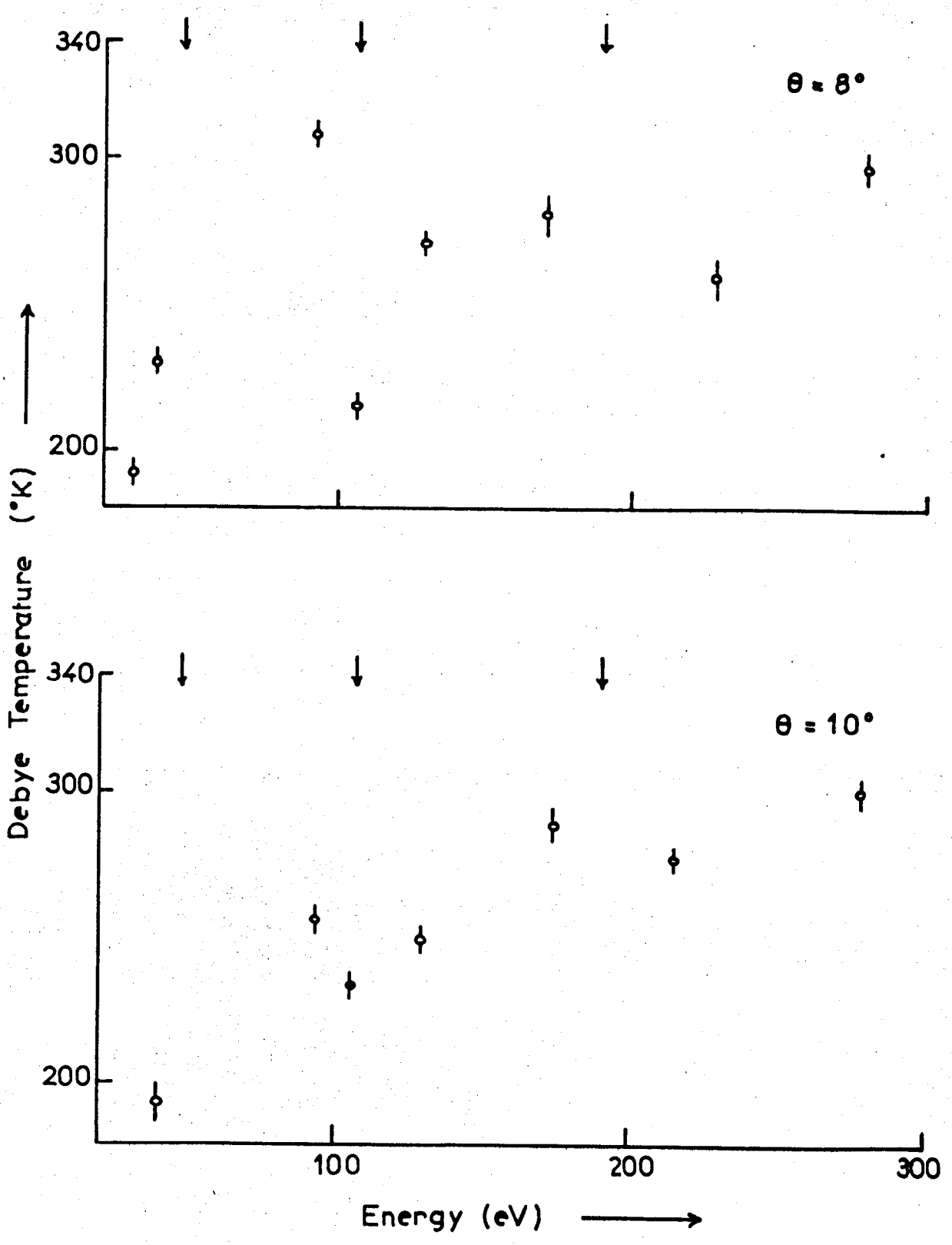
340
300
200
θ ≈ 8°
Debye Temperature (°K)
340
300
200
θ = 10°
100
200
300
Energy (eV)

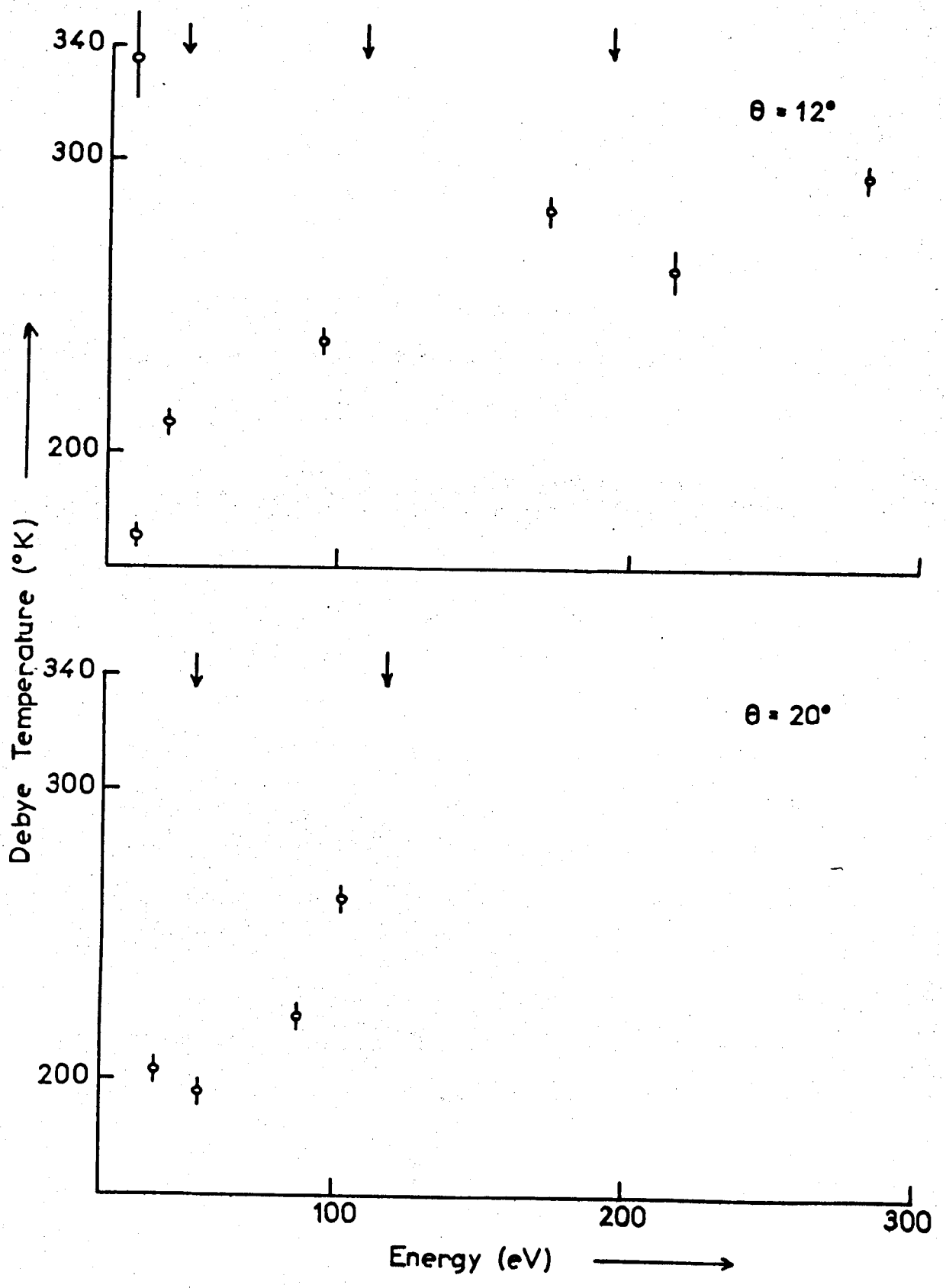
340
300
200
θ = 12°
340
300
200
θ = 20°
Debye Temperature (°K)
100
200
300
Energy (eV)

peaks, we do not get a smooth variation from low values gradually rising to meet the bulk value. The bulk value is, indeed, only reached in Figure 6.2-4 where data has been extended to much higher energies than in the other figures. Wilson has also observed this variability of Debye temperature from peak to peak in observations on Cr(100) and Mo(100)[28] and Lagally's results on (111) silver[22] also exhibit this behaviour, which he wrongly interprets as being due to the temperature induced peak shifts, an effect for which he made no allowance in taking his data.

Wilson's results indicate that for nominal Bragg peaks, the measured value of Debye temperature is somewhat higher than the local values. This is by no means as unambiguously defined for the results presented here. For example, if the (800) Bragg condition is at 187eV at 6°, are we to regard the experimental peak at 179eV or that at 161eV as the nominal Bragg peak? The former peak has a very much lower Debye temperature than the latter. Other examples may be picked out from these results where the peak nearest the Bragg condition does not have a local maximum in the Debye temperature.

Just about all we can in fact say about these results is that the effective Debye temperatures trend towards higher values as the energy of the incident electrons is increased, eventually saturating at the bulk value - which is shown rather by Wilson's results than by those presented here, where the required energies appear to be somewhat larger - but that extreme local variations occur.

Turning now to examination of the second relationship that we mentioned above, namely, how does the measured value of Debye temperature vary with

angle of incidence at a given incident energy? Rather than using a strictly constant incident energy, what we choose to look at is in fact the variation of Debye temperature for a given diffraction peak as it moves through $\underline{k}$-space as the angle of incidence is varied. We select such peaks by picking out on the $\underline{k}$-space plot series of peaks which appear to lie on the same loci, and may be thought to have the same diffraction origin.

Simple kinematical and simple multiple scattering theory would in fact tell us that they did have the same origin, i.e. the same scattering vector. Thus we would expect there to be not much variation in the Debye temperature of a given peak as it moves through $\underline{k}$-space.

The loci of the groups of peaks chosen are indicated on the $\underline{k}$-space plot of the intensity-energy spectrum of the specular beam from Cu(100) which is reproduced in Figure 6.2-9. In Figure 6.2-10 through 6.2-16, we plot the measured Debye temperatures for the peaks lying along each locus against the angle of incidence. The actual energy of each peak is also shown below the axis in each case. In no case is the Debye temperature constant with the changing angle of incidence, and in most cases marked local variations occur. For instance, in Figure 6.2-12, the peaks at 7° and 8° have apparent Debye temperatures very much higher than the peaks at the adjacent angles. No general trend is evident, however, in the data for the various loci.

We shall postpone further discussion of the results for this surface until we have presented the results for the (111) surface.

Figure 6.2-9 The $\underline{k}$-space plot of the Intensity-Energy Spectrum of the specular LEED beam from Cu(100) showing the peak loci chosen as discussed in the text for the sequence of data presented in Figures 6.2-10 through 6.2-16.

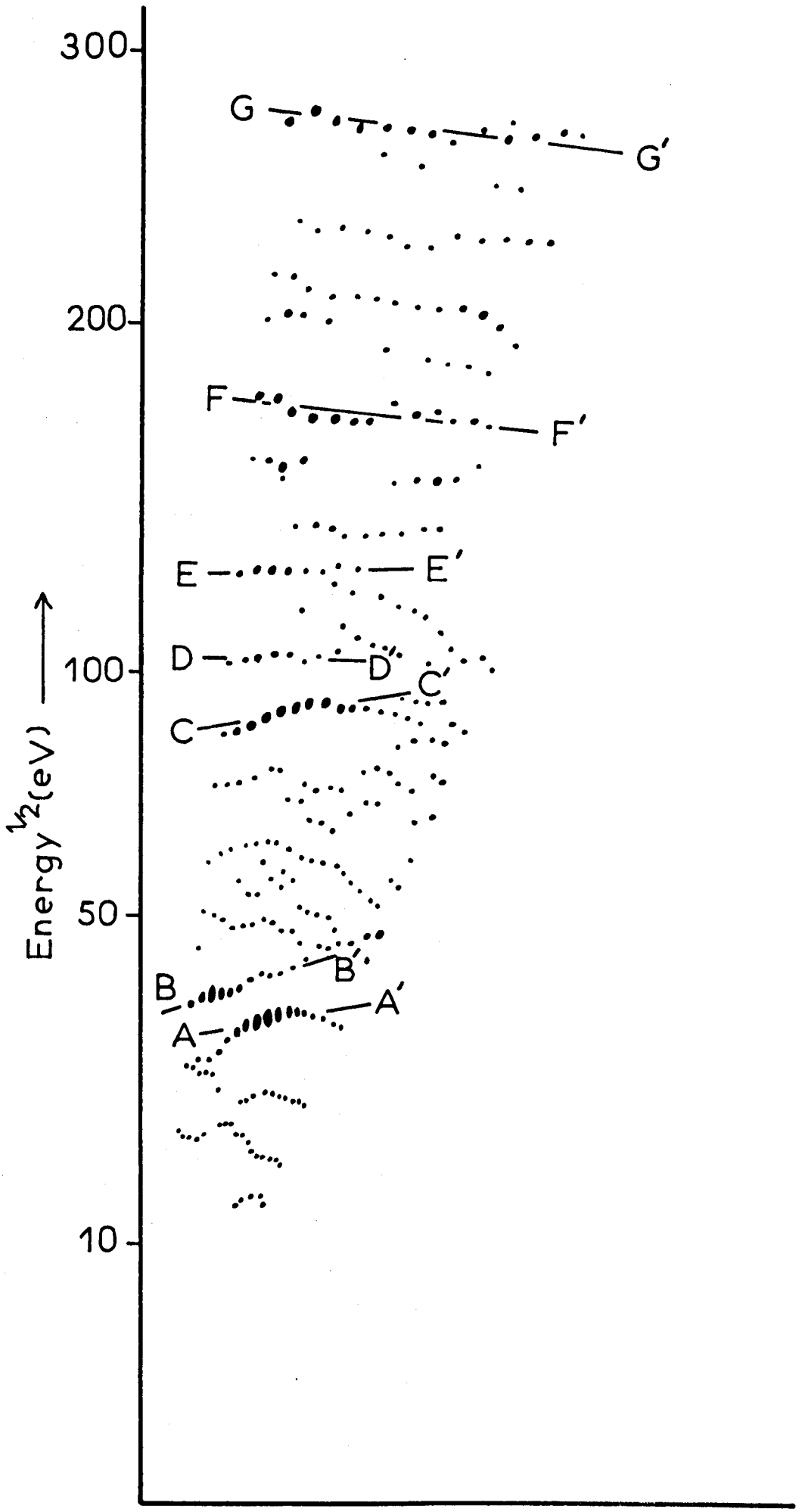
300
200
100
50
10
Energy ½ (eV)
G
G′
F
F′
E
E′
D
D′
C′
C
B′
B
A′
A

Figures 6.2-10 to 6.2-16 The variation of the measured Debye Temperatures with angle of incidence for diffraction peaks lying along the various loci indicated in Figure 6.2-9.

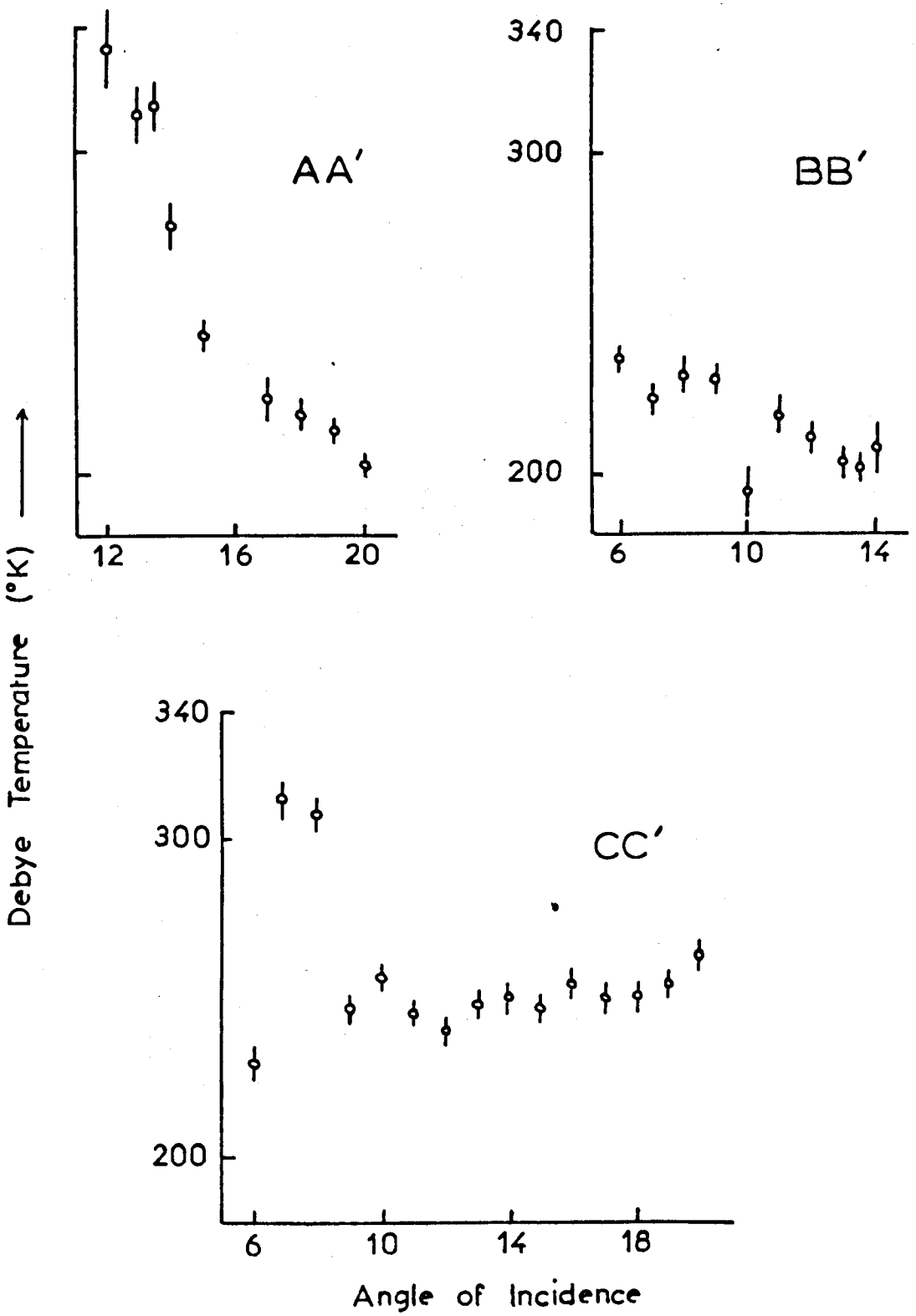
AA′
BB′
CC′
340
300
200
12
16
20
6
10
14
18
Debye Temperature (°K)
Angle of Incidence

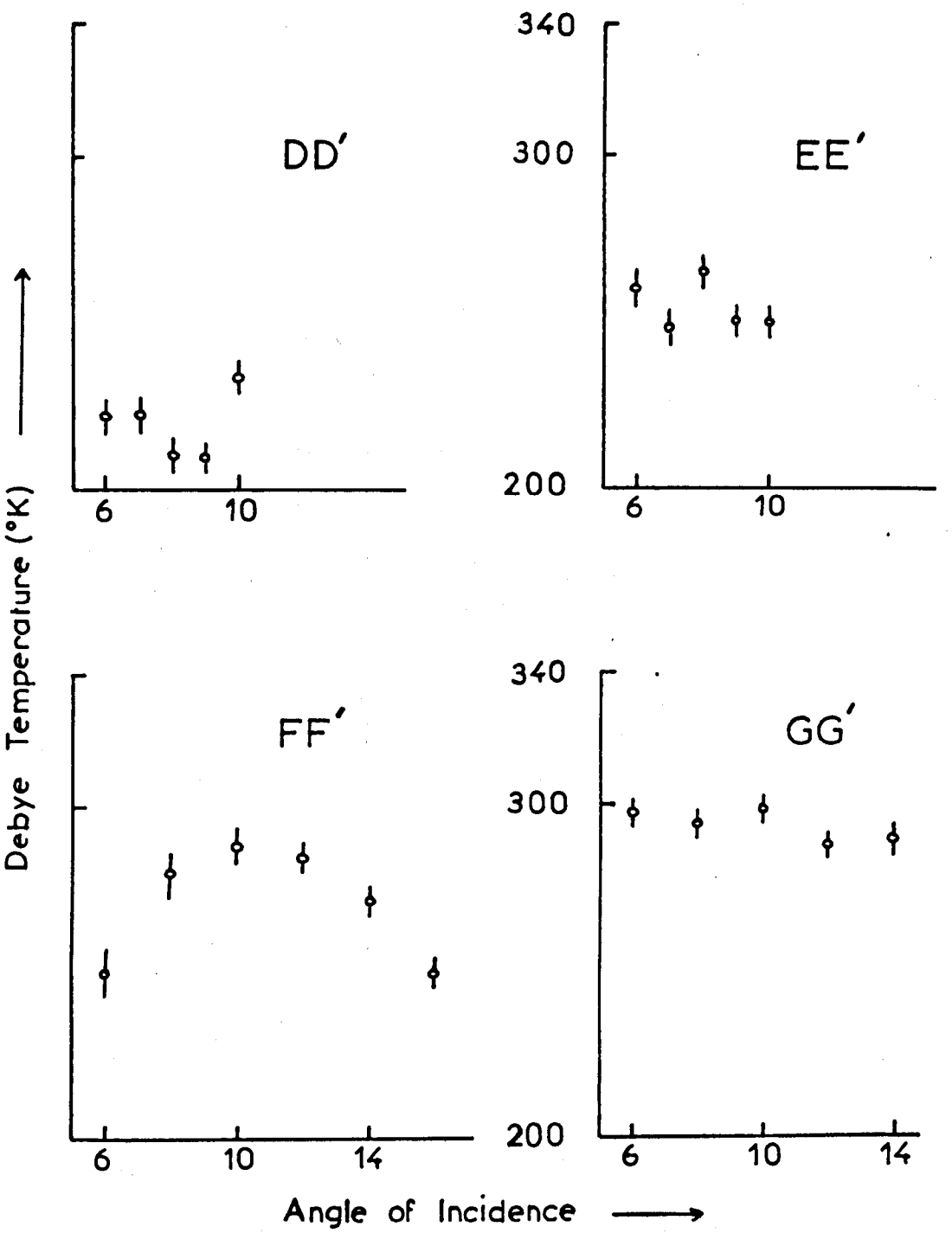
DD′
EE′
FF′
GG′
340
300
200
6
10
14
Debye Temperature (°K)
Angle of Incidence

6.2.5 - Measured Debye Temperatures for Cu(111)

Much the same general sort of comments can be made for the Debye plots derived for the various peaks in the intensity-energy spectra of the specular beam from the (111) surface of copper as were made for those from the (100) surface. The data available for this surface is, however, much sparser, and the Debye temperatures for the lower energy peaks are taken from the data of Woodruff and Seah[26]. It should be noted that in the evaluation of Debye temperatures, these authors include an inner potential correction of 14eV, and to obtain strict continuity with our data, the values quoted should be reduced by the factor given in equation 6.2-6.

Unfortunately, at these lower energies, the data does not extend to a high enough temperature to enable us to observe if anharmonicity sets in for this surface at the same temperature as for the (100) surface.

The measured values of Debye temperatures for this surface are listed in Table 6.2, those values obtained from the data of Woodruff and Seah being indicated by an asterisk.

In Figures 6.2-17 and 6.2-18 we plot the measured values of Debye temperatures as a function of energy for the angles of incidence of 6° and 14° respectively, and Figure 6.2-20 shows an angular plot similar to those plotted for the (100) surface for the locus HH' shown in Figure 6.2-19. Unfortunately, the limited data restricts us to these three separate plots.

Although the available data for this surface is much more limited than that for the (100) surface, it is evident that the overall behaviour of

TABLE 6.2

Measured Effective Debye Temperatures for Cu (111)

Angle of Incidence	Energy (eV)	Debye Temp. (^{o}K)
*6	25	244 ± 5
*6	67	278 ± 5
*6	130	270 ± 5
*6	211	279 ± 5
6	209	277 ± 8
6	420	337 ± 11
8	212	263 ± 6
8	308	311 ± 3
8	424	298 ± 7
10	210	270 ± 4
10	314	318 ± 9
*14	23	241 ± 5
*14	58	268 ± 5
*14	128	265 ± 5
*14	142	275 ± 5
*14	212	279 ± 5
14	300	297 ± 5
14	318	306 ± 4
14	340	276 ± 8
16	214	261 ± 3
16	243	263 ± 3
17	212	237 ± 8
17	242	276 ± 5
18	212	225 ± 5
18	240	276 ± 4
20	238	269 ± 4

* Data of Woodruff and Seah[26]. These values of Debye Temperatures include an Inner Potential Correction of 14eV.

Figures 6.2-17 and 6.2-18 The Debye Temperatures measured for various peaks in the intensity-energy spectrum of the specular LEED beam from the (111) surface of copper plotted as a function of peak energy for the angles of incidence of 6° and 14° respectively. In these Figures, the full circles represent points taken from the data of Woodruff and Seah, and include an inner potential correction of 15eV.

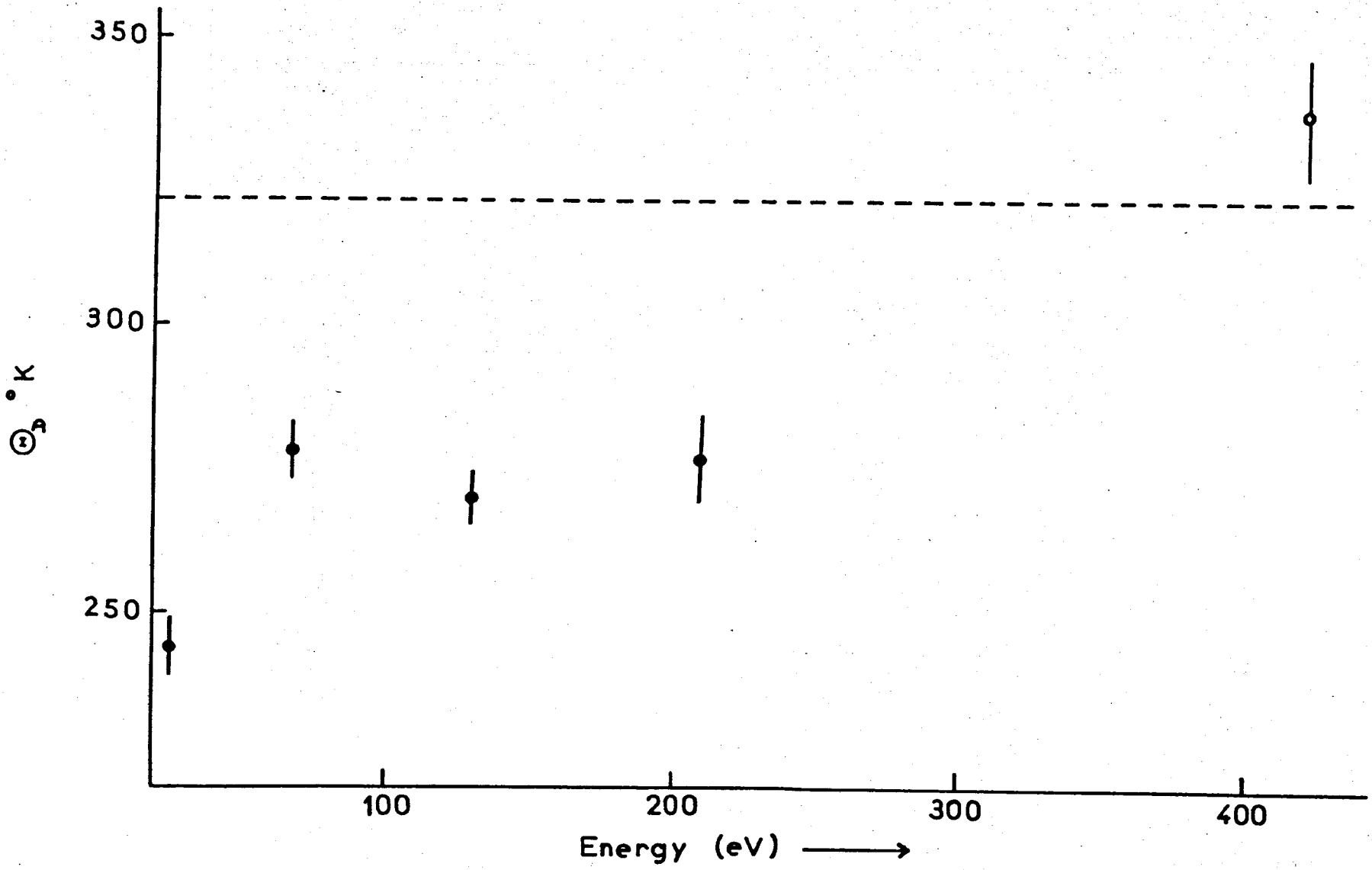

Figure 6.2-17

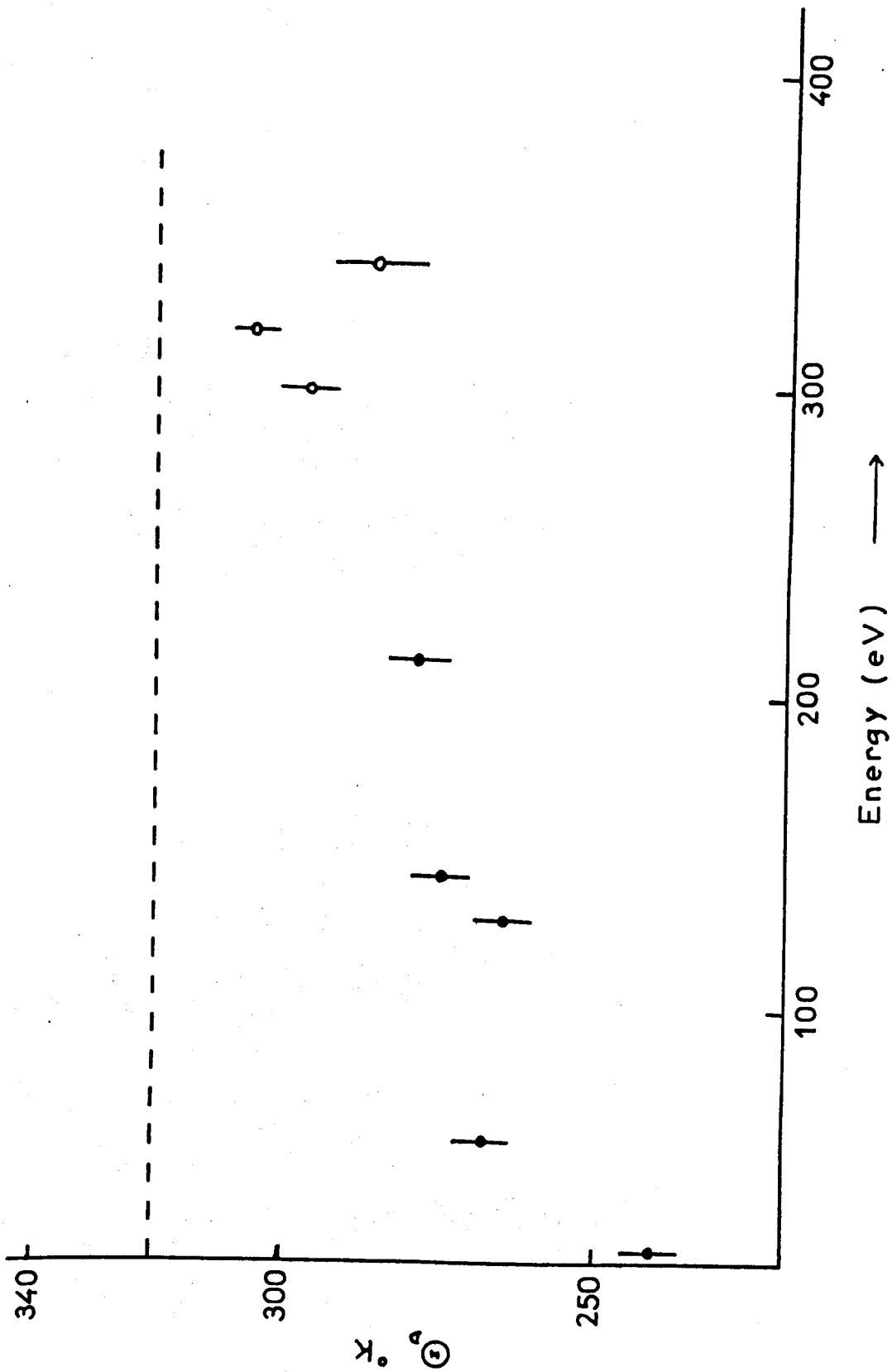

Figure 6.2-18

Figure 6.2-19 The $\underline{k}$-space plot of the intensity-energy spectrum of the specular LEED beam from Cu(111) showing the peak locus HH' chosen for Figure 6.2-20.

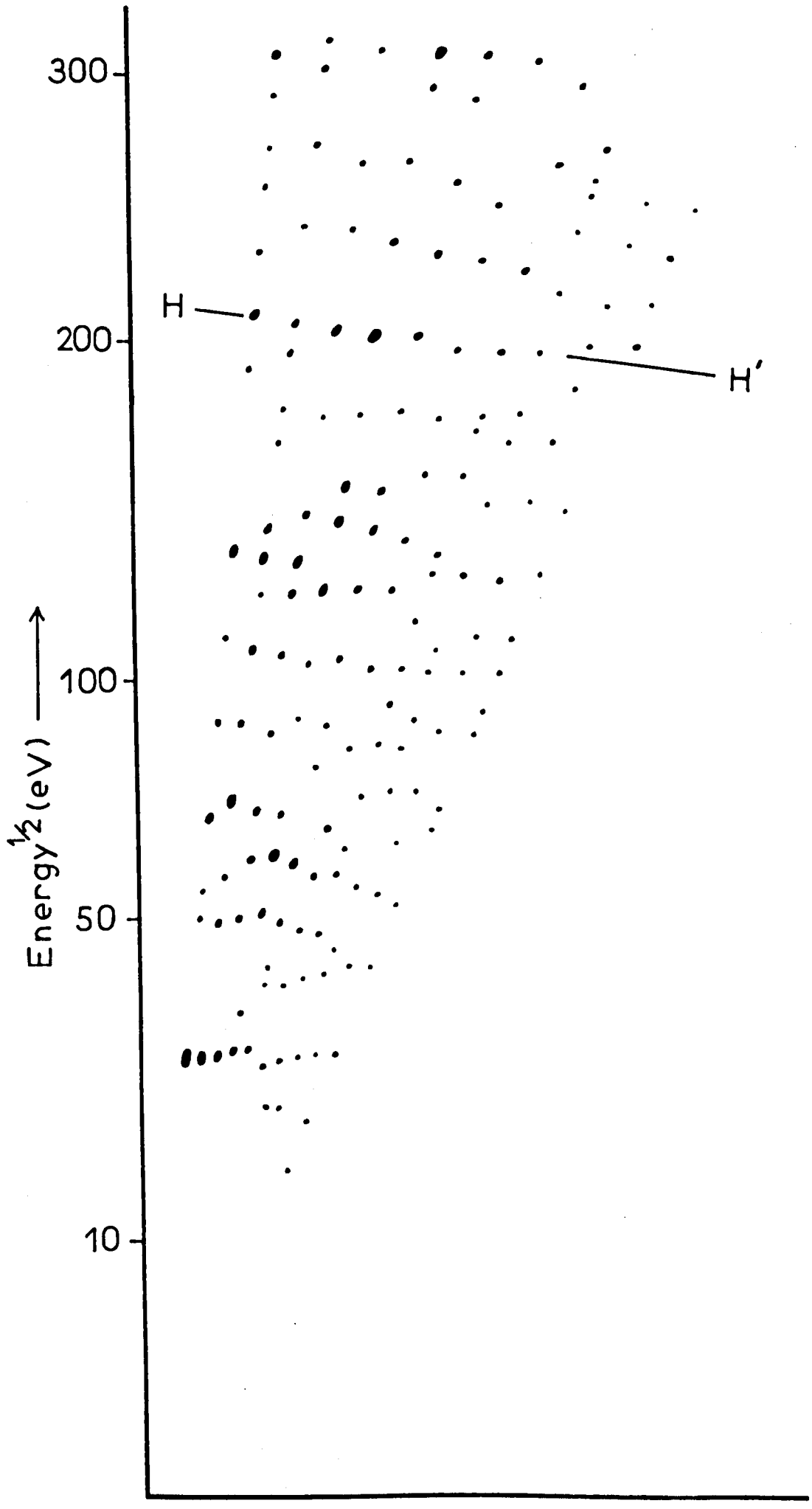
300
200
100
50
10
H
H'
Energy$^{1/2}$ (eV)

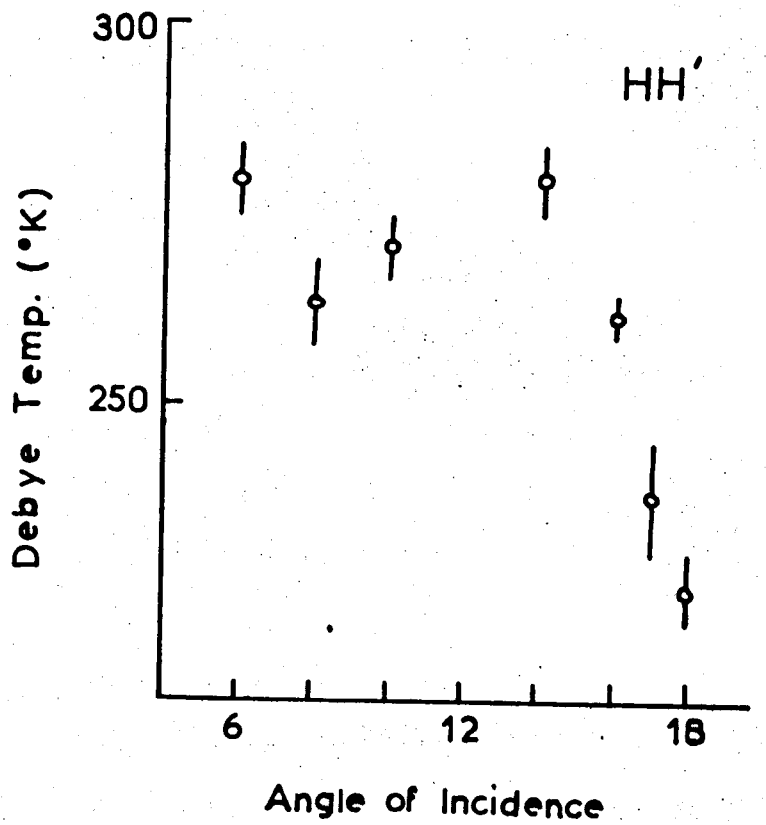

Figure 6.2-20. Variation of Debye Temperature with angle of incidence for a diffraction peak lying along the locus HH' in the Intensity-Energy Spectrum from the (111) surface of copper shown in the previous Figure.

the measured Debye temperatures as a function of the diffraction parameters is very similar to that found for the (100) surface, in that it is apparently rather random in detail, but with the same sort of general trends, i.e. increasing Debye temperature with energy, but only reaching the bulk value at comparatively high energies.

6.2.6 - Discussion

Given the results presented in the previous section, what conclusions can we draw? As we have seen, the behaviour of the Debye temperatures as a function of energy, and in particular, as a function of angle of incidence is at variance with the predictions of kinematical and pseudo-kinematical models of LEED, and constitutes yet another demonstration of the fundamentally dynamical nature of the LEED process.

The apparently random behaviour of the Debye temperature with energy of the incident electrons has been interpreted by Wilson[28] as being due to electrons near Bragg scattering conditions having greater extinction distances than those further away from the Bragg conditions, so that these electrons sample the atomic vibrations at a greater depth within the crystal and thus have Debye temperatures which are more bulk-like in character, or as being due to multiple scattering effects. As we have pointed out, the former type of behaviour is by no means as clearly demonstrated in this work, and so we are led to the conclusion that the apparently random behaviour of the Debye temperature as a function of diffraction conditions, superimposed on the general trend towards higher values as the energy of the incident electrons increases, is essentially a feature of the dynamical nature of the LEED process.

This conclusion is consistent with the recent theoretical discussion of the effects of including lattice vibrations into an inelastic collision model calculation presented by Laramore and Duke[36], where they find that the Debye temperatures calculated for various peaks in their theoretical spectra depend in a sensitive way on the precise nature of the diffraction parameters operating.

Current LEED theories based on the various multiple scattering approaches show that any given diffraction peak is, in general, the summation of flux scattered in many different diffraction processes, and that changing the diffraction parameters slightly can vary the detailed nature of such peaks by summing over a different diffraction series, without, however, greatly altering the observed overall profile of the diffraction peak in the intensity-energy spectrum. Since, however, the thermal behaviour of a diffraction peak is governed by the precise nature of each of the scattering processes contributing to the observed peak, it is not unreasonable that small changes in the diffraction parameters can give rise to such apparently disproportionately large changes in the thermal behaviour of the peak.

We therefore conclude that it is at present extremely speculative to try to draw any specific conclusions about the nature of surface atom vibrations, electron penetration depths, etc., from temperature dependent LEED data, but that the experimentally observed values of Debye temperatures should be regarded as a useful experimental parameter of the LEED problem, and will provide a sensitive test of the accuracy of any theory.

Nevertheless, as we mentioned earlier, the lowest observed value of the Debye temperature for any of the diffraction peaks in the intensity-energy

spectra ought to set a lower limit on the amplitude of vibration of the surface atoms in the surface normal direction. Applying this criterion to these two surfaces therefore gives a value of the ratio of the root mean square amplitude of vibration of the surface atoms to that of the bulk of at least (1.84 ± 0.16) for the (100) surface, and of (1.34 ± 0.14) for the (111) surface.

It is of interest to note before concluding the discussion on Debye temperatures that Horstmann[41] in studying the effects of temperature on the intensities of the diffraction rings produced by high energy electrons (51keV) passing through polycrystalline aluminium films observed a similar type of behaviour to that which we have described here. Rather than redefining the Debye temperature as is the normal practice in LEED work, he assumes, since the electrons are essentially sampling the bulk vibrations only, that the Debye-Waller factor is redefined as $-\alpha_g W$ instead of $-2W$. He then finds that for those reflections whose intensity can be adequately calculated within the framework of a kinematical analysis, that α_g is in fact usually fairly close to 2. However, for those reflections where a dynamical calculation is required in the intensity analysis, the values of α_g differ significantly from 2 in a rather random manner. In one case, he even shows a value of α_g which is negative, implying that the intensity of this ring in fact increases as the temperature is increased, an effect which has not yet been observed in LEED. He can, however, within the framework of the relatively simpler dynamical calculations required in high energy electron diffraction arrive at estimates of α_g which are in good agreement with the experimentally observed values. These results again confirm that the variability of the Debye temperature is essentially a feature of the dynamical nature of the process of electron

diffraction, and indicate that proper calculations of temperature dependent LEED intensities may well be able to reproduce the experimental results. A preliminary result of one such calculation will be discussed in § 6.5.

6.3 - The Effects of Temperature on Peak Widths and Shapes

It has been noted by previous authors[20,42] that the widths of diffraction peaks remain relatively constant from liquid nitrogen temperatures to almost the melting point of the crystal, and this is borne out in the present work. In the cases where a diffraction peak is very wide due to its being composed of one or more unresolved narrower peaks (within the limits of the envelope concept discussed in § 2.4.5), the individual peaks may have different Debye temperatures, and so as the temperature varies, the ratio of the peak heights of the individual components may vary, resulting in an overall change in the shape of the composite peak. Such variations may lead to rather better resolution of the components of such peaks at higher or lower temperatures, especially if combined with differential thermally induced peak shifts. Apart from this rather special case, however, for an apparently single diffraction peak in the intensity-energy spectrum, the peak width (FWHM) is virtually independent of temperature over the range of temperatures used in this work.

Similarly, for apparently single peaks in the intensity-energy spectra, the peak shape, or line profile, is independent of temperature. This is illustrated in Figure 6.3-1 for the large diffraction peak at 96eV at an angle of incidence of 13° in the spectrum from Cu(100). The upper

Figure 6.3-1 The upper trace is the profile in energy space of a diffraction peak at 97eV and an angle of incidence of 13° in the intensity-energy spectrum of the specular LEED beam from the (100) surface of copper at a temperature of about $70^{\circ}K$, and the lower trace is the profile of the same diffraction peak at about $390^{\circ}K$. The open circles are derived from the upper trace in the manner described in the text.

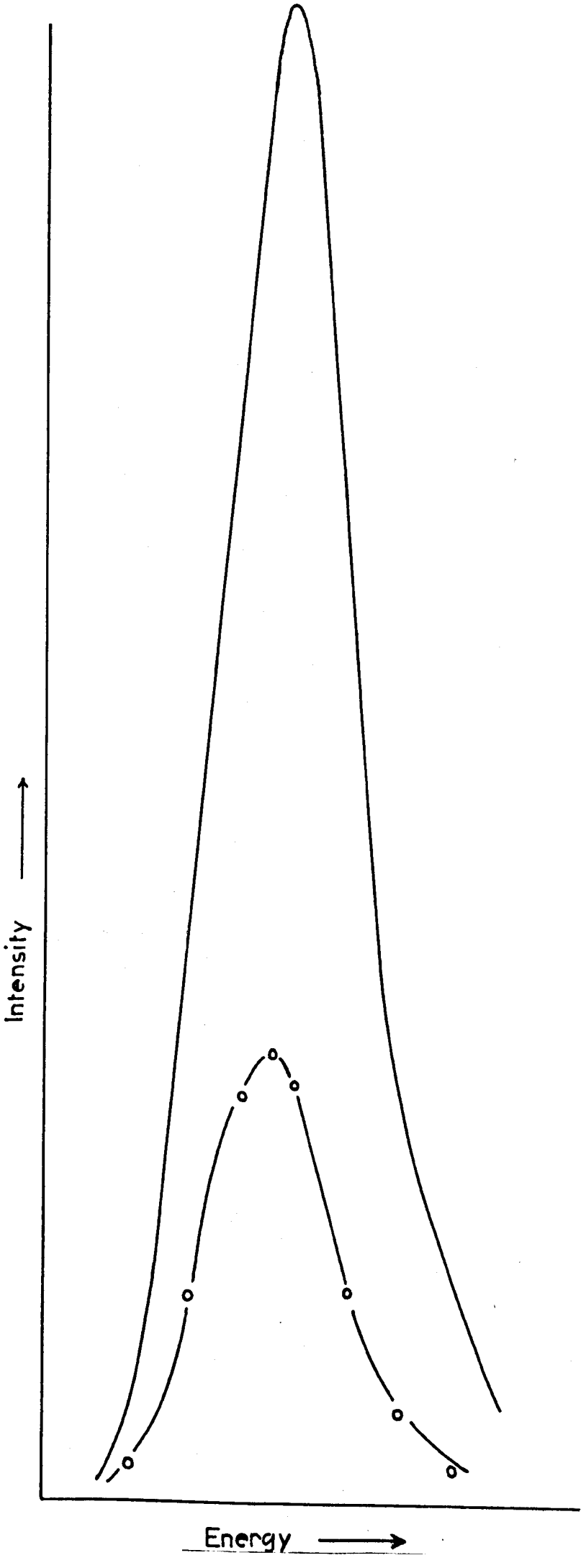
Intensity
Energy

curve is the trace of the profile at 50°K above room temperature and the lower trace is the profile of the same peak measured at 370°K above room temperature, a range in temperature over which the Debye plot is linear. The open circles are then derived from the upper curve in the following manner.

Let the coordinates of any point on the upper trace be (E_i, I_i). Then the coordinates of the open circle (E_i', I_i') corresponding to the point (E_i, I_i) are given by the transformation

$$E_i' = E_i - 1$$
$$I_i' = I_i \exp \frac{48\pi^2 E_i \hbar^2 \Delta T}{150 M k_B \Theta_D^2} \qquad (6.3 - 1)$$

where ΔT is the temperature difference between the two traces and Θ_D is the Debye temperature measured for the maximum of the diffraction peak. The reduction in the energy coordinate of 1eV is the observed temperature induced peak shift of the maximum over the temperature range used. In other words, the open circles are derived from the upper curve by multiplying the intensity of the upper curve at each point by the Debye-Waller factor assuming that the Debye temperature is unchanged across the peak, but taking into account its energy dependence, and then bodily shifting the derived curve through the observed shift in energy of the peak maximum in this temperature range.

The fit of the open circles to the experimentally measured curve at this temperature is very good, indicating both that the peak shape is almost independent of temperature, and that the Debye temperature is a constant across the peak, or at least any changes in the one are very effectively compensated for by changes in the other. Similar fits can be obtained for other well isolated peaks in the spectra.

We therefore conclude that the shape of diffraction peaks in energy space is independent of temperature, i.e. the shape is not primarily determined by the phonon scattering. McKinney has demonstrated[5] that the shape of a diffraction beam in real space is also unaffected by the temperature of the sample, so we may conclude that increasing the density of phonons in the sample affects only the distribution of intensity within a profile whose general shape is determined by the rigid lattice diffraction.

6.4 - Temperature Induced Peak Shifts

6.4.1 - The Causes of Peak Shifts

There are several basic effects which can lead to a change in position in energy space of a diffraction peak in the intensity-energy spectra as the temperature of the specimen is altered, and the more important of these have been discussed in detail by Woodruff and Seah[26].

The first and most obvious contribution is that due to the expansion in the crystal lattice as the temperature is increased. Laramore and Duke[36] have shown that, within the context of their calculations, increasing the lattice parameter of the model crystal without otherwise altering the scattering properties moves the diffraction maxima to lower energies without changing the distribution of intensity within the overall diffraction profile. Measurement of such shifts can therefore in principle be used to study the lattice expansion of the crystal, and especially any differential expansion occurring near the surface of the crystal. Wilson and Bastow[29] have shown that utilising a kinematical model for the diffraction process, an effective linear expansion coefficient, α, can be derived. If E is

the energy of the diffraction peak from which the coefficient is to be derived, then

$$\alpha = -\frac{1}{2}\frac{1}{E}\frac{\partial E}{\partial T} \qquad (6.4 - 1)$$

where $\frac{\partial E}{\partial T}$ is the rate of change of the energy of the diffraction peak with temperature.

By studying such effective linear expansion coefficients in detail for the diffraction peaks in a number of intensity-energy spectra, Wilson and Bastow[29] draw conclusions as to the nature of the interatomic potential near the surface of the crystal. However, there are other effects giving rise to temperature induced peak shifts which they do not appear to consider.

As is well known, the work function of a surface is a temperature dependent quantity, and for copper, the change in work function with temperature for the low index faces has been studied by Blevis and Crowell[43]. Their results for the (100) and (111) surfaces are shown in Figure 6.4-1, and show that as the temperature is raised, the work function decreases. This therefore also causes the diffraction peaks to move to lower energies as the temperature is increased, so this shift must be subtracted from the experimentally observed peak shifts.

Woodruff and Seah[26] also consider an apparent peak shift introduced due to the energy dependence of the Debye-Waller factor across any one diffraction peak. They show that if the peak profile is Gaussian in shape, then a peak shift ΔE is introduced where

$$\Delta E = 0.36\frac{W}{ET}E_{\frac{1}{2}}^2\Delta T \qquad (6.4 - 2)$$

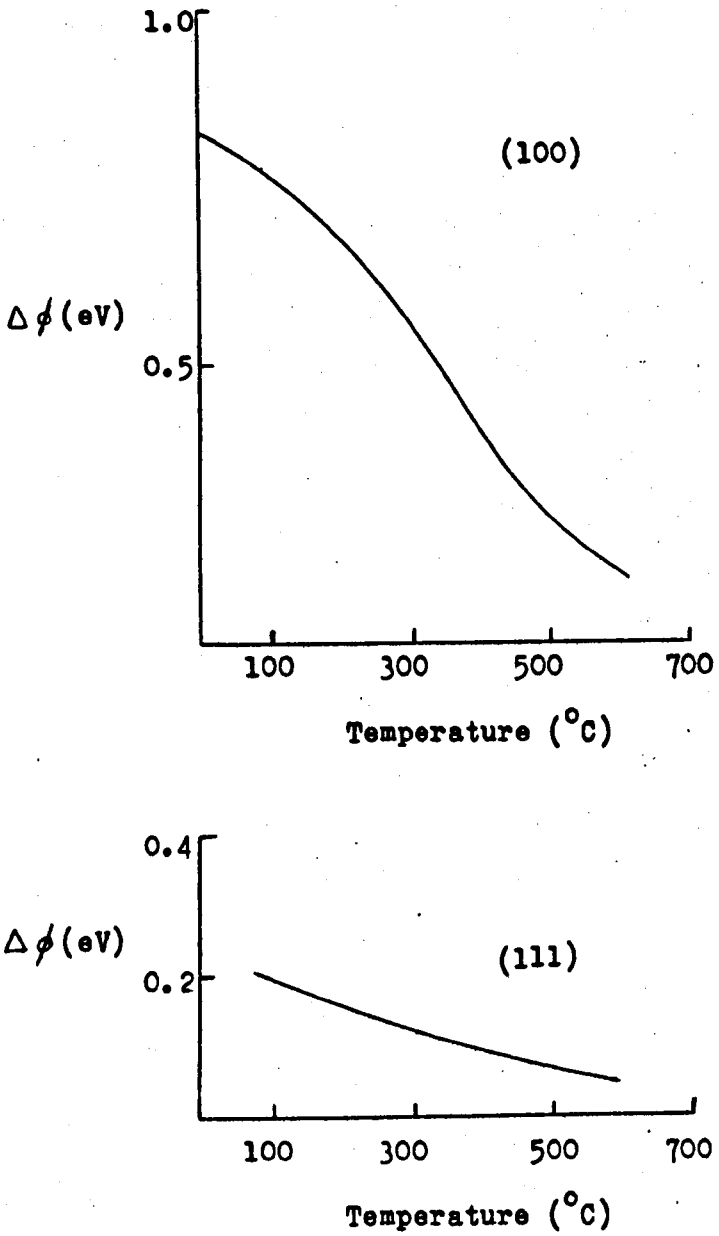

Figure 6.4-1. The data of Blevis and Crowell[43] on the change of work function ($\Delta\phi$) of the (100) and (111) faces of copper with increasing temperature.

where E is the energy of the peak

$E_{\frac{1}{2}}$ is the width (FWHM) of the peak

ΔT is the temperature range considered

and $2W$ is the Debye-Waller factor at energy E and temperature T.

This apparent shift, which is again to lower energies as the temperature is increased, is of comparable magnitude to the work function shifts, and should also be subtracted from the observed peak shift. It is assumed in deriving equation 6.4-2 that the Debye temperature across a diffraction peak is constant, which is as we saw in the last section a good assumption.

There are other possible sources of peak shifts which we should mention here, but will not consider in detail due to the complexities involved. As the crystal lattice expands, the density of the free electron gas in the crystal will be decreased, and the details of its inhomogeneity near the free surface may well be changed. This therefore may well lead to the interaction of the injected electron with the free electron gas being altered. In other words, the inner potential and the mean free path of the injected electrons may well be temperature dependent. Additionally, the precise scattering mechanisms involved in any one diffraction peak may change, as the lattice vibrations increase. For instance, it is known that the higher partial waves become more important in the diffraction series. These are at present totally unknown quantities, and may well affect the peak positions in an unknown manner. The extent of their significance must await the advent of more refined calculations.

6.4.2 - Experimental Values of Peak Shifts

Experimentally, it is observed that most peaks tend to shift towards lower

energies as the temperature of the sample is increased. In a few cases, however, a peak will remain at the same energy over the temperature range used here, or may even remain at a constant energy at the lower end of the temperature range but shift to lower energies as the temperature gets a bit higher. All three types of behaviour are exhibited occasionally by different peaks in the same set of spectra, so these more unusual effects are not an artefact introduced by instabilities in the apparatus. In no case however, has a peak been observed to move to higher energies as the temperature is increased.

However, since from these experimental peak shifts we have to subtract the shifts due to both the change in work function of the specimen and to the apparent Debye-Waller shift, it is apparent that we can arrive at values of the effective linear expansion coefficient which are either positive or negative - or even both in different temperature régimes - when we consider different diffraction peaks. In Figure 6.2-1, the most common trend - towards lower energies - can be clearly observed.

The peak shifts are in general very small, most commonly of the order of one or two electron volts for a temperature range of 500°K, but for a high energy peak may reach as much as 5eV. Thus any small instabilities in the accelerating potentials of the electron gun, etc., can cause significant errors in the data. The data points on a graph of peak shift against temperature tend therefore to be somewhat scattered, but it is usually possible to fit a straight line by eye to the data. Errors are assessed in this case by varying the fit of this line between plausible limits, and are therefore rather large.

Because of the smallness of the peak shifts, their overall effect on the profile of an intensity-energy spectrum is of secondary importance, but can obviously make a difference when trying to determine such quantities as inner potential corrections - especially at high energies. Nevertheless, it would be unfruitful to provide vast tables of measured peak shifts as a function of temperature for all the peaks appearing in the intensity-energy spectra studied here. What we therefore present here is the results obtained for certain of the peaks, chosen to illustrate the general trends of the data (or, more accurately, the general lack of trends in the data).

Table 6.3 lists respectively the observed "raw" peak shifts, the shift corrected for the change in work function, the shift corrected for this and for the Debye-Waller shift, and finally the effective linear expansion coefficient derived from the fully-corrected peak shift for some of the peaks in the intensity-energy spectrum of the specular beam from (100) copper. Since the work function shift is non-linear, and this has been allowed for in proceeding from the "raw" data, it is strictly speaking incorrect to draw straight lines through the data points for both "raw" shifts and work-function shifts, but owing to the scatter in the data, this is a refinement which we shall ignore here. Figure 6.4-2 shows a typical sequence of data for one diffraction peak.

In Figure 6.4-3 we show the linear expansion coefficient as a function of peak energy for peaks in the intensity-energy spectrum at an angle of incidence of 6°, and the mean bulk expansion coefficient of $20 \times 10^{-6}\ ^{\circ}K^{-1}$ is taken from the tables of Kaye and Laby[44]. Figure 6.4-4 shows these coefficients for the peaks in the spectrum which lie along the locus CC' of Figure 6.2-9 as a function of angle of incidence, and finally

TABLE 6.3

Temperature Induced Peak Shifts for Cu (100)

Θ	E_p	Θ_D	1.	2.	3.	4.
6	29	210 ± 1	19.6 ± 4.6	9.0 ± 2.1	5.1 ± 1.2	8.8 ± 2.0
6	37	235 ± 4	16.8 ± 3.9	9.1 ± 2.1	7.2 ± 1.6	9.7 ± 2.2
6	52	221 ± 5	63.0 ± 6.3	45.5 ± 4.5	41.0 ± 3.9	39.4 ± 3.8
6	61	261 ± 9	36.6 ± 4.0	29.4 ± 3.4	24.8 ± 3.1	20.3 ± 2.5
6	76	211 ± 5	12.3 ± 6.1	6.6 ± 3.1	4.3 ± 2.2	2.9 ± 1.5
6	105	221 ± 4	58.6 ± 7.2	49.3 ± 6.1	46.0 ± 5.5	21.9 ± 2.6
6	128	260 ± 3	48.5 ± 24.1	35.2 ± 15.1	14.4 ± 6.5	5.6 ± 2.6
6	161	290 ± 4	0 ± 1.2	-10.0 ± 2.1	-16.2 ± 3.4	-5.0 ± 1.0
6	179	250 ± 4	98.3 ± 13.3	85.0 ± 10.3	72.0 ± 8.9	20.1 ± 2.5
6	219	260 ± 5	128.0 ± 11.3	106.7 ± 8.1	90.0 ± 6.8	20.5 ± 1.5
6	277	298 ± 3	56.0 ± 4.2	48.7 ± 3.0	46.6 ± 2.8	8.4 ± 0.5
6	401	291 ± 4	193.3 ± 8.6	190.8 ± 8.1	169.3 ± 7.2	36.3 ± 1.5
7	90	311 ± 5	18.8 ± 4.1	16.0 ± 3.3	12.8 ± 2.6	7.1 ± 1.5
8	92	307 ± 3	39.4 ± 5.7	35.5 ± 4.5	32.0 ± 3.9	17.4 ± 2.3
9	93	246 ± 3	41.3 ± 5.8	37.3 ± 4.7	32.0 ± 4.0	17.3 ± 2.3
10	94	256 ± 2	46.6 ± 4.9	41.3 ± 4.0	35.3 ± 3.4	18.8 ± 1.8
11	95	245 ± 2	38.4 ± 6.3	30.9 ± 5.1	24.5 ± 4.0	12.9 ± 2.1
12	95	239 ± 2	37.2 ± 5.9	29.6 ± 4.8	22.4 ± 3.6	11.8 ± 1.9
13	97	247 ± 2	41.2 ± 6.4	32.0 ± 5.1	25.4 ± 4.0	13.1 ± 2.1
14	97.5	249 ± 3	38.3 ± 5.1	30.5 ± 3.9	24.5 ± 3.1	12.6 ± 1.6

In the table, Θ is the angle of incidence, E_p the energy and Θ_D the Debye temperature of the peak. Column 1 is the "raw" peak shift, column 2 the shift corrected for work function shift only, and column 3 the shift corrected for both work function and Debye-Waller shifts, all in units of 10^{-4}eV $^{o}K^{-1}$. Column 4 is the derived linear expansion coefficient in units of 10^{-6} $^{o}K^{-1}$.

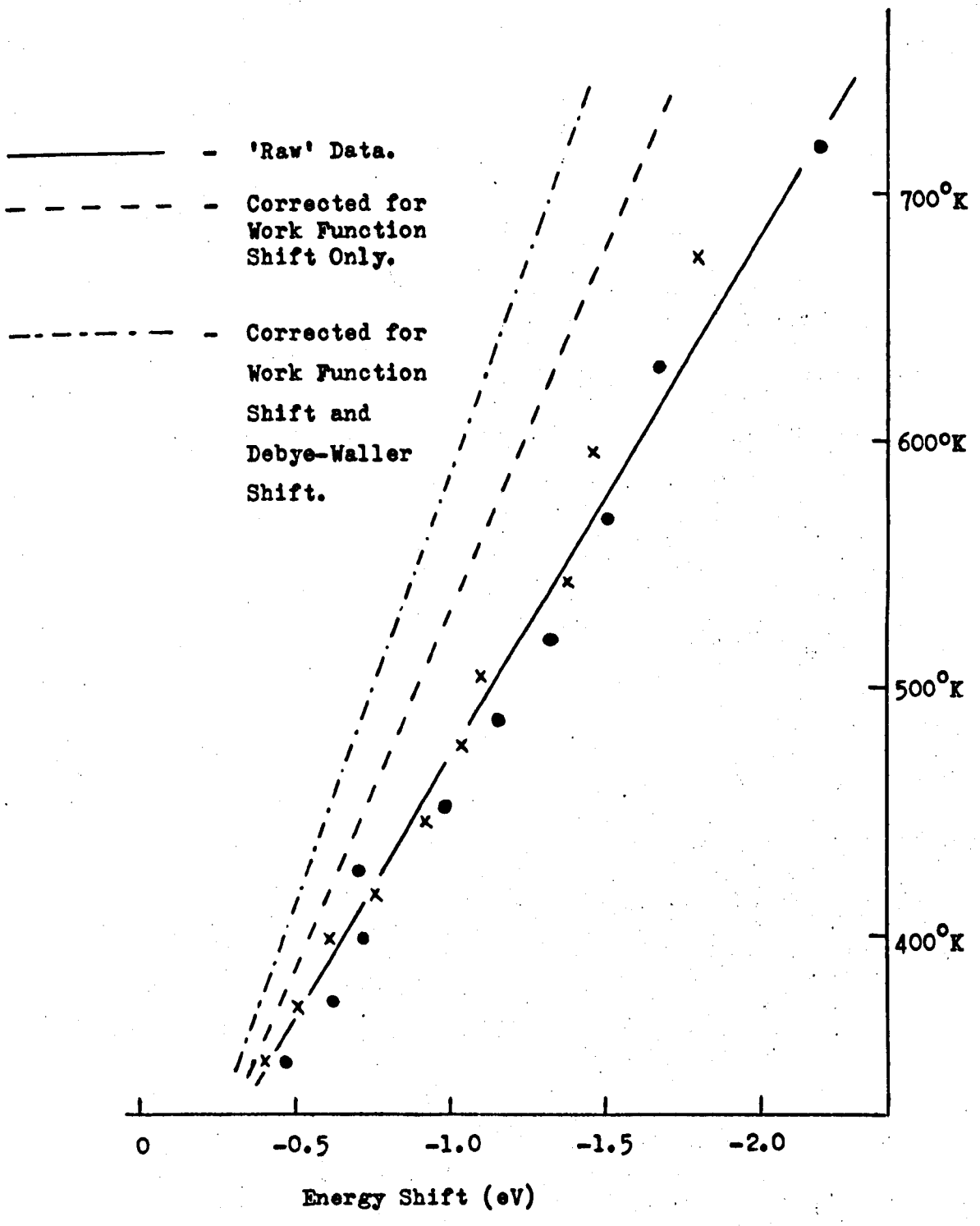

Figure 6.4-2. Sequence of data for the shift in energy of a diffraction peak at 97.5eV in the Intensity-Energy Spectrum from Cu(100). The crosses are for a scan with decreasing energy, and the circles for a scan with increasing energy. The corrections are applied as discussed in the text.

Figure 6.4-3 The derived linear expansion coefficients for various peaks in the Intensity-Energy Spectrum from the (100) surface of copper at an angle of incidence of 6° as a function of peak energy. The horizontal dashed line indicates the bulk linear expansion coefficients, and the short arrows at the top of the frame show the kinematical Bragg scattering conditions.

Figure 6.4-4 The derived linear expansion coefficients for peaks lying along the locus CC' of Figure 6.2-9 as a function of angle of incidence.

Figure 6.4-5 Temperature-induced peak shifts for various peaks in the Intensity-Energy Spectrum from the (100) surface of copper as a function of the Debye temperature of that peak.

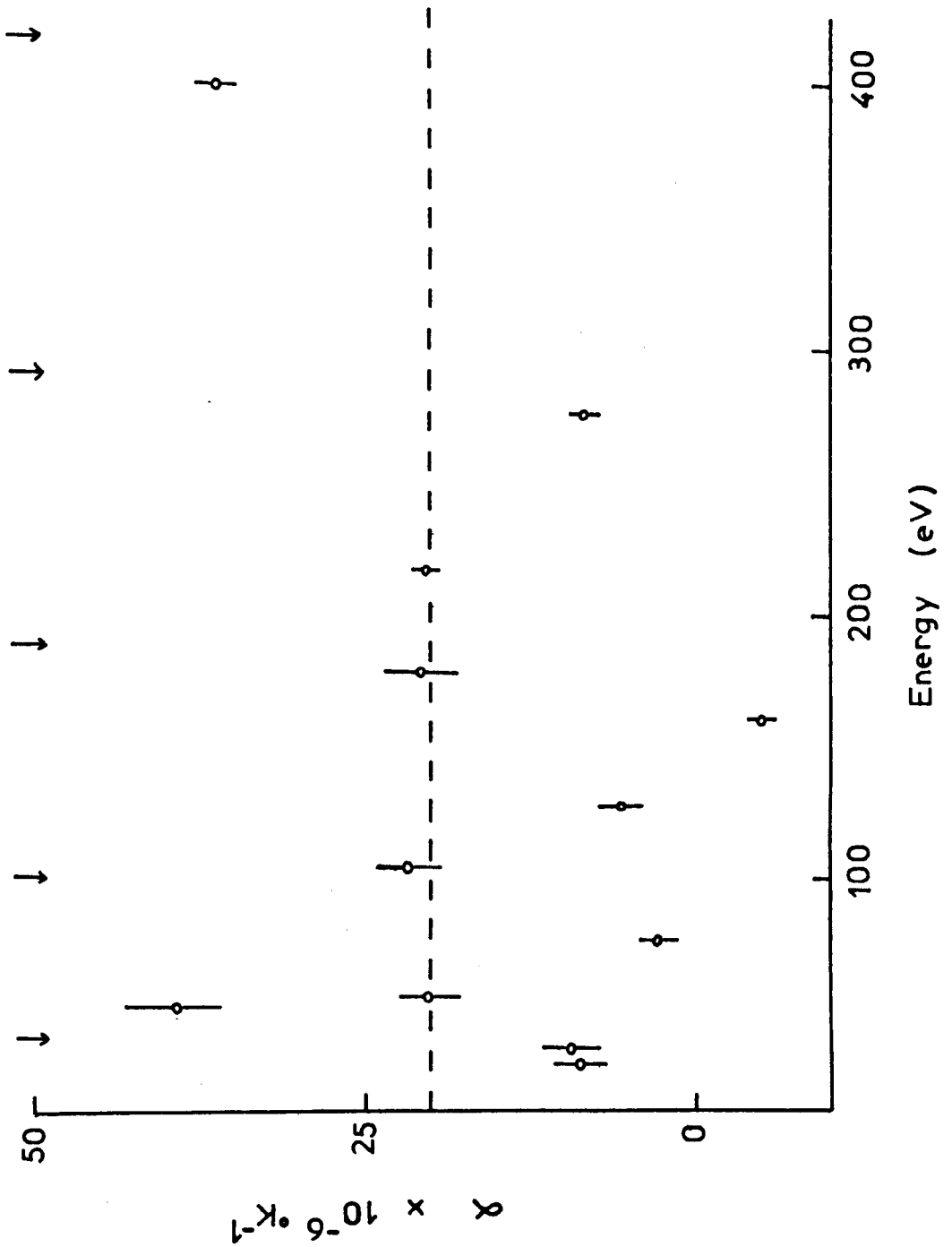

Figure 6.4-3

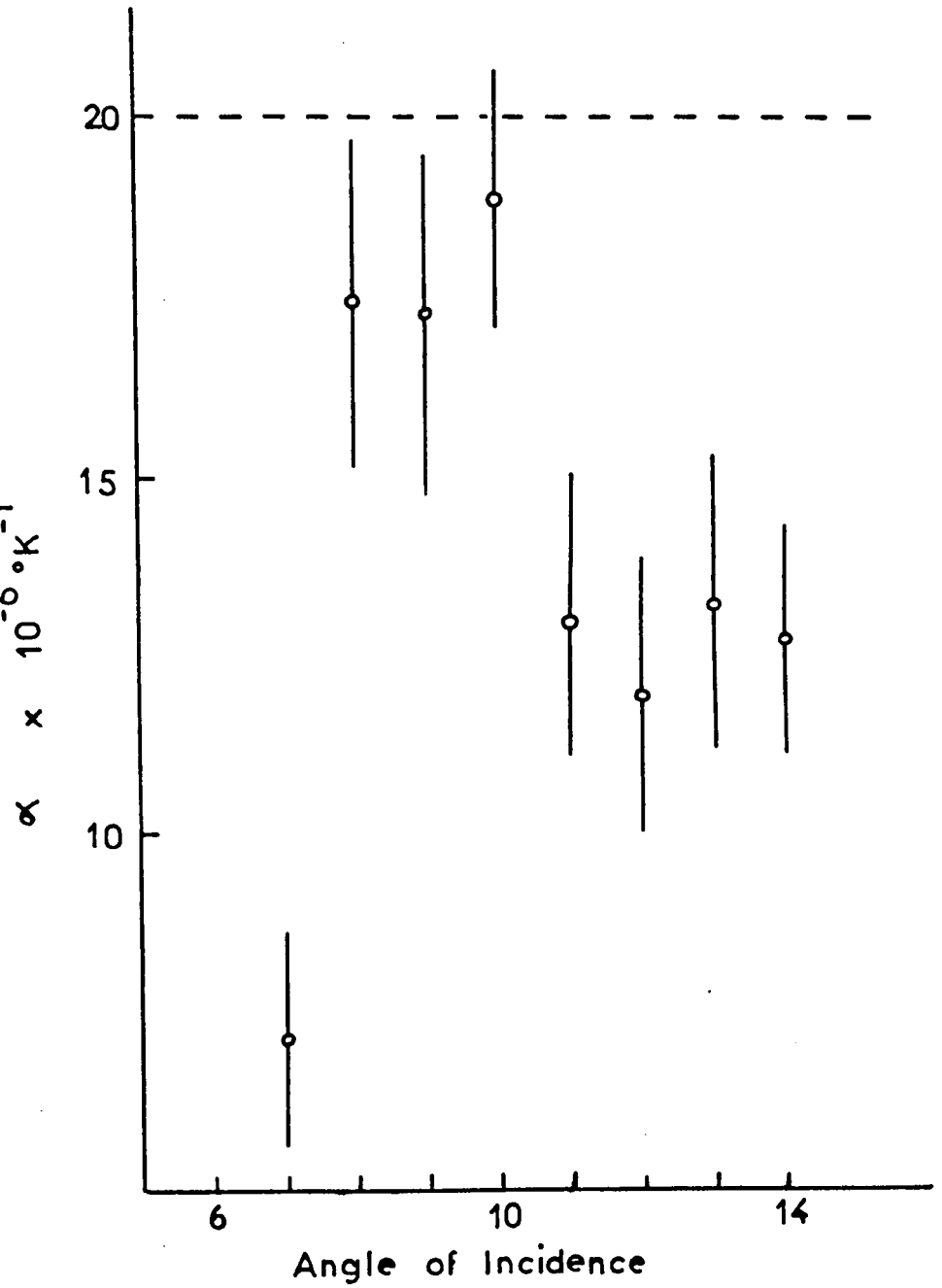

Figure 6.4-4

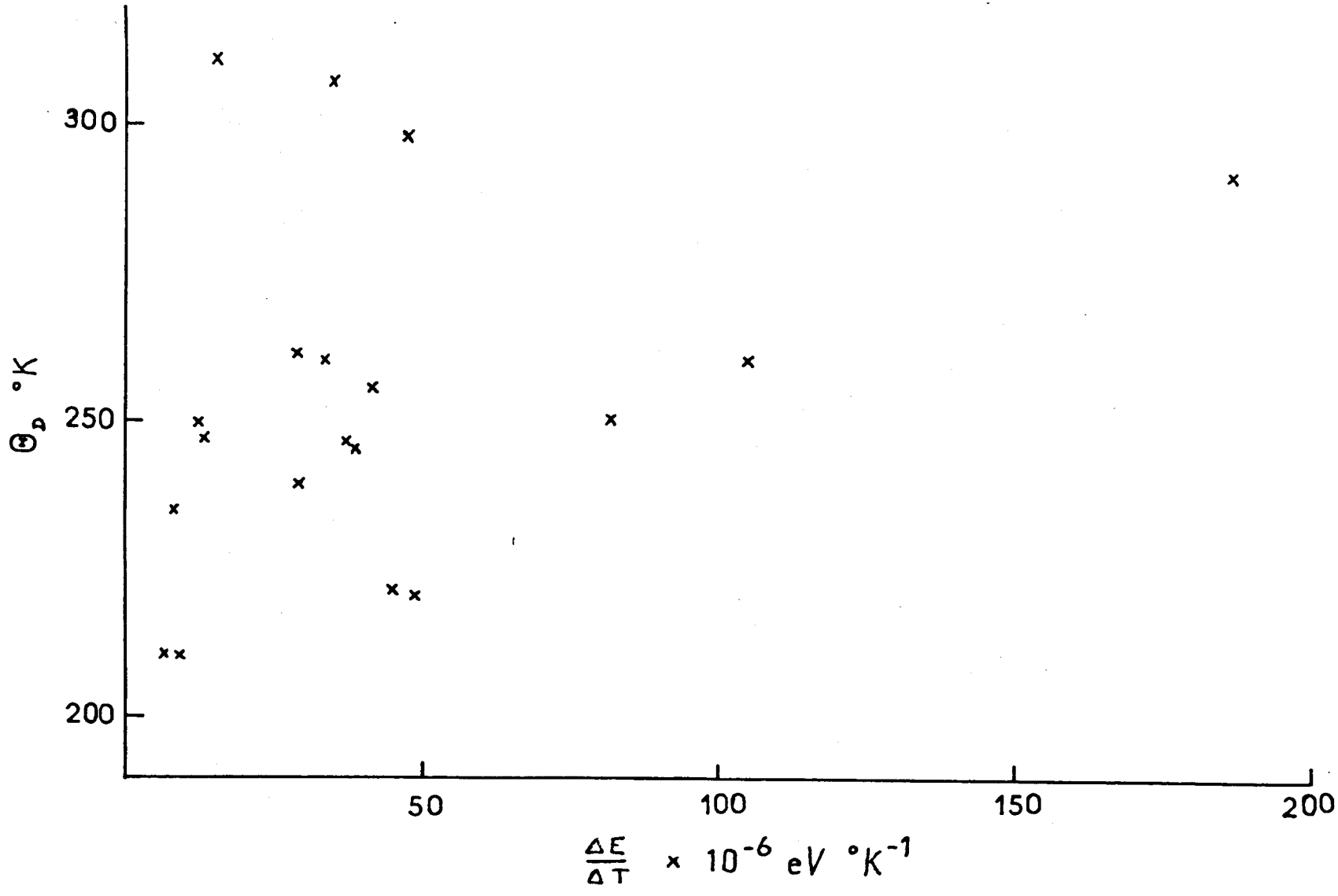
300
250
200
Θ_D °K
50
100
150
200
$\frac{\Delta E}{\Delta T}$ × 10^{-6} eV $°K^{-1}$

Figure 6.4-5

Figure 6.4-5 shows the peak shift corrected for work function only for all of the nineteen peaks as a function of the Debye temperature of these peaks. It is difficult to pick out any trends in any of these figures, since in no case is any consistent behaviour observable, other than to note that the derived linear expansion coefficients are certainly of the correct order of magnitude.

From this rather random behaviour of the peak shifts as a function of the diffraction parameters, we therefore conclude that they are in themselves intimately bound up with the details of the diffraction process, so that trying to proceed from this data to estimates of surface lattice expansions and interatomic potentials is somewhat hazardous.

6.5 - An Interesting Thermal Effect

An interesting effect was observed in the LEED intensity-energy spectrum from Cu(100) when the specimen was heated, and this has been reported in the literature[31]. Figure 6.5-1 shows a small section of the intensity-energy spectrum in the energy range 20 - 50eV for angles of incidence 11-14°. These peaks are part of the "split" (400) nominal Bragg peak discussed at length in § 5.2 In Figures 6.5-2 through 6.5-5 are shown the intensity-energy spectra at four angles of incidence as a function of temperature. In the case of the spectrum at 12.5° incidence, what was at room temperature a doublet of roughly equal intensities is markedly different at higher temperatures, and in the cases of the 11° and 12° spectra, the ratio of the intensities of the two elements of the doublet passes through unity in this temperature range. The Debye temperature for these peaks can be found in Table 6.1.

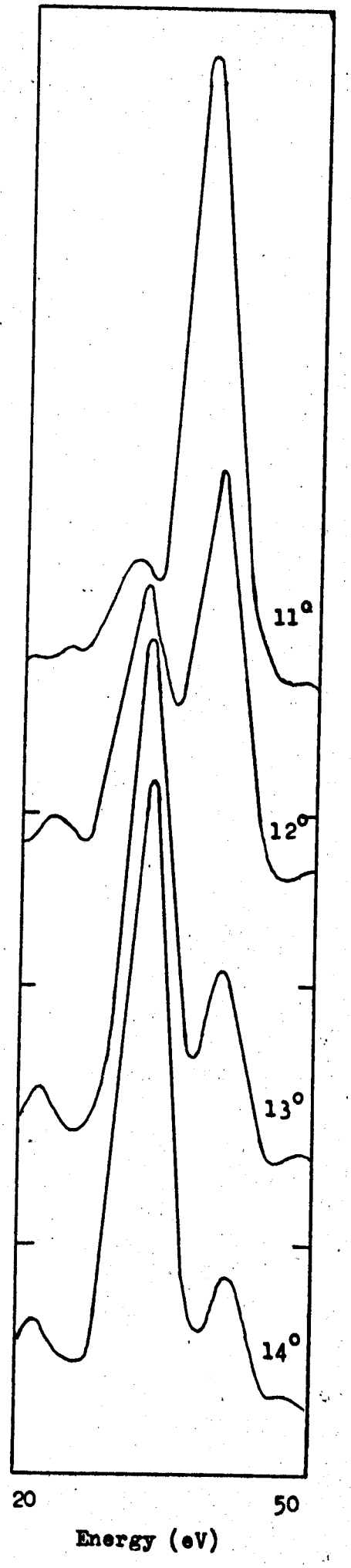

Figure 6.5-1. Portion of the Intensity-Energy Spectrum of the (100) Surface of copper.

Figures 6.5-2 to 6.5-5 The intensity-energy spectrum of the specular LEED beam from the (100) surface of copper as a function of temperature in the energy range 20-50eV at angles of incidence of 11°, 12°, 12.5° and 13° respectively.

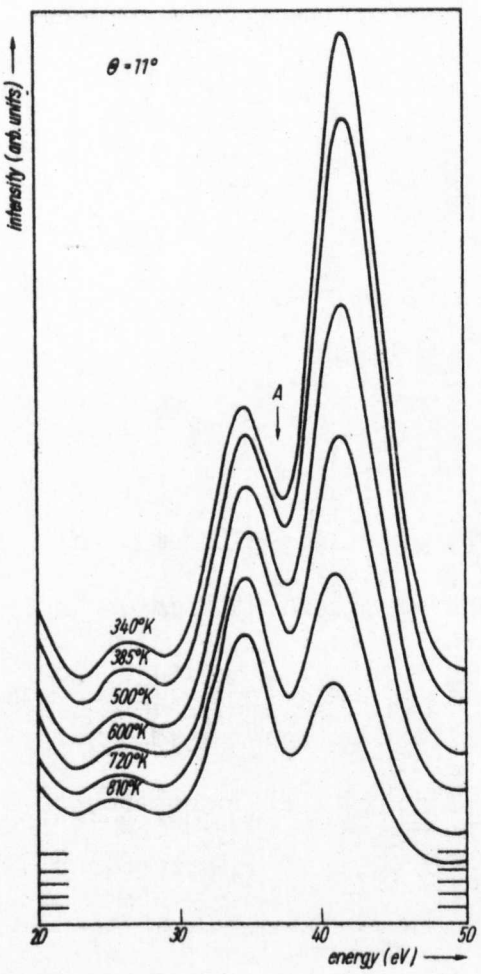
θ = 11°
intensity (arb. units)
A
340°K
385°K
500°K
600°K
720°K
810°K
20
30
40
50
energy (eV)

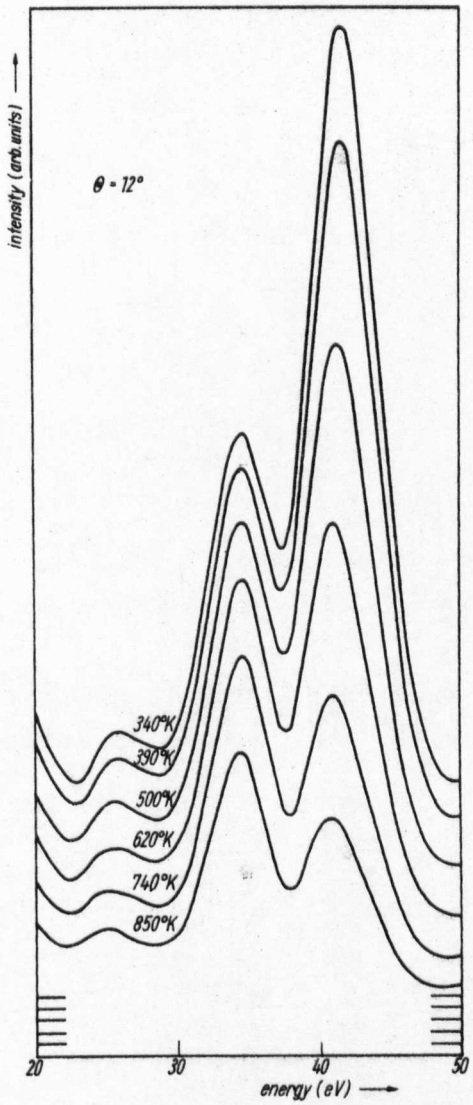
θ = 12°
intensity (arb. units)
340°K
390°K
500°K
620°K
740°K
850°K
20
30
40
50
energy (eV)

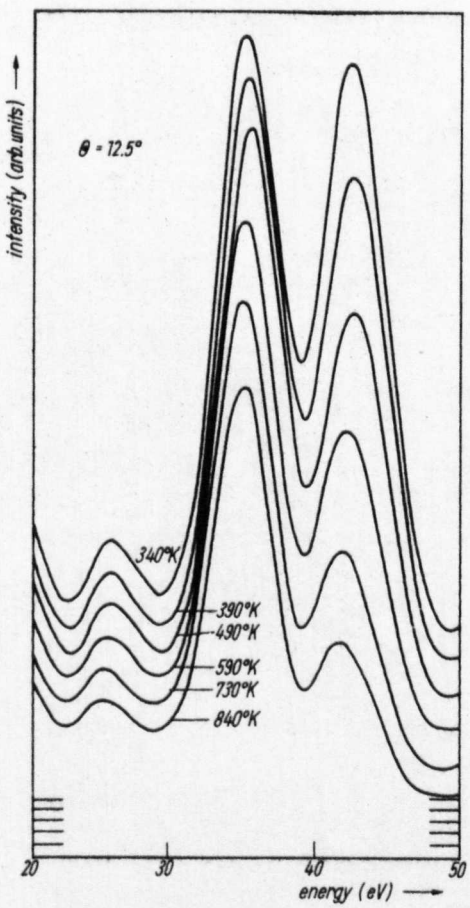
θ = 12.5°
intensity (arb. units)
340°K
390°K
490°K
590°K
730°K
840°K
20
30
40
50
energy (eV)

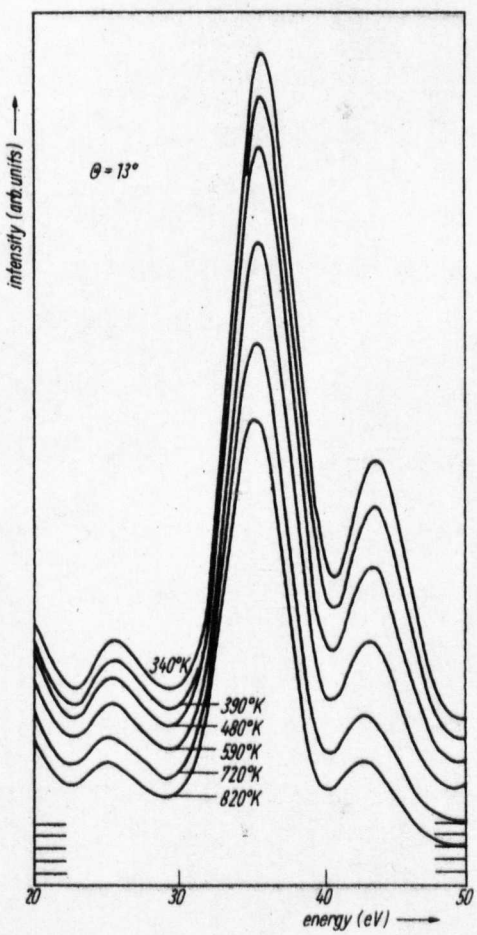
θ = 13°
intensity (arb. units)
340°K
390°K
480°K
590°K
720°K
820°K
20
30
40
50
energy (eV)

In view of the rapid change in the intensity-energy spectrum with angle of incidence, it might be thought that the effect is a spurious one, perhaps caused by some slight rotation of the specimen due to the specimen holder warping as it cooled. That the effect may not thus be readily explained away in terms of a real change in the angle of incidence is inferred from the reproducibility of the effect and its occurrence on both sides of the surface normal.

The effect may be explained simply in terms of the dependence of Debye temperatures on the precise diffraction mechanisms operating, even though we do not know these precise mechanisms.

Very recently, Holland has performed some calculations[45] on the effects of including thermal vibrations into an inelastic collision model analysis of this particular system, using a very crude model for the system. Briefly, he uses the phase shifts calculated for copper by Capart[46] to calculate the rigid lattice scattering of the electrons, and then builds in the thermal vibrations through an Einstein model with the Einstein temperature chosen as three quarters of the value of the bulk value of the Debye temperature. This procedure gives an Einstein frequency equal to the average frequency of the Debye phonon spectrum. Even though only the s-wave scattering is calculated, the general features of the measured intensity-energy spectra are reproduced. Figure 6.5-6, which should be compared with Figure 6.5-1, shows the results of this calculation. Apart from the obvious discrepancy in angles, which is an artefact introduced by ignoring the higher order phase shifts, the agreement is quite good. What is really interesting however, is that the general changes which occur in the intensity-energy spectrum as the temperature is changed are reproduced.

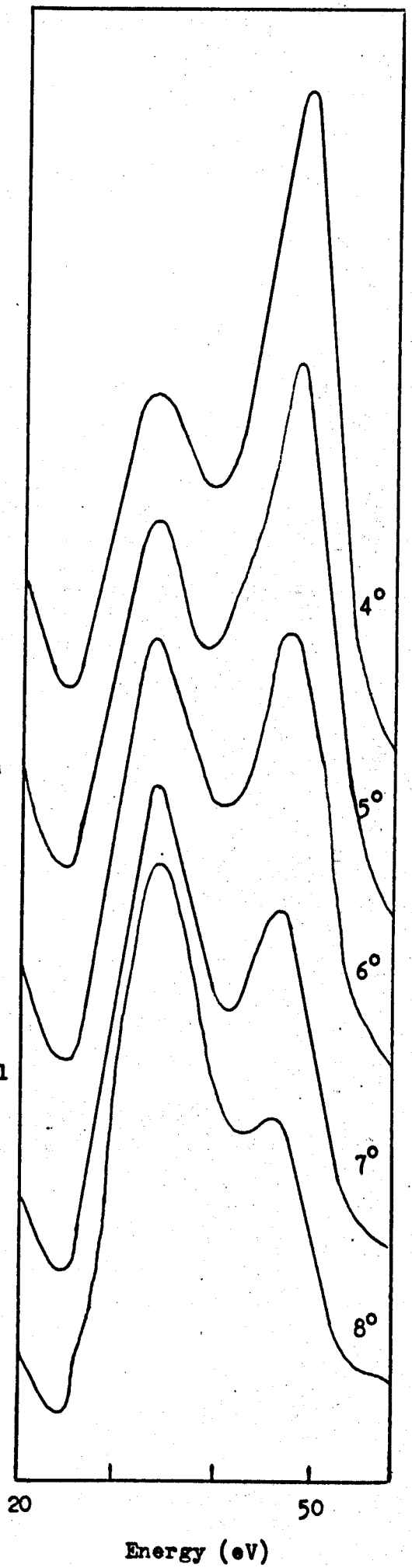

Figure 6.5-6. Part of the Intensity-Energy Spectrum for Cu(100) calculated by Holland. This should be compared with the experimental curves shown in Figure 6.5-1.

Figure 6.5-7 Comparison of a measured temperature-dependent intensity-energy spectrum from Cu(100) at an angle of incidence of 11° (left hand panel) and a similar spectrum calculated for an angle of incidence of 4° by Holland (right hand panel). The discrepancy in the angles is due to the calculation being performed within the framework of a purely s-wave analysis.

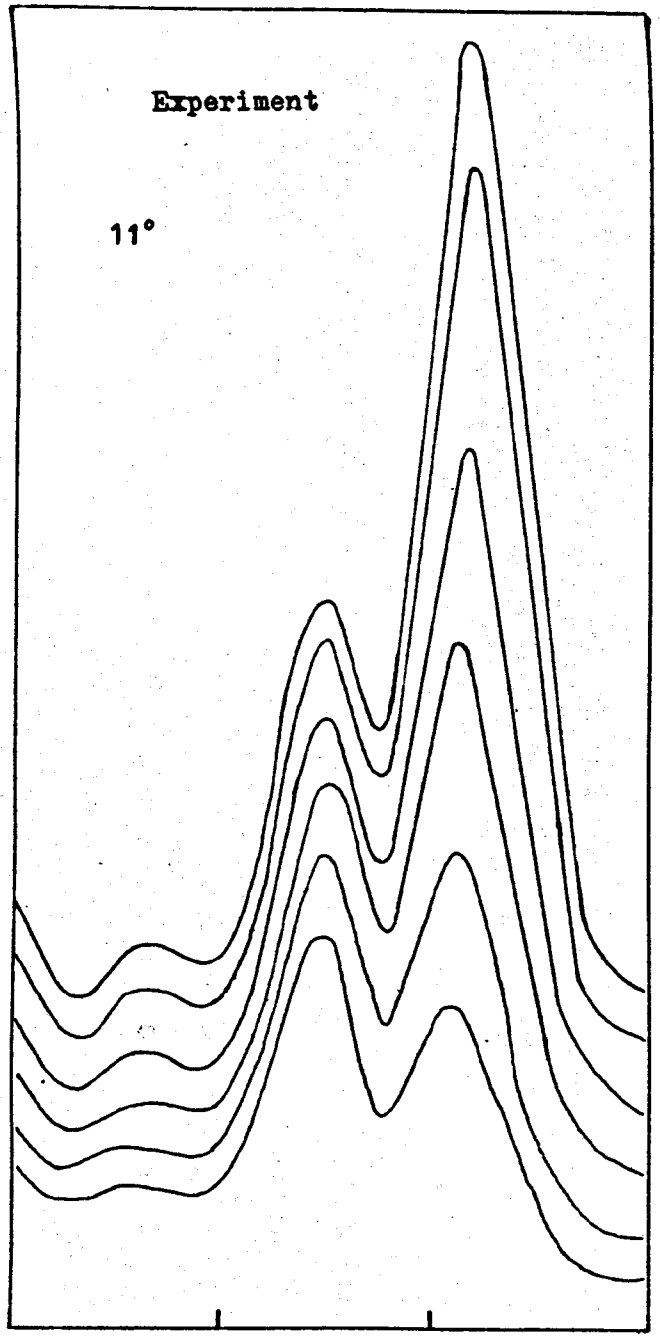
Experiment
11°

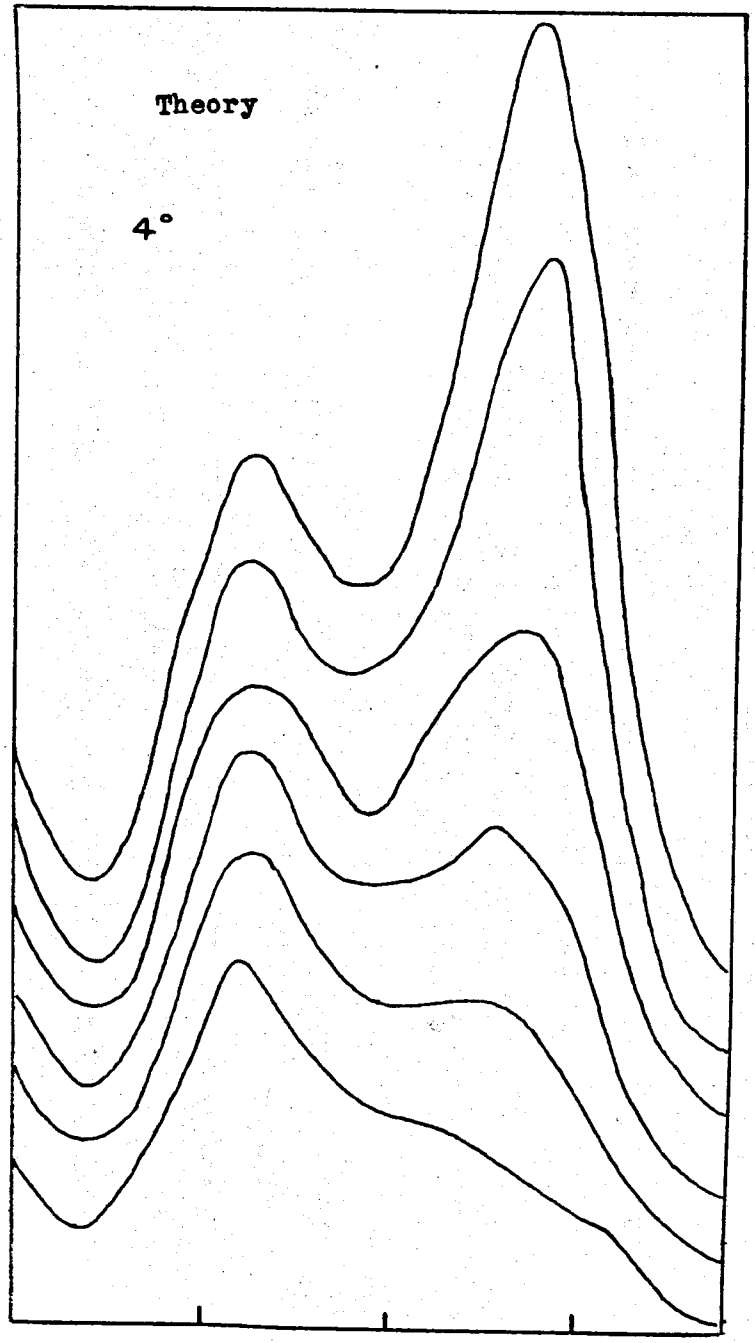
Theory
4°

This is shown in Figure 6.5-7 where the experimental 11° curve is shown beside the theoretical 4° curve. Although there is some discrepancy in detail, the qualitative reproduction of the experimental results is remarkable in view of the crudity of the model. These preliminary calculations are very encouraging, indicating that taking into account the thermal vibrations in a full calculation should have a good chance of reproducing the experimental detail.

6.6 - Summary and Conclusions

What we have seen in this chapter is that the effects of temperature on the intensity-energy spectra, and hence on the details of the LEED process, vary somewhat strikingly from the predictions of a kinematical model of the scattering process. The most important effect of increasing the temperature is to diminish the intensity of the elastic fraction of the scattered intensity, and hence to diminish the intensity of the peaks in the intensity-energy spectra. This diminution in intensity, which can be characterised in the case of each peak by an effective Debye temperature, is not constant from peak to peak, so that the overall profile of the intensity-energy spectrum is altered as the temperature is changed. Although the overall shape of a single diffraction peak is unaltered as a function of temperature, the positions of the diffraction maxima change. Such peak shifts are in themselves small enough to be ignored when comparing theory with experiment, but they must be taken into account in computing the Debye temperature for each peak. However, because of the rather random dependence of both Debye temperatures and peak shifts on the diffraction parameters, it is at present impossible to extract in any consistent fashion values for such properties of the crystal as surface

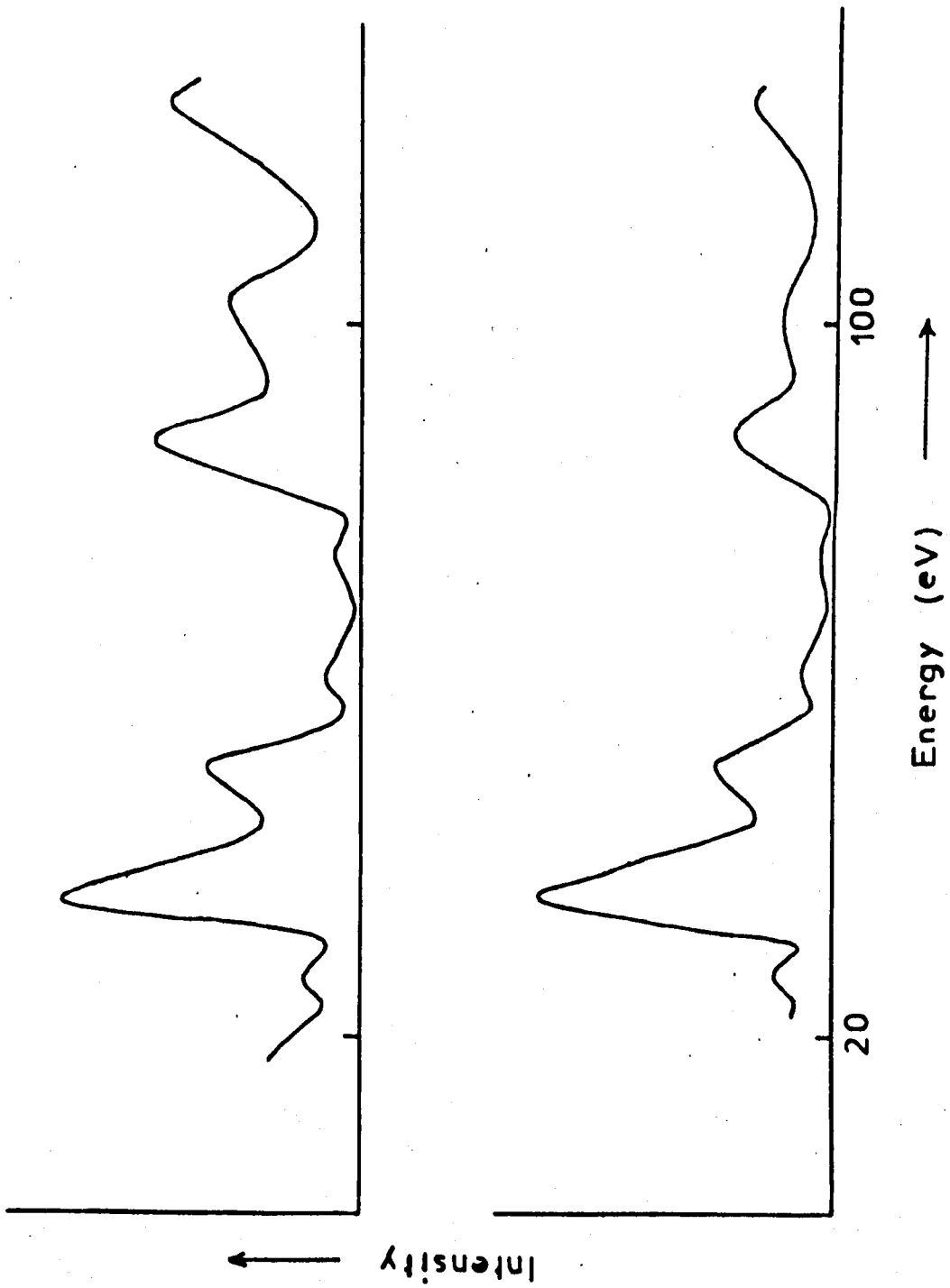

Figure 6.6-1. Comparison between a measured room temperature intensity-energy spectrum (lower panel) and the same spectrum extrapolated to $0^{\circ}K$ and normalised to the room temperature spectrum as described in the text (upper panel)

atom vibrations and lattice expansions from temperature dependent LEED data.

In the last chapter, we presented an intensity-energy spectrum extrapolated to absolute zero. This curve is redrawn in Figure 6.6-1 so that it may be compared directly with the room temperature spectrum. The $0^{\circ}K$ curve was obtained by multiplying the peaks in the room temperature curve by the Debye-Waller factor appropriate to that peak for the temperature range of $\sim 300^{\circ}K$, using the measured Debye temperatures of each peak, and then the peaks at 35eV in each curve were normalised to each other (and to one of the peaks in the other sets of data discussed in the last chapter). Peak shifts are, however, ignored. The main differences in the two curves in Figure 6.6-1 are the expected relatively greater increases in the higher energy peaks at the low temperature compared to the lower energy peaks, due to the energy dependence of the Debye-Waller factor, but there are also changes in relative intensities of the peaks which can be seen on close examination of the figure.

REFERENCES

1) V.E. Lashkarev and G.A. Kuzmin, Phys.J.Sowjet. 6 (1934), 211.
--- , Nature 134 (1934), 62.

2) A.U. McRae and L.H. Germer, Phys.Rev.Lett, 8 (1962), 489.

3) J. Aldag and R.M. Stern, Phys.Rev.Lett. 15 (1965), 857.

4) E.R. Jones, Thesis, University of Wisconsin (1965).

5) J.T. McKinney, Thesis, University of Wisconsin (1966).

6) E.R. Jones, J.T. McKinney and M.B. Webb, Phys.Rev. 151, (1966), 476.

7) H.B. Lyon and G.A. Somorjai, J.Chem.Phys. 44 (1966), 3707.

8) R.F. Barnes, Thesis, University of Wisconsin (1967).

9) H.B. Lyon and G.A. Somorjai, J.Chem.Phys. 46 (1967), 2539.

10) J.T. McKinney, E.R. Jones and M.B. Webb, Phys.Rev. 160 (1967), 523.

11) G. Allie, C.R.Acad.Sci.Paris, 266B (1968), 1568.

12) R.F. Barnes, M.G. Lagally and M.B. Webb, Phys. Rev. 171 (1968), 627.

13) C. Corotte, P. Ducros and A. Mascall, C.R.Acad.Sci.Paris, 267B (1968), 544.

14) R.M. Goodman, H.H. Farrell and G.A. Somorjai, J.Chem.Phys. 48 (1968), 1046.

15) M.G. Lagally and M.B. Webb, Phys.Rev.Lett. 21 (1968), 1388.

16) R. Riwan and G. Allie, C.R.Acad.Sci.Paris 266B (1968), 1568.

17) C.D. Gellatt, M.G. Lagally and M.B. Webb, Bull.Am.Phys.Soc. 14 (1969), 793.

18) R.M. Goodman, Thesis, University of California at Berkeley (1969).

19) J.A. Morabito, R.F. Steiger and G.A. Somorjai, Phys.Rev. 179 (1969), 638.

20) M.P. Seah and D.P. Woodruff, Phys.Lett. 30A (1969), 250.

21) D.P. Woodruff and M.P. Seah, Phys. Lett. 30A (1969), 263.

22) M.G. Lagally, Z. Naturforsch. 25a (1970), 1567.

23) R.J. Reid, Phys.Stat.Sol. (a) 2 (1970), K109.

24) D. Tabor and J.M. Wilson, Surface Science 20 (1970), 203.

25) J.B. Theeten, J.L. Domange and J. Bonnerot, Sol.State Comm. 8 (1970), 643.

26) D.P. Woodruff and M.P. Seah, Phys.Stat.Sol.(a) 1 (1970), 429.

27) S. Andersson and B. Kasemo, Sol.State Comm. 8 (1970), 1885.

28) D. Tabor, J.M. Wilson and T.J. Bastow, Surface Science, 26 (1971), 471.

29) J.M. Wilson and T.J. Bastow, Surface Science, 26 (1971), 461.

30) S. Mroz, Acta Physica Polonica 38 (1970), 321.

31) R.J. Reid, Phys.Stat.Sol.(a) 4 (1971), K211.

32) J.B. Biberian and M. Bienfait, C.R.Acad.Sci.Paris 270B (1970), 1301.

33) R.F. Wallis, B.C. Clark and R. Herman, 'Structure and Chemistry of Solid Surfaces' (Wiley, New York, 1969) Paper 17.

34) P.A. Wolff, Phys.Rev. 95 (1954), 56.

35) H. Taub, R.M. Stern and V.F. Dvoryankin, Phys.Stat.Sol. 33 (1969), 573.

36) G.E. Laramore and C.B. Duke, Phys.Rev.B 2 (1970), 4783.

37) A.A. Maradudin and P.A. Flinn, Phys.Rev. 129 (1963), 2529.

38) A.K. Singh and P.K. Sharma, J.Phys.Soc.Jap. 26 (1969), 425.

39) J.C. Tracy, Rev.Sci.Instrum. 39 (1968), 1300.

40) P.A. Flinn, G.M. McManus and J.A. Rayne, Phys.Rev. 123 (1961), 809.

41) M. Horstmann, Sol.State Comm. 2 (1964), 335.

42) E.G. McRae, private communication.

43) E.H. Blevis and C.R. Crowell, Phys.Rev. 133 (1964), 580.

44) G.W.C. Kaye and T.H. Laby, 'Tables of Physical and Chemical Constants' (Longmans, London, 1962), p. 54.

45) B.W. Holland, to be published.

46) G. Capart, Surface Science, 26 (1971), 429.

CHAPTER 7

CONCLUSIONS AND SUGGESTIONS FOR FURTHER WORK

7.1 - Conclusions

The scope of this thesis falls into two distinct sections, the work on the nature of the surface required to produce a "good" LEED pattern, and that on the effects of temperature on the LEED process. Both sections, however, are united in that they both throw doubt on previously held assumptions. The first part demonstrated that the constraints on the perfection of a crystal surface which would produce a "good" LEED pattern were much less rigorous than was previously supposed. In fact, only about 10% of the "illuminated" surface need be contributing to the observed pattern, and this was discussed in terms of the coherence of the electron beam. The second part examined in detail the effects of temperature on the intensity-energy spectra of the specular LEED beam from two of the low index faces of copper, looking at the changes in the profile of such spectra as the sample temperature varied. It showed that the effects were far from trivial, and that detailed experimental measurements of the Debye temperatures of the various diffraction peaks are required before detailed comparison of theory with experiment is attempted, but that such factors as peak shifts are relatively less important for such purposes. Contrary to the results of many previous, less detailed studies, the data presented here showed that it is as yet impossible to extract in any self-consistent way information about such things as surface atom vibrations, surface lattice expansion and so on. The corpus of work presented in Chapters 5 and 6, constitutes, however, one of the most detailed sets of experimental results at present available against which theories of LEED may be measured.

7.2 - Suggestions for Further Work

In order to provide a complete set of LEED data on any one system, it is necessary that the type of results discussed in this thesis should be extended to all the non-specular diffracted beams, and it would be advantageous to measure absolute scattered intensities. Once such a set of data is available, model calculations which specifically include the atomic vibrations could, in principle, be used to elucidate information about such things as surface atom vibrations, lattice expansion, interatomic potentials and so on. Once these are fully understood, studies of the elastic intensity scattered to all points of the Brillouin zone would be expected to yield information on the scattering of low energy electrons by surface defects, etc.

APPENDIX A1

Determination of Diffraction Angles from LEED Photographs

The geometry of the electron optics and the optical system used for photographing the diffraction patterns are as shown in the diagram.

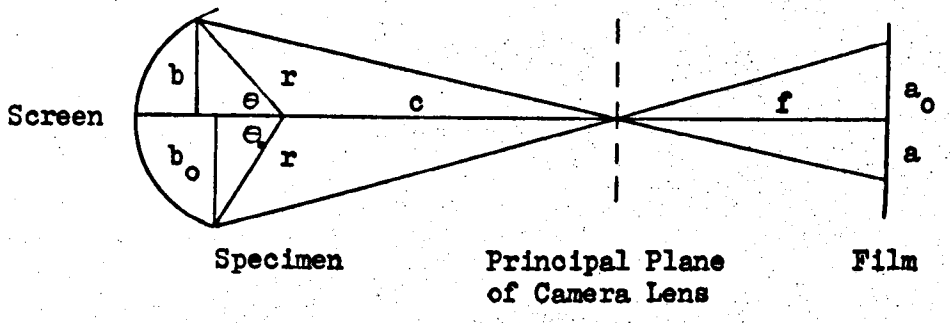

We know Θ_o, the angle subtended by the edge of the fluorescent screen at the centre of curvature of the grid-screen system, r_o, the radius of curvature of the screen, and hence we know b_o. a_o is measured directly from the photographic plate. The problem is to determine θ, the angle subtended by any diffraction spot and the centre of the screen at the centre of curvature of the screen (where we assume the specimen to be) in terms of $\frac{a}{a_o}$, the ratio of the distance of the diffraction spot from the centre of the photograph to that of the edge of the screen from the centre. In this way, we can ignore the magnification of the photograph we are using.

From similar triangles, we have

$$bf - ac = ar \cos\theta$$

$$\text{Hence} \quad \cos\theta = \cos\Theta_o \, \frac{bf - ac}{b_o f - a_o c} \cdot \frac{a_o}{a}$$

The solution of this equation requires a knowledge separately of f, the

distance between the principal point of the camera lens and the film, and of c, the distance between the centre of curvature of the screen and the principal point of the lens. These can be measured, and we can proceed from there.

However, if we do not wish to know the angles precisely, we can take the distance c to be of the order of 5r, a typical figure in this laboratory. (It is in fact the ratio of the specimen-screen distance to the distance between the specimen and the front of the viewing window).

We then have

$$\frac{\sin\theta}{\sin\theta_o} = \frac{b}{b_o} = \frac{a}{a_o} \cdot \frac{5 + \cos\theta}{5 + \cos\theta_o}$$

This can be solved for $\tan \frac{1}{2}\theta$ to give

$$\tan \tfrac{1}{2}\theta = \frac{-1 + (1 + 0.15 \frac{a}{a_o})^{\frac{1}{2}}}{0.15 \frac{a}{a_o}}$$

If, in addition, we allow the specimen to be situated at a point which is not the centre of curvature of the screen, the analysis becomes very much more complicated, and a general solution cannot be determined. In this case, it is better to 'calibrate' the screen in the manner described in the main body of the text.

APPENDIX A2

Coherence Lengths and Widths

Consider a beam of electrons of mean energy E and energy spread ΔE emitted by an extended radially symmetric source of diameter R and incident on a target at a distance L from the source. Let T be the point on the target on the axis of the system and let the source subtend a half angle α at T.

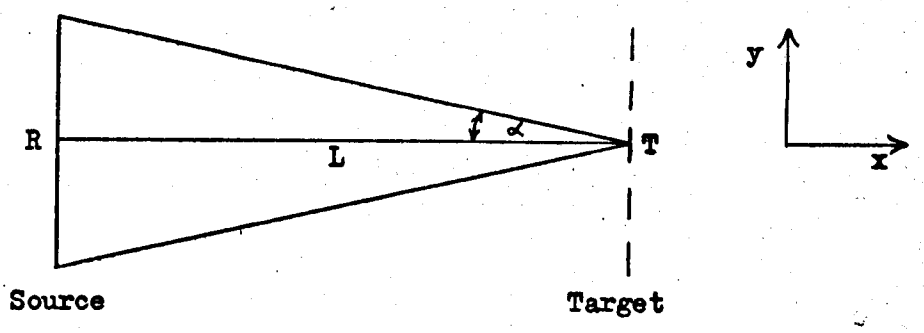

Take x and y axes as shown in the diagram.

The mean magnitude p of the momentum $\underline{p}$ of the electrons is then given by

$$p = \sqrt{2mE}$$

Thus the spread in p due to the energy spread in the beam is

$$\Delta p = \tfrac{1}{2}\sqrt{2m}\,\frac{\Delta E}{E^{\frac{1}{2}}}$$

Consider now the momentum along the x-axis, p_x. The maximum value of p_x is

$$p_x^{max} = \sqrt{2mE} + \tfrac{1}{2}\sqrt{2m}\,\frac{\Delta E}{E^{\frac{1}{2}}}$$

$$= \sqrt{2mE}\,(1 + \tfrac{1}{2}\frac{\Delta E}{E})$$

The minimum value of p_x is then

$$p_x^{min} = \sqrt{2mE}\,(1 - \tfrac{1}{4}\frac{\Delta E}{E})\cos\alpha$$

$$= \sqrt{2mE}\,(1 - \tfrac{1}{4}\frac{\Delta E}{E})\,\frac{2L}{(R^2 + 4L^2)^{\frac{1}{2}}}$$

So the spread in p_x is given by

$$p_x = p_x^{max} - p_x^{min}$$

$$\text{i.e.}\quad \Delta p_x = \sqrt{2mE}\,(1 + \tfrac{1}{4}\frac{\Delta E}{E}) - \sqrt{2mE}\,(1 - \tfrac{1}{4}\frac{\Delta E}{E})\,\frac{2L}{(R^2 + 4L^2)^{\frac{1}{2}}}$$

In a similar fashion, the spread in p_y is given by

$$\Delta p_y = 2\sqrt{2mE}\,(1 + \tfrac{1}{4}\frac{\Delta E}{E})\,\frac{R}{(R^2 + 4L^2)^{\frac{1}{2}}}$$

Thus applying the Uncertainty Principle in its limiting form

$$\Delta p_x \cdot \Delta x = \hbar$$

we get the minimum value of the coherence length Δx,

$$\Delta x = \frac{\hbar}{\sqrt{2mE}\left\{(1 + \tfrac{1}{4}\frac{\Delta E}{E}) - (1 - \tfrac{1}{4}\frac{\Delta E}{E})\,\frac{2L}{(R^2 + 4L^2)^{\frac{1}{2}}}\right\}} \qquad \text{(A2 - 1)}$$

and the coherence width Δy is,

$$\Delta y = \frac{\hbar}{2\sqrt{2mE}\,(1 + \tfrac{1}{4}\frac{\Delta E}{E})} \cdot \frac{(R^2 + 4L^2)^{\frac{1}{2}}}{R} \qquad \text{(A2 - 2)}$$

In the case where $R \ll L$ and $\Delta E \ll E$, these equations reduce to

$$\Delta x = \frac{2\hbar E}{\Delta E\sqrt{2mE}}$$

$$\Delta y = \frac{\hbar}{\sqrt{2mE}\,\beta} \qquad \text{where } \beta = \frac{R}{L}. \qquad \text{(A2 - 3)}$$

APPENDIX A3

The Debye - Waller Factor

The derivation presented here is based mainly on the treatment given in Maradudin *et al*[1].

On a single scattering model of electron diffraction, i.e. a purely kinematical model, the instantaneous intensity, I, of a diffracted beam is given by

$$I = |f_o|^2 \sum_{l,l'} \exp\left\{2\pi i\, \underline{S}\cdot\left[\underline{r}(l) - \underline{r}(l')\right]\right\} \qquad (A3 - 1)$$

where f_o is the atomic scattering factor

$\underline{S}$ is the scattering vector $\left(S = \frac{2\sin\theta}{\lambda}\right)$

$\underline{r}(l)$, $\underline{r}(l')$ are the position vectors of the l and l'th atoms, respectively, and l,l' run over all the points of the crystal lattice.

If we now consider the atoms as vibrating about the lattice points which are defined by the set of vectors $\left\{\underline{x}(l)\right\}$ such that the atomic displacement from $\underline{x}(l)$ is represented by $\underline{u}(l)$, then equation A3-1 becomes

$$I = |f_o|^2 \sum_{l,l'} \exp\left\{2\pi i\, \underline{S}\cdot\left[\underline{x}(l) - \underline{x}(l')\right]\right\} \exp\left\{2\pi i\, \underline{S}\cdot\left[\underline{u}(l) - \underline{u}(l')\right]\right\}$$

$$= I_o \sum_{l,l'} \exp\left\{2\pi i\, \underline{S}\cdot\left[\underline{u}(l) - \underline{u}(l')\right]\right\} \qquad (A3 - 2)$$

where I_o is the rigid lattice scattering factor, and the summation in A3-2 now contains all the effects of the vibrations.

What we require is the time averaged value, $\overline{I}$, of A3-2. As is usual in Statistical Mechanics, it is simpler to replace this time average by an ensemble average over the ensemble represented by the crystal Hamiltonian H.

For simplicity, we consider a crystal consisting of only one type of atom of mass m. Firstly, we wish to evaluate $\langle \exp\{iSu_\alpha(1)\}\rangle$ where $\underline{S}\cdot\underline{u}(1) = \sum_{\alpha=1}^{3} Su_\alpha(1)$. Then,

$$\langle \exp\{iSu_\alpha(1)\}\rangle = \frac{\mathrm{Tr}\exp\{-\beta H\}\exp\{iSu_\alpha(1)\}}{\mathrm{Tr}\exp\{-\beta H\}} \qquad \text{(A3 - 3)}$$

where $\beta = (k_B T)^{-1}$

k_B is Boltzmann's constant

T is the Absolute temperature

and Tr is the Trace operator of the matrix.

The Hamiltonian of the crystal is given in the Harmonic approximation by

$$H = \sum_{\underline{k},j} \hbar\omega(\underline{k},j)\left[a^*(\underline{k},j)a(\underline{k},j) + \tfrac{1}{2}\right] \qquad \text{(A3 - 4)}$$

where $\omega^2(\underline{k},j)$ are the eigenvalues of the dynamical matrix of the crystal, and $\omega, \underline{k}, j$ are respectively the frequency, wave vector and polarisations of the phonons. $a^*(\underline{k},j)$ and $a(\underline{k},j)$ are respectively the boson creation and annihilation operators for the phonons.

The amplitudes of the thermal vibrations can then be shown to be given in this representation by

$$u_\alpha(1) = \left(\frac{1}{mN}\right)^{\frac{1}{2}} \sum_{\underline{k},j} e_\alpha(\underline{k},j)\left(\frac{\hbar}{2\omega(\underline{k},j)}\right)^{\frac{1}{2}}\left[a^*(-\underline{k},j) + a(\underline{k},j)\right] x \exp\left\{2\pi i\, \underline{k}\cdot\underline{x}(1)\right\} \qquad \text{(A3 - 5)}$$

where the $e_\alpha(\underline{k},j)$ are the components of eigenvectors of the dynamical matrix of the crystal and N is the total number of atoms in the crystal.

By substituting A3-4 and A3-5 into A3-3 and factorising, we find, after some manipulation that

$$\langle \exp\{iSu_\alpha(1)\}\rangle = \exp\left\{-\tfrac{1}{2}S^2 \frac{\hbar}{2mN}\sum_{\underline{k},j}\frac{e_\alpha(\underline{k},j)e_\alpha^*(\underline{k},j)}{\omega(\underline{k},j)}\coth\tfrac{1}{2}\beta\hbar\omega(\underline{k},j)\right\} \qquad \text{(A3 - 6)}$$

By evaluating $\langle u_\alpha^2(1) \rangle$ in a similar manner, we may readily show that

$$\exp\{iSu_\alpha(1)\} = \exp\{-\tfrac{1}{2}S^2 \langle u_\alpha^2(1)\rangle\} \qquad (A3-7)$$

We are now in a position to evaluate $\langle \exp\{2\pi i\, \underline{S}\cdot[\underline{u}(1) - \underline{u}(1')]\}\rangle$.

Making use of A3-7 and substituting A3-5 into the expression, we arrive at the following equation

$$\bar{I} = \langle I_o \sum_{1,1'} \exp\{2\pi i\, \underline{S}.[\underline{u}(1) - \underline{u}(1')]\}\rangle$$

$$= |f_o|^2 \exp\{-\frac{4\pi^2}{Nm}\sum_{\underline{k},j}[\underline{S}.\underline{e}(\underline{k},j)]^2 E(\underline{k},j)\} \sum_{1,1'} \exp\{2\pi i\, \underline{S}.[\underline{x}(1) - \underline{x}(1')]$$

$$+ \frac{4\pi^2}{Nm}\sum_{\underline{k},j}[\underline{S}.\underline{e}(\underline{k},j)]^2 E(\underline{k},j)\cos 2\pi\underline{k}.[\underline{x}(1) - \underline{x}(1')]\}$$

where $E(\underline{k},j) = \frac{\hbar}{2\omega(\underline{k},j)} \coth \tfrac{1}{2}\beta\hbar\omega(\underline{k},j)$

Thus $\bar{I} = |f_o|^2 e^{-2W} I_o + |f_o|^2 e^{-2W} \sum_{1,1'} \exp\{\frac{4\pi^2}{Nm}\sum_{\underline{k},j}[\underline{S}.\underline{e}(\underline{k},j)]^2 E(\underline{k},j)$

$$\times \cos 2\pi\underline{k}.[\underline{x}(1) - \underline{x}(1')]\} \qquad (A3-8)$$

where $2W = \frac{4\pi^2}{Nm}\sum_{\underline{k},j}[\underline{S}.\underline{e}(\underline{k},j)]^2 E(\underline{k},j)$

i.e. $$2W = \frac{2\pi^2\hbar}{Nm}\sum_{\underline{k},j}[\underline{S}.\underline{e}(\underline{k},j)]^2 \frac{\coth \tfrac{1}{2}\beta\hbar\omega(\underline{k},j)}{\omega(\underline{k},j)} \qquad (A3-9)$$

This is the so - called Debye - Waller factor.

The first term in equation A3 - 8 is the rigid lattice scattering factor multiplied by the Debye - Waller factor, and so is a function sharply peaked at the reciprocal lattice points, diminished only in magnitude by a factor depending on the phonon distribution - and hence the temperature. The second term explicitly contains the phonon wave vector $\underline{k}$ and describes the phonon scattered electrons. We consider here only the first term, the zero phonon component.

Evaluation of the Debye - Waller factor in the general case is very difficult, and can really only be done numerically. However if we consider only the case of a cubic Bravais lattice, a considerable simplification occurs because of the cubic symmetry. In this case,

$$\left[\underline{S}.\ \underline{e}(\underline{k},j)\right]^2 = \frac{S^2}{3}$$

so $$2W = \frac{2\pi^2 S^2 \hbar^2}{3Nm} \sum_{\underline{k},j} \frac{\coth \frac{1}{2}\beta\hbar\omega(\underline{k},j)}{\omega(\underline{k},j)}$$

$$= 4\pi^2 S^2 \langle u_\alpha^2(1)\rangle$$

Now, $S = \frac{2\cos\theta}{\lambda}$, where θ is the angle of incidence and λ the wavelength of the electrons.

Hence $$\underline{2W = \frac{16\pi^2}{\lambda^2} \langle u_\alpha^2(1)\rangle \cos^2\theta} \qquad \text{(A3 - 10)}$$

It now only remains to evaluate $\langle u_\alpha^2(1)\rangle$

Now, as we have seen,

$$\langle u_\alpha^2(1)\rangle = \frac{\hbar}{6Nm} \sum_{\underline{k},j} \frac{\coth \frac{1}{2}\beta\hbar\omega(\underline{k},j)}{\omega(\underline{k},j)}$$

$$= \frac{\hbar}{6Nm} \int_0^\omega \frac{g(\omega)}{\omega} \coth \tfrac{1}{2}\beta\hbar\omega \, d\omega \qquad \text{(A3 - 11)}$$

for a continuous spectrum of the $\omega(\underline{k},j)$.

Any realistic evaluation of this quantity requires the substitution of a plausible function for the phonon frequency distribution $g(\omega)$, and in general the integration must be performed numerically. However, if we use the Debye frequency spectrum, we can proceed analytically.

Here,

$$g(\omega) = \frac{9N\omega^2}{\omega_M^3} \qquad 0 < \omega < \omega_M$$

$$= 0 \qquad \omega > \omega_M \qquad \text{(A3 - 12)}$$

Expanding $\coth \frac{1}{2}\beta\hbar\omega$ in the high temperature limit ($\frac{1}{\beta} \gg \hbar\omega$), we get

$$\langle u_\alpha^2(1)\rangle = \frac{\hbar}{6Nm}\int_0^{\omega_M} g(\omega)\left\{\frac{2k_BT}{\omega^2\hbar^2} + \frac{1}{6}\frac{\hbar}{k_BT} + \ldots\ldots\right\} d\omega$$

$$= \frac{3k_BT}{\omega_M^2} - \frac{\hbar^2}{6mk_BT} + \ldots\ldots \qquad (A3 - 13)$$

If we then put $\Theta_D = \frac{\hbar\omega_M}{k_B}$, where Θ_D is the characteristic Debye temperature and making the conventional approximation of ignoring all but the first term in the series A3 - 13, we get

$$2W = \frac{16\pi^2}{\lambda^2}\cos^2\theta\,\frac{3\hbar^2T}{mk_B\Theta_D^2} \qquad (A3 - 14)$$

This is the usual expression quoted for the Debye - Waller factor. It is worth summarising in conclusion the various approximations which have been made implicitly or explicitly in the above treatment, in order to define the area of validity of this expression. Firstly, the crystal Hamiltonian has been evaluated within the adiabatic and harmonic approximations for a monatomic crystal lattice, and the diffraction intensities calculated on a strict kinematical model, allowing no multiple scattering whatsoever. Finally, the phonon distribution has been calculated for a cubic Bravais lattice assuming a Debye frequency spectrum, evaluated in the high temperature limit.

REFERENCES

1) A.A. Maradudin, E.W. Montroll and G.H. Weiss, Sol. State Physics Supplement 3 (1963)